frontiers | Research Topics

Widely used and novel approaches of the measurement of arterial stiffness and central hemodynamic parameters: Is there a consensus on the horizon?

Edited by
János Nemcsik, Christopher Clemens Mayer, Andrea Guala, Bart Spronck and Dimitrios Terentes-Printzios

Published in
Frontiers in Physiology

ISSN 1664-8714
ISBN 978-2-83251-914-1
DOI 10.3389/978-2-83251-914-1

About Frontiers

Frontiers is more than just an open access publisher of scholarly articles: it is a pioneering approach to the world of academia, radically improving the way scholarly research is managed. The grand vision of Frontiers is a world where all people have an equal opportunity to seek, share and generate knowledge. Frontiers provides immediate and permanent online open access to all its publications, but this alone is not enough to realize our grand goals.

Frontiers journal series

The Frontiers journal series is a multi-tier and interdisciplinary set of open-access, online journals, promising a paradigm shift from the current review, selection and dissemination processes in academic publishing. All Frontiers journals are driven by researchers for researchers; therefore, they constitute a service to the scholarly community. At the same time, the *Frontiers journal series* operates on a revolutionary invention, the tiered publishing system, initially addressing specific communities of scholars, and gradually climbing up to broader public understanding, thus serving the interests of the lay society, too.

Dedication to quality

Each Frontiers article is a landmark of the highest quality, thanks to genuinely collaborative interactions between authors and review editors, who include some of the world's best academicians. Research must be certified by peers before entering a stream of knowledge that may eventually reach the public - and shape society; therefore, Frontiers only applies the most rigorous and unbiased reviews. Frontiers revolutionizes research publishing by freely delivering the most outstanding research, evaluated with no bias from both the academic and social point of view. By applying the most advanced information technologies, Frontiers is catapulting scholarly publishing into a new generation.

What are Frontiers Research Topics?

Frontiers Research Topics are very popular trademarks of the *Frontiers journals series*: they are collections of at least ten articles, all centered on a particular subject. With their unique mix of varied contributions from Original Research to Review Articles, Frontiers Research Topics unify the most influential researchers, the latest key findings and historical advances in a hot research area.

Find out more on how to host your own Frontiers Research Topic or contribute to one as an author by contacting the Frontiers editorial office: frontiersin.org/about/contact

Widely used and novel approaches of the measurement of arterial stiffness and central hemodynamic parameters: Is there a consensus on the horizon?

Topic editors

János Nemcsik — Semmelweis University, Hungary
Christopher Clemens Mayer — Austrian Institute of Technology (AIT), Austria
Andrea Guala — Vall d'Hebron Research Institute (VHIR), Spain
Bart Spronck — Maastricht University, Netherlands
Dimitrios Terentes-Printzios — University of Oxford, United Kingdom

Citation

Nemcsik, J., Mayer, C. C., Guala, A., Spronck, B., Terentes-Printzios, D., eds. (2023). *Widely used and novel approaches of the measurement of arterial stiffness and central hemodynamic parameters: Is there a consensus on the horizon?* Lausanne: Frontiers Media SA. doi: 10.3389/978-2-83251-914-1

Table of contents

frontiers | Frontiers in Physiology

TYPE Editorial
PUBLISHED 28 February 2023
DOI 10.3389/fphys.2023.1167257

OPEN ACCESS

EDITED AND REVIEWED BY
Gerald A. Meininger,
University of Missouri, United States

*CORRESPONDENCE
János Nemcsik,
janos.nemcsik@gmail.com

SPECIALTY SECTION
This article was submitted to Vascular Physiology, a section of the journal Frontiers in Physiology

RECEIVED 16 February 2023
ACCEPTED 23 February 2023
PUBLISHED 28 February 2023

CITATION
Nemcsik J, Mayer CC, Guala A, Terentes-Printzios D and Spronck B (2023), Editorial: Widely used and novel approaches of the measurement of arterial stiffness and central hemodynamic parameters: Is there a consensus on the horizon? *Front. Physiol.* 14:1167257. doi: 10.3389/fphys.2023.1167257

Editorial: Widely used and novel approaches of the measurement of arterial stiffness and central hemodynamic parameters: Is there a consensus on the horizon?

János Nemcsik[1]*, Christopher Clemens Mayer[2], Andrea Guala[3,4], Dimitrios Terentes-Printzios[5] and Bart Spronck[6,7]

[1]Department of Family Medicine, Faculty of Medicine, Semmelweis University, Budapest, Hungary, [2]Center for Health & Bioresources, AIT Austrian Institute of Technology, Vienna, Austria, [3]Vall d'Hebron Research Institute (VHIR), Barcelona, Spain, [4]CIBER-CV, Instituto de Salud Carlos III, Madrid, Spain, [5]1st Cardiology Department, Hippokration Hospital, National and Kapodistrian University of Athens, Athens, Greece, [6]Department of Biomedical Engineering, CARIM School for Cardiovascular Diseases, Maastricht University, Maastricht, Netherlands, [7]Macquarie Medical School, Faculty of Medicine, Health and Human Sciences, Macquarie University, Sydney, NSW, Australia

KEYWORDS

arterial stiffness, central blood pressure, pulse wave reflection, cardiovascular risk, modeling

Editorial on the Research Topic
Widely used and novel approaches of the measurement of arterial stiffness and central hemodynamic parameters: Is there a consensus on the horizon?

The evaluation of vascular biomarkers can help to identify patients with high cardiovascular risk providing opportunity for early preventive interventions to avoid clinical endpoints like cardiovascular morbidity and mortality. Recently a consensus paper was published on the clinical use of pulse wave velocity (PWV) (Park et al., 2022) suggesting that in the near future the importance of PWV measurements in everyday clinical practice will increase (Vlachopoulos et al., 2015).

This Research Topic provides nine articles (one review paper and eight original research papers) that deepen the knowledge in the field. The wide scope of these articles includes the role of circulating biomarkers in vascular ageing, *ex vivo* animal experiments, technical developments in the measurement of aortic stiffness, reference values of wave reflection parameters as measured in humans, acute effects of vasoactive drugs on arterial stiffness metrics, and a meta-analysis of the effects of antihypertensive medications on central hemodynamic characteristics.

The review paper by Gopcevic et al. gives an overview of circulating biomarkers related to vascular ageing including oxidative stress-based, inflammation-based, cell matrix-based and epigenetic-based biomarkers, the process of DNA methylation, and the importance of telomere length. This paper is a report from an international scientific collaboration on vascular ageing, called VascAgeNet (Climie et al., 2020a; Climie et al., 2020b).

De Moudt et al. demonstrated in isolated mouse aortic segments that both the extracellular matrix and vascular smooth muscle cells contribute to pressure-dependent

stiffness hysteresis. Stiffness hysteresis phenomena were contraction-, age-, and extracellular matrix-dependent, which suggests that vascular smooth muscle cells in interaction with the extracellular matrix contribute to the pressure-dependent pulse dampening in the aorta. These results warrant future studies in understanding the role of contractile cells of the aorta in arterial stiffening.

In the same *ex vivo* setup, Neutel et al. demonstrated that pulse pressure not only modulates the general stiffness of the tissue but also affects the physiological function of vascular smooth muscle cells. At lower pulse pressure the aortic segment showed a larger response to contractile stimuli strongly modulating stiffness, while at a higher pulse pressure, a smaller contraction-induced stiffness modulation was observed. This study contributes to the understanding of blood vessel biomechanics and could potentially yield new therapeutic insights.

Malik et al. provide an easier and less operator-dependent method based on ultrasound images to evaluate carotid artery mechanical properties. In 500 subjects, the single M-line ultrasound approach using the middle M-line was as accurate as the multiple M-line approach using 17 M-lines. Diameter, intima-media thickness, and Young's elastic modulus were not statistically significantly different when using one vs. 17 M-lines. Differences in distension and distensibility coefficient, though statistically significant, were of a clinically irrelevant magnitude.

Laser Doppler velocimetry enables contactless measurement of carotid-femoral pulse wave velocity, however, the developed CARDIS device requires now additional quality assessment which hampers its clinical usefulness. Seoni et al. explored two possible methods (template matching and matrix profile) for quality assessment to enable real-time feedback on signal quality in future versions of the device. The authors benchmarked these methods using visual scoring as a reference. Both methods were found to be suitable for the automated assessment of the signal quality of acceleration data measured from the skin at the neck and groin.

In the paper of Giudici et al., the authors used mechanistic correction of carotid PWV to distinguish acute and chronic effects of blood pressure on local arterial stiffness. They found that when comparing healthy individuals with patients with stage I and II hypertension, after mechanistic blood pressure correction, the difference in carotid PWV between the two groups was reduced by 68% and became statistically non-significant. These results suggest that moderate hypertension in middle-aged subjects has minor impact on common carotid artery stiffness independently of the acute effect of blood pressure. Further clinical investigations are required to evaluate the clinical utility of this method.

In the article of Fortier et al., the authors demonstrated the acute effect of nitroglycerine on the vasculature using an arterial stiffness gradient (the ratio between aortic PWV and muscular PWV). Besides preserved aortic stiffness, nitroglycerine acutely decreases muscular stiffness and wave reflection enabling higher pulsatility to reach the microcirculation. This effect could be harmful in the longer term, especially for high flow/low resistance organs like the kidneys and brain. The arterial stiffness gradient can potentially have stronger prognostic value than aortic (carotid-femoral) PWV *per se*, and its changes due to intervention using vasoactive agents (like antihypertensive drugs) could also bear clinical importance.

Zocalo and Bia provide very important age, height, and sex-specific reference intervals for pulse wave analysis/wave separation analysis-derived parameters like augmentation pressure, augmentation index, forward and backward components of aortic blood pressure, reflection magnitude, and reflection index. The age range of the reference population (n = 1,688) is between 2 and 84 years. These data form an important step in the future clinical utility of these parameters.

Cheng et al. performed an individual data meta-analysis on the effects of older and newer antihypertensive agents on central hemodynamic parameters. They found a more pronounced decrease in central systolic blood pressure, augmentation index, and augmentation pressure with newer antihypertensive agents (angiotensin converting enzyme inhibitors, angiotensin receptor blockers, and calcium channel blockers) compared to older medications (diuretics and alpha- and beta-blockers). These data support the therapeutic recommendations of current hypertension guidelines (Williams et al., 2018).

In summary, this Research Topic provided important results from both basic and clinical science demonstrating all levels of research of this scientific area. We hope that these valuable data will help to implement the knowledge in clinical practice and to improve cardiovascular outcome of patients.

Author contributions

JN was the chief editor of this Research Topic and wrote a draft of the editorial. CM, AG, DT-P, and BS were co-editors and reviewed critically the editorial providing huge intellectual imput.

Funding

JN, CM, AG, DT-P, and BS are members of and were supported by COST Action CA18216 "Network for Research in Vascular Ageing" supported by COST (European Cooperation in Science and Technology, www.cost.eu).

Conflict of interest

The authors declare that the research was conducted in the absence of any commercial or financial relationships that could be construed as a potential conflict of interest.

Publisher's note

References

Climie, R. E., Bruno, R. M., Hametner, B., Mayer, C. C., and Terentes-Printzios, D. (2020). Vascular age is not only atherosclerosis, it is also arteriosclerosis. *J. Am. Coll. Cardiol.* 76(2), 229–230. doi:10.1016/j.jacc.2020.03.081

Climie, R. E., Mayer, C. C., Bruno, R. M., and Hametner, B. (2020). Addressing the unmet needs of measuring vascular ageing in clinical practice–European COoperation in science and Technology action VascAgeNet. *Artery Res.* 26 (2), 71–75. doi:10.2991/artres.k.200328.001

Park, J. B., Sharman, J. E., Li, Y., Munakata, M., Shirai, K., Chen, C. H., et al. (2022). Expert consensus on the clinical use of pulse wave velocity in asia. *Pulse (Basel, Switz.* 10 (1-4), 1–18. doi:10.1159/000528208

Vlachopoulos, C., Xaplanteris, P., Aboyans, V., Brodmann, M., Cífková, R., Cosentino, F., et al. (2015). The role of vascular biomarkers for primary and secondary prevention. A position paper from the European society of cardiology working group on peripheral circulation: Endorsed by the association for research into arterial structure and Physiology (artery) society. *Atherosclerosis* 241 (2), 507–532. doi:10.1016/j.atherosclerosis.2015.05.007

Williams, B., Mancia, G., Spiering, W., Agabiti Rosei, E., Azizi, M., Burnier, M., et al. (2018). ESC/ESH guidelines for the management of arterial hypertension: The task force for the management of arterial hypertension of the European society of cardiology and the European society of hypertension: The task force for the management of arterial hypertension of the European society of cardiology and the European society of hypertension. *J. Hypertens.* 36(10), 1953–2041. doi:10.1097/HJH.0000000000001940

frontiers in Physiology

ORIGINAL RESEARCH
published: 28 September 2021
doi: 10.3389/fphys.2021.723972

Aortic Stiffness Hysteresis in Isolated Mouse Aortic Segments Is Intensified by Contractile Stimuli, Attenuated by Age, and Reversed by Elastin Degradation

Sofie De Moudt†, Arthur Leloup† and Paul Fransen†*

Physiopharmacology, Department Pharmaceutical Sciences, University of Antwerp, Antwerpen, Belgium

OPEN ACCESS

Edited by:
Bart Spronck, Maastricht University, Netherlands

Reviewed by:
Maria Bloksgaard, University of Southern Denmark, Denmark
Alessandro Giudici, Maastricht University, Netherlands

***Correspondence:**
Paul Fransen
paul.fransen@uantwerpen.be

†ORCID:
Sofie De Moudt
orcid.org/0000-0003-0060-128X
Arthur Leloup
orcid.org/0000-0003-2014-3618
Paul Fransen
orcid.org/0000-0002-4577-3416

Specialty section:
This article was submitted to Vascular Physiology, a section of the journal Frontiers in Physiology

Received: *11 June 2021*
Accepted: *23 August 2021*
Published: *28 September 2021*

Citation:
De Moudt S, Leloup A and Fransen P (2021) Aortic Stiffness Hysteresis in Isolated Mouse Aortic Segments Is Intensified by Contractile Stimuli, Attenuated by Age, and Reversed by Elastin Degradation. Front. Physiol. 12:723972. doi: 10.3389/fphys.2021.723972

Aim: Cyclic stretch of vascular tissue at any given pressure reveals greater dimensions during unloading than during loading, which determines the cardiac beat-by-beat hysteresis loop on the pressure-diameter/volume relationship. The present study did not focus on hysteresis during a single stretch cycle but investigated whether aortic stiffness determined during continuous stretch at different pressures also displayed hysteresis phenomena.

Methods: Aortic segments from C57Bl6 mice were mounted in the Rodent Oscillatory Set-up for Arterial Compliance (ROTSAC), where they were subjected to high frequency (10 Hz) cyclic stretch at alternating loads equivalent to a constant theoretical pulse pressure of 40 mm Hg. Diastolic and systolic diameter, compliance, and the Peterson elastic modulus (E_p), as a measure of aortic stiffness, was determined starting at cyclic stretch between alternating loads corresponding to 40 and 80 mm Hg, at each gradual load increase equivalent to 20 mm Hg, up to loads equivalent to pressures of 220 and 260 mm Hg (loading direction) and then repeated in the downward direction (unloading direction). This was performed in baseline conditions and following contraction by α_1 adrenergic stimulation with phenylephrine or by depolarization with high extracellular K^+ in aortas of young (5 months), aged (26 months) mice, and in segments treated with elastase.

Results: In baseline conditions, diastolic/systolic diameters and compliance for a pulse pressure of 40 mm Hg were larger at any given pressure upon unloading (decreasing pressure) than loading (increasing pressure) of the aortic segments. The pressure-aortic stiffness (E_p) relationship was similar in the loading and unloading directions, and aortic hysteresis was absent. On the other hand, hysteresis was evident after activation of the VSMCs with the α_1 adrenergic agonist phenylephrine and with depolarization by high extracellular K^+, especially after inhibition of basal NO release with L-NAME. Aortic stiffness was significantly smaller in the unloading than in the loading direction. In comparison with young mice, old-mouse aortic segments also displayed contraction-dependent aortic hysteresis, but hysteresis was shifted to a lower pressure range.

Elastase-treated segments showed higher stiffness upon unloading over nearly the whole pressure range.

Conclusions: Mouse aortic segments display pressure- and contraction-dependent diameter, compliance, and stiffness hysteresis phenomena, which are modulated by age and VSMC-extracellular matrix interactions. This may have implications for aortic biomechanics in pathophysiological conditions and aging.

Keywords: aortic stiffness, aging, pressure-dependent hysteresis, viscosity, constriction

INTRODUCTION

When the left ventricle of the heart ejects its blood into the circulation, the aorta undergoes large deformations to buffer the volume of the ejected blood. Thereby, the aorta acts as an elastic reservoir to store energy when dilating and to release this energy by elastic recoil during diastole. Evolution designed the aorta to optimize this heart-vessel coupling. The highest relative elastin content in the vascular tree is found in the blood vessels closer to the heart. These elastic arteries are characterized by stress-strain relationships with stress only gradually increasing with elevated pressure in the low pressure range (Armentano et al., 1995; Jesudason et al., 2007; Ratz, 2016). Although the relative VSMC content of the thoracic aorta is lower compared with any other part of the arterial tree, VSMCs are still the predominant cell type in the aortic wall thoracic aorta (Dinardo et al., 2014) and may play a determinant role in biomechanical behavior of the aorta (Qiu et al., 2010; Min et al., 2012; Saphirstein et al., 2013; Leloup et al., 2019). The VSMCs in the aorta are embedded in a plexus of elastin, collagen, and proteoglycans. The orientation and the quantity of these extracellular matrix (ECM) components are responsible for the arterial passive mechanical properties and crucially determine the non-linear stretch-strain relationship of the aorta (Wagenseil and Mecham, 2009, 2012; Charalambous et al., 2017). With aging, the compliance of the aorta slowly decreases, and the pulse-dampening properties are attenuated. It has been described that besides passive adaptations of the vessel wall, involving changes in the extracellular matrix (ECM), also, the intrinsic mechanical properties of the vascular smooth muscle cells (VSMCs) contribute to increased vascular stiffness in aging. In this process, both β_1-integrin and α-smooth muscle actin are likely major players in the age-dependent stiffening of VSMC (Qiu et al., 2010; Gao et al., 2014).

Elastic arteries such as the aorta are, however, not purely elastic but also exhibit viscous behavior. At any given pressure, they display greater dimensions during unloading than during loading, which determines a hysteresis loop on the pressure/volume relationship, a process known for a long time (Remington, 1955; Bergel, 1961a,b). This means that, on a cardiac beat-by-beat scale, part of the energy stored by the arterial wall during dilation (diastole to systole) is dissipated within the arterial wall during recoil (systole to diastole) (Bauer et al., 1979; Busse et al., 1981; Barra et al., 1993; Armentano et al., 1995; Boutouyrie et al., 1997). The pulsatile flow of the heart transforms to a nearly continuous flow in the peripheral capillaries. An *in vivo* and *in vitro* study of rat abdominal aorta revealed that the arterial wall viscosity was strongly influenced by steady and pulsatile mechanical load, but not by smooth muscle tone (Boutouyrie et al., 1998). Using cellular micro-biaxial stretching microscopy, Win et al. (2018) found that large-strain anisotropic stress caused hysteresis of individual VSMCs. This hysteresis was strongly dependent on load orientation and actin organization. When stretched along the primary fiber alignment, VSMCs exhibited hysteresis with unloading stresses smaller than loading stresses, while stretch in the transverse direction led to reverse hysteresis.

Arterial stiffness is inherently coupled to blood pressure, complicating the interpretation of arterial stiffness measurements in the *in vivo* situation. *In vivo*, acute manipulation (pharmacological or mechanical) of arterial pressure allows to compare arterial stiffness at the same level of pressure and to investigate the pressure sensitivity of arterial stiffness (Butlin et al., 2020). As far as we know, an *ex vivo* stiffness-pressure relationship, comparing isobaric aortic stiffness while increasing and decreasing pressure (as performed in *in vivo* studies), has never been studied before. In the present study, isolated mouse aortic segments were cyclically stretched in a highly controllable extracellular environment and at high frequency (10 Hz) to simulate the physiological heart rate in mice with the Rodent Oscillatory Tension Set-up to study Arterial Compliance (ROTSAC), an in-house-developed setup to study biomechanical properties of *ex vivo* intact aortic rings (Leloup et al., 2016). We did not intend to study classical hysteresis phenomena as observed in the beat-to-beat aortic diameter or lumen cross-sectional area-pressure relationship but aimed to study hysteresis phenomena in aortic compliance or stiffness pressure relationships when slower stepwise pressurization/depressurization was superimposed to the cyclic pulsation of the segments. Thereby, we hypothesized that VSMC contraction, mouse age, and extracellular matrix affected the pressure-stiffness relationship differently in the pressurization vs. depressurization direction in *ex vivo* mouse aortic segments.

Abbreviations: VSMC, vascular smooth muscle cell; ECM, extracellular matrix; ROTSAC, Rodent Oscillatory Set-up for Arterial Compliance; W, width of the aortic segment (as mounted in the ROTSAC set-p); D, calculated diameter; L, length of the aortic segment; E_p, Peterson elastic modulus; PP, pulse pressure; PE, phenylephrine; L-NAME, 300-μM NΩ-nitro-l-arginine methyl ester; RM ANOVA, repeated measures ANOVA.

METHODS AND MATERIALS

Animals

All animals were bred and housed in the University of Antwerp animal facility in standard cages with 12/12-h light-dark cycles,

with free access to regular chow and tap water. This study was approved by the Ethical Committee of the University of Antwerp (ECD2017-11), and all experiments were performed conforming to the Guide for the Care and Use of Laboratory Animals, published by the US National Institutes of Health (NIH Publication No. 85–23, revised 1996). The following C57Bl/6 (original substrain C57Bl/6JRj, Janvier Labs, France) male mouse animal groups were used: group 1, 4 to 7 months of age (n = 7, 5.8 ± 1.3 months), group 2, 5 months of age (n = 8, further named young, 5. ± 0.1 months), group 3, 26 months of age (n = 5, further named old, 26. ± 0.2 months), and group 4, 6 months of age (n = 5, further named elastase group, 6. ± 0.1 months). Comparisons between groups of mice only occurred between groups 2 and 3 mice. Both groups contained initially eight mice. Sample size was determined *a priori* with a statistical power of 90%, an effect size of 20% (pairwise comparison), and a coefficient of variation of 20%. The family-wise type I error was controlled at 5%. These figures (spread and effect size) were derived from historical data available at the lab. The study ended with unequal group sizes, because, in the aged group, three mice died before the *ex vivo* experiments started.

Aortic Tissue Preparation

Mice were euthanized by perforating the diaphragm while under deep anesthesia [sodium pentobarbital (Sanofi, Belgium), 250 mg kg-1, intraperitoneal]. The thoracic aorta was carefully removed and stripped of adherent tissue. Starting a ∼2 mm distally from the aortic arch, the descending aorta was cut into four segments of 2-mm length and immersed in Krebs Ringer (KR) solution (37°C, 95% O_2/5% CO_2, pH 7.4) containing (in mM): NaCl 118, KCl 4.7, $CaCl_2$ 2.5, KH_2PO_4 1.2, $MgSO_4$ 1.2, $NaHCO_3$ 25, CaEDTA 0.025, and glucose 11.1.

Rodent Oscillatory Set-Up for Arterial Compliance

Aortic segments were mounted between two parallel wire hooks in 10-ml organ baths. Force and displacement of the upper hook were measured and acquired at 0.4 kHz with a force-length transducer connected to a data acquisition system (Powerlab 8/30 and LabChart 8, ADInstruments). Because the segment is stretched between the two hooks, the extrapolated diameter of the vessel segment (D) at a given preload had to be derived from the displacement of the upper hook, being directly proportional to the inner circumference (**Figure 1**): $D = 2^* \frac{w}{\pi}$ with w (width) being the outer distance between the hooks (to approximate the inner circumference of the vessel segment) (see **Figure 1A**, 10 mN). Before each experiment, width (w) and length (l) were determined at six different preloads (10, 20, 30, 40, 50, and 60 mN), using a stereomicroscope and calibrated image software (**Figure 1**). To correct for the decrease in segment length with increased width and/or diameter (**Figure 1B**), the average length of the segment at each cycle (100 ms) was continuously derived from the diameter (D)-length (l) relationship using basic linear regression (**Figure 1C**).

To estimate the transmural pressure that would exist in the equilibrated vessel segment with the given distension force and dimensions, the following relationship was used: $P = \frac{F}{l^*D}$ with F being the force (preload); l, the length as derived from the linear regression in **Figure 1B** (∼2 mm); and D, the diameter of the vessel segment as derived from the displacement of the upper hook. Force was measured directly by the transducer. To simulate cyclic stretch of the segment between two theoretical transmural pressure levels, the preload was adjusted until the desired estimated diastolic and systolic pressure. Although we did not directly measure pressure in the ROTSAC setup but used diastolic and systolic preloads to calculate extrapolated pressures, we decided to use the term "pressure" to indicate "pressure equivalent load". At all pressures, a stretch amplitude corresponding to 40 mmHg was chosen to allow calculation of compliance and Peterson modulus. Compliance (C) was calculated as follows: $C = \frac{\Delta D}{\Delta P}$ with ΔD being the difference between systolic and diastolic diameter and ΔP being the pressure difference (i.e., 40 mm Hg). The Peterson modulus of elasticity (E_p) is a frequently used, vessel-size-independent measure of arterial stiffness (Gosling and Budge, 2003) and was calculated as follows: $E_p = D_0 * \frac{\Delta P}{\Delta D}$ with D_0 being the diastolic diameter. During all the experiments, the segments were continuously stretched directly after mounting them in the organ bath with a frequency of 10 Hz to mimic the physiological heart rate in mice (600 bpm) and at an estimated physiological pressure (diastolic 80-systolic 120 mmHg). At ∼60 min after isolation of the aorta from the animal, the experiments could be started.

Experimental Protocols

Our setup allows studying aortic stiffness in "isobaric" conditions when pressure is built up, which we have defined as the "loading" protocol or when pressure is released, which we have defined as the "unloading" protocol. These protocols were performed in various experimental conditions. By superimposing the slower loading/unloading protocols on top of the cyclic pulsation, we were able to continuously measure E_p, as a measure of aortic stiffness, at all applied pressure steps and in any experimental condition. In the present study, all measurements were performed over a broad pressure range (example of the loading/unloading protocols in **Figure 2**). The stretch amplitude always corresponded to 40 mmHg over the entire pressure range, which means that segment compliance had the same pressure dependency as diameter change but 40 times smaller. It took ∼5 min to acquire measurements over the entire pressure range (pressure up direction, loading), and, again, 5 min to return from the highest pressure back to the low pressure (40–80 mm Hg, pressure down direction, unloading). As mentioned before, at any given pressure, diameter-pressure (preload) loops as shown in **Figures 2B–D** could be determined. It is evident that the slope of the loop decreased considerably with higher pressure (right vs. left part of **Figure 2B**), with the addition of 2 μM PE in the presence of L-NAME (**Figure 2C**) and with the digestion of elastin with elastase (**Figure 2D**). This is reflected by the higher E_p values as indicated in each figure. Since diameter loops for single stretch cycles were not the topic of this research, the present study focused on the diastolic and systolic diameters, compliance, and stiffness parameter, E_p, along the entire pressure range during loading and unloading protocols (**Figure 2A**). At each pressure range, starting at 40–80 mm Hg and ending at

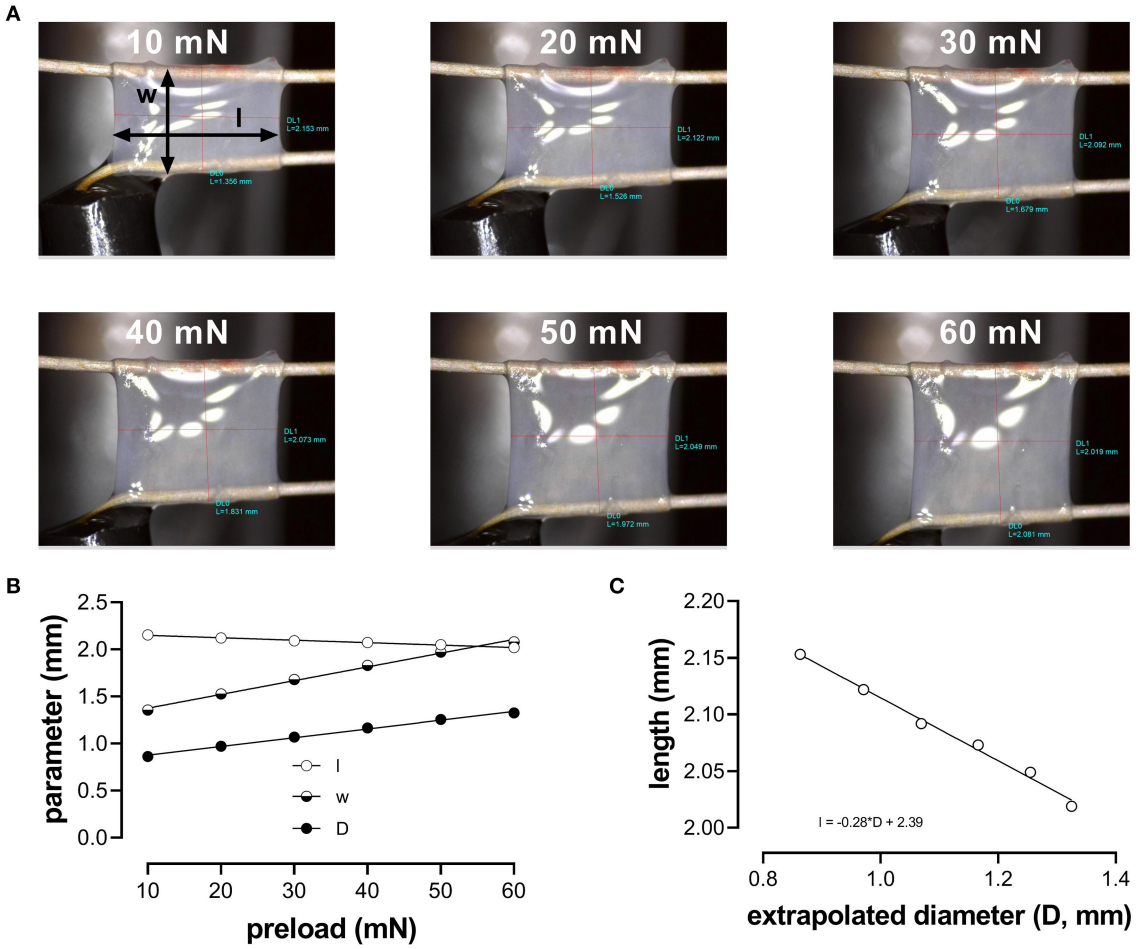

FIGURE 1 | Determination of the aortic segment extrapolated length and diameter. **(A)** Images of the aortic vessel segment at six different preloads between 10 and 60 mN; **(B)** length (l), width (w), and extrapolated diameter (D) as a function of preload; **(C)** relationship between length and extrapolated diameter (to obtain length at each calculated diameter to measure pressure).

200–240 mm Hg, diastolic/systolic diameters, compliance, and E_p were measured as the median value for the last 20–30 cycles before increasing or decreasing to the next pressure range.

Experimental Conditions

Group 1 mice: aortic segments (four per mouse) were subjected to cyclic stretch at increasing and decreasing pressure in KR solution. Because the effect of L-NAME was irreversible, subsequently, two segments were treated with 300-μM NΩ-nitro-l-arginine methyl ester (L-NAME) (Sigma-Aldrich, Belgium) to inhibit endothelial nitric oxide synthase (eNOS), followed by the loading/unloading protocols, and two segments did not receive L-NAME. Then, all segments received 2 μM PE, and the loading/unloading protocols were repeated. Since, in the experiments of group 1 mice, two segments received the same protocol, the mean of the data of the two segments was considered for further evaluation.

Groups 2 and 3 mice: aortic segments followed the same protocol as group 1 mouse segments. Young (group 2) and old (group 3) mouse aortic segments were studied separately but received the same experimental protocol. In the last loading/unloading protocol, two segments (one with and one without L-NAME) received 2 μM PE, and the other two segments (again one with and one without L-NAME) received the high extracellular (50 mM) K^+ concentration.

Group 4 mice: the loading/unloading protocol was applied to aortic segments in KR for all segments in the presence of L-NAME, after contraction with 2 μM PE, following the addition of 0.05 units elastase (ROTSAC 1), 0.1 units/ml elastase (ROTSAC 2), 0.1 mg/ml collagenase (ROTSAC 3), and 0.2 mg/ml collagenase (ROTSAC 4), and, finally, following the addition of 2 μM PE to all organ chambers. Only results for 0.1 units/ml elastase are shown in the present study. The data for 0.05 units/ml elastase and the data for collagenase showed effects on the E_p-pressure relationships, which were dependent on the enzyme activity and which will be the subject of a follow-up submission.

After each pressure curve, the organ chambers were thoroughly flushed with fresh KR solution. To obtain the 50-mM

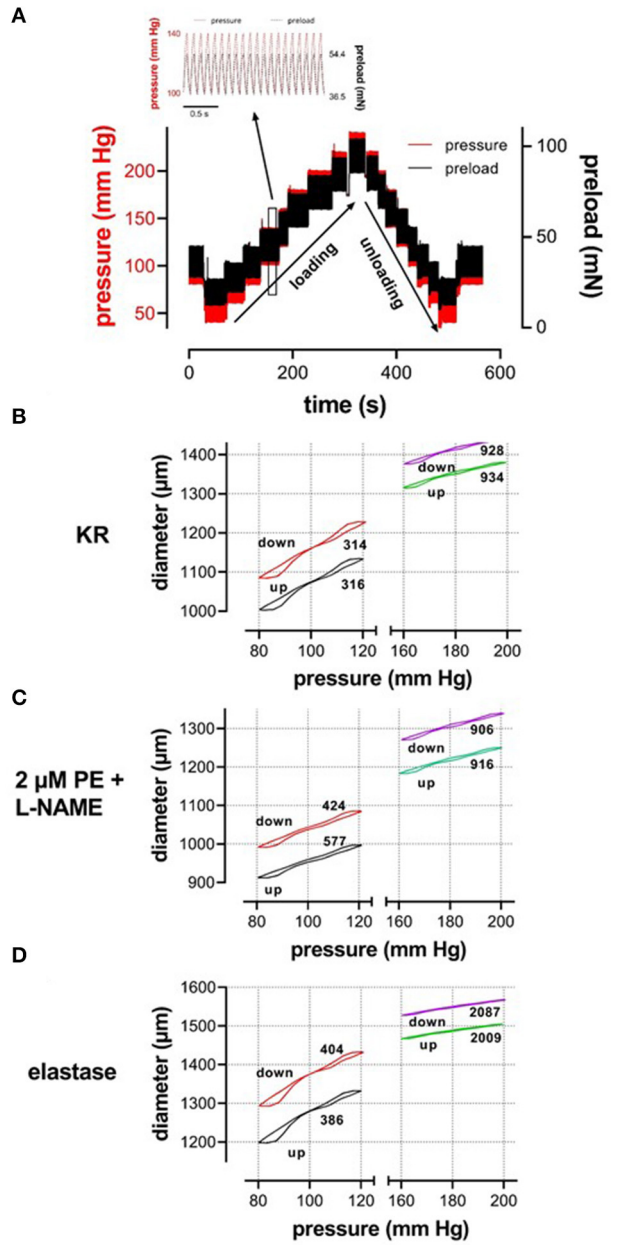

FIGURE 2 | (A) Test protocol applied to ROTSAC 1 to measure diameter, compliance, and Peterson modulus, E_p. Starting at diastolic and systolic preloads, according to 80 and 120 mm Hg, the preloads were adapted to obtain diastolic and systolic pressures of 40 and 80 mm Hg and subsequently increased by 20 mm Hg up to 200–240 mm Hg or higher (loading). Thereafter, the pressure was decreased back to 40–80 mm Hg (unloading) and, finally, to 80–120 mm Hg. In the insert, preload and calculated pressure are shown during the clamp of the segment at 10 Hz between 100 mm Hg (36.5 mN) and 140 mm Hg (54.4 mN). Similar protocols were applied to ROTSAC 2, 3, and 4 with the same pressure steps but other preloads. **(B–D)** Illustrate stretch-by-stretch diameter-pressure loops at 80–120 (black, red) and 160–200 (green, purple) during loading (up, black, green) and unloading (down, red, purple) in three experimental conditions: Krebs-Ringer (KR, **B**), 2 µM PE + 300-µM L-NAME **(C)**, and 0.1 mg/ml elastase **(D)**. The left y-axis refers to diastolic and systolic diameters at 80–120 mm Hg and the right axis to these parameters at 160–200 mm Hg. The y-axis scale is the same in all figures. The numbers along each loop indicate the E_p value in mm Hg.

K^+ solution, Na^+ in the KR solution was isosmotically replaced by K^+. All loading/unloading protocols and measurements were done on "steady state" contractions, achieved 30 min after the addition of PE or high K^+ to the organ chamber (Fransen et al., 2015). Because the present study was mainly interested in the role of smooth muscle cells in modulating stiffness, we mainly focused on segments in which basal NO release was inhibited by L-NAME and which can be considered as the control (KR) E_p-pressure relationship. Although E_p at 80–120 mm Hg was 299 ± 4 mm Hg and significantly rose to 328 ± 8 mm Hg ($n = 8$, $p < 0.05$) after the addition of 300 µM L-NAME, E_p pressure relationships were not statistically different between KR and KR + L-NAME (see **Supplementary Figure 1**).

Elastase (Elastase suspension, 26. mg P/ml, activity: 4.81 units/mg, Worthington, OH, USA) and collagenase (Collagenase type 2,310 units/mg, Worthington, OH, USA) were applied to the organ chambers for 30 min, while segments were stretched between 80 and 120 mm Hg. Then, the segments were washed three times with KR solution until the diameter change induced by elastase or collagenase was in steady state; after which, the experiment was continued.

Statistical Analyses

All results are expressed as the mean ± SEM, with *n* representing the number of mice, and analyses were performed using Prism 9.0 (GraphPad Software, La Jolla, CA, USA). The effects of VSMC contraction, pressure, and age on the measured vessel parameters were assessed using a repeated measures (RM) two-way or a three-way ANOVA, if appropriate. Sidak's *post-hoc* test was used to correct for multiple comparisons. Multiplicity-adjusted (when appropriate) *p*-values are reported in the figures and figure legends, a (family-wise) significance level of 5% was selected.

RESULTS

Diastolic and Systolic Diameter, Aortic Compliance, and Stiffness Are Pressure and Contraction Dependent

When repetitively stretched between 80 and 120 mm Hg, aortic segments of group 1 mice ($n = 7$) were stretched by 11 ± 0.2% and stretch slope of 2.38 ± 0.003 µm/mm Hg ($n = 7$), which is in accordance with normal stretch of 10% in the human aorta [13, 14]. As expected, extrapolated and calculated diastolic and systolic diameters were strongly dependent on the distension pressure. In baseline conditions after inhibition of basal NO release with 300 µM L-NAME (**Figures 3A,C,E,G**), the diastolic and systolic diameters of the aortic diameters increased with pressure. Diameters increased with pressure starting at 40–80 mm Hg up to 240–280 mm Hg (up) until a "maximum" diameter was attained of 1.36 ± 0.07 mm ($n = 7$) for diastolic pressure at 220 mm Hg and 1.39 ± 0.07 mm ($n = 7$) for systolic pressure at 260 mm Hg. Upon lowering diastolic and systolic pressure back down to 40–80 mm Hg (down, unloading), both diastolic and systolic diameters decreased but were significantly larger than during the pressure increase, indicating hysteresis. Diameter change between diastolic and systolic pressure divided

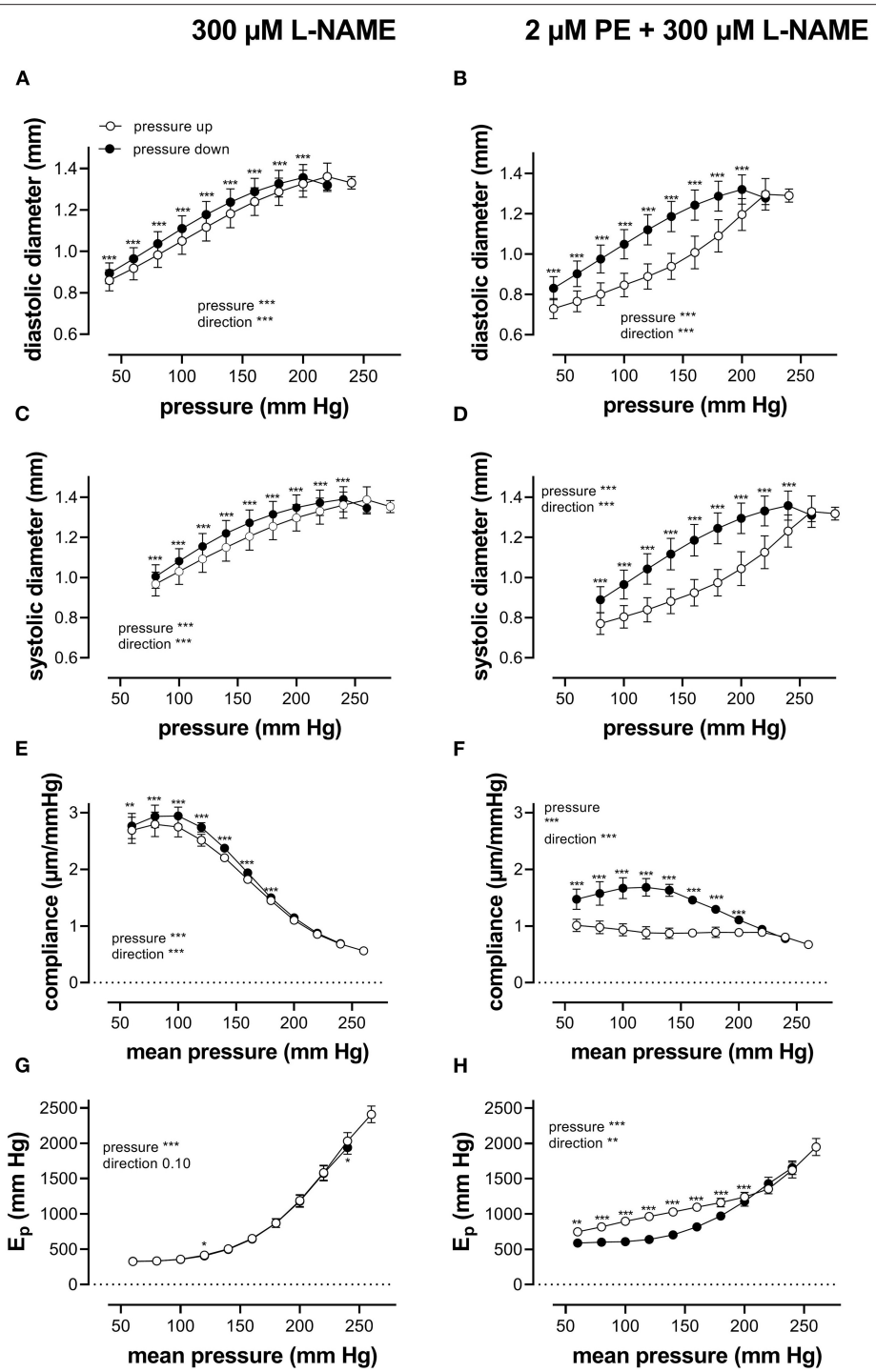

FIGURE 3 | Aortic segments displayed considerable pressure- and contraction-dependent hysteresis. Aortic segments were treated with 300-µM L-NAME in the absence **(A,C,E,G)** and presence **(B,D,F,H)** of 2 µM PE and subjected to cyclic stretch with an amplitude of 40 mm Hg, ranging from 40–80 mm Hg to 240–280 mm Hg (upward direction, open symbols, up) and back to 40–80 mm Hg (downward direction, closed symbols, down). Diastolic and systolic diameters **(A–D)**, compliance **(E,F)**, and Peterson's elastic modulus (E_p, **G,H**) were determined in aortic segments of 7 C57Bl6 mice (data points ± SEM). Data points for the upward pressure steps (open symbols, up) were compared at any given pressure with data points for the downward pressure steps (closed symbols, down) with two-way RM ANOVA with Sidak's multiple comparison test. $^*p < 0.05$, $^{**}p < 0.01$, and $^{***}p < 0.001$.

by the pulse pressure (40 mm Hg) revealed the compliance (in μm/mm Hg) (**Figure 3E**). Compliance measured during loading was significantly lower than for unloading in the pressure range below 160 mm Hg (140–180 mm Hg) but was similar for higher pressures. Finally, the aortic stiffness parameter, E_p, did not show significant hysteresis in baseline conditions (**Figure 3G**), and, at any given pressure, E_p, upon loading, was not different from E_p upon unloading.

Diameters, compliance, and Peterson modulus, E_p, were also determined in the presence of 2 μM PE at gradually increasing and decreasing pressures (**Figures 3B,D,F,H**) and the following depolarization with 50-mM extracellular K^+ (data not shown). After the addition of 2 μM PE in the presence of L-NAME, hysteresis was considerably increased for all parameters. As expected, diastolic and systolic diameters decrease with the addition of PE and after attaining maximal values of 1.30 ± 0.08 mm and 1.33 ± 0.08 mm ($n = 6$) at 240 and 280 mm Hg, respectively, diameters for the downward pressure steps were, at any given pressure, significantly increased when compared with the upward pressure steps (**Figures 3B,D**). Compliance (**Figure 3F**) was nearly three times lower when compared with control conditions (**Figure 3E**) and was almost pressure-independent for the upward pressure steps. Unloading resulted in clear pressure dependency but was not different from loading compliance for pressures above 220 mm Hg. Similar observations apply for E_p with significantly lower E_p values at any pressure below 220 mm Hg during unloading. We defined these lower stiffness values as "de-stiffening" of the aortic segments for the downward pressure steps below 220 mm Hg (**Figure 3H**). For depolarization with 50 mM K^+, similar results were obtained (see also **Figure 6**). Finally, it should be mentioned that when segments in the presence of PE and L-NAME were stretched at 80–120 mm Hg after the pressure protocol, it took about 20 to 30 min to attain E_p values comparable with E_p before the pressure protocol (see **Supplementary Figure 2**). Only after this "recovery" or "re-stiffening" period, another experimental protocol could be performed. These data suggest that the contractile state of vascular smooth muscle cells determines the hysteresis phenomena described in **Figure 3** and that at any given pressure, stiffness in unloading conditions is lower than stiffness in loading conditions, which we called de-stiffening.

Age and Contractile Stimulus Affect Aortic Stiffness

Pressure- and contraction-dependent hysteresis, as described above, was further studied in aortic segments of young (5 months, group 2, $n = 8$) and old (26 months, group 3, $n = 5$) mice. Contraction was not only induced by α_1-adrenergic stimulation with 2 μM PE but also by receptor-independent depolarization by 50 mM K^+ in the absence and presence of 300-μM L-NAME to inhibit basal endothelial NO release. **Figure 4** compares the effects of 2 μM PE and 50 mM K^+ before and after inhibition of basal NO release with 300-μM L-NAME in aortic segments of 5- and 26-month-old mice mounted in static, isometric conditions (100 mm Hg, **Figure 4A**) and dynamic, isobaric conditions (80–120 mm Hg, **Figure 4B**). The figure shows that maximal isometric force was higher after depolarization than following α_1 adrenoceptor stimulation, especially in aged mice but was not significantly age-dependent. In isobaric conditions, aortic stiffness was significantly increased by addition of L-NAME for PE-induced E_p increase in young animals. In the presence of L-NAME, E_p increased more after α_1 adrenoceptor stimulation than following depolarization with high K^+ in aged animals. Also, here, there was no significant age-dependent effect.

Pressure-Dependent Hysteresis Is Contraction- and Age-Dependent

Figures 5, **6** show E_p values for up- and downward pressure steps in the presence of 2 μM PE and 50 mM K^+ in the absence and presence of 300-μM L-NAME for aortic segments of young and old mice. E_p in control conditions (KR) was age- and pressure-dependent (**Figures 5**, **6A**) with significantly higher stiffness at elevated distension pressure for aortic segments of old mice. This age-dependent difference in aortic stiffness remained, following stimulating contraction with 2 μM PE or 50 mM K^+ in the absence (**Figures 5B**, **6B**) or presence (**Figures 5C**, **6C**) of L-NAME. Both contractile stimuli increase E_p at low and decrease E_p at high-distension pressures, especially in aortic segments of young mice. By subtracting the E_p values for the downward pressure steps from E_p values for the corresponding upward pressure steps, hysteresis is visualized as a pressure-dependent difference in E_p (ΔEp, **Figures 5D–F**, **6D–F**) with negative values corresponding to lower stiffness or "de-stiffening." In the absence of contractile stimuli, hysteresis was nearly absent. Following contraction of the aortic segments, hysteresis led to lower stiffness (negative values for △Ep) along the whole pressure range for aortic segments of young mice and was more evident in the absence of basal NO release (presence of 300-μM L-NAME) (**Figures 5F**, **6F**). In aortic segments of old mice, hysteresis in contracted segments was smaller for both contractile stimuli. Moreover, in these segments, lower stiffness in the pressure range from 40–80 up to 160–200 mm Hg turned to higher stiffness in the pressure range above 160–200 mm Hg.

In **Figure 7**, which reflects the same data as in **Figures 5**, **6**, hysteresis in young and old mice is compared for maximal contractions (NO release inhibited with L-NAME) induced by depolarization and α_1-adrenergic stimulation.

In young animals, hysteresis induced by contraction with PE or depolarization resulted in lower stiffness upon unloading along the whole pressure range up to 200 mm Hg, whereas, in old mice, hysteresis changed from lower to higher stiffness upon unloading at pressures above 160 mm Hg. Hysteresis by depolarization was significantly smaller in magnitude than hysteresis by PE, especially in the lower pressure range and for old animals.

Elastase Attenuates Pressure- and Contraction-Dependent Hysteresis

Because one of the characteristics of vascular aging is the age-dependent breakdown of elastin, aortic segments of group 4 mice were treated with 0.1 unit/ml elastase. In baseline conditions, the breakdown of elastin caused a significant increase of diastolic

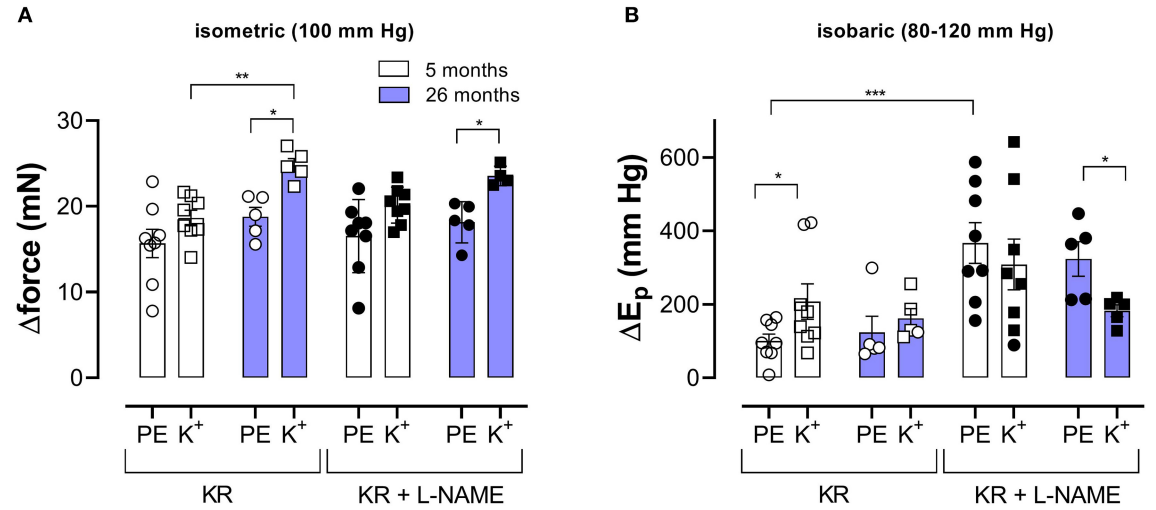

FIGURE 4 | α_1-Adrenergic stimulation and maximal depolarization of aortic segments cause different isometric and isobaric effects. Aortic segments were mounted in isometric (100 mm Hg, **A**) and isobaric (80–120 mm Hg, **B**) conditions and treated with 2 μM PE (circles) or depolarized with 50 mM K^+ (squares) in the absence (open symbols) and presence (closed symbols) of 300-μM L-NAME. The increase of force (Δorce) and E_p (ΔE_p) was determined in aortic segments of 5 (white bars) and 26 (blue bars) months old mice. Two-way RM ANOVA with Sidak's multiple comparison test. $^*p < 0.05$, $^{**}p < 0.01$, and $^{***}p < 0.001$.

and systolic diameters (**Figures 8A,B**), especially at physiological pressures. It is evident that at, high-distension pressure, diastolic and systolic diameters, after elastase treatment, are nearly the same. Hence, the compliance, which is defined as the change of diameter per mm Hg distension pressure, is approaching zero at high pressures (**Figure 8C**). At very low pressure (<100 mm Hg), compliance was higher than in control conditions and rapidly fell to below control levels at pressures above 100 mm Hg. Elastase-treated aortas were significantly stiffer than control aortas at pressures above 140 mm Hg (**Figure 8D**).

Diameters, compliance, and E_p were determined also in the presence of 2 μM PE and 300-μM L-NAME. To reveal the effects of PE in the absence and presence of elastase, the difference between the biomechanical parameters in the absence and presence of PE is displayed in **Figure 9**. In the absence of elastase, PE caused, as expected, decrease of diastolic and systolic diameters, reduced compliance, and elevated aortic stiffness. All these parameters were pressure-dependent, and PE was less effective at high-distension pressures (Leloup et al., 2019), and the pressure at which the PE effect caused higher compliance and lower E_p was ∼180–200 mm Hg. After degradation of elastin with elastase, all effects of PE were significantly attenuated in the physiological pressure range (decreased diameters and compliance, increased E_p). Furthermore, in the elastase-treated segments, the pressure at which the PE-induced decrease of compliance and increase of E_p changed a sign (higher compliance and lower E_p) and shifted to lower pressures by ±50 mm Hg.

Finally, pressure-dependent hysteresis was studied in the absence/presence of 2 μM PE and 300-μM L-NAME and absence /presence of elastase. The Δdiameter, Δcompliance, and ΔE_p values between upward and downward pressure steps at any given pressure (Δparameter by hysteresis) are shown in **Figure 10**. In the absence of contraction, hysteresis was only evident for diameters and compliance, but not for E_p. Elastase treatment was ineffective in affecting hysteresis for diameters, but compliance hysteresis was significantly attenuated at physiological pressures (**Figure 10E**). Hysteresis for all parameters was significantly intensified by contraction with PE in elastin-intact segments. Diameters and compliance were significantly increased for downward pressure steps, whereas segments were less stiff when the segments were unloaded at mean pressures below 160 mm Hg (**Figures 10B,D,F,H**). In segments treated with 0.1 unit/ml elastase, on the other hand, diameter and compliance hysteresis was reduced at pressures above 100 mm Hg. Hysteresis of aortic stiffness was completely reversed with higher stiffness at any given pressure upon unloading (positive ΔE_p values in **Figure 10H**).

DISCUSSION

The present study revealed that the ROTSAC equipment (Leloup et al., 2016) was suitable to study pressure dependency of arterial stiffness. The pressure-stiffness relationship of the present study displayed key features of anisotropic artery walls with non-linear behavior, being soft at low pressure and increasing stiffness at higher pressures. In this way, they perfectly resemble classical aortic stress-strain relationships (Hong et al., 2015). Moreover, the setup also allowed to study *ex vivo* viscoelastic properties and stiffness hysteresis of isolated mouse aortic segments. Indeed, dynamic testing of arterial stiffness, whether *in vivo* or *ex vivo*, should address viscoelasticity alongside the measurement of stiffness. *In vivo*, acute manipulation (pharmacological or mechanical) of arterial pressure allows to compare arterial stiffness at the same level of pressure in different animals and to investigate the pressure sensitivity of arterial stiffness (Butlin et al., 2020). For example, chronic hypertension has been

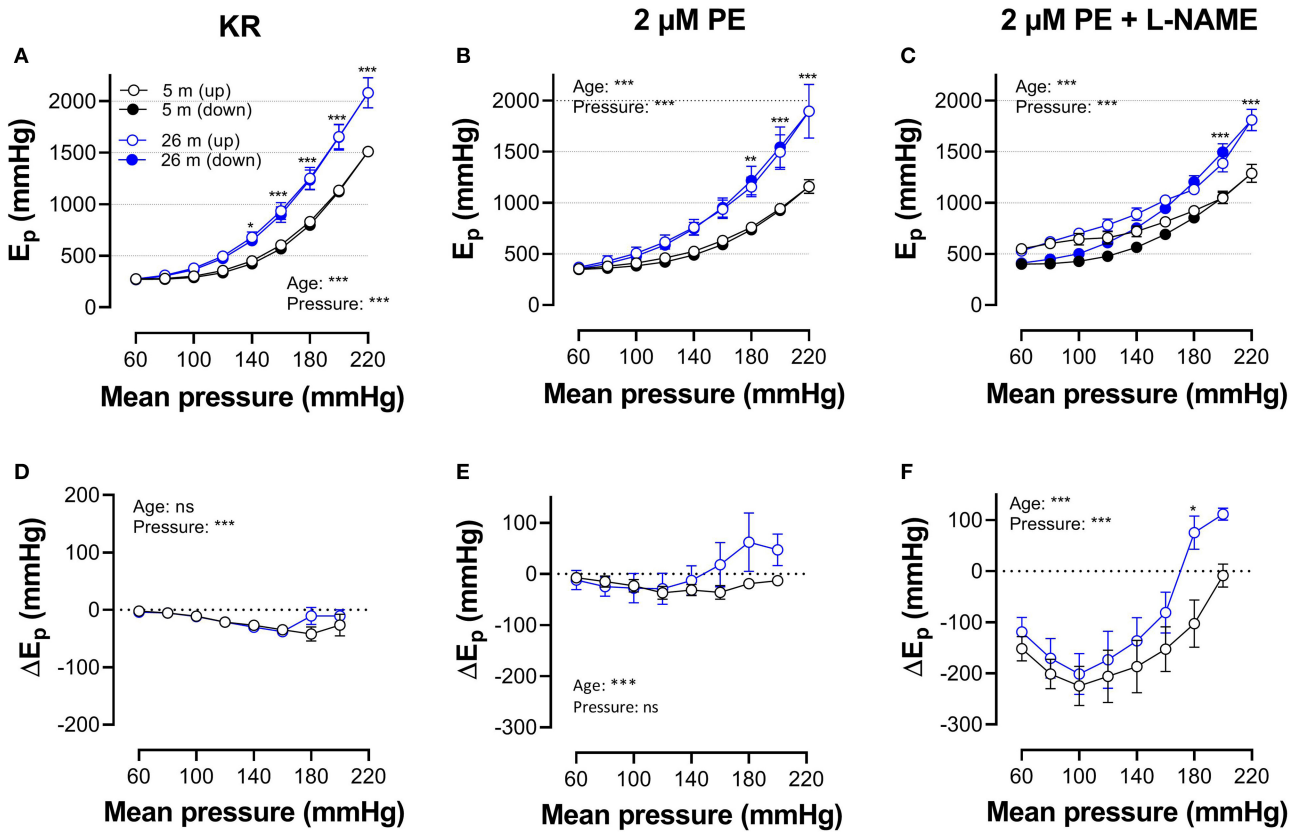

FIGURE 5 | Hysteresis is pressure, contraction and age dependent. Aortic segments of mice aged 5 months (black, $n = 8$) and 26 months (blue, $n = 5$) were subjected to upward (open symbols, up) and downward (closed symbols, down) pressure steps between 40 and 80 mm Hg to 200–240 mm Hg and back in control conditions (KR, **A,D**) in the presence of 2 µM PE **(B,E)** and 2 µM PE in the presence of 300-µM L-NAME to block endothelial NO release **(C,F)**. Absolute values of E_p are shown in **(A–C)**, whereas, in **(D–F)**, data points for the upward pressure steps (open symbols, up) were compared at any given pressure, with data points for the downward pressure steps (closed symbols, down) (stiffness hysteresis). Two-way RM ANOVA with Sidak's multiple comparison test, $^*p < 0.05$, $^{**}p < 0.01$, $^{***}p < 0.001$.

described to decrease the pressure sensitivity of arterial stiffness (Ng et al., 2012).

Aortic Stiffness Hysteresis

In the present study, the pressure-diameter relationship for a single-stretch cycle displayed hysteresis with smaller diameters upon increasing than upon decreasing stretch (**Figures 2B–D**). In general, it is assumed that cell stretch temporarily causes higher stress, followed by a return to the basal level. Hence, cyclic stretch is assumed to cause stress-strain hysteresis, with higher stresses during building up stretch than during subsequent stretch release. This has been demonstrated in numerous studies *in vivo* and *ex vivo* (Bauer et al., 1979; Langewouters et al., 1986; Armentano et al., 1995; Boutouyrie et al., 1997; Trepat et al., 2004) and illustrates the viscoelastic nature of blood vessels. The present study did not focus on hysteresis during a single-stretch cycle but investigated whether aortic stiffness also displayed hysteresis phenomena when segments were loaded and unloaded in a pressure range from 60 to 240 mm Hg, while subjected to continuous cyclic stretch with a constant PP of 40 mm Hg at high frequency. At increasing, and subsequently decreasing pressures, diastolic and systolic diameters, compliance, the aortic stiffness parameter, and Peterson's modulus or E_p were compared at any given pressure or mean pressure in the loading and unloading direction. In baseline conditions (KR), diastolic and systolic diameters and compliance for a pulse pressure of 40 mm Hg were smaller at any given pressure upon progressive loading of the segments than upon unloading. Stiffness hysteresis was, however, absent (**Figures 3A,C,E,G**), mainly because the diameter change in the loading and unloading direction was nearly the same. Hence, aortic stiffness gradually increases with pressure, but the pressure-stiffness relationship was similar in the loading (increasing pressure) and unloading (decreasing pressure) directions.

In general, it is assumed that the passive mechanical behavior of vascular walls is mainly governed by the extracellular matrix (collagen, elastic fibers, proteoglycans, and water), whereas the active mechanical contribution is due to the VSMCs (Holzapfel and Ogden, 2018; Butlin et al., 2020). The interactions between both in regulating aortic compliance are, however, complex

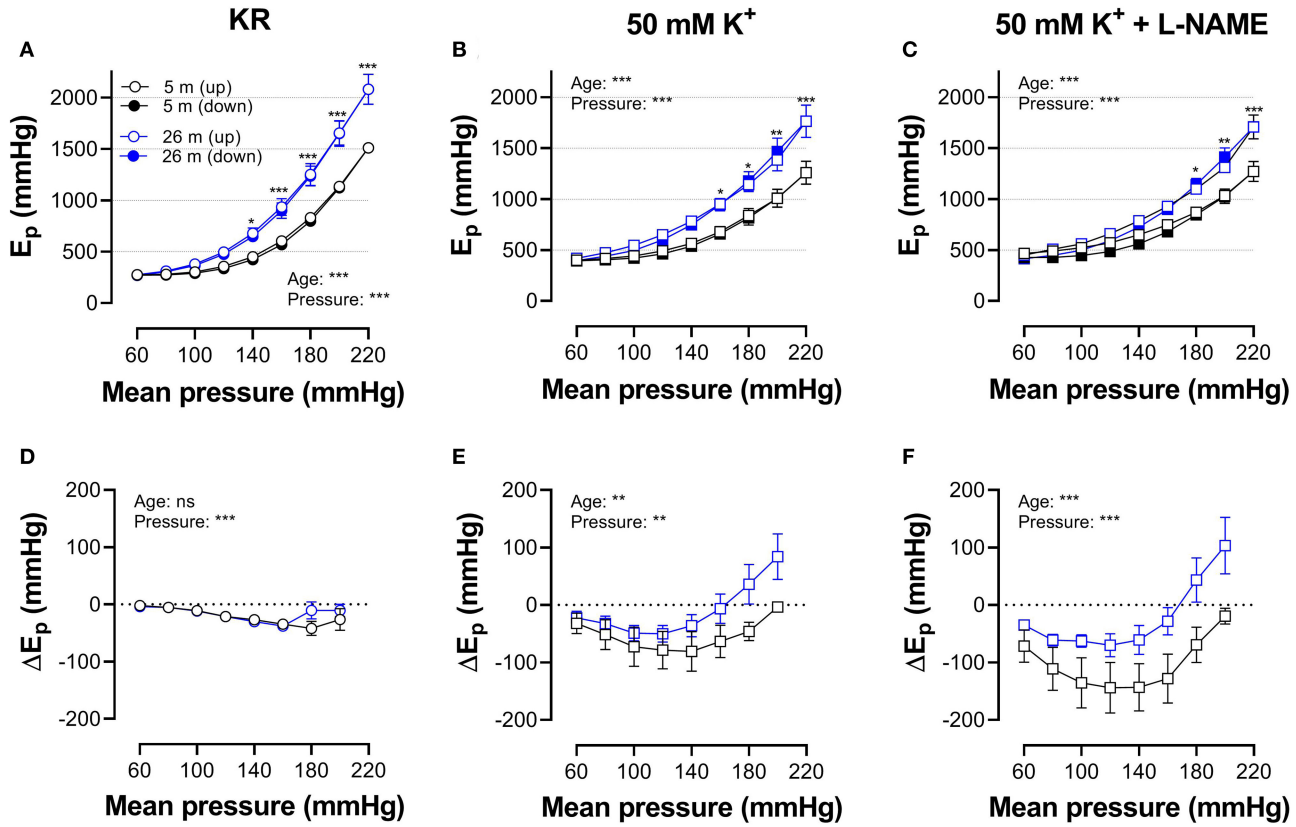

FIGURE 6 | Hysteresis is pressure, contraction, and age dependent. Aortic segments of mice aged 5 months (black, $n = 8$) and 26 months (blue, $n = 5$) were subjected to upward (open symbols, up) and downward (closed symbols, down) pressure steps between 40 and 80 mm Hg to 180–220 or 200–240 mm Hg and back in control conditions (KR, **A,D**) in the presence of 50 mM K^+ **(B,E)** and 50 mMK^+in the presence of 300-μM L-NAME to block endothelial NO release **(C,F)**. Absolute values of E_p are shown in **(A–C)**, whereas, in **(D–F)**, data points for the upward pressure steps (open symbols, up) were compared at any given pressure with data points for the downward pressure steps (closed symbols, down) (stiffness hysteresis). Two-way RM ANOVA with Sidak's multiple comparison test (old vs. young mice), $^*p < 0.05$, $^{**}p < 0.01$, $^{***}p < 0.001$.

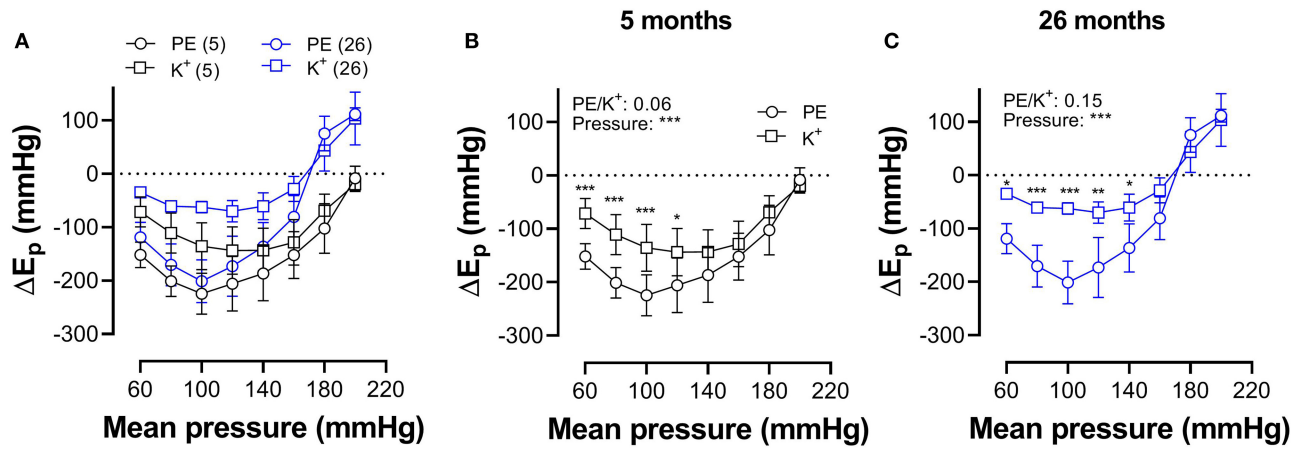

FIGURE 7 | Pressure-dependent hysteresis is affected by the contractile stimulus and by age. Data from **Figures 5F**, **6F** are combined in **Figure 6A** for mice of 5 months ($n = 8$, 5, black) and 26 months ($n = 5$, 26, blue). Contractions by 50 mM K^+ (squares) and 2 μM PE (circles) were elicited in the presence of L-NAME. Three-way ANOVA: pressure: ***; age 0.12; stimulus *; pressure/age: **; pressure/stimulus ***; age/stimulus 0.73. For clarity, **(A)** was repeated in **(B)** (for 5 months) and **(C)** (for 26 months). Two-way RM ANOVA with Sidak's multiple comparison test, $^*p < 0.05$, $^{**}p < 0.01$, $^{***}p < 0.001$.

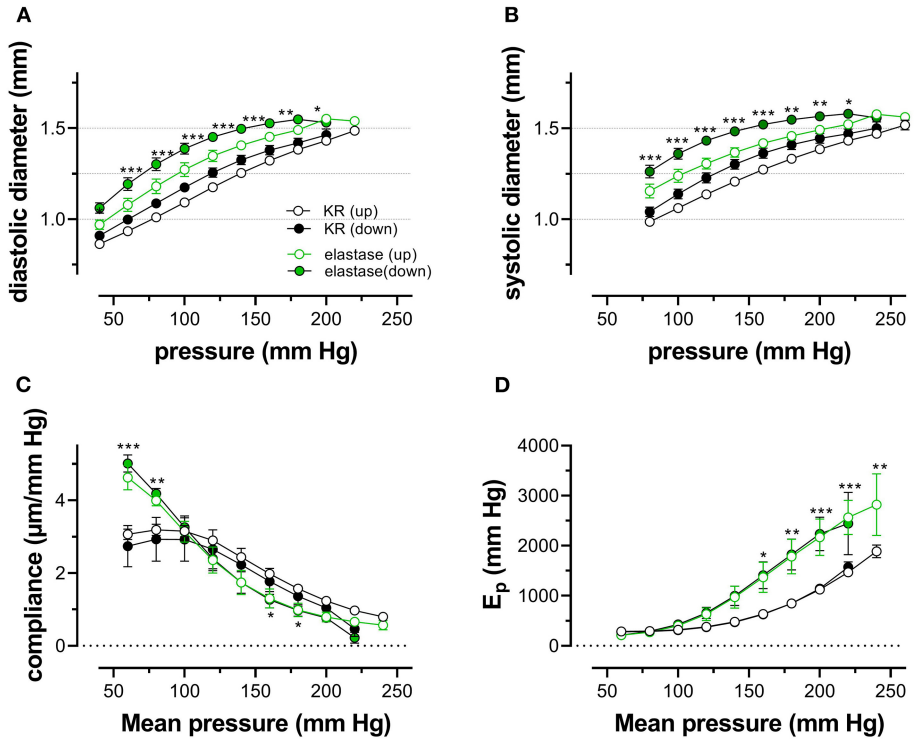

FIGURE 8 | Diastolic and systolic diameters, compliance, and stiffness are elastin dependent. Diastolic diameter **(A)**, systolic diameter **(B)**, compliance **(C)**, and Peterson modulus, E_p **(D)**, were measured in aortic segments in control conditions (black symbols) or after treatment with 0.1 unit/ml elastase (green symbols). Data points for the upward pressure steps (open symbols, up) were compared at any given pressure with data points for the downward pressure steps (closed symbols, down). Two-way RM ANOVA with Sidak's multiple comparison test (elastase vs. control), $^*p < 0.05$, $^{**}p < 0.01$, $^{***}p < 0.001$, $n = 5$.

and both are definitely crucial elements in the determination of arterial wall stiffness (Saphirstein et al., 2013; Hong et al., 2015; Lacolley et al., 2017). Elastic arteries, such as the aorta, are composed of alternating layers of smooth muscle and elastin-containing fibers. Elastin degradation with elastase caused prominent changes in the pressure-diameters, -compliance, and -stiffness relationships. Vessel diameters were significantly increased, compliance was larger at low pressure (60 mm Hg), but compromised at higher pressures, and E_p was significantly increased at pressures of 140 mm Hg. Similarly, the aorta of elastin heterozygous mice ($Eln^{+/-}$), in which about 60% of the normal elastin amount is present (Wagenseil and Mecham, 2009), is stiffer than the aorta of $Eln^{+/+}$ mice (Knutsen et al., 2018). The higher stiffness of $Eln^{+/-}$ or elastase-treated aortas is believed to be due to the redistribution of tensile force to the stiffer collagen. Because aging is accompanied by a gradual increase of elastin breaks and loss of elasticity, this process is also believed to be at the base of progressive arterial stiffening during aging. Also, the present study showed that, in comparison with "young" mice (5 months), aortic segments of old mice (26 months) displayed higher E_p values and aortic stiffness at mean pressures above 100 mm Hg.

Aortic Stiffness Hysteresis Modulation

The presence of a considerable amount of VSMCs in the aorta means that, by generating contractile force, they obviously contribute significantly to the material behavior of the artery wall (Qiu et al., 2010; Poythress et al., 2013; Saphirstein et al., 2013; Gao et al., 2014; Hong et al., 2015; Zhang et al., 2016). Aortic VSMC function can be significantly altered by cyclic stretch (Leloup et al., 2017), and, when subjected to high-frequency (10 Hz) stretch of about 10% in baseline conditions, it is expected that the ECM, together with actomyosin contraction and cytoskeletal remodeling, may produce viscoelastic-like stress relaxation and hysteresis. Thereby, it is assumed that VSMC may contribute markedly to different hysteresis behaviors under different loading regimes (Win et al., 2018).

In the presence of PE and L-NAME, aortic stiffness was almost independent of pressure when pressure was built up [compared with the reduced pressure-sensitivity of stiffness in hypertensive animals (Ng et al., 2012)]. Release of pressure reintroduced "control-like" pressure dependency with maximal compliance again in the physiological pressure range. When compared with baseline conditions, PE caused aortic stiffening in the pressure range between 60 and 180 mm Hg, but, at the highest pressure, stiffness was reduced (**Figure 5**). This has been explained by a shift in the load-bearing component from collagen at high pressures to the contractile VSMCs at lower pressures (Leloup et al., 2019). In the present study, pressure-induced hysteresis was dependent on the contractile state of the aortic VSMCs. In comparison with baseline conditions, contraction of the aortic VSMCs with α_1 adrenergic stimulation or with depolarization

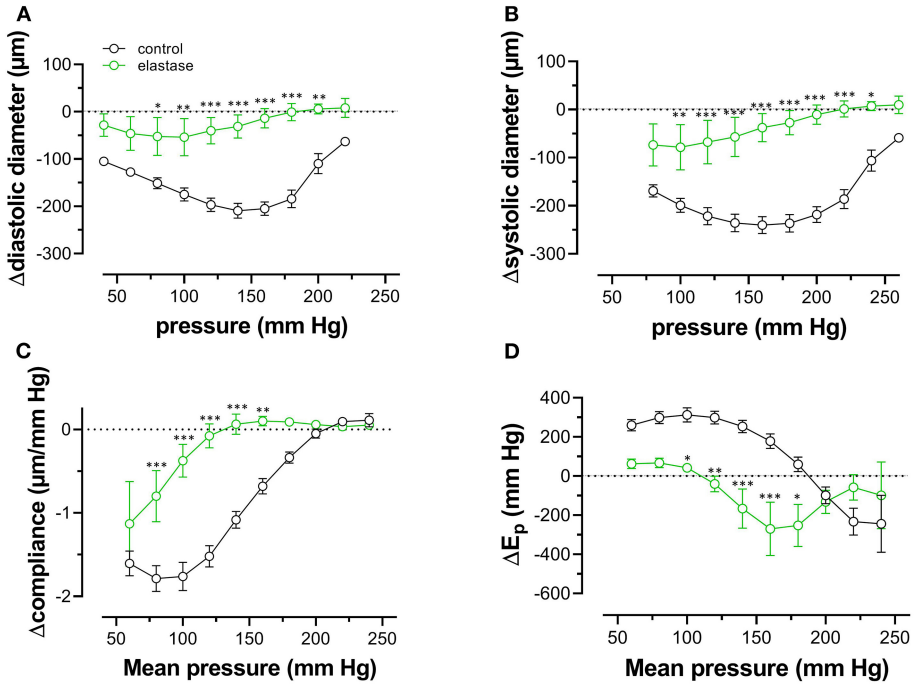

FIGURE 9 | Diastolic and systolic diameters, compliance, and stiffness in the presence of PE are elastin dependent. Diastolic diameter **(A)**, systolic diameter **(B)**, compliance **(C)**, and Peterson modulus, E_p **(D)**, were measured in aortic segments in the presence of 2 μM PE and 300-μM L-NAME in control conditions (black symbols) or after treatment with 0.1 unit/ml elastase (green symbols). Two-way RM ANOVA with Sidak's multiple comparison test (elastase vs. control), $^*p < 0.05$, $^{**}p < 0.01$, $^{***}p < 0.001$, $n = 5$.

by high extracellular K^+, especially after inhibition of basal NO release with L-NAME, caused more pronounced hysteresis of all parameters (**Figures 3B,D,F,H**). In this condition, now, also, clear hysteresis of the aortic stiffness parameter, E_p, occurred with lower stiffness ("de-stiffening") in the unloading than in the loading direction at any pressure given between 60 and 200 mm Hg. Both depolarization with high K^+ and α_1 adrenoceptor stimulation with PE caused aortic stiffness hysteresis. Although 50 mM K^+ caused larger isometric contractions than PE, stiffness increase by depolarization was significantly smaller than by PE (**Figure 4**). Furthermore, aortic stiffness hysteresis was more pronounced for PE than for 50 mM K^+. The largest difference between upward and downward pressure change was observed at physiological pressures for PE and slightly higher pressures for depolarization (**Figure 7**). This is the pressure range where the tensile force is mainly absorbed by the contracted VSMCs, suggesting that aortic VSMCs, indeed, play a major role in aortic stiffening, stiffness hysteresis phenomena, and aortic viscosity. The more pronounced hysteresis for PE-induced stiffening may be explained by the stronger activation of Rho/Rho kinase in receptor-mediated (adrenoceptor, PE) than non-receptor-mediated (high K^+) contraction. Rho-linked signaling mechanisms have been linked to mechanotransduction *via* modulation of focal adhesions (Jang et al., 2005; Sun et al., 2012). Focal adhesion sites, where the VSMC cytoskeleton is linked to ECM components through integrin-based interactions (Saphirstein et al., 2013; Lacolley et al., 2017), permit adequate force transmission from the contracted VSMC to the vascular wall *via* the extracellular matrix, thereby enabling stiffness development. Pharmacological inhibition of focal adhesions results in a more than 60% decrease in vascular stiffening, highlighting their importance in the VSMC contribution to arterial stiffness (Min et al., 2012; Poythress et al., 2013; Gao et al., 2014).

On the other hand, the continuous connection of the elastin fibers to the contractile units in the VSMCs of the aortic wall, which has been termed the "elastin-contractile unit" (Milewicz et al., 2017), is a prerequisite for performing contraction. The present study confirmed these observations. The effects of PE-induced constriction on diameters, compliance, and E_p were reduced by 70 to 100% at low to high pressure. At the high-pressure elastase-treated aortic segment, stiffness was even insensitive to the presence of PE. The "elastin-contractile unit" (Milewicz et al., 2017) may also affect the viscoelastic properties and hysteresis of the aorta. In aortic segments treated with elastase and subjected to PE in the presence of L-NAME, degradation of elastin caused hysteresis, which was exactly the opposite of stiffness hysteresis in elastin-intact aortic segments. At any given mean pressure in the unloading conditions, aortic stiffness was higher than in the loading condition (**Figure 10**). This "reverse" hysteresis was also observed in single VSMCs exposed to stretch transverse to primary fiber alignment (Win

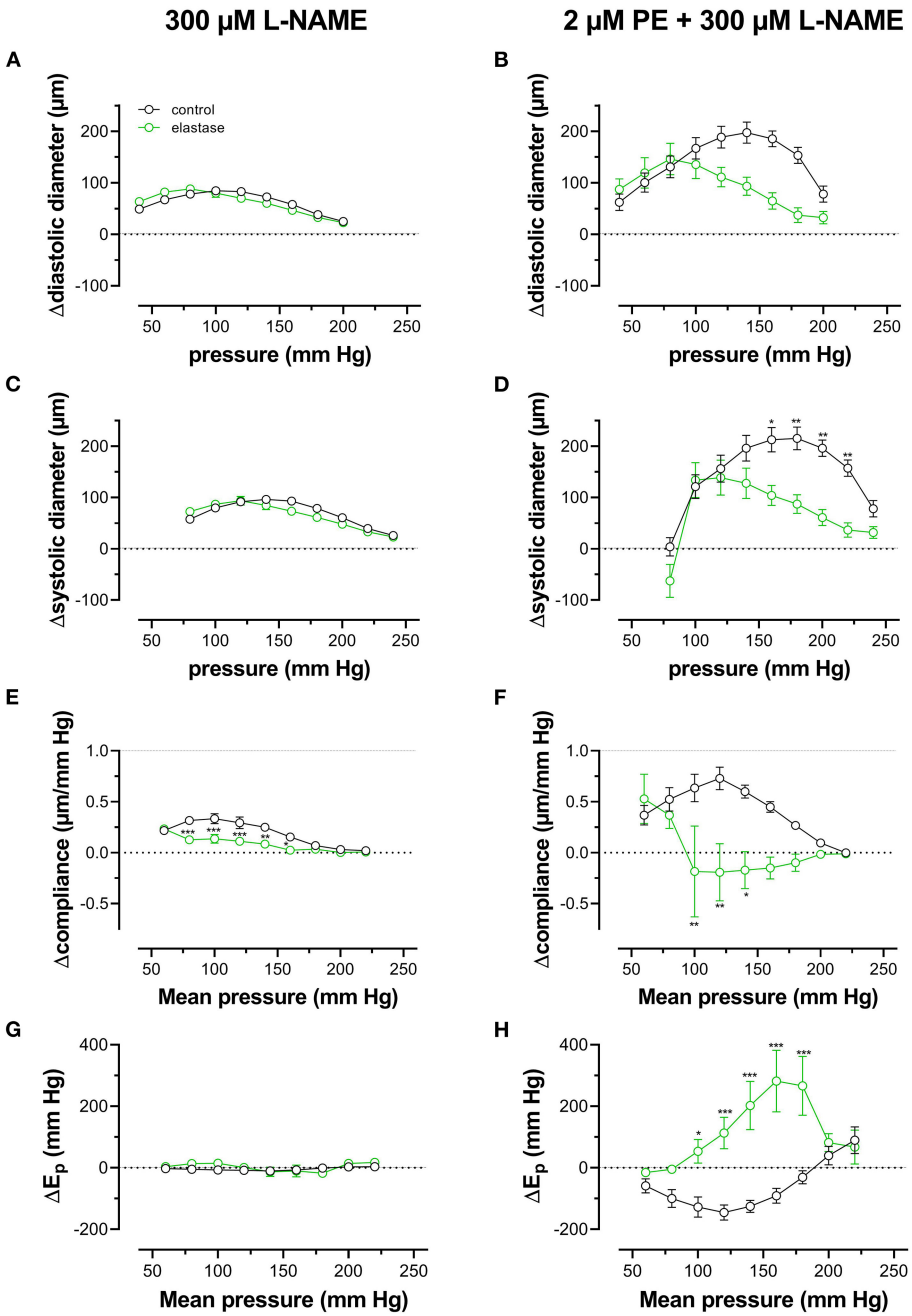

FIGURE 10 | Pressure-dependent hysteresis induced by contraction with PE is elastin dependent. Diastolic **(A,B)** and systolic diameters **(C,D)**, compliance **(E,F)**, and E_p **(G,H)** were determined in untreated (black) and elastase-treated (0.1 unit/ml, green) aortic segments in KR **(A,C,E,G)** and in the presence of 2 µM PE/300-µM L-NAME **(B,D,F,H)**. Data points for the upward pressure steps were compared at any given pressure with data points for the downward pressure steps (stiffness hysteresis). Hence, positive values for diameter and compliance refer to larger diameters and compliance for downward pressure steps. Negative values for E_p correspond to lower stiffness for the downward pressure steps ("de-stiffening"). Two-way RM ANOVA with Sidak's multiple comparison test, $^{*}p < 0.05$, $^{**}p < 0.01$, $^{***}p < 0.001$, $n = 5$.

et al., 2018), suggesting that rearrangement of the ECM occurred after elastin digestion in our experiments may affect viscous properties of the aortic segments.

Aging and VSMC stimulation with depolarization or α_1 adrenoceptor stimulation changed the typical biomechanical behavior of the aorta. The most prominent effect of aging was the increased aortic stiffness along the entire pressure range investigated. Especially at higher-distension pressure, aortic stiffness was increased. Moreover, stiffness hysteresis in the aorta of old mice was of a mixed type. Stiffness at mean

pressures above 160 mm Hg was higher for pressure release than for pressure increase. Below 160 mm Hg, normal hysteresis was present with stiffness being lower in the unloading than loading direction. Aorta segments of young mice showed normal stiffness hysteresis at mean pressures below 200 mm Hg, about 40 mm Hg above the turning point in aortas of old animals. It is well-known that aging causes migration of VSMCs from the media to the intima, wall thickening, and artery stiffening because of the fragmentation and degradation of elastin, cross-linking, collagen remodeling, and ECM irregularities (Toda et al., 1980; Greenwald, 2007; Tsamis et al., 2013). The fact that elastin degradation with elastase turned normal pressure-dependent hysteresis of contracted aortic segments to "reverse" hysteresis may indicate that the mixed hysteresis observed in aortic segments of old mice is due to the age-dependent elastin degradation and/or the elevated number of elastin breaks. However, many different structural and biochemical changes occur within the vessel wall with aging (Ungvari et al., 2018), and recent studies have shown an increase in VSMC cellular stiffness with aging (Qiu et al., 2010). Aging is characterized by an increase in α smooth muscle actin, the stress fiber-specific isoform for VSMCs, which is central to mechanotransduction by transmitting force to the ECM *via* integrins (Qiu et al., 2010). Hence, also, with aging, focal adhesion assembly and disassembly may be affected. In aortas of old mice, the inhibitory effects of the Src inhibitor PP2 on agonist-induced stress, stiffness, and phosphotyrosine increase are lost, suggesting the regulatory pathways related to focal adhesion are attenuated with aging (Gao et al., 2014).

Physiological Impact, Shortcomings, and Future Directions of This Study

Because of its distinguished location between the contracting and ejecting left ventricle of the heart and the rest of the circulation, the compliance and stiffness of the aorta play a pivotal role in cardiovascular health. The elastic properties of the aorta undoubtedly contribute to the blood buffering capacity of this blood vessel, as well as its viscous properties in the dynamic regulation of wall properties. Results of the present study indicate that both ECM and VSMCs contribute to the pressure-dependent stiffness hysteresis observed as the difference between loading and unloading stiffness along a pressure range from 60 to 240 mm Hg. To investigate this in more detail, more experiments with elastase, collagenase, and factors involved in focal adhesion dynamics are expected to further elucidate the pressure-, age- and contraction-dependent biomechanics of the aorta. An important physiological aspect of the viscous properties of the aortic wall might be a de-stiffening effect of acute exercise. During exercise, diastolic pressure hardly changes, whereas systolic pressure is elevated dependent on the exercise intensity, leading to an increase of pulse pressure. The results of the present study suggest that immediately after an exercise bout, diastolic and systolic diameters are larger than before exercise and dependent on the contractile state of the VSMCs; this may lead to aortic de-stiffening and a higher blood buffering capacity of the aorta immediately after the exercise bout.

One of the main shortcomings of this study is that aortic segments were not pressurized and were only subjected to uniaxial stretch. *Ex vivo* organ bath studies on isolated aortic segments have been performed extensively in the past few decades. In many cases, researchers focused on the isometric force at non-physiological preloads or stress-strain relationships under static conditions. Recently, a new setup to study biaxial biomechanics of mouse carotid artery under pulsatile conditions has been described (van der Bruggen et al., 2021). With this setup, it was demonstrated that pulse wave velocity, distensibility, and compliance coefficients of murine carotid artery depended on the amount of axial stretch. Although our ROTSAC system uses uniaxial stretch of large mouse aortic segments (diameter $\pm$ 1 mm) or larger, it allows to continuously stretch aortic segments at high frequency of 10 Hz (600 beats/min) or even more and to apply extrapolated pressure differences of up to 100 mm Hg. In this way, the ROTSAC setup allows simulating various pulsatile conditions or bouts of exercise. In the ROTSAC setup, compliance of the segments was defined as the change in diameter (between systolic and diastolic pressures) per mm Hg pressure. In general, compliance refers to the change of volume per mm Hg pressure. We preferred to keep the change of diameter per mm Hg, because diameters were directly measured and extrapolated in the present setup. Also, wall thickness was not measured and considered. Therefore, we were not able to measure wall stress. It should be mentioned that, to apply a calculated pressure of 100 mm Hg to the aortic segments, it was found that aortic segments of young mice needed a preload of 27. $\pm$ 0.6 mN ($n = 8$) vs. 30. $\pm$ 0.4 mN ($n = 5$, $p < 0.01$) for segments of old mice. Probably, this is due to the higher wall thickness of aortas isolated from aged mice.

The advantage of the ROTSAC setup is related to (i) the ability to independently control mechanical and pharmacological stimulation, (ii) the ability to expose the vessel to a physiological stretch rate, (iii) the ability to study several aortic segments of the same mouse, segments of different mice or different experimental protocols at the same time, and (iv) to compare effects of mechanical or pharmacological stimuli at the same extrapolated transmural pressure (isobaric measurements). These advantages might be especially relevant to aortic segments, given it is the significant visco-elastic behavior and (patho)physiological role in overall hemodynamics. Furthermore, the knowledge of the physiological role of VSMC contraction and relaxation in the aorta is still largely lacking, and data collected with the ROTSAC setup are expected to further contribute to a better understanding of the role of (contractile) cells in the aorta. It is evident that the ROTSAC setup cannot simply replace or be translated into the *in vivo* setting. Use of a biaxial pressurized myograph, which can be used for larger diameter vessels (300–1,000 μm) with (van der Bruggen et al., 2021) or without pulsation (Bersi et al., 2016), may result in additional experiments to demonstrate the (patho)physiological implications of the observations of the present study.

CONCLUSION

The present study revealed that the ROTSAC equipment (Leloup et al., 2016) was suitable to study pressure dependency of arterial stiffness in different, well-controllable experimental conditions. Loading and unloading of aortic segments along a pressure range from 60 to 240 mm Hg and back, while continuously stretching the segments equivalent to a pulse pressure of 40 mm Hg to measure aortic compliance and stiffness, revealed that both the ECM and the VSMCs contribute to pressure-dependent stiffness hysteresis. Stiffness hysteresis phenomena were contraction, age, and ECM dependent, which suggests that VSMCs, in interaction with their ECM, contribute to a pressure-dependent pulse-dampening capacity of the aorta. The presumable role of focal adhesions as the link between VSMC cytoskeleton, integrins, and ECM in aortic stiffness hysteresis in the pulse-dampening capacity of the aorta might be a subject for future studies.

DATA AVAILABILITY STATEMENT

The raw data supporting the conclusions of this article will be made available by the authors, without undue reservation.

ETHICS STATEMENT

The animal study was reviewed and approved by Ethical Committee of the University of Antwerp.

AUTHOR CONTRIBUTIONS

SD, AL, and PF contributed to the conception and design of the study performed the statistical analysis and wrote the first draft of the manuscript. All authors contributed to manuscript revisions, read and approved the submitted version.

FUNDING

This work was supported by the University of Antwerp (GOA-BOF, grant 33931). AL was fellow of the FWO-Flanders (Belgium).

SUPPLEMENTARY MATERIAL

The Supplementary Material for this article can be found online at: https://www.frontiersin.org/articles/10.3389/fphys.2021.723972/full#supplementary-material

REFERENCES

Armentano, R. L., Barra, J. G., Levenson, J., Simon, A., and Pichel, R. H. (1995). Arterial wall mechanics in conscious dogs. assessment of viscous, inertial, and elastic moduli to characterize aortic wall behavior. *Circ. Res.* 76, 468–478. doi: 10.1161/01.RES.76.3.468

Barra, J. G., Armentano, R. L., Levenson, J., Fischer, E. I., Pichel, R. H., and Simon, A. (1993). Assessment of smooth muscle contribution to descending thoracic aortic elastic mechanics in conscious dogs. *Circ.Res.* 73, 1040–1050. doi: 10.1161/01.RES.73.6.1040

Bauer, R. D., Busse, R., Schabert, A., Summa, Y., and Wetterer, E. (1979). Separate determination of the pulsatile elastic and viscous forces developed in the arterial wall in vivo. *Pflugers Arch.* 380, 221–226. doi: 10.1007/BF00582900

Bergel, D. H. (1961a). The dynamic elastic properties of the arterial wall. *J. Physiol.* 156, 458–469. doi: 10.1113/jphysiol.1961.sp006687

Bergel, D. H. (1961b). The static elastic properties of the arterial wall. *J. Physiol.* 156, 445–457. doi: 10.1113/jphysiol.1961.sp006686

Bersi, M. R., Bellini, C., Wu, J., Montaniel, K. R. C., Harrison, D. G., and Humphrey, J. D. (2016). Excessive adventitial remodeling leads to early aortic maladaptation in angiotensin-induced hypertension. *Hypertension* 67, 890–896. doi: 10.1161/HYPERTENSIONAHA.115.06262

Boutouyrie, P., Bezie, Y., Lacolley, P., Challande, P., Chamiot-Clerc, P., Benetos, A., et al. (1997). In vivo/in vitro comparison of rat abdominal aorta wall viscosity. influence of endothelial function. *Arterioscler. Thromb. Vasc. Biol.* 17, 1346–1355. doi: 10.1161/01.ATV.17.7.1346

Boutouyrie, P., Boumaza, S., Challande, P., Lacolley, P., and Laurent, S. (1998). Smooth muscle tone and arterial wall viscosity: an in vivo/in vitro study. *Hypertension* 32, 360–364. doi: 10.1161/01.HYP.32.2.360

Busse, R., Bauer, R. D., Sattler, T., and Schabert, A. (1981). Dependence of elastic and viscous properties of elastic arteries on circumferential wall stress at two different smooth muscle tones. *Pflugers Arch.* 390, 113–119. doi: 10.1007/BF00590192

Butlin, M., Tan, I., Spronck, B., and Avolio, A. P. (2020). Measuring arterial stiffness in animal experimental studies. *Arterioscler. Thromb. Vasc. Biol.* 40, 1068–1077. doi: 10.1161/ATVBAHA.119.313861

Charalambous, H. P., Roussis, P. C., and Giannakopoulos, A. E. (2017). Viscoelastic dynamic arterial response. *Comput. Biol. Med.* 89, 337–354. doi: 10.1016/j.compbiomed.2017.07.028

Dinardo, C. L., Venturini, G., Zhou, E. H., Watanabe, I. S., Campos, L. C., Dariolli, R., et al. (2014). Variation of mechanical properties and quantitative proteomics of VSMC along the arterial tree. *Am. J. Physiol. Heart Circ. Physiol.* 306, H505–516. doi: 10.1152/ajpheart.00655.2013

Fransen, P., Van Hove, C. E., Leloup, A. J., Martinet, W., De Meyer, G. R., Lemmens, K., et al. (2015). Dissecting out the Complex Ca2+-Mediated Phenylephrine-Induced Contractions of Mouse Aortic Segments. *PLoS.ONE.* 10:e0121634. doi: 10.1371/journal.pone.0121634

Gao, Y. Z., Saphirstein, R. J., Yamin, R., Suki, B., and Morgan, K. G. (2014). Aging impairs smooth muscle-mediated regulation of aortic stiffness: a defect in shock absorption function? *Am. J. Physiol. Heart Circ. Physiol.* 307, H1252–1261. doi: 10.1152/ajpheart.00392.2014

Gosling, R. G., and Budge, M. M. (2003). Terminology for describing the elastic behavior of arteries. *Hypertension* 41, 1180–1182. doi: 10.1161/01.HYP.0000072271.36866.2A

Greenwald, S. E. (2007). Ageing of the conduit arteries. *J. Pathol.* 211, 157–172. doi: 10.1002/path.2101

Holzapfel, G. A., and Ogden, R. W. (2018). Biomechanical relevance of the microstructure in artery walls with a focus on passive and active components. *Am. J. Physiol. Heart Circul. Physiol.* 315, H540–H549. doi: 10.1152/ajpheart.00117.2018

Hong, Z., Reeves, K. J., Sun, Z., Li, Z., Brown, N. J., and Meininger, G. A. (2015). Vascular smooth muscle cell stiffness and adhesion to collagen I modified by vasoactive agonists. *PLoS ONE* 10:e0119533. doi: 10.1371/journal.pone.0119533

Jang, G. J., Ahn, D. S., Cho, Y. E., Morgan, K. G., and Lee, Y. H. (2005). C2-ceramide induces vasodilation in phenylephrine-induced pre-contracted rat thoracic aorta: role of RhoA/Rho-kinase and intracellular Ca2+ concentration. *Naunyn Schmiedebergs Arch.Pharmacol.* 372, 242–250. doi: 10.1007/s00210-005-0008-3

Jesudason, R., Black, L., Majumdar, A., Stone, P., and Suki, B. (2007). Differential effects of static and cyclic stretching during elastase digestion on the mechanical properties of extracellular matrices. *J. Appl. Physiol.* 103, 803–811. doi: 10.1152/japplphysiol.00057.2007

Knutsen, R. H., Beeman, S. C., Broekelmann, T. J., Liu, D., Tsang, K. M., Kovacs, A., et al. (2018). Minoxidil improves vascular compliance, restores cerebral blood flow, and alters extracellular matrix gene expression in a model of chronic vascular stiffness. *Am. J. Physiol. Heart Circ. Physiol.* 315, H18–H32. doi: 10.1152/ajpheart.00683.2017

Lacolley, P., Regnault, V., Segers, P., and Laurent, S. (2017). Vascular smooth muscle cells and arterial stiffening: relevance in development, aging, and disease. *Physiol. Rev.* 97, 1555–1617. doi: 10.1152/physrev.00003.2017

Langewouters, G. J., Zwart, A., Busse, R., and Wesseling, K. H. (1986). Pressure-diameter relationships of segments of human finger arteries. *Clin. Phys. Physiol. Meas.* 7, 43–56. doi: 10.1088/0143-0815/7/1/003

Leloup, A., De Moudt, S., Van Hove, C., and Fransen, P. (2017). Cyclic stretch alters vascular reactivity of mouse aortic segments. *Front. Physiol.* 8:858. doi: 10.3389/fphys.2017.00858

Leloup, A. J., Van Hove, C. E., Kurdi, A., De Moudt, S., Martinet, W., De Meyer, G. R., et al. (2016). A novel set-up for the ex vivo analysis of mechanical properties of mouse aortic segments stretched at physiological pressure and frequency. *J. Physiol.* 594, 6105–6115. doi: 10.1113/JP272623

Leloup, A. J. A., Van Hove, C. E., De Moudt, S., De Meyer, G. R. Y., De Keulenaer, G. W., and Fransen, P. (2019). Vascular smooth muscle cell contraction and relaxation in the isolated aorta: a critical regulator of large artery compliance. *Physiol. Rep.* 7, e13934. doi: 10.14814/phy2.13934

Milewicz, D. M., Trybus, K. M., Guo, D. C., Sweeney, H. L., Regalado, E., Kamm, K., et al. (2017). Altered smooth muscle cell force generation as a driver of thoracic aortic aneurysms and dissections. *Arterioscler. Thromb. Vascul. Biol.* 37, 26–34. doi: 10.1161/ATVBAHA.116.303229

Min, J., Reznichenko, M., Poythress, R. H., Gallant, C. M., Vetterkind, S., Li, Y., et al. (2012). Src modulates contractile vascular smooth muscle function via regulation of focal adhesions. *J. Cell. Physiol.* 227, 3585–3592. doi: 10.1002/jcp.24062

Ng, K., Butlin, M., and Avolio, A. P. (2012). Persistent effect of early, brief angiotensin-converting enzyme inhibition on segmental pressure dependency of aortic stiffness in spontaneously hypertensive rats. *J. Hypertens.* 30, 1782–1790. doi: 10.1097/HJH.0b013e3283562e35

Poythress, R. H., Gallant, C., Vetterkind, S., and Morgan, K. G. (2013). Vasoconstrictor-induced endocytic recycling regulates focal adhesion protein localization and function in vascular smooth muscle. *Am. J. Physiol. Cell Physiol.* 305, C215–227. doi: 10.1152/ajpcell.00103.2013

Qiu, H., Zhu, Y., Sun, Z., Trzeciakowski, J. P., Gansner, M., Depre, C., et al. (2010). Short communication: vascular smooth muscle cell stiffness as a mechanism for increased aortic stiffness with aging. *Circ. Res.* 107, 615–619. doi: 10.1161/CIRCRESAHA.110.221846

Ratz, P. H. (2016). Mechanics of Vascular Smooth Muscle. *Compr. Physiol.* 6, 111–168. doi: 10.1002/cphy.c140072

Remington, J. W. (1955). Hysteresis loop behavior of the aorta and other extensible tissues. *Am. J. Physiol.* 180, 83–95. doi: 10.1152/ajplegacy.1954.180.1.83

Saphirstein, R. J., Gao, Y. Z., Jensen, M. H., Gallant, C. M., Vetterkind, S., Moore, J. R., et al. (2013). The focal adhesion: a regulated component of aortic stiffness. *PLoS ONE* 8:e62461. doi: 10.1371/journal.pone.0062461

Sun, Z., Li, Z., and Meininger, G. A. (2012). Mechanotransduction through fibronectin-integrin focal adhesion in microvascular smooth muscle cells: is calcium essential? *Am. J. Physiol. Heart Circ. Physiol.* 302, H1965–1973. doi: 10.1152/ajpheart.00598.2011

Toda, T., Tsuda, N., Nishimori, I., Leszczynski, D. E., and Kummerow, F. A. (1980). Morphometrical analysis of the aging process in human arteries and aorta. *Acta. Anat.* 106, 35–44. doi: 10.1159/000145167

Trepat, X., Grabulosa, M., Puig, F., Maksym, G. N., Navajas, D., and Farre, R. (2004). Viscoelasticity of human alveolar epithelial cells subjected to stretch. *Am. J. Physiol. Lung Cell. Mol. Physiol.* 287, L1025–1034. doi: 10.1152/ajplung.00077.2004

Tsamis, A., Krawiec, J. T., and Vorp, D. A. (2013). Elastin and collagen fibre microstructure of the human aorta in ageing and disease: a review. *J.R.Soc.Interface* 10:20121004. doi: 10.1098/rsif.2012.1004

Ungvari, Z., Tarantini, S., Donato, A. J., Galvan, V., and Csiszar, A. (2018). Mechanisms of Vascular Aging. *Circ. Res.* 123, 849–867. doi: 10.1161/CIRCRESAHA.118.311378

van der Bruggen, M. M., Reesink, K. D., Spronck, P. J. M., Bitsch, N., Hameleers, J., Megens, R. T. A., et al. (2021). An integrated set-up for ex vivo characterisation of biaxial murine artery biomechanics under pulsatile conditions. *Sci. Rep.* 11:2671. doi: 10.1038/s41598-021-81151-5

Wagenseil, J. E., and Mecham, R. P. (2009). Vascular extracellular matrix and arterial mechanics. *Physiol. Rev.* 89, 957–989. doi: 10.1152/physrev.00041.2008

Wagenseil, J. E., and Mecham, R. P. (2012). Elastin in Large Artery Stiffness and Hypertension. *J. Cardiovasc. Transl. Res.* 5, 264–273. doi: 10.1007/s12265-012-9349-8

Win, Z., Buksa, J. M., and Alford, P. W. (2018). Architecture-dependent anisotropic hysteresis in smooth muscle cells. *Biophys. J.* 115, 2044–2054. doi: 10.1016/j.bpj.2018.09.027

Zhang, J., Zhao, X., Vatner, D. E., McNulty, T., Bishop, S., Sun, Z., et al. (2016). Extracellular matrix disarray as a mechanism for greater abdominal versus thoracic aortic stiffness with aging in primates. *Arterioscler. Thromb. Vasc. Biol.* 36, 700–706. doi: 10.1161/ATVBAHA.115.306563

Conflict of Interest: The authors declare that the research was conducted in the absence of any commercial or financial relationships that could be construed as a potential conflict of interest.

Publisher's Note: All claims expressed in this article are solely those of the authors and do not necessarily represent those of their affiliated organizations, or those of the publisher, the editors and the reviewers. Any product that may be evaluated in this article, or claim that may be made by its manufacturer, is not guaranteed or endorsed by the publisher.

frontiers in Physiology

ORIGINAL RESEARCH
published: 22 October 2021
doi: 10.3389/fphys.2021.741346

High Pulsatile Load Decreases Arterial Stiffness: An *ex vivo* Study

*Cédric H. G. Neutel[1], Giulia Corradin[2], Pauline Puylaert[3], Guido R. Y. De Meyer[3], Wim Martinet[3] and Pieter-Jan Guns[1]**

[1] Laboratory of Physiopharmacology, Faculty of Medicine and Health Sciences, University of Antwerp, Campus Drie Eiken, Antwerp, Belgium, [2] Department of Pharmaceutical and Pharmacological Sciences, University of Padua, Padua, Italy, [3] Laboratory of Physiopharmacology, Faculty of Pharmaceutical, Biomedical and Veterinary Sciences, University of Antwerp, Campus Drie Eiken, Antwerp, Belgium

Measuring arterial stiffness has recently gained a lot of interest because it is a strong predictor for cardiovascular events and all-cause mortality. However, assessing blood vessel stiffness is not easy and the *in vivo* measurements currently used provide only limited information. *Ex vivo* experiments allow for a more thorough investigation of (altered) arterial biomechanical properties. Such experiments can be performed either statically or dynamically, where the latter better corresponds to physiological conditions. In a dynamic setup, arterial segments oscillate between two predefined forces, mimicking the diastolic and systolic pressures from an *in vivo* setting. Consequently, these oscillations result in a pulsatile load (i.e., the pulse pressure). The importance of pulse pressure on the *ex vivo* measurement of arterial stiffness is not completely understood. Here, we demonstrate that pulsatile load modulates the overall stiffness of the aortic tissue in an *ex vivo* setup. More specifically, increasing pulsatile load softens the aortic tissue. Moreover, vascular smooth muscle cell (VSMC) function was affected by pulse pressure. VSMC contraction and basal tonus showed a dependence on the amplitude of the applied pulse pressure. In addition, two distinct regions of the aorta, namely the thoracic descending aorta (TDA) and the abdominal infrarenal aorta (AIA), responded differently to changes in pulse pressure. Our data indicate that pulse pressure alters *ex vivo* measurements of arterial stiffness and should be considered as an important variable in future experiments. More research should be conducted in order to determine which biomechanical properties are affected due to changes in pulse pressure. The elucidation of the underlying pulse pressure-sensitive properties would improve our understanding of blood vessel biomechanics and could potentially yield new therapeutic insights.

Keywords: pulse pressure, arterial stiffness, biomechanics, infrarenal aorta, thoracic descending aorta, VSMC

OPEN ACCESS

Edited by:
Bart Spronck,
Maastricht University, Netherlands

Reviewed by:
Alessandro Giudici,
Maastricht University, Netherlands
Isabella Tan,
Macquarie University, Australia

***Correspondence:**
Pieter-Jan Guns
pieter-jan.guns@uantwerpen.be

Specialty section:
This article was submitted to Vascular Physiology, a section of the journal Frontiers in Physiology

Received: *14 July 2021*
Accepted: *23 September 2021*
Published: *22 October 2021*

Citation:
Neutel CHG, Corradin G, Puylaert P, De Meyer GRY, Martinet W and Guns P-J (2021) High Pulsatile Load Decreases Arterial Stiffness: An ex vivo Study. Front. Physiol. 12:741346. doi: 10.3389/fphys.2021.741346

INTRODUCTION

Large artery stiffness is a strong predictor of cardiovascular events and all-cause mortality and directly impacts blood pressure. Evidently, measurement of arterial stiffness *in vivo* and *ex vivo* has gained a lot of interest (Vlachopoulos et al., 2010; Leloup et al., 2016; Avolio et al., 2018). Determining pulse wave velocity (PWV) is the cornerstone for the *in vivo* measurement of arterial stiffness (Butlin et al., 2020). However, PWV does not make a distinction between the contribution of different components of the vessel wall to the overall stiffness. *Ex vivo* measurements of arterial stiffness may provide more insight into the mechanisms that cause blood vessel stiffening. Such *ex vivo* measurements can

reveal important (altered) biomechanical properties of blood vessels, which can advance the research field of "vascular mechanomedicine" (Naruse, 2018).

Measuring blood vessel stiffness *ex vivo* can either be done in a static or a dynamic manner. However, the biomechanical behavior of blood vessels differs between stationary and oscillatory experiments (Cox, 1974; Glaser et al., 1995; Lénárd et al., 2000). Therefore, assessing arterial stiffness under pulsatile conditions is favorable, as it is more representative of physiological conditions. Pulsatile *ex vivo* setups such as the bi-axial stretching setup of van der Bruggen M. M. et al. (2021) or the dynamic intraluminal pressure testing system by Santelices et al. (2007) are able to produce quasi-physiological pressure waveforms. In these setups, pulsatile load/stretch can be mimicked in *ex vivo* conditions, allowing a dynamic assessment of blood vessel stiffness.

Our research group previously developed a wire myography-based organ bath setup, called ROTSAC, that enables imposing different pulsatile stretching conditions (Leloup et al., 2016). Using this setup, the role of vascular smooth muscle cells (VSMCs) and endothelial cells (ECs) in arterial viscoelasticity was extensively studied (Leloup et al., 2017, 2019, 2020; De Munck et al., 2020; Bosman et al., 2021). In these experiments, the pulsatile load was kept at a pulse pressure of 40 mmHg to mimic the physiological condition. However, the amplitude of the pulsatile stretch is known to modulate mechanosensitive properties of the blood vessel, such as contractile properties, stress fiber alignment, cell morphology and gene expression in both ECs and VSMCs (Birukov, 2009; Haghighipour et al., 2010; Hsu et al., 2010). Moreover, the viscoelastic properties of the arterial wall, which modulate the stiffness of the vessel, can be affected by altered dynamic loading conditions (Tan et al., 2016; Xiao et al., 2017; Butlin et al., 2020). Therefore, instead of assessing the "pressure"–"strain" relationship at a single fixed pulse pressure, altering the stretch amplitude/pulse pressure could reveal other biomechanical responses which would otherwise be neglected.

In the present study, we investigated how altering the amplitude of the pulsatile stretch (i.e., the pulsatile load) *ex vivo* affects the measurement of arterial stiffness. We aimed to illustrate how VSMC function and arterial viscoelastic properties are affected with altered loading conditions. Specifically, VSMC contraction and relaxation were studied under different pulse pressures to assess whether their functionality is dependent on the pulsatile load. Finally, we compared the descending aorta with the infrarenal aorta in this model to assess differential effects of pulsatile stretch on an elastic and muscular artery, respectively.

MATERIALS AND METHODS

Mice and Tissue Preparation

Seven male C57BL/6J mice (6 months old; Charles River Laboratories, France) were used in the present study. All animals were housed in the animal facility of the University of Antwerp in standard cages with 12 h-12 h light-dark cycles and had free access to regular chow and tap water. The animals were euthanized by perforating the diaphragm while under anesthesia [sodium pentobarbital (Sanofi, Belgium), 75 mg/kg i.p.]. The descending and infrarenal aorta were carefully removed and stripped of adherent tissue. The tissue was cut into segments of 2 mm. In all experiments, segments from the same anatomical location were used in order to minimize variability due to the heterogeneity in blood vessel composition along the aortic tree. The segments were immersed in Krebs Ringer (KR) solution (37°C, 95% O_2/5% CO_2, pH 7.4) containing (in mM): NaCl 118, KCl 4.7, $CaCl_2$ 2.5, KH_2PO_4 1.2, $MgSO_4$ 1.2, $NaHCO_3$ 25, CaEDTA 0.025 and glucose 11.1. The study was waived by the local ethics committee, according to article 3 of the EU legislation (L 276/38, 2010).

Rodent Oscillatory Tension Set-Up to Study Arterial Compliance (ROTSAC)

The *ex vivo* stiffness of the aortic vessels was determined *via* ROTSAC measurements as previously described (Leloup et al., 2016). In brief, aortic segments were mounted between two parallel wire hooks in 10 mL organ baths. Force and displacement of the upper hook were controlled and measured with a force-length transducer. The segments were continuously stretched between alternating preloads, corresponding to a "diastolic" and "systolic" transmural pressure at a frequency of 10 Hz. The Laplace relationship was used to calculate the transmural pressure. At any given pressure, calibration of the upper hook allowed the calculation of the vessel diameter (both systolic and diastolic diameter) and the Peterson pressure-strain modulus of elasticity (Ep). The Ep was calculated as follows:

$$Ep = D_0 . \frac{\triangle P}{\triangle D}$$

With D_0 the diastolic diameter. To dissect how pulse pressure affects the stiffness of the blood vessel, the amplitude of the oscillations was changed to generate higher or lower pulsatile stretches. However, mean pressure is an important regulator of *ex vivo* stiffness (Leloup et al., 2016). Therefore, altering pulse pressure should be done in such a manner that the mean pressures between pulse pressures are equal (**Figure 1**). In our setup, the duration of the diastolic and systolic phase are equal (50 ms for each phase). Therefore, mean transmural pressure is calculated as:

$$Mean\ Pressure = \frac{(Diastolic\ Pressure + Systolic\ pressure)}{2}$$

To increase pulse pressure, diastolic pressures were decreased and systolic pressures were increased in equal increments, leading to different pulse pressures, but equal mean pressures. Hence, the effect of a larger or smaller pulse can be assessed in isobaric conditions. The mean pressures were incrementally increased for all pulse pressures to assess the relationship between the non-linear increase in pressure-mediated stiffness and pulse pressure. All the measurements were conducted on the same aortic segment in order to make paired comparisons. A KCl solution (50 mM in Krebs) as well as the NO donor diethylamine NONOate (DEANO, 2 μM) were used to elicit VSMC contraction and relaxation, respectively. The resulting stiffness was measured at steady state conditions (i.e., 20 min

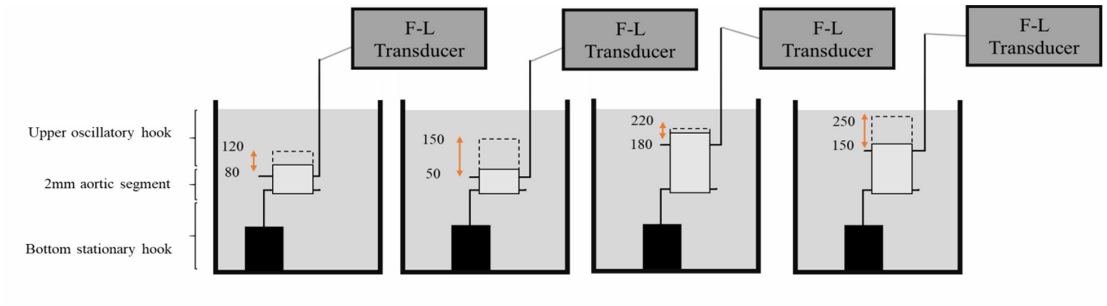

"Systolic" Pressure	120 mmHg	150 mmHg	220 mmHg	250 mmHg
"Diastolic" Pressure	80 mmHg	50 mmHg	180 mmHg	150 mmHg
Mean Pressure	**100 mmHg**	**100 mmHg**	**200 mmHg**	**200 mmHg**
Pulse Pressure	**40 mmHg**	**100 mmHg**	**40 mmHg**	**100 mmHg**

FIGURE 1 | Altering pulsatile load *ex vivo*. To increase the pulse pressure at equal mean pressure, the diastolic and systolic pressures are decreased and increased, respectively, with equal increments. A segment that oscillates between 80 mmHg diastolic pressure and 120 mmHg systolic pressure, is exposed to a mean pressure of 100 mmHg and a pulse pressure of 40 mmHg. Alternatively, a segment that oscillates between 50 mmHg diastolic pressure and 150 mmHg systolic pressure, is exposed to an equal mean pressure of 100 mmHg but an increased pulse pressure of 100 mmHg. F-L Transducer = Force-Length Transducer.

after contraction or relaxation). The segments were washed three times after VSMC contraction in order to remove KCl before administering DEANO.

Experimental Pulse Pressure Protocol

Five different pulse pressures were chosen to be implemented in the experimental protocol. The pulse pressure of 40 mmHg was considered as "physiological" pulse pressure and was therefore used as a reference for the other pulse pressures. One sub-physiological and three supra-physiological pulse pressures were included in the protocol (20 mmHg and 60, 80, and 100 mmHg, respectively). In this protocol, the mean pressure was increased from 80 to 200 mmHg in steps of 20 mmHg (see **Supplementary Figure 1**). The same pulse pressure protocol was applied to each vessel segment in three different conditions (Krebs, KCl, and DEANO). There was a waiting period of 30 min between conditions. Unless otherwise mentioned, segments from the thoracic descending aorta (TDA) were used in this study.

Statistics

All results are expressed as mean ± SEM with n representing the number of mice. Statistical analyses were performed in GraphPad Prism 7.0. Statistical tests are mentioned in the figure and/or table legends. Significance was accepted at $P < 0.05$.

RESULTS

Pulse Pressure Modulates the Non-linear Pressure-Stiffness Relationship

Increasing pulse pressure augmented the maximum distension of the thoracic aortic segment (**Figure 2A**). The maximum distension (%) for pulse pressures of 20, 40, 60, 80, and 100 mmHg at a mean pressure of 100 mmHg were 6 ± 0.3, 13 ± 0.6, 20 ± 1, 28 ± 2, and 36 ± 2, respectively. Changing pulse pressure, alters both the D0 and the compliance (**Figures 2B,C**). Increasing mean pressure increases the Ep (**Figure 2D**). The pulse pressure significantly changed the pressure-stiffness relationship (**Figures 2D,E** and **Table 1**). Ep for each pulse pressure was different at every mean pressure ($p < 0.0001$), meaning that pulse pressure alters the stiffness of the same blood vessel (**Figure 2D**). Statistical comparisons in **Table 1** were made to 40 mmHg pulse pressure, which was considered as the basal, physiological pulse pressure. Additionally, the interaction between pulse pressure and pressure was significant ($p < 0.0001$). A sub analysis was conducted for different pulse pressures at a mean pressure of 100 mmHg and demonstrated that pulse pressure significantly affects both D0 ($p < 0.0001$) and $\Delta P/\Delta D$ ($p = 0.001$) (**Supplementary Figure 2**). This indicates that changes in Ep reflect both changes in diastolic diameter and altered compliance.

Pulse Pressure Modulates Vascular Smooth Muscle Cell Reactivity

The Pulse pressure-pressure-stiffness relationships were also investigated following constriction of aortic segments by depolarization with high extracellular K + or following removal of basal tonus with exogenous NO (DEANO) (**Figure 3**). The results for contraction and relaxation are shown in **Tables 2**, **3**, respectively. We previously reported that VSMC contraction increases stiffness at low, physiological pressures, but decreases stiffness at higher, non-physiological pressures (Leloup et al., 2019). The comparisons between 50 mM KCl (50K) contraction induced stiffness at different pulse pressures and their uncontracted state are listed in **Table 2**. At pulse pressures of 20 and 40 mmHg, 50K increased the stiffness significantly at "low" mean pressures (80–140 mmHg) and decreased stiffness significantly at "high" mean pressures (180–200 mmHg) (**Figure 3A**). For the pulse pressures 60, 80, and 100 mmHg, 50K only decreased the stiffness significantly ($p < 0.0001$) at "high" mean pressures (160–200 mmHg).

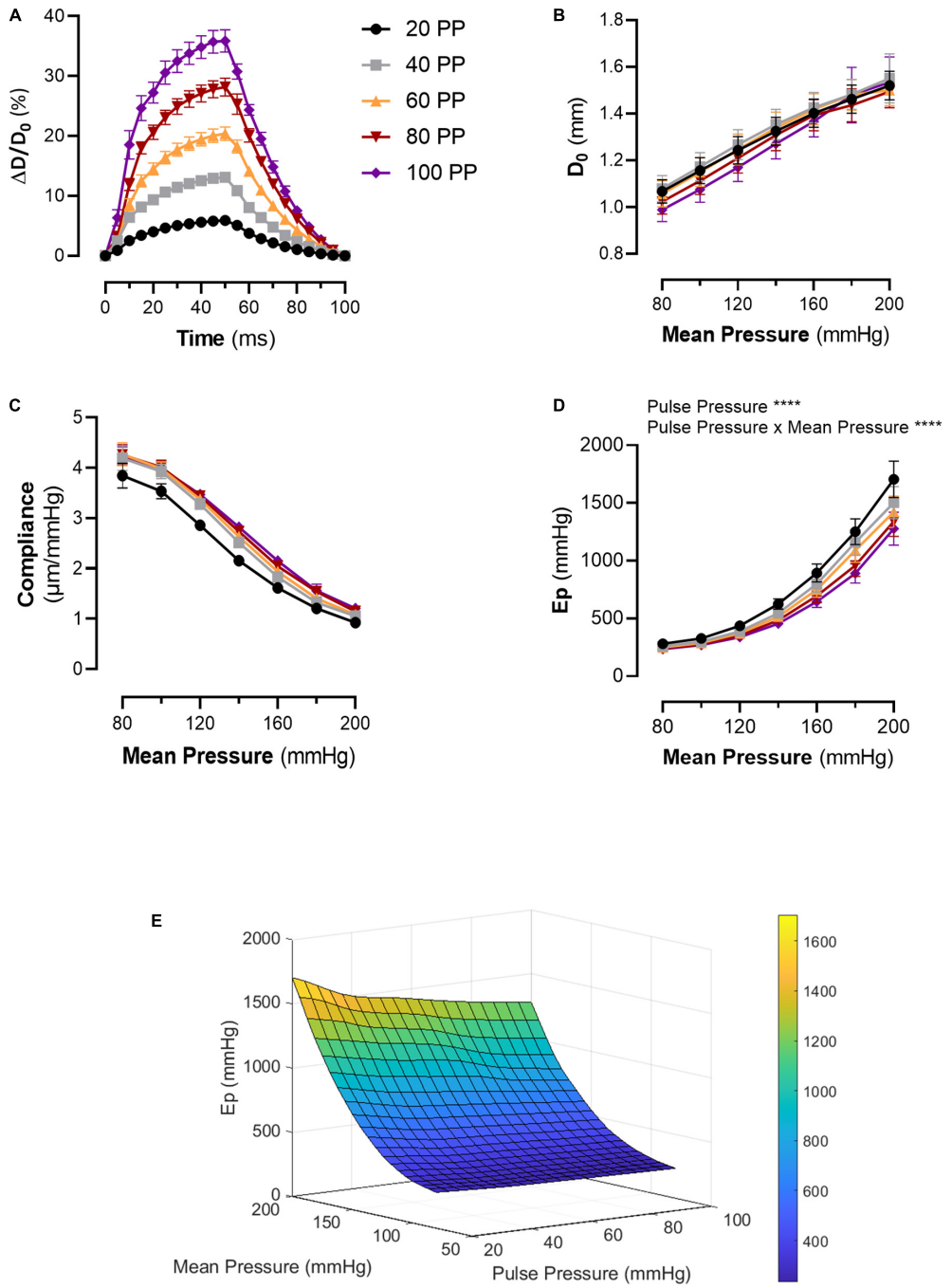

FIGURE 2 | Pulsatile load modulates the pressure-stiffness relationship. **(A)** Mean distension of a single cycle (100 ms) of thoracic aorta segments at different pulse pressures. Tracings were downsampled to 5 ms intervals. **(B)** Diastolic diameter is altered by the applied pulse pressure, as expected due to the nature of the setup. **(C)** The relationship between compliance, pulse pressure and mean pressure. **(D)** The pressure-stiffness relationship is modulated by the pulse pressure. At low pulse pressures, the pressure-mediated increase in Ep is significantly augmented, while the inverse is true for increasing pulse pressures. **(E)** Surface plot representing the mean interpolated data. $n = 7$. Ep, Peterson's modulus of elasticity; PP, pulse pressure.

After 50K elicited contraction, all measurements (Ep) were significantly ($p < 0.0001$) different from each other. The ΔEp was significantly different between 20 and 40 mmHg pulse pressure, at the "low" mean pressures, indicating a stronger response to 50K in the former (**Figure 3B**).

Adding DEANO to the aortic segments removed the basal tonus of the VSMCs (Leloup et al., 2018). The comparisons before and after DEANO administration at different pulse pressures are listed in **Table 3**. Overall, at most pressures, there was no clear effect of removal of basal tonus by DEANO. However, at

TABLE 1 | Effect of differential pulse pressure on blood vessel stiffness.

Mean pressure (mmHg)	Peterson's modulus (Ep, mmHg)				
	20 PP	**40 PP**	**60 PP**	**80 PP**	**100 PP**
80	(280 ± 9)**	(259 ± 8)	(248 ± 7)**	(241 ± 7)**	(234 ± 7)**
100	(328 ± 11)***	(298 ± 10)	(288 ± 12)**	(277 ± 11)***	(270 ± 10)***
120	(437 ± 23)***	(388 ± 22)	(371 ± 22)**	(353 ± 20)***	(338 ± 18)***
140	(625 ± 45)***	(545 ± 42)	(516 ± 41)***	(484 ± 36)***	(454 ± 31)***
160	(894 ± 79)**	(798 ± 71)	(748 ± 65)***	(695 ± 60)***	(645 ± 50)**
180	(1250 ± 112)**	(1158 ± 111)	(1089 ± 105)**	(958 ± 96)**	(890 ± 84)**
200	(1705 ± 158)*	(1502 ± 140)	(1424 ± 136)*	(1339 ± 130)**	(1277 ± 141)**

*Data is expressed as (Mean ± SEM), n = 7. Repeated measures two-way ANOVA with Sidak post hoc test for multiple comparisons (comparisons are made with 40 PP as reference). *p < 0.05; **p < 0.01; ***p < 0.001. PP, pulse pressure (mmHg).*

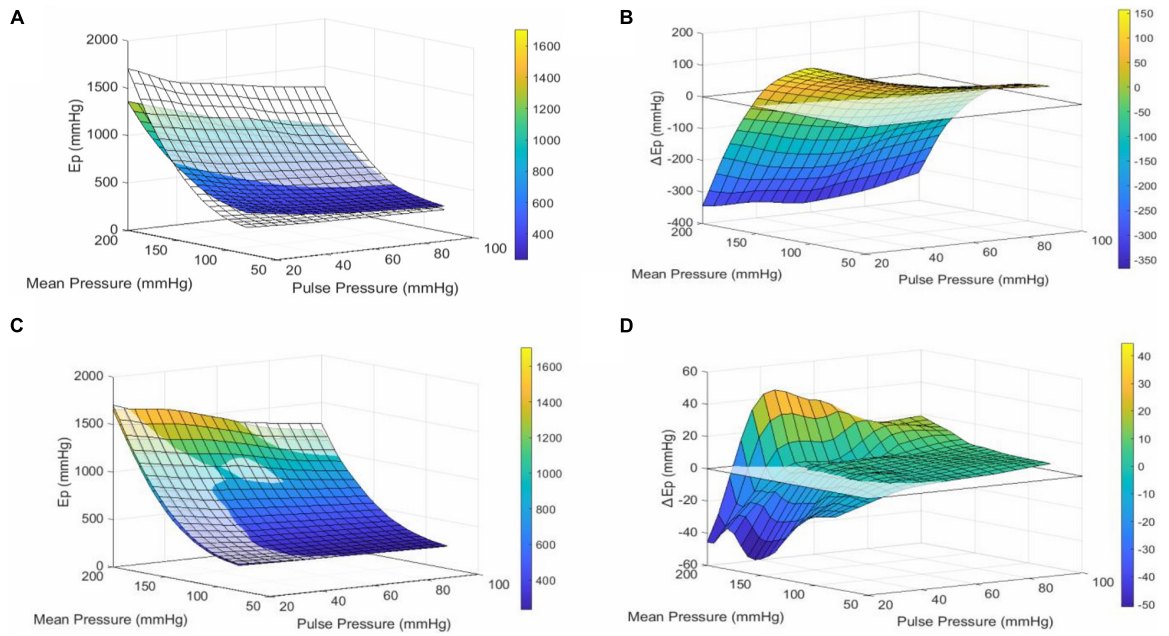

FIGURE 3 | Pulse Pressure alters VSMC reactivity. **(A)** Surface plot of the mean interpolated raw data. The transparent surface plot is the uncontracted, basal state of the aortic segment, while the colored surface plot shows the same segment in 50 mM KCl-induced contracted state. At low mean pressures (80–140 mmHg), contraction of VSMCs makes the segment stiffer, while at high mean pressures (140–200 mmHg), the vessel is less stiff when contracted. This effect is consistent for all pulse pressures. **(B)** Surface plot of the mean interpolated data of the difference in stiffness between contracted and uncontracted state (contracted–basal). **(C)** Surface plot of the mean interpolated raw data. The transparent surface plot is the uncontracted, basal state of the aortic segment while the colored surface plot shows the same segment treated with 2 μM DEANO. **(D)** Surface plot of the mean interpolated data of the difference in stiffness (Ep) between relaxed and basal state (relaxed–basal). *n* = 7. Ep, Peterson's modulus of elasticity; ΔEP, $EP_{contraction}$–$EP_{uncontracted}$; PP, pulse pressure.

20 mmHg pulse pressure Ep was significantly decreased at mean pressures of 140, 160, and 200 mmHg ($p < 0.01$) (**Figure 3D**). A detailed overview of the effects of 50K and DEANO per pulse pressure can be found in the **Supplementary Material** (**Supplementary Figure 3**).

Comparison of Biomechanical Properties of the Thoracic Descending Aorta and the Abdominal Infrarenal Aorta

Overall, Ep for the infrarenal artery was higher than Ep for the descending thoracic aorta, indicating a higher stiffness of the infrarenal artery in all conditions. The individual results are listed in **Table 4**. Whereas differences in Ep between the descending and infrarenal aorta were significant ($p < 0.05$–$p < 0.01$) at mean pressures of 80, 100, 120, and 140 mmHg for a pulse pressure of 20 mmHg, significant differences ($p < 0.05$) were only observed at mean pressures of 100, 120, and 140 mmHg for a pulse pressure of 40 mmHg and at 120 mmHg mean pressure for a pulse pressure of 60 mmHg (**Figure 4**). At higher pulse pressures, the difference in stiffness between the descending and infrarenal aorta did not reach significance.

DISCUSSION

In this study, we demonstrated that increasing *ex vivo* pulsatile load alters the non-linear relationship between pressure

TABLE 2 | Blood vessel stiffness before and after 50 mM KCl induced VSMC contraction at different pulse pressures.

Mean pressure (mmHg)	Peterson's modulus (Ep, mmHg)														
	20 PP			40 PP			60 PP			80 PP			100 PP		
	Basal	50K	ΔEp	Basal	50K	ΔEp	Basal	50K	ΔEp	Basal	50K	ΔEp	Basal	50K	ΔEp
80	(280 ± 9)	(436 ± 17)****	(156 ± 17)	(259 ± 8)	(362 ± 12)*	(103 ± 13)#	(248 ± 7)	(319 ± 8)	(71 ± 8)	(241 ± 7)	(291 ± 7)	(50 ± 6)	(234 ± 7)	(272 ± 7)	(38 ± 4)
100	(328 ± 11)	(483 ± 17)****	(155 ± 18)	(298 ± 10)	(395 ± 12)*	(96 ± 15)#	(288 ± 12)	(348 ± 9)	(60 ± 10)	(277 ± 11)	(321 ± 9)	(44 ± 8)	(270 ± 10)	(301 ± 9)	(32 ± 6)
120	(437 ± 23)	(560 ± 22)****	(123 ± 22)	(388 ± 22)	(464 ± 16)	(76 ± 19)	(371 ± 22)	(408 ± 14)	(37 ± 13)	(353 ± 20)	(375 ± 14)	(22 ± 10)	(338 ± 18)	(353 ± 13)	(15 ± 7)
140	(625 ± 45)	(695 ± 29)*	(71 ± 29)	(545 ± 42)	(575 ± 27)	(30 ± 22)	(516 ± 41)	(506 ± 25)	(−10 ± 18)	(484 ± 36)	(464 ± 23)	(−20 ± 15)	(454 ± 31)	(434 ± 21)	(−21 ± 11)
160	(894 ± 79)	(863 ± 43)	(−32 ± 41)	(798 ± 71)	(731 ± 43)	(−67 ± 31)	(748 ± 65)	(654 ± 41)*	(−94 ± 26)	(695 ± 60)	(602 ± 38)**	(−93 ± 23)	(645 ± 50)	(562 ± 35)**	(−83 ± 17)
180	(1250 ± 112)	(1079 ± 67)****	(−171 ± 49)	(1158 ± 111)	(938 ± 62)****	(−221 ± 54)	(1089 ± 105)	(854 ± 63)****	(−235 ± 44)	(958 ± 96)	(762 ± 61)****	(−196 ± 38)	(890 ± 84)	(717 ± 57)****	(−174 ± 31)
200	(1705 ± 158)	(1360 ± 98)****	(−345 ± 62)	(1502 ± 140)	(1206 ± 90)****	(−349 ± 63)	(1424 ± 136)	(1056 ± 85)****	(−368 ± 58)	(1339 ± 130)	(990 ± 84)****	(−350 ± 52)	(1277 ± 141)	(880 ± 73)****	(−312 ± 72)

*Comparisons are made between the Ep at "50K" and "Basal" (conditions) at the same pulse pressure. Data is expressed as (Mean ± SEM), n = 7. *p < 0.05; **p < 0.01; ***p < 0.001; ****p < 0.0001, #P < 0.05 ("#" = Compared to the ΔEp at 20PP), Repeated measures two-way ANOVA with Sidak post hoc test for multiple comparisons. PP, pulse pressure (mmHg), ΔEp, Ep_{50K}–Ep_{Basal}.*

TABLE 3 | Blood vessel stiffness before and after DEANO-induced VSMC relaxation at different pulse pressures.

Mean pressure (mmHg)	Peterson's modulus (Ep, mmHg)														
	20 PP			40 PP			60 PP			80 PP			100 PP		
	Basal	DEANO	ΔEp	Basal	DEANO	ΔEp	Basal	DEANO	ΔEp	Basal	DEANO	ΔEp	Basal	DEANO	ΔEp
80	(280 ± 9)	(265 ± 6)	(−15 ± 4)	(259 ± 8)	(254 ± 7)	(−5 ± 2)	(248 ± 7)	(248 ± 8)	(0 ± 3)	(241 ± 7)	(242 ± 8)	(1 ± 2)	(234 ± 7)	(238 ± 8)	(4 ± 1)
100	(328 ± 11)	(310 ± 10)	(−18 ± 4)	(298 ± 10)	(297 ± 11)	(−1 ± 3)	(288 ± 12)	(289 ± 13)	(1 ± 3)	(277 ± 11)	(281 ± 12)	(4 ± 3)	(270 ± 10)	(274 ± 11)	(4 ± 2)
120	(437 ± 23)	(409 ± 23)	(−28 ± 4)	(388 ± 22)	(387 ± 23)	(−1 ± 5)	(371 ± 22)	(372 ± 23)	(1 ± 4)	(353 ± 20)	(357 ± 21)	(4 ± 3)	(338 ± 18)	(343 ± 18)	(5 ± 2)
140	(625 ± 45)	(579 ± 43)**	(−46 ± 10)	(545 ± 42)	(543 ± 41)	(−2 ± 7)	(516 ± 41)	(518 ± 41)	(2 ± 6)	(484 ± 36)	(488 ± 37)	(4 ± 6)	(454 ± 31)	(461 ± 32)	(6 ± 4)
160	(894 ± 79)	(844 ± 73)**	(−51 ± 11)	(798 ± 71)	(796 ± 70)	(−2 ± 9)	(748 ± 65)	(752 ± 67)	(3 ± 10)	(695 ± 60)	(700 ± 60)	(5 ± 8)	(645 ± 50)	(653 ± 53)	(8 ± 7)
180	(1250 ± 112)	(1216 ± 113)	(−35 ± 15)	(1158 ± 111)	(1155 ± 110)	(−3 ± 14)	(1089 ± 105)	(1089 ± 102)	(−1 ± 14)	(958 ± 96)	(976 ± 103)	(18 ± 9)	(890 ± 84)	(904 ± 90)	(14 ± 7)
200	(1705 ± 158)	(1659 ± 143)**	(−46 ± 32)	(1502 ± 140)	(1602 ± 146)*	(41 ± 26)	(1424 ± 136)	(1459 ± 151)*	(36 ± 21)	(1339 ± 130)	(1289 ± 147)	(18 ± 16)	(1277 ± 142)	(1211 ± 153)	(19 ± 18)

*Comparisons are made between the Ep at "DEANO" and "Basal" (conditions) at the same pulse pressure. Data is expressed as (Mean ± SEM), n = 7, *p < 0.05; **p < 0.01. Repeated measures two-way ANOVA with Sidak post hoc test for multiple comparisons. PP, pulse pressure (mmHg), ΔEp = Ep_{DEANO}–Ep_{Basal}.*

TABLE 4 | Difference in stiffness between the thoracic descending aorta (TDA) and the abdominal infrarenal aorta (AIA) at different pulse and mean pressures.

Mean pressure (mmHg)	Peterson's modulus (Ep, mmHg)															
	20 PP			40 PP			60 PP			80 PP			100 PP			
	TDA	IR	ΔEp	TDA	IR	ΔEp	TDA	IR	ΔEp	TDA	IR	ΔEp	TDA	IR	ΔEp	
80	(280 ± 9)	(339 ± 15)*	(59 ± 16)	(259 ± 8)	(296 ± 12)	(37 ± 14)	(248 ± 7)	(274 ± 11)	(26 ± 13)	(241 ± 7)	(259 ± 10)	(18 ± 14)	(234 ± 7)	(242 ± 8)	(9 ± 12)	
100	(328 ± 11)	(430 ± 17)**	(102 ± 21)	(298 ± 10)	(368 ± 15)*	(70 ± 21)	(288 ± 12)	(343 ± 13)	(55 ± 20)	(277 ± 11)	(322 ± 12)	(45 ± 19)	(270 ± 10)	(306 ± 11)	(36 ± 17)	
120	(437 ± 23)	(599 ± 25)**	(162 ± 35)	(388 ± 22)	(502 ± 18)*	(114 ± 32)	(371 ± 22)	(465 ± 16)*	(94 ± 31)	(353 ± 20)	(431 ± 14)	(78 ± 28)	(338 ± 18)	(406 ± 13)	(69 ± 25)	
140	(625 ± 45)	(835 ± 38)*	(211 ± 49)	(545 ± 42)	(727 ± 26)*	(182 ± 48)	(516 ± 41)	(666 ± 22)	(150 ± 47)	(484 ± 36)	(614 ± 20)	(130 ± 43)	(454 ± 31)	(566 ± 16)	(112 ± 37)	
160	(894 ± 79)	(1135 ± 55)	(241 ± 76)	(798 ± 71)	(1033 ± 40)	(235 ± 71)	(748 ± 65)	(950 ± 39)	(201 ± 70)	(695 ± 60)	(875 ± 32)	(180 ± 63)	(645 ± 50)	(805 ± 28)	(160 ± 55)	
180	(1250 ± 112)	(1452 ± 64)	(202 ± 111)	(1158 ± 111)	(1368 ± 60)	(210 ± 106)	(1089 ± 105)	(1288 ± 56)	(198 ± 105)	(958 ± 96)	(1202 ± 49)	(246 ± 97)	(890 ± 84)	(1114 ± 41)	(226 ± 85)	
200	(1705 ± 158)	(1761 ± 84)	(57 ± 160)	(1502 ± 140)	(1695 ± 79)	(182 ± 143)	(1424 ± 136)	(1636 ± 76)	(211 ± 142)	(1339 ± 130)	(1545 ± 69)	(204 ± 137)	(1277 ± 141)	(1426 ± 64)	(233 ± 158)	

*Data is expressed as (Mean ± SEM), n = 7. *p < 0.05; **p < 0.01. Repeated measures two-way ANOVA with Sidak post hoc test for multiple comparisons. Comparisons are made between the TDA and the IR subjected to the same PP. PP, pulse pressure (mmHg), TDA, thoracic descending aorta, IR, abdominal infrarenal aorta.*

and blood vessel stiffness, making the aortic tissue softer. Additionally, the magnitude of the applied pulsatile load altered the response of VSMCs to a contractile stimulus. Finally, we compared the stiffness of the TDA with that of the abdominal infrarenal aorta (AIA). Interestingly, while it is known that the AIA is a stiffer blood vessel compared to the TDA, the difference between the AIA and the TDA becomes less apparent when higher *ex vivo* pulse pressures are applied. These findings suggest that pulsatile load *ex vivo* alters the properties of aortic tissue and therefore impacts the measurement of arterial stiffness. Importantly, it was not the aim of the present study to unravel the altered molecular/biomechanical mechanisms when changing pulse pressure, but rather how manipulating this neglected parameter influences the *ex vivo* measurement of arterial stiffness. Nonetheless, these findings indicate that pulse pressure can be used as an additional variable parameter to better understand arterial stiffening in subsequent studies.

In our setup, whether a segment oscillates at a pulse pressure of 20 or 100 mmHg, both pulses happen at an equal frequency of 10 Hz. Therefore, a segment oscillating at a pulse pressure of 100 mmHg has a higher deformation rate than a segment oscillating at a pulse pressure of 20 mmHg. Our results are in agreement with previous work demonstrating that deformation rate is inversely correlated with the stiffness of (porcine) aortic segments (Delgadillo et al., 2010). Others have reported dissonant results as well. For example, pulse frequency and heart rate have been found to be positively correlated with the dynamic modulus of arteries and PWV, respectively, Bergel (1961), Learoyd and Taylor (1966), Tan et al. (2018), Spronck et al. (2021). However, most of these studies assess the effect of altered pulse frequency on arterial stiffness, which is different from this study since the pulse frequency was kept constant while the ΔP was altered to simulate different pulse pressures. Hydrogels, microtissues and whole tissues such as lung and liver are known to exhibit strain-modulated alterations in viscoelasticity, attributed to, among others, the disruption of crosslinks, protein unfolding and the movement of fluid (Chaudhuri, 2017; Barenholz-Cohen et al., 2020; Walker et al., 2020). Therefore, by applying a larger pulse pressure *ex vivo*, both the larger deformation rate and the higher strain of the aortic segments would lead to alterations in viscoelasticity, expressed as a decreased stiffness. Which viscous or elastic elements are altered in aortic tissue due to increased deformation rate, is largely unclear. In physics, it is known that increasing the strain rate decreases the viscosity of fluids. Since aortic segments are filled with fluid both intracellularly and in the extracellular matrix, follow-up research should assess how altered internal fluid movement/viscosity (due to a change in deformation rate and maximum strain) affects the stiffness of blood vessels, which is similar to the "poro-viscoelastic model" (Caccavo and Lamberti, 2017). Alternatively, while changes in viscoelasticity due to altered pulse pressure are a plausible explanation for the "softening" of the aortic segments, the presence of the Mullins effect cannot be excluded. The Mullins effect (i.e., softening after an initial deformation) has been described by others within cyclic loading of aortic tissue and differs from viscoelasticity (Sokolis, 2007; Horny et al., 2010; Sarangi, 2010; Weisbecker et al., 2013). The Mullins

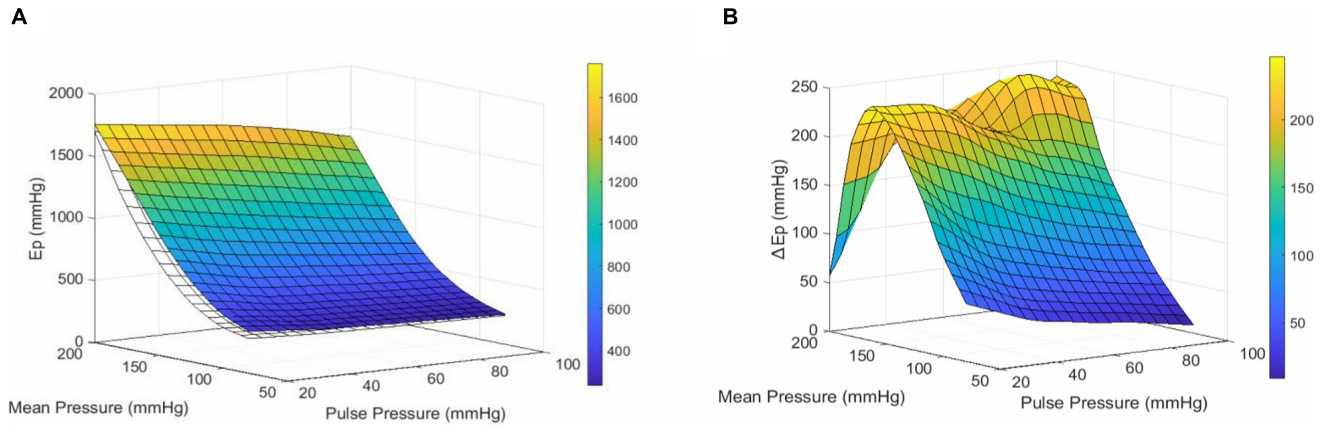

FIGURE 4 | Comparison of the stiffness-profile of the thoracic descending and abdominal infrarenal aorta. **(A)** Surface plot representing the mean Ep of the descending aorta (transparent/white) and the infrarenal aorta (colored) at different pulse & mean pressures. **(B)** Surface plot representing the mean difference in Ep (ΔEP) between the infrarenal and thoracic aorta for every pulse & mean pressure. Ep, Peterson's modulus of elasticity; ΔEP, $EP_{infrarenalaorta}$–$EP_{descendingaorta}$; PP, pulse pressure.

effect goes with residual strain and has been attributed to the interacting properties of elastin and collagen fibers (Sokolis, 2007; Horny et al., 2010; Sarangi, 2010; Weisbecker et al., 2013). To summarize, we have shown that in our setup, increasing pulse pressure softens aortic tissue, by increasing the strain rate. Accordingly, changing the cyclic pulsatile load modulates the (viscoelastic) properties of blood vessels.

Furthermore, our results suggest that contraction-induced stiffness is dependent on the pulsatile load. At lower pulse pressure, the aortic segment produces a larger response to contractile stimuli (50 mM KCl) and therefore generates a higher apparent stiffness. The opposite is true for higher pulse pressures, where a smaller increase in stiffness is observed after introducing a contractile stimulus. Interestingly, this difference is only noticeable at (relatively) low pressures, where the magnitude of the pulse pressure determines the contraction-induced stiffness. However, at pressures above 160 mmHg, there is no difference between a low or high pulse pressure, yet there is an overall difference between the contracted and uncontracted state. This indicates that at higher pressures, the effect of pulse pressure becomes inferior to the effect of pressure itself. One explanation for this phenomenon could be that the efficacy of contraction is dependent on the applied (pulsatile) strain. At low pressures (100 mmHg), the amplitude of the stretch is mainly determined by the pulse pressure. However, at high pressures (200 mmHg), the pressure itself mainly determines the maximum stretch of the aortic segment while the pulse pressure is not able to change the distension much more, causing smaller oscillations (data not shown). This rationale is in line with previously published findings, where the amplitude of the applied stretch controls intracellular calcium levels as well as the reactivity of aortic VSMCs to contractile stimuli (Monaghan et al., 2011; Hutcheson et al., 2012; Leloup et al., 2017). Moreover, mechanical stretch modulates the contractile apparatus of VSMCs, reorganizing the cytoskeleton and promoting focal adhesion (FA) growth (Halka et al., 2008; Chen et al., 2013; De, 2018; Chatterjee et al., 2019). Therefore, rapid responses to altered stretch, such as both FA kinase and ERK1/2 phosphorylation, could explain why adjusting pulse pressure *ex vivo* modulates the excitability of VSMCs toward contraction, but only at low, physiological pressures (Chen et al., 2013; Hu et al., 2014).

Besides the pronounced effect on VSMC contraction-induced stiffness, small, but significant, differences were observed upon removal of basal VSMC tonus by DEANO. Whether these small effects have any physiological relevance is unclear but should not be ruled out. Future research should investigate whether basal tonus is truly affected by pulsatile load.

In the first set of experiments, we focused on the TDA, which is mainly a very elastic artery. The TDA has an important physiological role in dampening the pressure wave generated by the left ventricle. In contrast, the AIA is generally a stiffer blood vessel, having a higher collagen to elastin ratio compared to the TDA (Bia et al., 2005; Cuomo et al., 2017). In the present study, we demonstrated *ex vivo* that the AIA is stiffer than the TDA within the same animal at pressures ranging from 80 to 140 mmHg, but only when low pulse pressures were applied (20–60 mmHg). At higher pulsatile loads, the effect was less pronounced and did not reach statistical significance, in terms of Ep. This means that increased pulsatile load differentially affects the mechanical properties of the AIA and the TDA, and, in essence, shows how *ex vivo* pulsatile load affects the comparison in stiffness between different tissues.

To date, it has not been fully elucidated what biomechanical mechanisms are modulated by *ex vivo* pulse pressure and how they translate to our observed differences and cardiovascular pathologies in general. It is generally accepted that arterial stiffness contributes to an increased pulse pressure *in vivo* (Mitchell et al., 2004, 2010; van der Bruggen M. et al., 2021). In the current work, we have investigated whether there is a reverse crosstalk between pulse pressure and artery stiffness, which is difficult to unequivocally assess *in vivo*. One study (Said et al., 2018) reported that pulse pressure is an independent predictor

of CVD mortality. Similarly, a retrospective study based on the data of the Framingham Heart Study has shown that the forward wave amplitude of the blood pressure, but not the mean arterial pressure, is associated with CVD events (Cooper et al., 2015). While these studies suggest an important role of pulsatile load in CVD, the observational design of these studies, make it difficult to determine whether these are causal relationships. On the other hand, observations in orthotopic heart transplant patients provide complementary insights. Patients equipped with a continuous-flow left ventricular assist device (LVAD) show increased aortic stiffness in the first year after transplantation, opposed to patients who received a pulsatile LVAD (Patel et al., 2017). Additionally, acute aerobic exercise, a condition in which pulse pressure is increased due to increased stroke volume, is known to increase arterial compliance (Kingwell et al., 1997; Tanaka et al., 2000; Maeda et al., 2008; Sharman and LaGerche, 2015). In general, these findings provide direct evidence that pulsatile load affects aortic properties, which is in line with our findings. Therefore, future research should investigate how (dynamic) pulsatile load affects mechanical properties of the aortic wall to enhance our understanding of blood vessel micro- and macromechanics (Bia et al., 2005).

LIMITATIONS

While the standard for measuring stiffness of arterial tissue *ex vivo* is evaluation of stress-strain relationships (Butlin et al., 2020), the nature of our ROTSAC set-up does not allow to assess vascular wall stress, since the wall thickness/cross-sectional area cannot be measured. Alternatively, the Peterson's modulus (Ep) is another, widely used, metric to evaluate blood vessel stiffness (Gosling and Budge, 2003; Santelices et al., 2007; Spronck and Humphrey, 2019). The parameters necessary to calculate Ep are easy to obtain, after translating force into pressure using the Laplace relationship. Ep integrates changes in D0 and ΔD which were both manipulated by the applied pressure protocol. Previous publications from our research group have demonstrated that Ep is a valid metric yielding similar results to other commonly used metrics for arterial stiffness (Leloup et al., 2016; De Munck et al., 2020; Bosman et al., 2021). Another limitation relates to the non-randomized order in which the mean pressures and pulse pressures were changed due to practical reasons. However, pilot experiments did not reveal significant crossover effects. Lastly, all experiments were performed at a frequency of 10 Hz, reflecting the physiological heart rate of mice. From a theoretical perspective, investigating different frequencies would be interesting but beyond the scope of the current work.

CONCLUSION

We demonstrated that pulse pressure (i.e., pulsatile load) is a valuable parameter when assessing *ex vivo* blood vessel stiffness. Altering the amplitude of the cyclic oscillations not only modulates the general stiffness of the tissue but also affects the physiological function of VSMCs. While more research is needed to investigate the mechanisms responsible for altered stiffness due to changes in pulsatile load, pulse pressure provides additional insight into the capacity of a blood vessel to resist (cyclic) deformation.

DATA AVAILABILITY STATEMENT

The original contributions presented in the study are included in the article/**Supplementary Material**, further inquiries can be directed to the corresponding author/s.

AUTHOR CONTRIBUTIONS

CN, WM, and P-JG designed the study. CN and GC performed the experiments. CN drafted the manuscript. PP, GD, WM, and P-JG critically read and revised the manuscript. All authors contributed to the article and approved the submitted version.

FUNDING

This work was supported by the University of Antwerp (GOA 33931 and DOCPRO 36663). CN and PP are fellows of the Fund for Scientific Research (FWO)-Flanders (Grant Nos. 1S24720N and 11A2620N).

ACKNOWLEDGMENTS

We are grateful to Bronwen Martin for critical reading of the manuscript. We would like to warmly thank Paul Fransen for sharing his extensive expertise on vascular biology and wish him all the best with his retirement. Paul has been the initiator of research on arterial stiffness in our laboratory and is the scientific father of the ROTSAC. During his career, Paul has been an excellent mentor for many students and has been an incredible source of scientific and personal inspiration. We will take care of your ROTSAC baby and try to continue the work you have started. We will miss you, as well as the hot coffee you prepared every morning.

SUPPLEMENTARY MATERIAL

The Supplementary Material for this article can be found online at: https://www.frontiersin.org/articles/10.3389/fphys.2021.741346/full#supplementary-material

Supplementary Figure 1 | The pulse pressure protocol. The mean pressure was increased from 80 to 200 mmHg in steps of 20 mmHg. This was done five times, with each time a different pulse pressure. The order of pulse pressures (PP) was the same between all experiments and started with a PP of 20 mmHg and ended with a PP of 100 mmHg. The same pulse pressure protocol was applied to each vessel segment in three different conditions (Krebs, KCl, and DEANO). There was a waiting period of 30 min between conditions.

Supplementary Figure 2 | Pulse pressure alters diastolic diameter (D0) and ΔP/ΔD Increasing pulse pressure decreases both **(A)** the diastolic diameter (D0)

and **(B)** the inverse of the compliance (ΔP/ΔD) which both contribute to the decrease in **(C)** Ep due to increasing pulse pressure. Data is expressed as (Mean ± SEM), $n = 7$, $^{*}p < 0.05$; $^{**}p < 0.01$; $^{***}p < 0.001$, $^{****}p < 0.0001$ Repeated measures One-Way ANOVA with Holm-Sidak *post hoc* test for multiple comparisons [data is compared to; control (= 40 mmHg)]. ΔP/ΔD, inverse of compliance; D0, Diastolic diameter; Ep, Peterson's modulus of elasticity.

Supplementary Figure 3 | The effect of VSMC contraction and basal tonus on Ep per pulse pressure. The relationship between stiffness and pressure (Ep–Mean pressure) under contracting and relaxing conditions at a pulse pressure of **(A)** 20 mmHg, **(B)** 40 mmHg, **(C)** 60 mmHg, **(D)** 80 mmHg, and **(E)** 100 mmHg. Ep, Peterson's modulus of elasticity; 50K, 50 mM KCl; PP, Pulse pressure.

REFERENCES

Avolio, A. P., Kuznetsova, T., Heyndrickx, G. R., Kerkhof, P. L. M., and Li, J. K. (2018). Arterial flow, pulse pressure and pulse wave velocity in men and women at various ages. *Adv. Exp. Med. Biol.* 1065, 153–168. doi: 10.1007/978-3-319-77932-4_10

Barenholz-Cohen, T., Merkher, Y., Haj, J., Shechter, D., Kirchmeier, D., Shaked, Y., et al. (2020). Lung mechanics modifications facilitating metastasis are mediated in part by breast cancer-derived extracellular vesicles. *Int. J. Cancer* 147, 2924–2933.

Bergel, D. H. (1961). The dynamic elastic properties of the arterial wall. *J. Physiol.* 156, 458–469. doi: 10.1113/jphysiol.1961.sp006687

Bia, D., Aguirre, I., Zócalo, Y., Devera, L., Cabrera Fischer, E., and Armentano, R. (2005). [Regional differences in viscosity, elasticity and wall buffering function in systemic arteries: pulse wave analysis of the arterial pressure-diameter relationship]. *Rev. Esp. Cardiol.* 58, 167–174. doi: 10.1016/s1885-5857(06)60360-5

Birukov, K. G. (2009). Cyclic stretch, reactive oxygen species, and vascular remodeling. *Antioxid Redox Signal.* 11, 1651–1667. doi: 10.1089/ars.2008.2390

Bosman, M., Favere, K., Neutel, C. H. G., Jacobs, G., De Meyer, G. R. Y., Martinet, W., et al. (2021). Doxorubicin induces arterial stiffness: a comprehensive in vivo and ex vivo evaluation of vascular toxicity in mice. *Toxicol. Lett.* 346, 23–33. doi: 10.1016/j.toxlet.2021.04.015

Butlin, M., Tan, I., Spronck, B., and Avolio, A. P. (2020). Measuring arterial stiffness in animal experimental studies. *Arterioscler. Thromb. Vasc. Biol.* 40, 1068–1077.

Caccavo, D., and Lamberti, G. (2017). PoroViscoElastic model to describe hydrogels' behavior. *Mater. Sci. Eng. C* 76, 102–113. doi: 10.1016/j.msec.2017.02.155

Chatterjee, A., Kondaiah, P., and Gundiah, N. (2019). Stress fiber growth and remodeling determines cellular morphomechanics under uniaxial cyclic stretch. *bioRxiv* [Preprint]. doi: 10.1101/622092

Chaudhuri, O. (2017). Viscoelastic hydrogels for 3D cell culture. *Biomater. Sci.* 5, 1480–1490. doi: 10.1039/c7bm00261k

Chen, Y., Pasapera, A. M., Koretsky, A. P., and Waterman, C. M. (2013). Orientation-specific responses to sustained uniaxial stretching in focal adhesion growth and turnover. *Proc. Natl. Acad. Sci. U.S.A.* 110, E2352–E2361.

Cooper, L. L., Rong, J., Benjamin, E. J., Larson, M. G., Levy, D., Vita, J. A., et al. (2015). Components of hemodynamic load and cardiovascular events: the Framingham Heart Study. *Circulation* 131, 354–361. discussion 61 doi: 10.1161/circulationaha.114.011357

Cox, R. H. (1974). Three-dimensional mechanics of arterial segments in vitro: methods. *J. Appl. Physiol.* 36, 381–384. doi: 10.1152/jappl.1974.36.3.381

Cuomo, F., Roccabianca, S., Dillon-Murphy, D., Xiao, N., Humphrey, J. D., and Figueroa, C. A. (2017). Effects of age-associated regional changes in aortic stiffness on human hemodynamics revealed by computational modeling. *PLoS One* 12:e0173177. doi: 10.1371/journal.pone.0173177

De, R. (2018). A general model of focal adhesion orientation dynamics in response to static and cyclic stretch. *Commun. Biol.* 1:81.

De Munck, D. G., Leloup, A. J. A., De Meyer, G. R. Y., Martinet, W., and Fransen, P. (2020). Defective autophagy in vascular smooth muscle cells increases passive stiffness of the mouse aortic vessel wall. *Pflugers Arch.* 472, 1031–1040. doi: 10.1007/s00424-020-02408-y

Delgadillo, J. O. V., Delorme, S., Mora, V., DiRaddo, R., and Hatzikiriakos, S. G. (2010). Effect of deformation rate on the mechanical properties of arteries. *J. Biomed. Sci. Eng.* 03, 123–137.

Glaser, E., Lacolley, P., Boutouyrie, P., Sacunha, R., Lucet, B., Safar, M. E., et al. (1995). Dynamic versus static compliance of the carotid artery in living Wistar-Kyoto rats. *J. Vasc. Res.* 32, 254–265. doi: 10.1159/000159100

Gosling, R. G., and Budge, M. M. (2003). Terminology for describing the elastic behavior of arteries. *Hypertension* 41, 1180–1182. doi: 10.1161/01.hyp.0000072271.36866.2a

Haghighipour, N., Tafazzoli-Shadpour, M., Shokrgozar, M. A., and Amini, S. (2010). Effects of cyclic stretch waveform on endothelial cell morphology using fractal analysis. *Artif. Organs.* 34, 481–490. doi: 10.1111/j.1525-1594.2010.01003.x

Halka, A. T., Turner, N. J., Carter, A., Ghosh, J., Murphy, M. O., Kirton, J. P., et al. (2008). The effects of stretch on vascular smooth muscle cell phenotype in vitro. *Cardiovasc. Pathol.* 17, 98–102. doi: 10.1016/j.carpath.2007.03.001

Horny, L., Gultova, E., Chlup, H., Sedlacek, R., Kronek, J., Vesely, J., et al. (eds) (2010). *Mullins Effect in Human Aorta Described With Limiting Extensibility Evolution*. Berlin: Springer Berlin Heidelberg.

Hsu, H. J., Lee, C. F., Locke, A., Vanderzyl, S. Q., and Kaunas, R. (2010). Stretch-induced stress fiber remodeling and the activations of JNK and ERK depend on mechanical strain rate, but not FAK. *PLoS One* 5:e12470. doi: 10.1371/journal.pone.0012470

Hu, B., Song, J. T., Qu, H. Y., Bi, C. L., Huang, X. Z., Liu, X. X., et al. (2014). Mechanical stretch suppresses microRNA-145 expression by activating extracellular signal-regulated kinase 1/2 and upregulating angiotensin-converting enzyme to alter vascular smooth muscle cell phenotype. *PLoS One* 9:e96338. doi: 10.1371/journal.pone.0096338

Hutcheson, J. D., Venkataraman, R., Baudenbacher, F. J., and Merryman, W. D. (2012). Intracellular Ca(2+) accumulation is strain-dependent and correlates with apoptosis in aortic valve fibroblasts. *J. Biomech.* 45, 888–894. doi: 10.1016/j.jbiomech.2011.11.031

Kingwell, B. A., Berry, K. L., Cameron, J. D., Jennings, G. L., and Dart, A. M. (1997). Arterial compliance increases after moderate-intensity cycling. *Am. J. Physiol.* 273, H2186–H2191.

Learoyd, B. M., and Taylor, M. G. (1966). Alterations with age in the viscoelastic properties of human arterial walls. *Circ. Res.* 18, 278–292. doi: 10.1161/01.res.18.3.278

Leloup, A., De Moudt, S., Van Hove, C., and Fransen, P. (2017). Cyclic stretch alters vascular reactivity of mouse aortic segments. *Front. Physiol.* 8:858. doi: 10.3389/fphys.2017.00858

Leloup, A. J., Van Hove, C. E., Kurdi, A., De Moudt, S., Martinet, W., De Meyer, G. R., et al. (2016). A novel set-up for the ex vivo analysis of mechanical properties of mouse aortic segments stretched at physiological pressure and frequency. *J. Physiol.* 594, 6105–6115. doi: 10.1113/jp272623

Leloup, A. J. A., De Moudt, S., Van Hove, C. E., Dugaucquier, L., Vermeulen, Z., Segers, V. F. M., et al. (2018). Short-term angiotensin II treatment affects large artery biomechanics and function in the absence of small artery alterations in mice. *Front. Physiol.* 9:582. doi: 10.3389/fphys.2018.00582

Leloup, A. J. A., Hove, C. E. V., Moudt, S. D., Keulenaer, G. W. D., and Fransen, P. (2020). Ex vivo aortic stiffness in mice with different eNOS activity. *Am. J. Physiol. Heart Circ. Physiol.* 318, H1233–H1244.

Leloup, A. J. A., Van Hove, C. E., De Moudt, S., De Meyer, G. R. Y., De Keulenaer, G. W., and Fransen, P. (2019). Vascular smooth muscle cell contraction and relaxation in the isolated aorta: a critical regulator of large artery compliance. *Physiol. Rep.* 7:e13934. doi: 10.14814/phy2.13934

Lénárd, Z., Fülöp, D., Visontai, Z., Jokkel, G., Reneman, R., and Kollai, M. (2000). Static versus dynamic distensibility of the carotid artery in humans. *J. Vasc. Res.* 37, 103–111. doi: 10.1159/000025721

Maeda, S., Tanabe, T., Otsuki, T., Sugawara, J., Ajisaka, R., and Matsuda, M. (2008). Acute exercise increases systemic arterial compliance after 6-month exercise training in older women. *Hypertens. Res.* 31, 377–381. doi: 10.1291/hypres.31.377

Mitchell, G. F., Parise, H., Benjamin, E. J., Larson, M. G., Keyes, M. J., Vita, J. A., et al. (2004). Changes in arterial stiffness and wave reflection with advancing

age in healthy men and women. *Hypertension* 43, 1239–1245. doi: 10.1161/01.hyp.0000128420.01881.aa

Mitchell, G. F., Wang, N., Palmisano, J. N., Larson, M. G., Hamburg, N. M., Vita, J. A., et al. (2010). Hemodynamic correlates of blood pressure across the adult age spectrum. *Circulation* 122, 1379–1386. doi: 10.1161/circulationaha.109.914507

Monaghan, K., Baker, S. A., Dwyer, L., Hatton, W. C., Sik Park, K., Sanders, K. M., et al. (2011). The stretch-dependent potassium channel TREK-1 and its function in murine myometrium. *J. Physiol.* 589(Pt 5), 1221–1233. doi: 10.1113/jphysiol.2010.203869

Naruse, K. (2018). Mechanomedicine. *Biophys. Rev.* 10, 1257–1262. doi: 10.1007/s12551-018-0459-7

Patel, A. C., Dodson, R. B., Cornwell, W. K. III, Hunter, K. S., Cleveland, J. C. Jr., Brieke, A., et al. (2017). Dynamic changes in aortic vascular stiffness in patients bridged to transplant with continuous-flow left ventricular assist devices. *JACC Heart Fail.* 5, 449–459. doi: 10.1016/j.jchf.2016.12.009

Said, M. A., Eppinga, R. N., Lipsic, E., Verweij, N., and van der Harst, P. (2018). . Relationship of arterial stiffness index and pulse pressure with cardiovascular disease and mortality. *J. Am. Heart Assoc.* 7:e007621.

Santelices, L. C., Calano, S. J., Erhart, J. C., Prantil, R. L., Haney, J. L., Vorp, D. A., et al. (2007). Experimental system for ex vivo measurement of murine aortic stiffness. *Physiol. Meas.* 28, N39–N49.

Sarangi, S. (ed.) (2010). *On the Mullins Effect of Soft-Biological Tissues: A Comparison Between Material Models with Experimental Results*. Berlin: Springer Berlin Heidelberg.

Sharman, J. E., and LaGerche, A. (2015). Exercise blood pressure: clinical relevance and correct measurement. *J. Hum. Hypertens.* 29, 351–358. doi: 10.1038/jhh.2014.84

Sokolis, D. P. (2007). Three-part passive constitutive laws for the aorta in simple elongation. *J. Med. Eng. Technol.* 31, 397–409. doi: 10.1080/03091900600700533

Spronck, B., and Humphrey, J. D. (2019). Arterial stiffness: different metrics, different meanings. *J. Biomech. Eng.* 141, 0910041–09100412.

Spronck, B., Tan, I., Reesink, K. D., Georgevsky, D., Delhaas, T., Avolio, A. P., et al. (2021). Heart rate and blood pressure dependence of aortic distensibility in rats: comparison of measured and calculated pulse wave velocity. *J. Hypertens.* 39, 117–126. doi: 10.1097/hjh.0000000000002608

Tan, I., Butlin, M., Spronck, B., Xiao, H., and Avolio, A. (2018). Effect of heart rate on arterial stiffness as assessed by pulse wave velocity. *Curr. Hypertens. Rev.* 14, 107–122.

Tan, I., Spronck, B., Kiat, H., Barin, E., Reesink, K. D., Delhaas, T., et al. (2016). Heart rate dependency of large artery stiffness. *Hypertension* 68, 236–242. doi: 10.1161/hypertensionaha.116.07462

Tanaka, H., Dinenno, F. A., Monahan, K. D., Clevenger, C. M., DeSouza, C. A., and Seals, D. R. (2000). Aging, habitual exercise, and dynamic arterial compliance. *Circulation* 102, 1270–1275. doi: 10.1161/01.cir.102.11.1270

van der Bruggen, M., Spronck, B., Bos, S., Heusinkveld, M. H. G., Taddei, S., Ghiadoni, L., et al. (2021). Pressure-corrected carotid stiffness and young's modulus: evaluation in an outpatient clinic setting. *Am. J. Hypertens.* 34, 737–743. doi: 10.1093/ajh/hpab028

van der Bruggen, M. M., Reesink, K. D., Spronck, P. J. M., Bitsch, N., Hameleers, J., Megens, R. T. A., et al. (2021). An integrated set-up for ex vivo characterisation of biaxial murine artery biomechanics under pulsatile conditions. *Sci. Rep. U. K.* 11:2671.

Vlachopoulos, C., Aznaouridis, K., and Stefanadis, C. (2010). Prediction of cardiovascular events and all-cause mortality with arterial stiffness: a systematic review and meta-analysis. *J. Am. Coll. Cardiol.* 55, 1318–1327. doi: 10.1016/j.jacc.2009.10.061

Walker, M., Rizzuto, P., Godin, M., and Pelling, A. E. (2020). Structural and mechanical remodeling of the cytoskeleton maintains tensional homeostasis in 3D microtissues under acute dynamic stretch. *Sci. Rep. U. K.* 10:7696.

Weisbecker, H., Viertler, C., Pierce, D. M., and Holzapfel, G. A. (2013). The role of elastin and collagen in the softening behavior of the human thoracic aortic media. *J. Biomech.* 46, 1859–1865. doi: 10.1016/j.jbiomech.2013.04.025

Xiao, H., Tan, I., Butlin, M., Li, D., and Avolio, A. P. (2017). Arterial viscoelasticity: role in the dependency of pulse wave velocity on heart rate in conduit arteries. *Am. J. Physiol. Heart Circ. Physiol.* 312, H1185–H1194.

Conflict of Interest: The authors declare that the research was conducted in the absence of any commercial or financial relationships that could be construed as a potential conflict of interest.

frontiers in Physiology

ORIGINAL RESEARCH
published: 24 November 2021
doi: 10.3389/fphys.2021.762586

Antihypertensive Treatment and Central Arterial Hemodynamics: A Meta-Analysis of Randomized Controlled Trials

*Yi-Bang Cheng, Jia-Hui Xia, Yan Li and Ji-Guang Wang**

Shanghai Key Laboratory of Hypertension, Department of Cardiovascular Medicine, Centre for Epidemiological Studies and Clinical Trials, National Research Centre for Translational Medicine, Ruijin Hospital, Shanghai Institute of Hypertension, Shanghai Jiao Tong University School of Medicine, Shanghai, China

Background: Antihypertensive treatment may have different effects on central arterial hemodynamics. The extent of the difference in effects between various antihypertensive drugs remains undefined.

Methods: We conducted a systematic review and meta-analysis of randomized controlled trials that explored the effects of antihypertensive agents on both central and peripheral systolic blood pressure (SBP) and pulse pressure (PP) or central augmentation index, with a special focus on the comparison between newer [renin-angiotensin-aldosterone system (RAS) inhibitors and calcium-channel blockers (CCBs)] and older antihypertensive agents (diuretics and β- and α -blockers).

Results: In total, 20 studies (n = 2,498) were included. Compared with diuretics (10 studies), β-blockers (16 studies), or an α-blocker (1 study), RAS inhibitors (21 studies), and CCBs (6 studies) more efficaciously ($P < 0.001$) reduced both central and peripheral SBP by a weighted mean difference of −5.63 (−6.50 to −4.76 mmHg) and −1.97 mmHg (−2.99 to −0.95 mmHg), respectively. Compared with older agents, the newer agents also more efficaciously ($P < 0.001$) reduced central PP (−3.27 mmHg; −4.95 to −1.59 mmHg), augmentation index (−6.11%; −7.94 to −4.29) and augmentation (−3.35 mmHg; −5.28 to –1.42 mmHg) but not peripheral PP ($p \geq 0.09$). Accordingly, the newer agents reduced central-to-peripheral PP amplification significantly less than the older agents (0.11 mmHg; 0.05 to 0.17 mmHg; $P < 0.001$).

Conclusion: Newer agents, such as RAS inhibitors and CCBs, were significantly more efficacious than older agents in their effects on central hemodynamics.

Keywords: antihypertensive treatment, central blood pressure, augmentation index, randomized controlled trial, drug

OPEN ACCESS

Edited by:
Christopher Clemens Mayer, Austrian Institute of Technology (AIT), Austria

Reviewed by:
Stefano Omboni, Istituto Italiano di Telemedicina, Italy
Enrique Rodilla, Hospital de Sagunto, Spain

****Correspondence:***
Ji-Guang Wang
jiguangwang@aim.com

Specialty section:
This article was submitted to Vascular Physiology, a section of the journal Frontiers in Physiology

Received: *22 August 2021*
Accepted: *22 October 2021*
Published: *24 November 2021*

Citation:
Cheng Y-B, Xia J-H, Li Y and Wang J-G (2021) Antihypertensive Treatment and Central Arterial Hemodynamics: A Meta-Analysis of Randomized Controlled Trials. Front. Physiol. 12:762586. doi: 10.3389/fphys.2021.762586

INTRODUCTION

When the blood flows from the central large elastic aorta to the peripheral smaller muscular arteries, systolic blood pressure (SBP) increases, without significant changes in diastolic blood pressure and mean arterial pressure, resulting in widened pulse pressure (PP). Although brachial blood pressure highly correlates with central blood pressure, substantial individual discrepancies between

the central and peripheral blood pressure exist. Several studies have shown that the association between target-organ damage and SBP and PP is stronger for the central arteries than the brachial arteries (Kollias et al., 2016). Indeed, in a meta-analysis of 11 studies that included 5,648 subjects followed up for 3.8 years, central PP showed borderline superiority to brachial PP in the prediction of cardiovascular events (Vlachopoulos et al., 2010). Similar results were obtained in at least two recent systematic reviews and meta-analyses (Li et al., 2019; Vieceli et al., 2021).

Previous studies have shown that various classes of antihypertensive drugs may have different treatment effects between the central and peripheral arterial sites and that the newer antihypertensive agents, such as renin-angiotensin-aldosterone (RAS) inhibitors and calcium-channel blockers (CCBs), might be more efficacious than the older ones, such as diuretics, β-blockers, and α-blockers in the effect on central hemodynamics. The Conduit Artery Function Evaluation (CAFE) study, a substudy of the Anglo-Scandinavian Cardiac Outcomes Trial (ASCOT), showed that treatment with amlodipine/perindopril was more efficacious than with atenolol/bendroflume thiazide in reducing central SBP and PP by 4.3 and 3.0 mmHg, respectively, despite similar reductions in the brachial arteries (Williams et al., 2006). The cardiovascular benefits of treatment with amlodipine and perindopril observed in ASCOT (Dahlöf et al., 2005) might have been resulted at least in part from the lowering of central blood pressure, although other hemodynamic effects, such as reduced blood pressure variability, might have also played a part (Rothwell et al., 2010). In fact, there is a growing interest in central blood pressure as a target of treatment in hypertension.

In this comparative meta-analysis of randomized controlled trials, we investigated the effects of the newer agents vs. older antihypertensive agents on various central hemodynamic measurements.

MATERIALS AND METHODS

Search Strategy and Selection Criteria

Our meta-analysis strictly followed the recommendations of the *Preferred Reporting Items for Systematic Reviews and Meta-Analysis: The PRISMA Statement* (Moher et al., 2009). A total of 5,158 abstracts and full-text articles were retrieved systematically from electronic databases (PubMed, Embase, and Cochrane Central Register of Controlled Trials) and searched manually on September 15, 2020. The search key terms included "central pressure," "aortic pressure," "carotid pressure," "pulse amplification," "central-to-peripheral pulse pressure ratio," "augmentation index," "antihypertensive drug," "antihypertensive treatment," and "antihypertensive agent." We limited our search to studies published in peer-reviewed journals in English. We checked the reference lists of review and original articles identified by the electronic search to find other potentially eligible studies.

The selection criteria for the inclusion of clinical trials in this meta-analysis were as follows: parallel-group randomized actively controlled trials in humans, the duration of treatment was no less than 4 weeks, and peripheral and central SBP or augmentation index after intervention were reported in a published article. Studies were excluded if the intervention was not an antihypertensive drug, or if the comparison was within the same drug class, between two newer (RAS inhibitors and CCBs) or older agents (diuretics and β- or α-blockers) or with a combination antihypertensive therapy.

Data Extraction and Quality Assessment

Data extraction was performed using predefined data fields. Variables included author name, year of publication, study design, study population, number of patients, study intervention, duration of treatment and specifications of the blood pressure measuring device and other methods for blood pressure measurement, arterial sites, and the algorithm for augmentation index estimation. Baseline and post-intervention mean values of central and peripheral hemodynamic measurements for the experimental and control groups were extracted with standard deviation (SD), standard error of mean (SEM), or 95% confidence intervals (CIs) separately.

Central hemodynamic measurements included central systolic and diastolic blood pressure (mmHg), central PP (mmHg), augmentation pressure (mmHg), and augmentation index (%). Central augmentation pressure was the absolute difference between the second peak (P2) and the first peak (P1) of the central blood pressure wave. The central augmentation index was calculated either as the ratio of the P2 to the P1, or as augmentation pressure (P2−P1) divided by PP, expressed in percent. Peripheral measurements were brachial SBP and diastolic blood pressure and PP. Central-to-peripheral PP amplification was calculated as the ratio of the central PP to the peripheral PP.

When multiple usable groups were available within an individual study, the data were counted as another study in the meta-analysis. Methodological quality was assessed using the Jadad scores (Jadad et al., 1996). Study selection, quality assessment, and data extraction were performed independently by two investigators (Y-BC and J-HX) in an unblinded standardized manner. Disagreements were resolved by negotiation or consensus with a third authoritative investigator (J-GW).

Data Analysis

For each comparison within each trial, we calculated the absolute differences between the experimental and control groups. If significant between-group differences in any outcome measure were reported at baseline, we calculated the absolute difference in the mean changes over time. The pooled effect for each grouping of trials was derived from the point estimate for each separate trial weighted by the inverse of the variance ($1/SE^2$). Heterogeneity of effect sizes was tested across trials using the χ^2 test. If trials were homogeneous ($p < 0.10$), a fixed-effects model was used to calculate pooled effect sizes. Otherwise, a random-effects model was applied to calculate overall differences. Net treatment effects on central pressure and augmentation index were determined by subtracting the mean change in the experimental group from the corresponding mean change in the

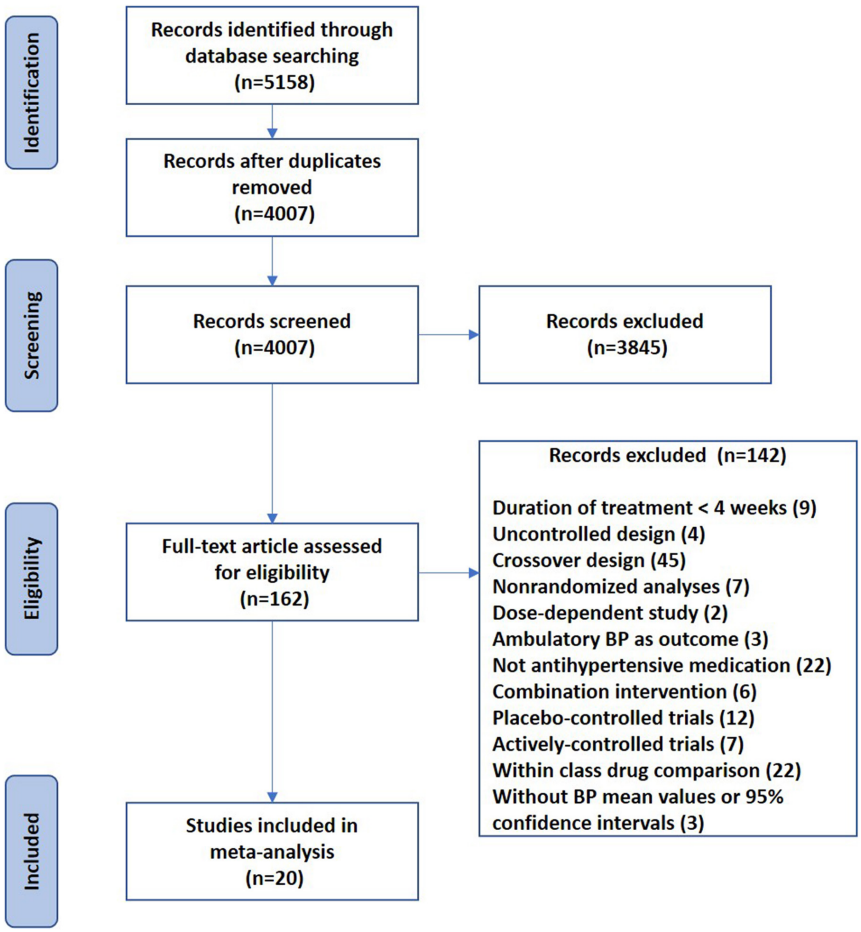

FIGURE 1 | Flow diagram of the selection procedure for studies.

control group. We performed all aforementioned computations and statistical analyses in Stata version 15 (Stata Corp LP, College Station, TX, United States). SEM was converted to SD [SE = SD/$\sqrt{}$(sample size)], and CIs were calculated [CI = mean difference ± (SEM × 1.96)], as appropriate.

Publication bias was assessed using the Egger's statistic and visual inspection of funnel plots. Potential heterogeneity was further inspected by visual inspection of the data and by subgroup and sensitivity analyses. We performed subgroup analyses based on the classes of drugs, sensitivity analyses by limiting to studies with a Jadad score of ≥3, central blood pressure *via* the radial approach with the SphygmoCor device (AtCor Medical, Sydney, NSW, Australia), and a primary diagnosis of hypertension. All *p*-values were calculated from two-tailed tests of statistical significance with a type 1 error of 5%.

RESULTS

Characteristics of the Studies

Figure 1 shows the flow diagram of the selection procedure for studies. The initial literature search retrieved 5,158 potentially eligible articles, and 4,007 records remained after removing duplicates. After having reviewed the title and abstract, 3,845 were excluded. Of the 162 full-text articles retrieved, 142 original articles were excluded for various reasons (**Figure 1**), leaving 20 eligible original articles in the analysis (Chen et al., 1995; Klingbeil et al., 2002; Ariff et al., 2006; Dart et al., 2007; Jiang et al., 2007; Schneider et al., 2008; Mackenzie et al., 2009; Matsui et al., 2009; Boutouyrie et al., 2010; Doi et al., 2010; Vitale et al., 2012; Kubota et al., 2013; Radchenko et al., 2013; Kim et al., 2014; Koumaras et al., 2014; Ghiadoni et al., 2017; Jekell et al., 2017; Miyoshi et al., 2017; Webster et al., 2017; Choi et al., 2018), comparing RAS inhibitors ($n = 21$) or CCBs ($n = 6$) with diuretics, β-blockers, or an α-blocker (**Table 1**).

These 20 trials included a total of 2,498 participants. The mean age of the study participants ranged from 35.5 (Webster et al., 2017) to 71.6 years (Dart et al., 2007), the proportion of women from 21.0% (Ghiadoni et al., 2017) to 100% (Webster et al., 2017), and the mean follow-up time from 6 (Klingbeil et al., 2002) to 52 weeks (Ariff et al., 2006). The study design was double-blinded in 10 studies, open in 9 studies, and not reported in 1 study. Central hemodynamics was estimated non-invasively from radial, carotid, and brachial applanation tonometry in 16

TABLE 1 | Trials of the renin-angiotensin-aldosterone system (RAS) inhibitors and calcium-channel blockers (CCBs) vs. diuretics, β-blockers, and α -blockers.

First author	Year	Blinding	Patients	No of patients	Treatment	Arterial site	Device	Algorithm*	Measurements	Follow-up	Jadad
ACEIs vs. diuretics											
Dart A. M.	2007	Open	HT	479	ACEI vs. diuretic	Carotid	Millar	–	cBP	4 y	3
Jiang X. J.	2007	Double	HT	101	Enalapril vs. indapamide	Radial	SphygmoCor	(P2−P1)/PP	cBP and AI	8 w	3
Mackenzie I. S.	2009	Double	HT	28	Perindopril vs. bendrofluazide	Radial	SphygmoCor	(P2−P1)/PP	cBP, AP, and AI	10 w	3
ACEIs vs. β -blockers											
Chen C. H.	1995	Double	HT	79	Fosinopril vs. atenolol	Carotid	Millar	(P2−P1)/PP	AI	8 w	2
Mackenzie I. S.	2009	Double	HT	32	Perindopril vs. atenolol	Radial	SphygmoCor	(P2−P1)/PP	cBP, AP, and AI	10 w	3
Koumaras C.	2014	Unknown	HT	37	Quinapril vs. atenolol	Radial	SphygmoCor	(P2−P1)/PP	cBP and AI	10 w	2
Koumaras C.	2014	Unknown	HT	37	Quinapril vs. nebivolol	Radial	SphygmoCor	(P2−P1)/PP	cBP and AI	10 w	2
ACEIs vs. α -blockers											
Jekell A.	2017	Double	HT	61	Doxazosin vs. ramipril	Radial	SphygmoCor	(P2−P1)/PP	cBP and AI	12 w	7
Angiotensin-receptor blockers (ARBs) vs. diuretics											
Klingbeil A. U.	2002	Double	HT	40	Valsartan vs. HCTZ	Radial	SphygmoCor	P2/P1	cBP, AP, and AI	6 w	4
ARBs vs. β -blockers											
Ariff B.	2006	Double	HT	88	Candesartan vs. atenolol	Carotid	Millar	–	cBP	52 w	3
Schneider M. P.	2008	Double	HT	156	Irbesartan vs. atenolol	Radial	SphygmoCor	(P2−P1)/PP	cBP, AP, and AI	18 m	3
Boutouyrie P.	2010	Open	HT	393	Valsartan vs. atenolol	Radial	SphygmoCor	(P2−P1)/PP	cBP and AI	24 w	5
Radchenko G. D.	2013	Open	HT	59	Losartan vs. bisoprolol	Radial	SphygmoCor	(P2−P1)/PP	cBP and AI	6 m	2
Choi M. H.	2018	Double	Ischemic stroke	70	Valsartan vs. atenolol	Radial	Omron	(P2−P1)/PP	cBP and AI	12 w	4
Choi M. H.	2018	Double	Ischemic stroke	70	Fimasartan vs. atenolol	Radial	Omron	(P2−P1)/PP	cBP and AI	12 w	4
Kim E. J.	2014	Open	HT	182	Losartan vs. carvedilol	Radial	Hanbyul Meditech	(P2−P1)/PP	cBP and AI	24 w	5
Vitale C.	2012	Double	HT	65	Irbesartan vs. nebivolol	Radial	SphygmoCor	(P2−P1)/PP	cBP and AI	8 w	5
Renin inhibitors vs. diuretics											
Kubota Y.	2013	Open	HT	30	Aliskiren vs. HCTZ	Radial	Omron	P2/P1	cBP and AI	12 w	2
Miyoshi T.	2017	Open	HT	97	Aliskiren vs. trichlormethiazide	Radial	Omron	P2/P1	cBP and AI	24 w	5
Renin inhibitors vs. β -blockers											
Koumaras C.	2014	Unknown	HT	35	Aliskiren vs. atenolol	Radial	SphygmoCor	(P2−P1)/PP	cBP and AI	10 w	2
Koumaras C.	2014	Unknown	HT	35	Aliskiren vs. nebivolol	Radial	SphygmoCor	(P2−P1)/PP	cBP and AI	10 w	2
CCBs vs. diuretics											
Mackenzie I. S.	2009	Double	HT	27	Lercanidipine vs. bendrofluazide	Radial	SphygmoCor	(P2−P1)/PP	cBP, AP, and AI	10 w	4
Matsui Y.	2009	Open	HT	207	Azelnidipine vs. HCTZ	Radial	SphygmoCor	(P2−P1)/PP	cBP, AP, and AI	24 w	3
Doi M.	2010	Open	HT	37	Azelnidipine vs. trichlormethiazide	Radial	Omron	P2/P1	cBP and AI	6 m	3
Ghiadoni L.	2017	Open	Metabolic syndrome	76	Lercanidipine vs. HCTZ	Radial	SphygmoCor	(P2−P1)/PP@HR75	cBP, AP, and AI	24 w	3
CCBs vs. β -blockers											
Mackenzie I. S.	2009	Double	HT	31	Lercanidipine vs. atenolol	Radial	SphygmoCor	(P2−P1)/PP	cBP, AP, and AI	10 w	3
Webster L. M.	2017	Open	HT in pregnancy	112	Nifedipine vs. labetalol	Brachial	Arteriograph	(P2−P1)/PP	cBP and AI	130 d	2

*Studies are listed in the order of the year of publication per category. *Augmentation index was calculated either by the ratio of the second peak (P2) to the first peak (P1) of the central blood pressure wave or by augmentation pressure (P2−P1) divided by PP, expressed in percent. @HR75 indicated that the augmentation index was adjusted by heart rate at 75 bpm. d, days; w, weeks; m, months; y, years; HT, hypertension; HCTZ, hydrochlorothiazide; cBP, central blood pressure; AP, augmentation pressure; AI, augmentation index.*

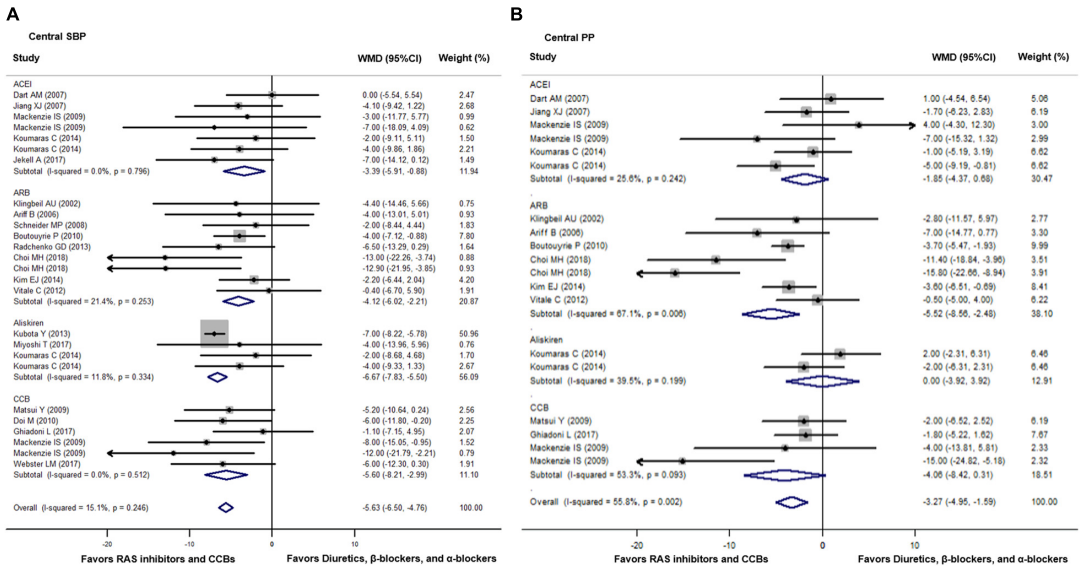

FIGURE 2 | Effect of angiotensin-converting enzyme inhibitors (ACEIs), angiotensin-receptor blockers (ARBs), renin inhibitors, and calcium-channel blockers (CCBs) vs. diuretics, β-blockers, and α-blockers on central systolic blood pressure (SBP, **A**) and pulse pressure (PP, **B**). Weights are from the fixed **(A)** and random **(B)** effects analyses. RAS indicates renin-angiotensin-aldosterone system. Dots represent mean difference of each study. The size of the squares is proportional to the sample size. Horizontal lines represent the 95% confidence intervals (CI). Open diamonds represent the weighted mean difference (WMD) with 95% CI.

studies, 3 studies, and 1 study, respectively. Radial tonometry was performed using the SphygmoCor device (n = 11), (Omron Healthcare, Kyoto, Japan) (n = 4), or (Hanbyul Meditech, Jeonju, Korea) (n = 1).

Renin-Angiotensin-Aldosterone System Inhibitors and Calcium-Channel Blockers vs. Diuretics, β-Blockers, and α-Blockers

In total, we performed analyses in 20 trials with 1,250 and 1,248 participants in the treatment groups of newer and older antihypertensive drugs, respectively (**Table 1**). Newer antihypertensive agents consisted of an ACEI in eight trials (n = 854), an ARB in nine trials (n = 1,123), a renin inhibitor in four trials (n = 197), and a CCB in six trials (n = 490).

Compared with diuretics (n = 10), β-blockers (n = 16), or an α-blocker (n = 1), the weighted mean differences in the central SBP were statistically significant for ACEIs (n = 7) by −3.39 mmHg (−5.91 to −0.89, p = 0.008), for ARBs (n = 9) by −4.12 mmHg (−6.02 to −2.21, $p < 0.001$), for renin inhibitors (n = 4) by −6.67 mmHg (−7.83 to −5.50, $p < 0.001$), and for CCBs (n = 6) by −5.60 mmHg (−8.21 to −2.99, $p < 0.001$). No significant heterogeneity was noticed within all four classes of newer drugs ($p \geq 0.24$). The overall weighted mean difference in the central SBP across all 20 trials was −5.63 mmHg (−6.50 to −4.76, $p < 0.001$; I^2 = 15.1%, P for heterogeneity = 0.25). The weighted mean differences in central PP were statistically significant for ARBs (n = 7) by −5.52 mmHg (−8.56 to −2.48, p = 0.006) but not significant for ACEIs (n = 6), renin inhibitors (n = 2), or CCBs (n = 4, $p \geq 0.07$). The overall weighted mean difference in central PP across 12 studies with data was −3.27 mmHg (−4.95 to −1.59, $p < 0.001$; I^2 = 55.8%, P for heterogeneity = 0.002, **Figure 2**).

Compared with diuretics (n = 9), β-blockers (n = 15), or an α-blocker (n = 1), the weighted mean differences in the central augmentation index were statistically significant for ACEIs (n = 7) by −4.89% (−7.28 to −2.50, p = 0.001), for ARBs (n = 8) by −9.20% (−12.54 to −5.86, $p < 0.001$), and for CCBs (n = 6) by −5.27% (−9.14 to −1.40, p = 0.008). The overall weighted mean difference in the central augmentation index across 18 studies with data was −6.11% (−7.94 to −4.29, $p < 0.001$; I^2 = 67.5%, P for heterogeneity < 0.001, **Figure 3**). In addition, across five trials with data, the overall weighted mean difference in the central augmentation pressure was −3.35 mmHg (−5.28 to −1.42, $p < 0.001$; I^2 = 55.7%, P for heterogeneity = 0.03, **Figure 4**).

With regard to peripheral measurements, the weighted mean difference was significant for SBP across 19 trials by −1.97 mmHg (−2.99 to −0.95, $p < 0.001$; I^2 = 0.0%, P for heterogeneity = 0.67), but not for PP across 9 studies [−0.90 mmHg (−1.92 to 0.13 mmHg), p = 0.09; I^2 = 25.8%, P for heterogeneity = 0.16, **Supplementary Figure 1**].

Compared with diuretics (n = 3) or β-blockers (n = 4), the overall weighted mean differences in central-to-peripheral PP amplification were significantly smaller across four trials with either ACEIs (n = 2), ARBs (n = 2), or CCBs (n = 3) by 0.11 mmHg (0.05 to 0.17, $p < 0.001$; I^2 = 54.3%, P for heterogeneity = 0.041, **Figure 5**).

Publication Bias and Sensitivity Analysis

No publication bias was suggested by visual inspection of funnel plot in reporting changes in central SBP (**Figure 6**, the Egger's test, $p \geq 0.08$).

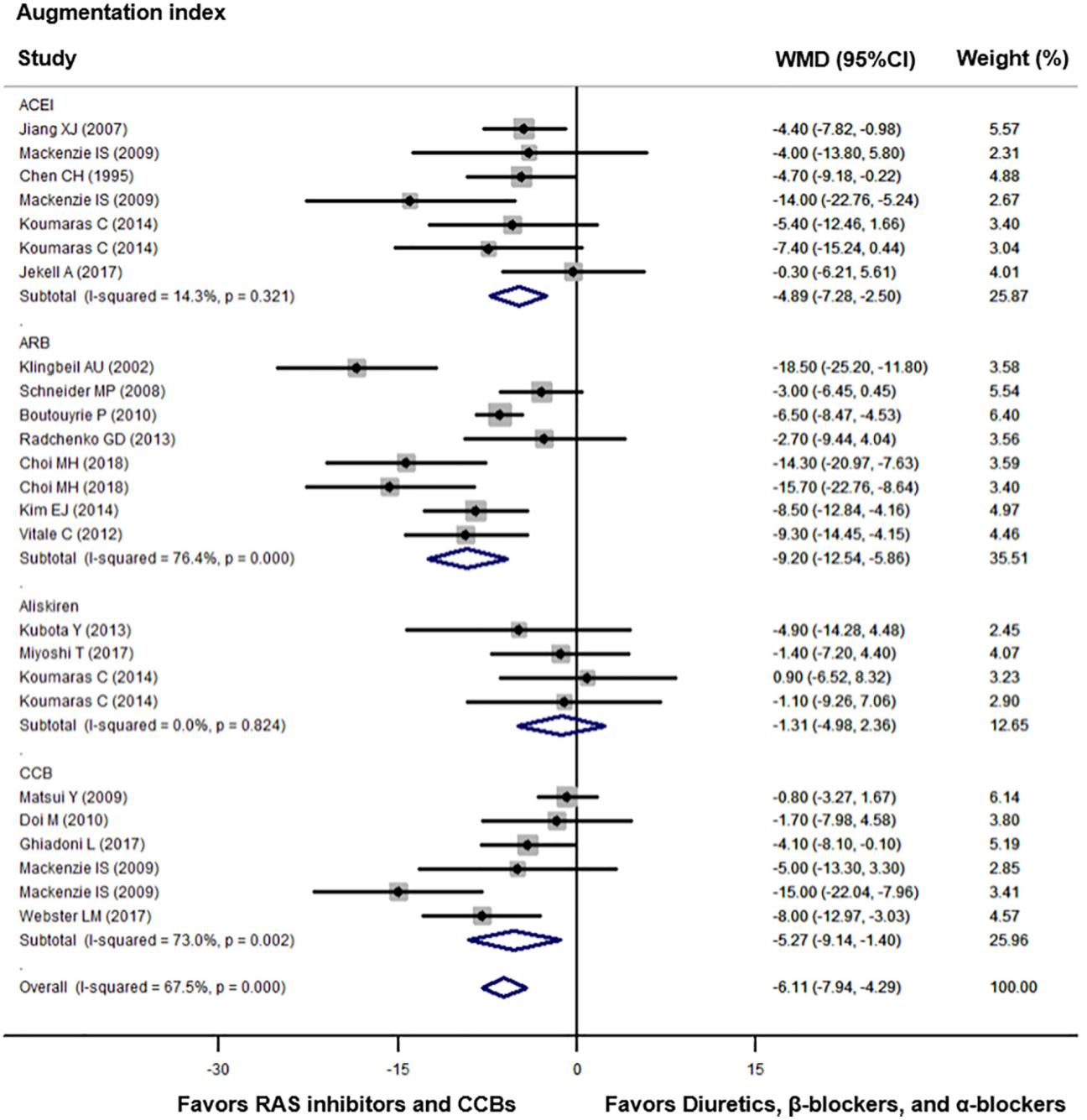

FIGURE 3 | Effect of angiotensin-converting enzyme inhibitors (ACEIs), angiotensin-receptor blockers (ARBs), renin inhibitors, and calcium-channel blockers (CCBs) vs. diuretics, β-blockers, and α-blockers on central augmentation index. Weights are from the random-effects analysis. For further details, see legends in **Figure 2**.

We also repeated analyses in subgroups according to the prespecified characteristics. In these subgroup analyses, the weighted mean differences were in agreement with the overall results (**Supplementary Table 1**).

When the trials of diuretics (n = 10) and β-blockers (n = 16) were compared, these older antihypertensive drugs behaved similar to the effects on the central SBP (n = 25) and peripheral SBP and PP (n = 24, $p \geq 0.17$), but different to the effects on central PP (n = 19), central-to-peripheral PP amplification (n = 7), and central augmentation index (n = 24) in favor of β-blockers ($p \leq 0.002$, **Supplementary Table 2**). Furthermore, when the trials of vasodilating (n = 4) and non-vasodilating β-blockers (n = 12) were compared, these two classes of β-blockers did not show significant difference in the effects on central and peripheral arterial hemodynamics ($p \geq 0.15$, **Supplementary Table 3**).

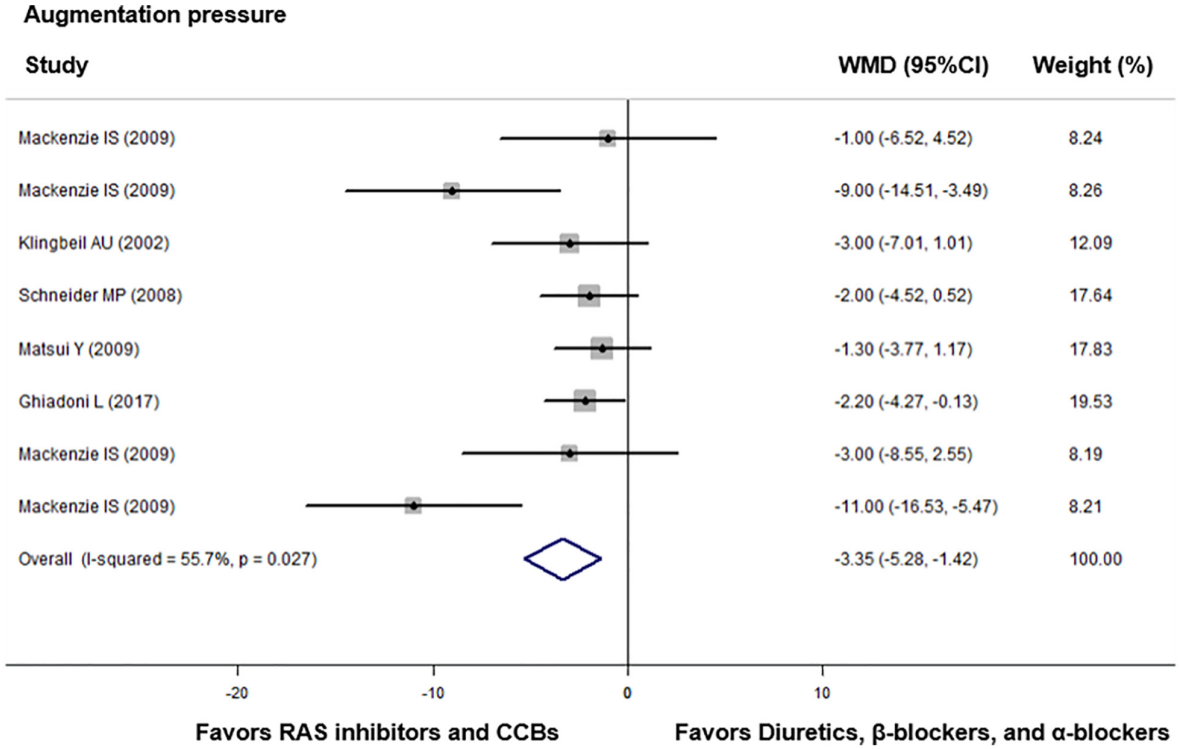

FIGURE 4 | Effect of angiotensin-converting enzyme inhibitors (ACEIs), angiotensin-receptor blockers (ARBs), renin inhibitors, and calcium-channel blockers (CCBs) vs. diuretics, β-blockers, and α-blockers on central augmentation pressure. Weights are from the fixed-effects analysis. For further details, see legends in **Figure 2**.

DISCUSSION

This meta-analysis showed the differential effects of various antihypertensive drug classes on central hemodynamics. These results might help explain why some antihypertensive drugs, such as the β-blocker atenolol, were less efficacious in reducing the risk of stroke and cardiovascular mortality (Carlberg et al., 2004; McEniery, 2009), although it is generally believed that blood pressure reduction *per se* matters more than the choice of antihypertensive agents.

London et al. (1994) first conducted a controlled, blinded study to compare perindopril and nitrendipine in patients on chronic hemodialysis with a focus on central hemodynamic effects of vasoactive antihypertensive agents. The results showed that 12 months of treatment with ACEI and CCB had similar effects on augmentation index and carotid blood pressure. The following REASON study (Asmar et al., 2001) revealed in 471 hypertensive participants who were followed for 12 months that the combination of indapamide and perindopril decreased brachial SBP and PP more significantly than atenolol, with an adjusted between-group difference of −6.02 (95% CI, −8.90 to −3.14) and −5.57 mmHg (95% CI, −7.70 to −3.44), respectively. Similar adjusted between-group differences were observed for central SBP [−12.52 mmHg (95% CI, −17.97 to −7.08)] and PP [−10.34 mmHg (95% CI, −14.12 to −6.56)], and for carotid [−5.57% (95% CI, −10.77 to −0.36)] and aortic augmentation indices [−5.17% (95% CI, −7.74 to −2.61)].

A series of subsequent studies revealed a discrepancy in antihypertensive treatment on central and peripheral blood pressure. In a meta-analyses of 24 trials, Manisty and Hughes (2013) reported that treatment with β-blockers and diuretics posed a significantly less reduction in the central SBP than the brachial SBP by 6.9 and 6.8 mmHg, respectively, whereas other agents of monotherapy similarly lowered central and brachial SBP. Similar results were confirmed by McGaughey et al. (2016) in another meta-analyses of 52 studies with 4,381 participants and 58 studies with 3,716 participants for central SBP and augmentation index, respectively. Fifteen of the included studies had a crossover design, and 46 studies had a parallel group comparison design. Overall, antihypertensive drugs reduced brachial SBP more than central SBP by 2.52 mmHg, which was mainly attributed to the 5.19 mmHg greater reduction in the central-to-brachial amplification observed in β-blockers. Moreover, a significant reduction in the augmentation index was seen with RAS inhibitors, CCBs, and diuretics, but not β-blockers or α-blockers.

Both of the aforementioned meta-analyses were based on summary statistics instead of individual-subject data. The calculated differences in brachial and central SBP were less standardized in statistical analysis, such as adjustment for confounding factors. We tabulated head-to-head comparisons of various antihypertensive drugs regarding the effect on arterial hemodynamics. Despite similar reductions in peripheral PP, RAS inhibitors, and CCBs were more effective in reducing

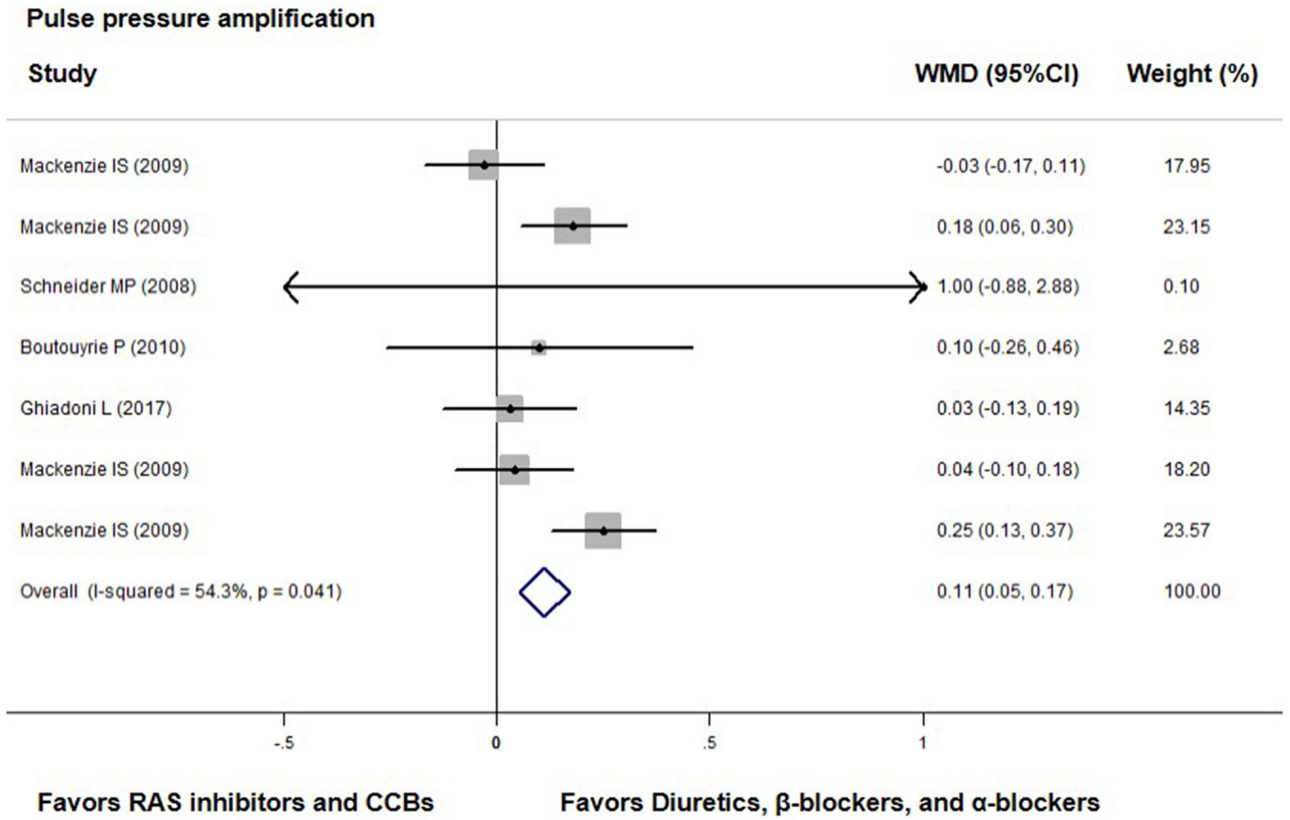

FIGURE 5 | Effect of angiotensin-converting enzyme inhibitors (ACEIs), angiotensin-receptor blockers (ARBs), renin inhibitors, and calcium-channel blockers (CCBs) vs. diuretics, β-blockers, and α-blockers on central-to-peripheral pulse pressure amplification. Weights are from the fixed-effects analysis. For further details, see legends in **Figure 2**.

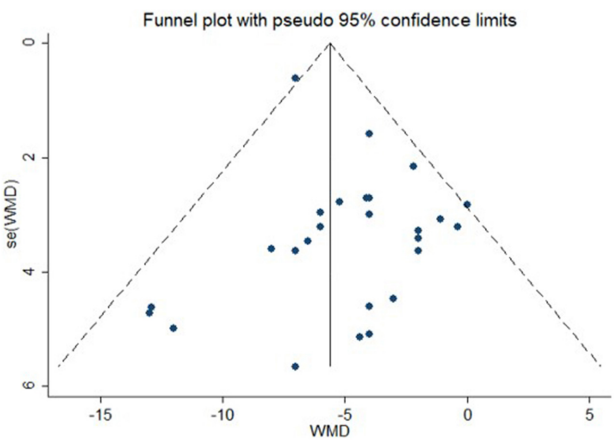

FIGURE 6 | Funnel plot with pseudo 95% confidence limits for publication bias of actively controlled studies on central systolic blood pressure. WMD indicates weighted mean difference.

central PP than diuretics, β-blockers, and α-blockers. Newer antihypertensive agents significantly reduced more central blood pressure and augmentation than older agents.

The mechanisms for these differential treatment effects on central hemodynamics remain under investigation. As non-vasodilating β-blockers showed much less central blood pressure-lowering effect than the other classes of antihypertensive drugs, heart rate and vascular dilation or constriction must play a major role in the regulation of central hemodynamics. Indeed, in a meta-regression analysis (Ding et al., 2013), we previously found that slowing heart rate may to a large extent explain the less efficacy of β-blockers vs. the other classes of antihypertensive drugs. Although not shown in our present meta-analysis probably because of a limited number of trials, the vasoactive property must also play an important part in the central hemodynamic regulation. Indeed, a previous head-to-head comparison study showed divergent effects between vasodilating (nebivolol) and non-vasodilating (atenolol) β-blockers (Redón et al., 2014). Studies on the I_f inhibitor ivabradine provided further evidence. In a randomized, double-blind placebo-controlled, crossover study (Dillinger et al., 2015) in 12 patients with stable coronary artery disease, normal blood pressure, a sinus heart rate ≥70 beats per minute and β-blocker therapy, ivabradine treatment for 3 weeks reduced heart rate (−15.8 ± 7.7 vs. 0.3 ± 5.8 beats per minute, p = 0.001) and increased left ventricular ejection time (18.5 ± 17.8 vs. 2.8 ± 19.3 ms, p = 0.074) and diastolic perfusion time (215.6 ± 105.3 vs. −3.0 ± 55.8 ms,

p = 0.0005), but did not significantly increase central SBP (−4.0 ± 9.6 vs. 2.4 ± 12.0 mmHg, p = 0.13) or augmentation index (−0.8% ± 10.0% vs. 0.3% ± 7.6%, p = 0.87). Taken together, it is probably the interaction between heart rate and vasoactive property that determines the extent of central pressure augmentation from wave reflections. This hypothesis may be tested in future animal experiments as well as human research. In addition, thiazide diuretics might be different in the central hemodynamic effects, for instance, between the so-called thiazide-type and thiazide-like diuretics. However, the present analysis did not allow us to perform this comparison because the thiazide-like diuretic was only used in one of the nine studies.

A major limitation of our meta-analysis was that two recent studies on an even newer antihypertensive drug class, i.e., angiotensin receptor neprilysin inhibitor (ARNI), were not included, because the comparative drug was an ARB (Schmieder et al., 2017; Williams et al., 2017), which was defined as a newer agent in the present analysis. In the PARAMETER (The Prospective comparison of Angiotensin Receptor neprilysin inhibitor with Angiotensin receptor blocker MEasuring arterial sTiffness in the eldERly) study, sacubitril/valsartan reduced central aortic systolic pressure (primary outcome) greater than olmesartan [between-treatment difference: −3.7 mmHg (95% CI, −6.4 to −0.9), p = 0.01] after 12 weeks of treatment but not after 52 weeks of treatment, probably because more subjects in the olmesartan group required add-on antihypertensive therapy than in the sacubitril/valsartan group (47% vs. 32%, $p < 0.002$). Indeed, Schmieder found that sacubitril/valsartan reduced central aortic PP to a greater extent than olmesartan (−3.5 mmHg, p = 0.01) after 52 weeks of treatment, with similar add-on treatment of amlodipine in the two groups (17.5% vs. 29.8%, p = 0.12). These observations shed some light on the potential beneficial effect of novel antihypertensive agents on central hemodynamics.

CONCLUSION

Antihypertensive drug treatment with RAS inhibitors and CCBs was more efficacious than that with diuretics, β-blockers, and α-blockers in the central hemodynamic effects. At present, there is still no direct evidence regarding the clinical relevance of central hemodynamics for decision-making in the management of hypertension and cardiovascular prevention. Therefore, it is imperative to run adequately powered outcome trials to investigate whether central hemodynamic measurements are clinically useful in guiding antihypertensive treatment and other cardiovascular therapeutic approaches for the prevention of cardiovascular events.

DATA AVAILABILITY STATEMENT

The original contributions presented in the study are included in the article/**Supplementary Material**, further inquiries can be directed to the corresponding author/s.

AUTHOR CONTRIBUTIONS

J-GW and Y-BC conceived the study, performed the statistical analyses, and prepared the first draft of the manuscript. Y-BC and J-HX coordinated the data extraction. All authors participated in the interpretation of the data and approved the final version of the manuscript.

FUNDING

This study investigators were financially supported by grants from the National Natural Science Foundation of China (91639203, 81770455, 82070432, and 82070435), Ministry of Science and Technology (2018YFC1704902), and Ministry of Health (2016YFC0900902), Beijing, China, from the Shanghai Commissions of Science and Technology (grant 19DZ2340200 and "Sailing Program" 19YF1441000), and Health ("Three-Year Action Program of Shanghai Municipality for Strengthening the Construction of Public Health System" GWV-10.1-XK05 and a special grant for "leading academics"), Shanghai, China, and from the Clinical Research Program, Ruijin Hospital, Shanghai Jiao Tong University School of Medicine (grant 2018CR010), Shanghai, China.

SUPPLEMENTARY MATERIAL

The Supplementary Material for this article can be found online at: https://www.frontiersin.org/articles/10.3389/fphys.2021.762586/full#supplementary-material

REFERENCES

Ariff, B., Zambanini, A., Vamadeva, S., Barratt, D., Xu, Y., Sever, P., et al. (2006). Candesartan- and atenolol-based treatments induce different patterns of carotid artery and left ventricular remodeling in hypertension. *Stroke* 37, 2381–2384. doi: 10.1161/01.STR.0000236839.69658.c5

Asmar, R. G., London, G. M., O'Rourke, M. E., Mallion, J. M., Romero, R., Rahn, K. H., et al. (2001). Amelioration of arterial properties with a perindopril-indapamide very-low-dose combination. *J. Hypertens. Suppl.* 19, S15–S20.

Boutouyrie, P., Achouba, A., Trunet, P., Laurent, S., and Group, E. T. (2010). Amlodipine-valsartan combination decreases central systolic blood pressure more effectively than the amlodipine-atenolol combination: the explor study. *Hypertension* 55, 1314–1322. doi: 10.1161/HYPERTENSIONAHA.109.148999

Carlberg, B., Samuelsson, O., and Lindholm, L. H. (2004). Atenolol in hypertension: is it a wise choice? *Lancet* 364, 1684–1689. doi: 10.1016/S0140-6736(04)17355-8

Chen, C. H., Ting, C. T., Lin, S. J., Hsu, T. L., Yin, F. C., Siu, C. O., et al. (1995). Different effects of fosinopril and atenolol on wave reflections in hypertensive patients. *Hypertension* 25, 1034–1041. doi: 10.1161/01.hyp.25.5.1034

Choi, M. H., Lee, J. S., Lee, S. E., Lee, S. J., Yoon, D., Park, R. W., et al. (2018). Central and cerebral haemodynamic changes after antihypertensive therapy in ischaemic stroke patients: a double-blind randomised trial. *Sci. Rep*. 8:1556. doi: 10.1038/s41598-018-19998-4

Dahlöf, B., Sever, P. S., Poulter, N. R., Wedel, H., Beevers, D. G., Caulfield, M., et al. (2005). Prevention of cardiovascular events with an antihypertensive regimen of amlodipine adding perindopril as required versus atenolol adding bendroflumethiazide as required, in the anglo-scandinavian cardiac outcomes trial-blood pressure lowering Arm (ASCOT-BPLA): a multicentre randomised controlled trial. *Lancet* 366, 895–906. doi: 10.1016/S0140-6736(05)67185-1

Dart, A. M., Cameron, J. D., Gatzka, C. D., Willson, K., Liang, Y. L., Berry, K. L., et al. (2007). Similar effects of treatment on central and brachial blood pressures in older hypertensive subjects in the second australian national blood pressure trial. *Hypertension* 49, 1242–1247. doi: 10.1161/HYPERTENSIONAHA.106.085803

Dillinger, J. G., Maher, V., Vitale, C., Henry, P., Logeart, D., Manzo Silberman, S., et al. (2015). Impact of ivabradine on central aortic blood pressure and myocardial perfusion in patients with stable coronary artery disease. *Hypertension* 66, 1138–1144. doi: 10.1161/HYPERTENSIONAHA.115.06091

Ding, F. H., Li, Y., Li, L. H., and Wang, J. G. (2013). Impact of heart rate on central hemodynamics and stroke: a meta-analysis of beta-blocker trials. *Am. J. Hypertens.* 26, 118–125. doi: 10.1093/ajh/hps003

Doi, M., Miyoshi, T., Hirohata, S., Kamikawa, S., Usui, S., Kaji, Y., et al. (2010). Combination therapy of calcium channel blocker and angiotensin II receptor blocker reduces augmentation index in hypertensive patients. *Am. J. Med. Sci.* 339, 433–439. doi: 10.1097/MAJ.0b013e3181d658c4

Ghiadoni, L., Bruno, R. M., Cartoni, G., Stea, F., Magagna, A., Virdis, A., et al. (2017). Combination therapy with lercanidipine and enalapril reduced central blood pressure augmentation in hypertensive patients with metabolic syndrome. *Vascul. Pharmacol.* 92, 16–21. doi: 10.1016/j.vph.2015.06.004

Jadad, A. R., Moore, R. A., Carroll, D., Jenkinson, C., Reynolds, D. J., Gavaghan, D. J., et al. (1996). Assessing the quality of reports of randomized clinical trials: is blinding necessary? *Control Clin. Trials* 17, 1–12. doi: 10.1016/0197-2456(95)00134-4

Jekell, A., Kalani, M., and Kahan, T. (2017). The effects of alpha 1-adrenoceptor blockade and angiotensin converting enzyme inhibition on central and brachial blood pressure and vascular reactivity: the doxazosin-ramipril study. *Heart Vessels* 32, 674–684. doi: 10.1007/s00380-016-0924-9

Jiang, X. J., O'Rourke, M. F., Zhang, Y. Q., He, X. Y., and Liu, L. S. (2007). Superior effect of an angiotensin-converting enzyme inhibitor over a diuretic for reducing aortic systolic pressure. *J. Hypertens.* 25, 1095–1099. doi: 10.1097/HJH.0b013e3280ac1533

Kim, E. J., Song, W. H., Lee, J. U., Shin, M. S., Lee, S., Kim, B. O., et al. (2014). Efficacy of losartan and carvedilol on central hemodynamics in hypertensives: a prospective, randomized, open, blinded end point, multicenter study. *Hypertens. Res.* 37, 50–56. doi: 10.1038/hr.2013.112

Klingbeil, A. U., John, S., Schneider, M. P., Jacobi, J., Weidinger, G., and Schmieder, R. E. (2002). AT1-receptor blockade improves augmentation index: a double-blind, randomized, controlled study. *J. Hypertens.* 20, 2423–2428. doi: 10.1097/00004872-200212000-00022

Kollias, A., Lagou, S., Zeniodi, M. E., Boubouchairopoulou, N., and Stergiou, G. S. (2016). Association of central versus brachial blood pressure with target-organ damage: systematic review and meta-analysis. *Hypertension* 67, 183–190. doi: 10.1161/HYPERTENSIONAHA.115.06066

Koumaras, C., Tziomalos, K., Stavrinou, E., Katsiki, N., Athyros, V. G., Mikhailidis, D. P., et al. (2014). Effects of renin-angiotensin-aldosterone system inhibitors and beta-blockers on markers of arterial stiffness. *J. Am. Soc. Hypertens.* 8, 74–82. doi: 10.1016/j.jash.2013.09.001

Kubota, Y., Takahashi, H., Asai, K., Yasutake, M., and Mizuno, K. (2013). The influence of a direct renin inhibitor on the central blood pressure. *J. Nippon Med. Sch.* 80, 25–33. doi: 10.1272/jnms.80.25

Li, W. F., Huang, Y. Q., and Feng, Y. Q. (2019). Association between central haemodynamics and risk of all-cause mortality and cardiovascular disease: a systematic review and meta-analysis. *J. Hum. Hypertens.* 33, 531–541. doi: 10.1038/s41371-019-0187-x

London, G. M., Pannier, B., Guerin, A. P., Marchais, S. J., Safar, M. E., and Cuche, J. L. (1994). Cardiac hypertrophy, aortic compliance, peripheral resistance, and wave reflection in end-stage renal disease. Comparative effects of ACE inhibition and calcium channel blockade. *Circulation* 90, 2786–2796. doi: 10.1161/01.cir.90.6.2786

Mackenzie, I. S., McEniery, C. M., Dhakam, Z., Brown, M. J., Cockcroft, J. R., and Wilkinson, I. B. (2009). Comparison of the effects of antihypertensive agents on central blood pressure and arterial stiffness in isolated systolic hypertension. *Hypertension* 54, 409–413. doi: 10.1161/HYPERTENSIONAHA.109.133801

Manisty, C. H., and Hughes, A. D. (2013). Meta-analysis of the comparative effects of different classes of antihypertensive agents on brachial and central systolic blood pressure, and augmentation index. *Br. J. Clin. Pharmacol.* 75, 79–92. doi: 10.1111/j.1365-2125.2012.04342.x

Matsui, Y., Eguchi, K., O'Rourke, M. F., Ishikawa, J., Miyashita, H., Shimada, K., et al. (2009). Differential effects between a calcium channel blocker and a diuretic when used in combination with angiotensin II receptor blocker on central aortic pressure in hypertensive patients. *Hypertension* 54, 716–723. doi: 10.1161/HYPERTENSIONAHA.109.131466

McEniery, C. M. (2009). Antihypertensive drugs and central blood pressure. *Curr. Hypertens. Rep.* 11, 253–259. doi: 10.1007/s11906-009-0043-4

McGaughey, T. J., Fletcher, E. A., and Shah, S. A. (2016). Impact of antihypertensive agents on central systolic blood pressure and augmentation index: a meta-analysis. *Am. J. Hypertens.* 29, 448–457. doi: 10.1093/ajh/hpv134

Miyoshi, T., Murakami, T., Sakuragi, S., Doi, M., Nanba, S., Mima, A., et al. (2017). Comparable effect of aliskiren or a diuretic added on an angiotensin II receptor blocker on augmentation index in hypertension: a multicentre, prospective, randomised study. *Open Heart* 4:e000591. doi: 10.1136/openhrt-2017-000591

Moher, D., Liberati, A., Tetzlaff, J., Altman, D. G., and Group, P. (2009). Preferred reporting items for systematic reviews and meta-analyses: the PRISMA statement. *Ann. Intern. Med.* 151, 264–9, W64. doi: 10.7326/0003-4819-151-4-200908180-00135

Radchenko, G. D., Sirenko, Y. M., Kushnir, S. M., Torbas, O. O., and Dobrokhod, A. S. (2013). Comparative effectiveness of a fixed-dose combination of losartan + HCTZ versus bisoprolol + HCTZ in patients with moderate-to-severe hypertension: results of the 6-month ELIZA trial. *Vasc. Health Risk Manag.* 9, 535–549. doi: 10.2147/VHRM.S44568

Redón, J., Pascual-Izuel, J. M., Rodilla, E., Vicente, A., Oliván, J., Bonet, J., et al. (2014). Effects of nebivolol and atenolol on central aortic pressure in hypertensive patients: a multicenter, randomized, double-blind study. *Blood Press* 23, 181–188. doi: 10.3109/08037051.2013.840421

Rothwell, P. M., Howard, S. C., Dolan, E., O'Brien, E., Dobson, J. E., Dahlöf, B., et al. (2010). Prognostic significance of visit-to-visit variability, maximum systolic blood pressure, and episodic hypertension. *Lancet* 375, 895–905. doi: 10.1016/S0140-6736(10)60308-X

Schmieder, R. E., Wagner, F., Mayr, M., Delles, C., Ott, C., Keicher, C., et al. (2017). The effect of sacubitril/valsartan compared to olmesartan on cardiovascular remodelling in subjects with essential hypertension: the results of a randomized, double-blind, active-controlled study. *Eur. Heart J.* 38, 3308–3317. doi: 10.1093/eurheartj/ehx525

Schneider, M. P., Delles, C., Klingbeil, A. U., Ludwig, M., Kolloch, R. E., Krekler, M., et al. (2008). Effect of angiotensin receptor blockade on central haemodynamics in essential hypertension: results of a randomised trial. *J. Renin Angiotensin Aldosterone Syst.* 9, 49–56. doi: 10.3317/jraas.2008.003

Vieceli, T., Brambilla, B., Pereira, R. Q., Dellamea, B. S., Stein, A. T., and Grezzana, G. B. (2021). Prediction of all-cause and cardiovascular mortality using central hemodynamic indices among elderly people: systematic review and meta-analysis. *Sao Paulo Med. J.* 139, 123–126. doi: 10.1590/1516-3180.2020.0364.R1.0412020

Vitale, C., Marazzi, G., Iellamo, F., Spoletini, I., Dall'Armi, V., Fini, M., et al. (2012). Effects of nebivolol or irbesartan in combination with hydrochlorothiazide on vascular functions in newly-diagnosed hypertensive patients: the NINFE (Nebivololo, Irbesartan Nella Funzione Endoteliale) study. *Int. J. Cardiol.* 155, 279–284. doi: 10.1016/j.ijcard.2011.10.099

Vlachopoulos, C., Aznaouridis, K., and Stefanadis, C. (2010). Prediction of cardiovascular events and all-cause mortality with arterial stiffness: a systematic review and meta-analysis. *J. Am. Coll. Cardiol.* 55, 1318–1327. doi: 10.1016/j.jacc.2009.10.061

Webster, L. M., Myers, J. E., Nelson-Piercy, C., Harding, K., Cruickshank, J. K., Watt-Coote, I., et al. (2017). Labetalol versus nifedipine as antihypertensive treatment for chronic hypertension in pregnancy: a randomized controlled trial. *Hypertension* 70, 915–922. doi: 10.1161/HYPERTENSIONAHA.117.09972

Williams, B., Cockcroft, J. R., Kario, K., Zappe, D. H., Brunel, P. C., Wang, Q., et al. (2017). Effects of sacubitril/valsartan versus olmesartan on central hemodynamics in the elderly with systolic hypertension: the parameter study. *Hypertension* 69, 411–420. doi: 10.1161/HYPERTENSIONAHA.116.08556

Williams, B., Lacy, P. S., Thom, S. M., Cruickshank, K., Stanton, A., Collier, D., et al. (2006). Differential impact of blood pressure-lowering drugs on central aortic pressure and clinical outcomes: principal results of the conduit artery function evaluation (CAFE) study. *Circulation* 113, 1213–1225. doi: 10.1161/CIRCULATIONAHA.105.595496

Conflict of Interest: J-GW reports receiving lecture and consulting fees from Novartis, Omron, and Viatris.

The remaining authors declare that the research was conducted in the absence of any commercial or financial relationships that could be construed as a potential conflict of interest.

Publisher's Note: All claims expressed in this article are solely those of the authors and do not necessarily represent those of their affiliated organizations, or those of the publisher, the editors and the reviewers. Any product that may be evaluated in this article, or claim that may be made by its manufacturer, is not guaranteed or endorsed by the publisher.

frontiers in Physiology

REVIEW
published: 14 December 2021
doi: 10.3389/fphys.2021.789690

Pathophysiology of Circulating Biomarkers and Relationship With Vascular Aging: A Review of the Literature From VascAgeNet Group on Circulating Biomarkers, European Cooperation in Science and Technology Action 18216

Kristina R. Gopcevic[1], Eugenia Gkaliagkousi[2], János Nemcsik[3,4], Ömür Acet[5], M. Rosa Bernal-Lopez[6], Rosa M. Bruno[7], Rachel E. Climie[7,8,9], Nikolaos Fountoulakis[10], Emil Fraenkel[11], Antonios Lazaridis[2], Petras Navickas[12], Keith D. Rochfort[13], Agnė Šatrauskienė[12,14], Jūratė Zupkauskienė[12] and Dimitrios Terentes-Printzios[15]*

[1] Laboratory for Analytics of Biomolecules, Department of Chemistry in Medicine, Faculty of Medicine, Belgrade, Serbia, [2] 3rd Department of Internal Medicine, Papageorgiou Hospital, Faculty of Medicine, Aristotle University of Thessaloniki, Thessaloniki, Greece, [3] Department of Family Medicine, Semmelweis University, Budapest, Hungary, [4] Health Service of ZUGLO, Department of Family Medicine, Budapest, Hungary, [5] Vocational School of Health Science, Pharmacy Services Program, Tarsus University, Tarsus, Turkey, [6] Internal Medicine Department, Regional University Hospital of Malaga, Instituto de Investigacion Biomedica de Malaga, University of Malaga, CIBER Fisiopatología de la Obesidad y la Nutrición, Instituto de Salud Carlos III, Málaga, Spain, [7] Unversite de Paris, INSERM, U970, Paris Cardiovascular Research Center, Paris, France, [8] Menzies Institute for Medical Research, University of Tasmania, Hobart, TAS, Australia, [9] Sports Cardiology Lab, Clinical Research Domain, Baker Heart and Diabetes Institute, Melbourne, VIC, Australia, [10] Faculty of Life Sciences and Medicine, King's College London - Waterloo Campus, London, United Kingdom, [11] 1st Department of Internal Medicine, University Hospital and Pavol Jozef Šafárik University in Košice, Košice, Slovakia, [12] Clinic of Cardiac and Vascular Diseases, Institute of Clinical Medicine, Faculty of Medicine, Vilnius University, Vilnius, Lithuania, [13] School of Nursing, Psychotherapy and Community Health, Dublin City University, Dublin, Ireland, [14] Centre of Cardiology and Angiology, Vilnius University Hospital Santaros Klinikos, Vilnius, Lithuania, [15] First Department of Cardiology, Hippokration Hospital, Medical School, National and Kapodistrian University of Athens, Athens, Greece

OPEN ACCESS

Edited by:
Carlos R. Tirapelli, University of São Paulo, Brazil

Reviewed by:
Eliana Hiromi Akamine, University of São Paulo, Brazil
Tiago J. Costa, Johns Hopkins University School of Medicine, United States

***Correspondence:**
Kristina R. Gopcevic
kristinagopcevic@yahoo.com

Specialty section:
This article was submitted to Vascular Physiology, a section of the journal Frontiers in Physiology

Received: *05 October 2021*
Accepted: *17 November 2021*
Published: *14 December 2021*

Citation:
Gopcevic KR, Gkaliagkousi E, Nemcsik J, Acet Ö, Bernal-Lopez MR, Bruno RM, Climie RE, Fountoulakis N, Fraenkel E, Lazaridis A, Navickas P, Rochfort KD, Šatrauskienė A, Zupkauskienė J and Terentes-Printzios D (2021) Pathophysiology of Circulating Biomarkers and Relationship With Vascular Aging: A Review of the Literature From VascAgeNet Group on Circulating Biomarkers, European Cooperation in Science and Technology Action 18216. Front. Physiol. 12:789690. doi: 10.3389/fphys.2021.789690

Impairment of the arteries is a product of sustained exposure to various deleterious factors and progresses with time; a phenomenon inherent to vascular aging. Oxidative stress, inflammation, the accumulation of harmful agents in high cardiovascular risk conditions, changes to the extracellular matrix, and/or alterations of the epigenetic modification of molecules, are all vital pathophysiological processes proven to contribute to vascular aging, and also lead to changes in levels of associated circulating molecules. Many of these molecules are consequently recognized as markers of vascular impairment and accelerated vascular aging in clinical and research settings, however, for these molecules to be classified as biomarkers of vascular aging, further criteria must be met. In this paper, we conducted a scoping literature review identifying thirty of the most important, and eight less important, biomarkers of vascular aging. Herein, we overview a selection of the most important molecules connected with the above-mentioned pathological conditions and study their usefulness as circulating biomarkers of vascular aging.

Keywords: vascular aging, circulating biomarkers, oxidative stress, inflammation, cellular matrix, epigenetics

INTRODUCTION

The process of aging is defined as 'significant physiological alterations which lead to increased susceptibility to disease and risk of death.' To assess the changes leading to biological aging, molecular and cellular biomarkers, as well as non-invasive imaging techniques, can be applied (Ferrucci et al., 2020). Aging can be viewed as a cell-specific deterioration process mainly caused by genomic instability, telomere shortening, epigenetic changes, and a loss of proteostasis (Crimmins et al., 2008; Freitas-Rodríguez et al., 2017). Moreover, many relevant age-related changes occur at the intercellular level too, which call for a more integrative approach of the aging process (Groenwagen et al., 2016; Sena et al., 2018).

Vascular aging is a natural process, happening with advanced age, and is associated with structural and functional changes in the vascular wall. This is evident in the structural properties of the blood vessels, in that for example, the larger elastic arteries exhibit an increase in collagen content, covalent crosslinking of the collagen, elastin fracture, and calcification and reduction in the elastin content. Increased vascular smooth muscle growth is also a hallmark, in addition to an increase in wall thickness (i.e., the media to lumen ratio). In terms of changes in the functional properties, these are related mainly to aspects of endothelial dysfunction and decreased nitric oxide (NO) production. Finally, and perhaps the major consequence and observable change associated with vascular aging is reduced compliance/increased arterial stiffness of the arterial wall, which is recognized as the hallmark of vascular dysfunction in healthy aging. Importantly, the afore mentioned processes which are associated with vascular aging are accelerated in cardiovascular, and other disease states, and development or onset of these pathophysiological states can result in vascular aging developing earlier in life as compared to natural aging (Nilsson et al., 2008). In this way, as aging is characterized as a chronic progressive proinflammatory phenotype (Franceschi et al., 2000), indirectly controlled by a network of cellular and molecular defense mechanisms, the events which lead to the early development of vascular aging sees many of these mechanisms activated and in turn influence aspects of vascular tree. As such, inflammaging; the gradually adaptive process of the body which leads to a proinflammatory status with advancing age, is central to vascular aging (Kirkwood, 2018).

Another central hallmark and key driver of aging is senescence. Cellular senescence is a state of a durable, irreversible cell-cycle arrest of previously replication-competent cells, which plays a dual role in physiology and disease (Gorgoulis et al., 2019). In this regard, transient induction of senescence followed by tissue remodeling has been recognized as a beneficial mechanism to eliminate damaged or aged cells (He and Sharpless, 2017). Conversely, persistent senescence and inability to eliminate the excess damaged cells, has been linked with detrimental effects leading to inflammation, which as mentioned, is an essential pathophysiological mechanism inextricably linked to tissue dysfunction which characterizes aging and the aging-related diseases (Di Micco et al., 2021).

The term biomarker refers to a broad range of biological measures that can be objectively measured and evaluated as indicators of normal biological and pathogenic processes or pharmacologic responses to a therapeutic intervention (Biomarkers Definitions Working Group, 2001). Specific to aging, or indeed vascular aging, there is currently no standard set of biomarkers in clinical trials yet. The authors of this manuscript were convened within the European Cooperation in Science and Technology (COST) Action on vascular aging international scientific network (CA18216 - Network for Research in Vascular Aging, VascAgeNet[1], action duration 4 years (November 5, 2019–November 4, 2023) and a comprehensive literature review was conducted specific to this.

In the following, we introduce a selection of identified molecules/cellular aspect which demonstrate potential in addressing the aforementioned deficit, and provide an overview of their usefulness as circulating biomarkers of vascular aging.

METHODOLOGY

In order to identify all relevant studies a literature search was conducted using PubMed. Research articles were also selected manually from the reference lists of articles. The search strategy used the terms "circulating biomarker," "cardiovascular disease (CVD)," "aging," "vascular aging," and the initial selection of biomarkers was refined by those which appeared in most studies, and importantly met the criteria introduced by Vlachopoulos et al. (2015). As a result, **Supplementary Table S1** contains the list of extracellular biomarkers which meet these requisites, and are proven to be involved in: inflammation (3), alterations to the cellular matrix (5), aging of the kidney (1), stress response and mitochondria (1), nutrient signaling (1) and epigenetics (3). **Supplementary Table S2** contains a subset of miRNA-based biomarkers which have been shown to be involved in influencing genetics (1), the cell matrix (1), inflammation (1), angiogenesis, cell adhesion, and inflammation (1), mitochondria biogenesis and metabolism (2), and metabolism (2). We then further refined this list, ranking the biomarkers based on their influence on: underlying mechanisms related to vascular aging, involvements in disease, proof of concept, prospective validation, incremental value, clinical utility, clinical outcomes, cost-effectiveness, ease of use, methodological consensus and finally reference value (Vlachopoulos et al., 2015). In doing so, we selected only those which aligned closest with the aforementioned criteria. Further refinement of biomarkers was then based on: (1) clinical utility; (2) cost effectiveness; (3) ease of use; (4) methodological consensus; and (5) reference values (cut-off values).

In conducting the literature search, duplicated studies were identified and removed. The abstracts and titles of article retrieved were screened to exclude the irrelevant studies. Full-text articles were then examined to determine whether they met the inclusion criteria. Inclusion criteria were: (1) studies investigating the association of a biomarker with CVDs, and vascular aging; (2) studies using blood serum or plasma for biomarker analysis; and (3) peer-reviewed articles and all types of reviews published in English between January 1989 and October 2021. Unpublished

[1] www.vascagenet.eu

theses, reports, and conference proceedings were excluded. Data were extracted using a standardized form by the reviewers and verified by another reviewers.

We aim to address the vascular aging phenomenon of different factors within the scope of COST 18216 "Network for Research in Vascular Aging" action. For each selected biomarker, we present the data according to four different sections: pathophysiology, association with physiological aging and vascular markers, association with CVD and measurement method. This review describes important molecules associated with pathological conditions and their implications for their usefulness as biomarkers of circulating vascular aging and showing relevant data on outcomes whenever available. Reviews, guidelines, and consensus papers are also included.

RESULTS

Thirty of the most important and pertinent biomarkers related to inflammation, matrix injury, stress response and mitochondria, nutrient signaling, vascular senescence, thrombotic events and epigenetic were identified; and eight of the less important biomarkers related to genetics, matrix remodeling, angiogenesis, cell inflammation, mitochondrial biogenesis, metabolism (**Supplementary Tables S1, S2**).

Application of stated criteria to the available literature to the identified 38 biomarkers resulted in a short list of circulating biomarkers: oxidative stress based – superoxide dismutase (SOD); inflammation based – high sensitivity C-reactive protein (hsCRP) and interleukin-6 (IL-6); cellular matrix based – matrix metalloproteinases (MMPs), growth differentiation factor-15 (GDF-15); epigenetic based – micro ribonucleic acids (miRNAs), DNA methylation and telomere length (**Figure 1**).

CIRCULATING BIOMARKERS RELATED TO VASCULAR AGING

Oxidative Stress-Based Circulating Biomarkers

Reactive Oxygen and Nitrogen Species

Pathophysiology

Reactive oxygen and nitrogen species (RONS) are formed by the use of molecular oxygen by aerobic organisms and play an essential role in physiology and pathophysiology of aerobic life (Li et al., 2016). RONS are a group of small reactive molecules, including radicals and non-radicals, that are derived from oxygen metabolism. RONS with unpaired electrons are considered as free radicals. Free radicals such as superoxide ion ($O_2^{\bullet -}$) and hydroxyl radical ($OH^{\bullet -}$), are unstable in nature and subsequently have short biological half-lives (Stevenson et al., 2020). Non-radicals in comparison; such as hydrogen peroxide (H_2O_2), singlet oxygen ($^1O_2$), peroxynitrite ($ONOO^-$) and hypochlorous acid (HOCl), are more stable in contrast and thus exhibit longer half-lives as compared to their free radical counterparts. Mitochondrial respiration is a major source of reactive oxygen species (ROS) within most cells. As electrons are transferred between the complexes of the electron transport chain, some of these electrons can 'leak' out to react directly with oxygen to form superoxide (Shields et al., 2021). A hallmark of aging is the progressive loss of mitochondrial function and in turn reduction in mitochondrial-derived ROS (Santos et al., 2018).

In that way, whilst aging sees a reduction in mitochondrial levels of ROS, with respect to the vascular system, there are several other sources of RONS which play a role in promoting oxidative stress; most notably; the enzymatic sources of RONS; which have been the subject of extensive investigation the last number of years. Notably, NADPH oxidases (NOX); which utilizes electrons donated from NADPH to convert molecular oxygen to $O_2^{\bullet -}$, myeloperoxidases (MPO); which converts H_2O_2 to HOCl, xanthine oxidase (XO); which produces $O_2^{\bullet -}$ anions during the breakdown of purines to uric acid, SOD; which converts $O_2^{\bullet -}$ anions to H_2O_2 and oxygen, and monoamine oxidase; which decomposes dopamine and produces H_2O_2 (Shields et al., 2021), are among the most prominent sources of vascular ROS, closely followed by lipoxygenase (LOX), cyclooxygenase (COX), angiotensin II, and cytochrome P450 1B1.

According to numerous published data, RONS have a dual role in an organism: RONS contribute to aging but they also play a crucial role in cell signaling and development, thus serving a beneficial role. In the vascular system, physiological levels of RONS are essential for normal vascular functions including endothelial homeostasis and smooth muscle cell contraction (Salisbury and Bronas, 2015). For example, the free radical nitric oxide (NO), which is produced by endothelial nitric oxide synthase (eNOS) by the vascular endothelium, is very important in the regulation of blood flow and vasodilation (Chen et al., 2018). However, any imbalance between prooxidant and antioxidant mechanisms, often called "redox potential," can play an important role in vascular aging (Ferrini et al., 2004). Excessive levels of ROS have been shown to cause vascular remodeling by inducing proliferation and migration of vascular smooth muscle cells, vascular cell damage, the recruitment of inflammatory cells, lipid peroxidation, activation of metalloproteinases and deposition of extracellular matrix (Chen et al., 2018). The initiation and progression of disease states such as hypertension, atherosclerosis, restenosis and abdominal aortic aneurysm are among the main vascular diseases in which oxidative stress has been shown to play a key role (Tejero et al., 2019).

With respect to reactive nitrogen species (RNS), a large proportion of their production stems from the activity of eNOS. Under pathological conditions, eNOS can also produce $O_2^{\bullet -}$ which contributes directly to ROS levels. The $O_2^{\bullet -}$ can now react with the NO produced by the same enzyme to produce peroxynitrite ($ONOO^-$), which has been shown to directly damage cellular components, or further react with other molecules to create other types of RNS; nitric dioxide ($NO_2^{\bullet}$), nitrate radical ($NO_3^{\bullet}$), nitrous acid (HNO_2), nitrite (NO_2^-), nitrosyl cation (NO^+), nitroxyl anion (NO^-), peroxynitrous acid (ONOOH), dinitrogen trioxide (N_2O_3). Similar to peroxynitrite, these RNS have also been shown to cause similar nitrosative damage to cellular component, but also have functional roles in cell signaling and pathogen defense (Shields et al., 2021).

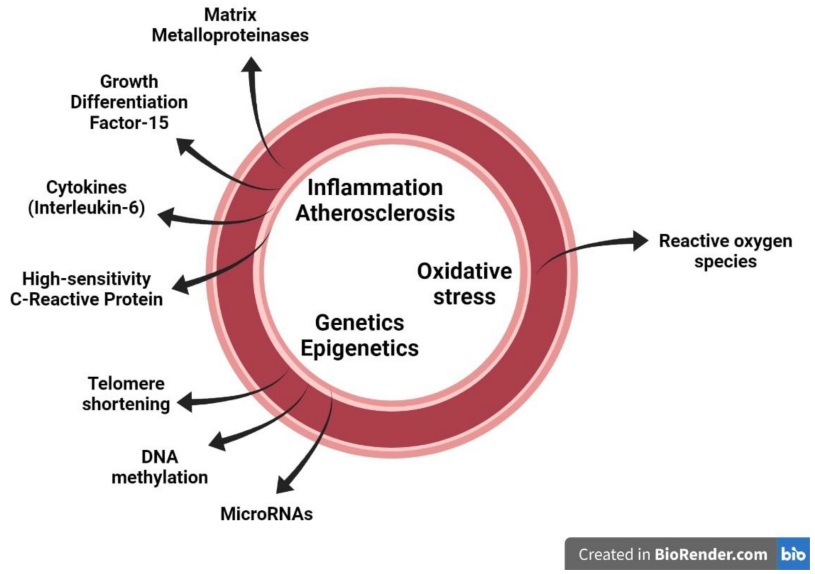

FIGURE 1 | Several circulating biomarkers which are proposed to mirror the major pathophysiological mechanisms that contribute to vascular aging in the vascular wall, namely inflammation/atherosclerosis, oxidative stress and genetics-epigenetics.

Excessive levels of RONS are mainly generated by and credited to the NOX family of enzymes. The NOX family are the only family of enzymes which produce RONS as its primary function (Lassegue et al., 2012; Montezano and Touyz, 2014), and in general NOX-derived ROS are important regulators of endothelial function and vascular tone. However, the excessive reduction of molecular oxygen to superoxide anion $O_2^{\bullet -}$ by members of this family has been linked to vascular disease and biological aging, directly and indirectly, via several pathogenic pathways (Blankenberg et al., 2003). For example, $O_2^{\bullet -}$ from NOX enzymes initiates the process of eNOS uncoupling which promotes accelerated vascular aging in CVD. Moreover, SOD dismutates the superoxide anion to H_2O_2 which is able to form highly reactive hydroxyl ions ($OH^{\bullet}$) (Gong et al., 2014), that are extremely reactive and cause damage to the cell membrane phospholipids and proteins (Liguori et al., 2018). All seven family members of the NOX family are major producers of RONS in mammalian cells, yet NOX-1, -2. -3, -4, and -5 are variably expressed in the vascular system by endothelial cells or vascular smooth muscle cells, and are among those identified as having a predominant role, through their specific generation of $O_2^{\bullet -}$ or H_2O_2, in progressing vascular disease (Ighodaro and Akinloye, 2018). Of note, the exact pathophysiological significance of NOX-5 is still unclear, but according to the review of Touyz et al. (2019), this enzyme is important in the physiological regulation of sperm motility, lymphocyte differentiation and interestingly vascular contraction. Emerging evidence has implicated its hyperactivation in the onset and development of CVD, as well as kidney injury and cancer.

Furthermore, in fully understanding the redox dynamics central to pathophysiological disease states, attention has been directed toward the inherent physiological defense mechanisms which protect the body against oxidative stress. The most important enzymatic systems include SOD, catalase (CAT), glutathione peroxidase (GPx), glutaredoxin (Grx), thioredoxin (Trx), peroxiredoxin (Prx) and glutathione S-transferase (GST). These antioxidant enzymes catalytically remove ROS in their own unique way; for example, SOD dismutases $O_2^{\bullet -}$ into H_2O_2, which is in turn degraded by CAT or GPx into water and molecular oxygen. Grx and Trx act to protect thiol-containing proteins by repairing damage caused by ROS by transferring electrons to the disulfide bonds of the damaged proteins in order to repair them and restore them back to its reduced form. Prx is a cysteine containing enzyme that reduces the activity of peroxides, while GSTs act synergistically with GPx to reduce lipid peroxidation.

Among the non-enzymatic antioxidants, the most pertinent is glutathione (GSH); which is essential for the activity of GPx and Grx in returning each to their active state. *N*-Acetyl cysteine (NAC) is important in the formation of GSH acting as its precursor molecule, whilst also participating in redox reactions by donating electrons toward the detoxification of ROS which are present in the vicinity. Finally, Vitamin C and E are important water-soluble antioxidants which scavenge oxygen free radicals in the environment and prevent the oxidation of cholesterol. Vitamin E also acts as an inhibitor of lipid peroxidation (Nandi et al., 2019; Shields et al., 2021).

Association With physiological Aging and Vascular Markers

One of the main features of aging is a progressive loss of tissue and organ function over time. In accordance with the free radical theory of aging; age-associated functional losses are due to the accumulation of oxidative damage to macromolecules (lipids, DNA, and proteins) caused by RONS. The exact mechanism of aging caused by oxidative stress is still unclear, but oxidative stress and aging are becoming increasingly recognized as intertwined biological events as increased RONS production is observed with

aging. A wealth of experimental data confirms oxidative stress disrupts critical signaling pathways owing to the damage inflicted to the aforementioned macromolecular molecules/structures of cells and tissues. These changes in signaling pathways are correlative to those associated with cellular aging; a physiological mechanism that reduces/halts cell proliferation in response to damage incurred during the replication cycle (Papaconstantinou, 2019). Senescent cells acquire an irreversible senescence-associated secretory phenotype (SASP) involving secretion of soluble factors (interleukins, chemokines, and growth factors), degradative enzymes like MMPs, and insoluble proteins/extracellular matrix (ECM) components. For example, adoption of a senescent phenotype in endothelial cells leads to impaired endothelium-dependent vasodilation and upregulation of inflammatory gene expression in aged vasculature (Donato et al., 2015). This data and others, have implicated RONS as inducers of cellular senescence in directly acting on various components associated with SASP (Liguori et al., 2018).

Thereafter, RONS-mediated events are concurrent with vascular inflammation and the development and progression of atherosclerosis and accelerated atherosclerotic damage (Wu et al., 2014; Kattoor et al., 2017). Recent experimental data have linked RONS production with the development of aortic stiffening, while conversely, indirect clinical evidence supports the beneficial effect of antioxidant therapies in reducing arterial stiffness (Ashor et al., 2014; Canugovi et al., 2019).

Association With Cardiovascular Disease

Substantial evidence clearly shows that oxidative stress, through inflammation, endothelial dysfunction, and other pro-atherosclerotic mechanisms, plays a pivotal role in the pathophysiology of CVD and highly cardiovascular (CV) risk disorders including hypertension, dyslipidemia, peripheral artery disease, metabolic syndrome, and diabetes mellitus (DM) (Loperena and Harrison, 2017; Touyz and Delles, 2019). Of note, several studies have suggested that therapeutic interventions using antioxidants have prevented CV progression. For example, supplementation of Vitamin A, C, and E have demonstrated positive effects in short-term secondary CV prevention, though their exact role in vascular health remains divisive (Ashor et al., 2016). Other trials aimed at addressing the redox balance in individuals are perceived in much the same way; caloric restriction (reduced CV aging and increased chronic disease protection), nutraceuticals (reduction of blood pressure and oxidative stress, with concomitant increases in NO release), and dietary supplements such as fish oil and green tea (improvement in endothelial function, reduction in inflammation and oxidative stress). Moreover, endogenous forms of antioxidant enzymes are now available (SOD, CAT, and Gpx), whilst efforts are ongoing to produce other mimetics or scavenging molecules of similar capabilities, though no molecule has conclusively been successful, while others are still in trials (Izzo et al., 2021). Similarly, direct evidence linking excessive RONS production to CV mortality is currently lacking due to the complexity in the pathophysiology of CVD, hence oxidative stress has been rendered a key contributing factor but not the primary pathogenetic mechanism. Despite these complexities, clinical data from several trials investigating classical antioxidant treatments, but not medications possessing indirect antioxidant properties, have yet to present conclusive evidence of either no benefit or even harm (Senoner and Dichtl, 2019).

It is worth to mention that many studies have suggested the possible therapeutic application of antioxidants. Among antioxidants, vitamin E and C have shown some effect in short term secondary CV prevention, but their role in vascular health remains controversial (Ashor et al., 2016; Izzo et al., 2016). Even more controversial is the supplementation with vitamin A, which even worsened all-cause mortality (Izzo et al., 2021). In some trials antiaging and antioxidant strategies have been documented. They include: caloric restriction (CV aging and chronic disease protection) (Ashor et al., 2016); nutraceuticals (reduction of blood pressure and oxidative stress, increase of NO release; Ashor et al., 2016); dietary supplements such as: fish oil, green tea, vitamin C and A (improvement of endothelial function, reduction of inflammation and oxidative stress) (Ashor et al., 2016). Until now it is impossible to use endogenous antioxidant enzymes, SOD, catalase or GPx, or any synthetic deriving molecule. Several attempts have been made to create such molecules or scavenging enzymes, but so far, no elements have been successful, and other molecules are still in trials (Izzo et al., 2021).

One of the new molecules emerging as important mediators regulating oxidation and inflammation in the vasculature and heart is osteoprotegerin, which may act through reduction in apoptosis and preservation of the matrix structure. Although osteoprotegerin can affect vascular function, its cardiac effects seem to be direct and independent of effects on the vasculature (Guzik and Touyz, 2017). Finding new molecules and new ways to address aging and oxidative stress is fundamental to find new potential application for cardiovascular prevention and treatment.

Measurement of Reactive and Nitrogen Oxygen Species

Owing to their extremely short half-lives, it is currently incredibly difficult to accurately measure and assess RONS levels (Rice et al., 2012). Markers of oxidative stress are either molecules modified by interactions with ROS, or molecules of the antioxidant system changed in response to increased redox stress (Tanguy et al., 2000). In that way, targeting the molecules upstream of RONS represents the current best way to assess RONS levels indirectly, and the most commonly used markers in CV research include isoprostanes (IsoPs), malondialdehyde (MDA), nitrotyrosine, *S*-glutathionylation, MPO, oxidized LDL, ROS induced changes to gene expression, glutathione peroxidase (GPX), and isoforms of SOD (Zarzuelo et al., 2013). The measurement of SOD is perhaps one of the most accepted means of measuring RONS activity owing to their levels reflecting their activity catalyzing the dismutation of the strong superoxide radical (O_2^-) thus maintaining redox balance and preventing accumulation of injurious ROS (He et al., 2009). There are three distinct SOD isoforms which include the Cu/Zn superoxide dismutase (SOD1), MnSOD (SOD2), and ECM superoxide dismutase (ECM-SOD/SOD3), and as these isoforms remain stable even when the erythrocytes of the samples are hemolyzed

and stored frozen (Pierce et al., 2011), they are suggested to be a suitable biomarker for estimation of oxidative stress (Thangaswamy et al., 2012).

Inflammation-Based Circulating Biomarkers

Nowadays, it is strongly believed that aging and age-associated diseases share many common physiologic and pathophysiologic pathways which seem to converge on inflammation. In fact, at the cellular level, aging is characterized by a state of chronic, sterile, low-grade inflammation (i.e., inflammaging), and it is considered a pre-status mechanism for many age-associated diseases such as cancer, diabetes mellitus (DM) and CVD (Franceschi et al., 2020). Based on the study of Franceschi et al. (2000), inflammaging is the expansion of the network theory of aging and the remodeling theory of aging (Franceschi, 1989; Franceschi and Cossarizza, 1995). Based on the remodeling theory, inflammaging is the gradual adaptive process of the body; the net result of which is a regulation of malignant damage sustained by the body as a result of a trade-off with the immune system. Despite the lack of agreement on definitions and terminology surrounding inflammaging, the prevailing consensus is that the primary feature of such is an increase in the proinflammatory status with advancing age (Kirkwood, 2018).

From an evolutionary perspective, inflammaging is primarily driven by several endogenous signals including the accumulation of misplaced and misfolded self-molecules from damaged or senescent cells. Among the several inflammatory factors, the key molecules associated with inflammaging and aging are the elevated pro-inflammatory cytokines, especially interleukin (IL)-6 and C-reactive protein (CRP) (Singh and Newman, 2011). Various studies have described production of IL-6 by endothelial cells. More specifically, it has been described that human umbilical vein endothelial cells (HUVECs) can produce IL-6 via a G-protein, calcium, and NF-kB-dependent pathway upon stimulation of the protease-activated receptors (PAR) PAR-1 or PAR-2. The effects of both PAR-1 and PAR-2 agonists on the endothelial cells are greatly enhanced by concomitant stimulation by endotoxin (lipopolysaccharide, LPS) or tumor necrosis factor-a (TNF-a) (Chi et al., 2001). In addition, in acute inflammation, it has been shown that thrombin (a procoagulant and proinflammatory molecule) may induce monocyte recruitment through endothelial activation by inducing monocyte chemotactic protein-1 (MCP-1) secretion indirectly through an autocrine loop involving endothelial IL-6 secretion (Marin et al., 2001). Bacterial endotoxin or inflammatory cytokines, such as IL-1 or TNF-alpha have also been shown to stimulate IL-6 production in adult vascular endothelial cells (Loppnow and Libby, 1989; Naka et al., 2002; Puel and Casanova, 2019).

Interleukin-6

Pathophysiology

Interleukin-6 is a small, 21 kDa glycoprotein produced by numerous cell types, including but not limited to; dendritic cells, macrophages, monocytes, T cells and vascular cells. IL-6 binds to its receptor (IL-6R), thus activating the Janus kinase (JAK) tyrosine kinases and the downstream signal transducer and activator of transcription (STAT). The net result is a pleiotropic tissue activity predominantly directed toward the initiation of inflammation and the elevation of acute phase reactants including CRP (Hirano and Murakami, 2020).

Association With Physiological Aging and Vascular Markers

Based on current knowledge, IL-6 is a well-acknowledged sensitive biomarker of low-grade inflammation and is among the best candidates within the interleukin family as a representative biomarker of vascular aging (Puzianowska-Kuźnicka et al., 2016). IL-6 has been positively associated with vascular markers of aging such as pulse wave velocity (PWV) in healthy men and patients with chronic kidney disease (Nishida et al., 2007; Peyster et al., 2017), and carotid intima-media thickness (cIMT) (Huang et al., 2016). Additionally, IL-6 levels have been found to increase in an age-dependent manner in two cohorts of older individuals (Puzianowska-Kuźnicka et al., 2016; Stevenson et al., 2018). Similarly, in a recent meta-analysis including 12421 values for IL-6 in the blood of healthy adult male and female donors, it was found that for every 1-year increase in age, there was a significant increase of IL-6 values by 0.05 pg/ml (Said et al., 2021). Moreover, there is substantial evidence that IL-6 contributes to hypertension as levels of IL-6 have been correlated with blood pressure in hypertensive subjects and are reduced by treatment with angiotensin II-receptor blockade (Vázquez-Oliva et al., 2005). A similar study corroborates this relationship in demonstrating that angiotensin II-receptor inhibitor significantly reduces IL-6 levels in hypertensive patients (Tsutamoto et al., 2000; Manabe et al., 2005).

Hypertension and atherosclerosis are associated with accumulation of cellular senescence biomarkers in the vascular wall; a hallmark often associated with vascular dysfunction (Kovacic et al., 2011). Additional risk factors for CVD; such as smoking, hyperlipidemia, or DM, are also associated with accelerated decline of vascular function (Cunha et al., 2017). Hypertension is inherently associated with accelerated vascular aging and, therefore, research on such has assisted in understanding the vascular remodeling that occurs with age (Lakatta, 2007; Huang et al., 2018). Early vascular aging—a term introduced in the context of premature development of vascular stiffness and remodeling by Nilsson et al. (2009) and Cunha et al. (2017) is a key feature of hypertension (Lakatta, 2007; Guzik and Touyz, 2017). In hypertensive patients, the vascular wall activates monocytes, which increases the release of IL-6 (Guzik and Touyz, 2017; Loperena et al., 2018). Concurrently, the existence of a chronic inflammatory state has been reported in elderly age, and has been shown to be caused by an increase in the levels of IL-6 and TNF-alpha (Derhovanessian et al., 2009). In that way, recent advances in hypertension research have unraveled novel inflammatory, and oxidative mechanisms, of vascular dysfunction that underlie accelerated vascular aging in hypertension and associated CVD (Passacquale et al., 2016).

Association With Cardiovascular Disease

A wealth of data exists confirming the association between increased IL-6 levels and CV mortality and morbidity

(Libby et al., 2002; Rao et al., 2005; Danesh et al., 2008; Compté et al., 2013; Ridker et al., 2018; Batra et al., 2021).

More specifically, in the population-based Cardiovascular Health Study, elevated plasma IL-6 levels were found to significantly associate with death across multiple causes and strongly predict future mortality (Walston et al., 2009). Similarly, higher IL-6 levels were associated with increased mortality in older adults in the Framingham Heart Study (Roubenoff, 2003). More recently, it was demonstrated that for each SD increase in log IL-6, there was a 25% increase in the risk of future CV events (Kaptoge et al., 2014). Several studies described the association of IL-6 and cardiovascular mortality and morbidity (Held et al., 2017; Wainstein et al., 2017; Ridker et al., 2018).

Measurement of Interleukin-6

Kenis et al. (2002) examined the stability of IL-6 in human serum using an accelerated stability testing protocol according to the Arrhenius equation. In this study, the effect of time delay between blood sampling and sample processing, clotting temperature and repeated freeze-thaw cycles on serum levels of these proteins were determined. It was concluded that serum samples for the determination of IL-6 can be stored at −20°C for several years (Kenis et al., 2002). Graham et al. (2017) studied the impact of initial and multiple subsequent freeze-thaw cycles on pro-inflammatory including IL-6, anti-inflammatory, acute phase proteins and other biomarkers. The authors found that the examined biomarkers on their panel remained stable for analysis despite multiple freeze-thaw cycles. Together, these data provide the foundation and confidence for large scale analyses of panels of inflammatory biomarkers to provide better understanding of immunological mechanisms underlying health versus disease (Graham et al., 2017).

The foremost way of measuring IL-6 levels in a biological sample is by enzyme-linked immunosorbent assays (ELISA) which are readily available from numerous companies today. For this analysis, sample volumes as little as 50 μL are measurable, with sample matrices including but not limited to serum, plasma, cell culture supernatant. Most ELISA formats allow for a measurable range of 1.56–100 pg/mL (Tecan manufacturer of ELISA kits). Owing to the nature of ELISA-based methods, results of the study Gong et al. (2019), highlighted a number of variables which can affect levels of cytokine in a sample. It was found that incorrect sample handling procedures played a key role in the obtained results. For example, plasma and serum sampling require their own individual protocols. With respect to IL-6, unseparated EDTA plasma can keep IL-6 stable for up to 24 h, whereas with unseparated serum it is recommended to measure IL-6 as soon as possible. Despite these potential obstacles, ELISAs have improved upon earlier methods which utilized flow cytometry and determined the levels of IL-6 based on the cellular response to the cytokine and the employment of a dose-response curve. In comparison, levels of cytokines like IL-6 and their respective activity can now be rapidly determined in accordance with the World Health Organization (WHO) cytokine standards; taking as little as a few hours to achieve, in comparison to previous methods which took days in comparison (Simard et al., 2014).

High Sensitivity-C-Reactive Protein

Pathophysiology

C-reactive protein or high sensitivity (hs)-CRP is an acute-phase reactant and a nonspecific inflammatory biomarker whose production is stimulated in response to inflammatory mediators including IL-6 and IL-1. It is predominantly secreted by hepatocytes in the form of pentameric molecules, although low-level expression of CRP in other cells has also been observed. Levels of CRP have been shown to increase rapidly up to 1,000-fold at sites of trauma, infection or inflammation, and accordingly, rapidly decrease upon resolution of the causative condition. Measurement of hs-CRP is therefore widely used to monitor various inflammatory states.

Association With Physiological Aging and Vascular Markers

Increasing evidence shows that hs-CRP is not only an inflammatory biomarker but also an important risk factor associated with aging and aging-related diseases (Tang et al., 2017). Pertinent to this, it has been demonstrated that hs-CRP levels increase in an age-dependent manner across aging elderly populations without evident CVD. Relatively, hs-CRP levels are significantly lower in healthy aging adults compared to those with aging-related diseases (Puzianowska-Kuźnicka et al., 2016). Moreover, high hs-CRP levels are associated with decreased physical and cognitive performance which are strongly related to the natural aging process (Puzianowska-Kuźnicka et al., 2016; Tegeler et al., 2016), and, additionally, with several aging diseases like sarcopenia (Lee et al., 2020), deep white matter lesions, ischemic stroke, and heart failure (van Wezenbeek et al., 2018).

Concerning the association of hs-CRP with vascular disease, a connection between hs-CRP and atherosclerosis has long been established since hs-CRP directly binds oxidized low-density lipoprotein cholesterol (LDL-C) and has been shown to be present within atherosclerotic plaques. As a result, hs-CRP contributes to plaque instability and exerts a highly proatherogenic effect (Singh et al., 2008; Conte E. et al., 2020). Moreover, hs-CRP has been associated with indices of vascular stiffness. Relatively, hs-CRP has been found to positively correlate and, additionally, predict elevated PWV over and above traditional CV risk factors and in various diseased populations (Nakhai-Pour et al., 2007; Mozos et al., 2019). In addition, hs-CRP has been positively correlated with markers of carotid stiffness including cIMT (Liao et al., 2014).

Association With Cardiovascular Disease

The association between elevated hs-CRP levels and CVD is well established since most large-scale clinical trials have used a hs-CRP cut off point of 2 mg/l for determining increased CV risk, and a handful of studies have shown a consistent association of hs-CRP levels above 3 mg/l with CV events (Möhlenkamp et al., 2011). Additionally, it has been demonstrated that hs-CRP levels are able to predict future CV events. In a large meta-analysis of 160,309 individuals without a history of vascular disease, among a total of 27,769 patients who suffered fatal or nonfatal events, hs-CRP was associated with a significantly increased risk for coronary heart disease (CHD), stroke, and vascular mortality (Kaptoge et al., 2009). Similarly, ample studies have confirmed

that elevated hs-CRP concentrations can independently predict the risk of all-cause and CV mortality in different populations including the general population and patients with CHD (Li et al., 2017; Stumpf et al., 2017).

Due to its strong association with CVD, many mathematical models have tried to incorporate hs-CRP in order to improve CV risk prediction owing to the high correlation of hs-CRP with multiple risk factors. Subsequently, hs-CRP has been included in the position paper of the European Society of Cardiology and the Artery Society (Vlachopoulos et al., 2015), and it has been integrated into numerous guidelines in different pathological CV conditions (for primary and secondary CVD prevention). However, the class of recommendations for hs-CRP as circulating biomarker related to vascular wall biology may be measured as part of refined risk assessment only in patients with an unusual or moderate risk, whose profile is mostly class IIb with a level of evidence B, but not in asymptomatic low-risk or high-risk individuals (class III and level of evidence B recommendation) (Perk et al., 2012; Vlachopoulos et al., 2015). Therefore, there seems to be a modest support of the incremental value of hs-CRP, and it is debatable whether its measurement can provide a consistent and clinically meaningful incremental predictive value in risk prediction and reclassification (Yousuf et al., 2013).

Measurement of High Sensitivity-C-Reactive Protein

The standard CRP turbidimetric immunoassay measures markedly high levels of the protein in the range from 10 to 1000 mg/L. On the contrary, the hs-CRP assay accurately detects even lower, basal levels of CRP in the range from 0.5 to 10 mg/L which belongs to the currently accepted CV risk assessment range of 0.20–10.0 mg/l.

Cell Matrix Based Circulating Biomarkers

Matrix Metalloproteinases

Pathophysiology

Proteases degrade proteins by hydrolyzing their peptide bonds, and in their action control and influence many key physiological and pathological processes (López-Otín and Hunter, 2010). An essential part of each cell; the ECM can be modified during aging by protease dysfunction. Imbalances or altered activity of certain proteases can ultimately affect the structure and composition of the ECM, thus altering its ability to perform its biological functions; differentiation, proliferation, migration and survival (Freitas-Rodríguez et al., 2017). Matrix MMPs are a family of multidomain calcium-dependent, zinc-containing endopeptidases, activated by inflammatory signaling. They are able to degrade ECM molecules, have been shown to have a crucial role in aspects of aging, hypertension and atherosclerosis within the arterial wall (Wang et al., 2014). Activated MMPs influence arterial remodeling by promoting endothelial inflammation, intimal-medial thickening, elastin fiber network destruction, arterial fibrosis, calcification and adventitial expansion. Importantly, it was shown that aging enhances MMP-2/-7/-9/-14 activity in the aortic wall, namely via increases in Ang II-mediated signaling, proinflammation, fibrosis and elastin fragmentation (Wang et al., 2015). Conversely, human tissue inhibitors of matrix metalloproteinases (TIMPs) are four glycoproteins responsible for the inhibition of MMPs and thereby are also involved in and influence degradation of ECM.

Association With Physiological Aging and Vascular Markers

There is significant discordance between current and previous studies regarding the association of MMPs with age. For example, in a study including 93 healthy adults of different ethnic origins, no associations were found between MMP-2 and MMP-9 with age (Tayebjee et al., 2005), nor any gender influence. Similarly, in 699 adults of the Framingham study, MMP-9 was not associated with age (Sundström et al., 2004). In a subsequent study including 77 subjects with no evidence of CVD, significant positive correlations between MMP-2 and MMP-7, and a significant negative correlation between MMP-9 and age were found (Bonnema et al., 2007). Recently, Basisty et al. (2020), in using proteomic technology, identified increased levels of MMP-1, MMP-2 and their regulators TIMP1 and TIMP2 as secreted by senescent cells in human plasma (Basisty et al., 2020). Interestingly, age-related changes in the cardiac proteome have been also shown to be MMP-9 dependent (Iyer et al., 2016), while age-related MMP-2 upregulation occurs in the human aorta (McNulty et al., 2005).

Taking into account the crucial role of MMPs into vascular pathophysiology, a certain link with vascular function markers is anticipated. Indeed, it has been shown that plasma MMP-1 levels display a positive correlation with both PWV and augmentation index (AIx) after adjustment for age and mean arterial pressure in a cohort of normotensive and hypertensive individuals (McNulty et al., 2005). Similarly, MMP-9 levels have been positively correlated with aortic and brachial PWV in patients with hypertension including isolated systolic hypertension (Yasmin et al., 2005; Tan et al., 2007; Gkaliagkousi et al., 2012), whereas MMP-2 and MMP-3 have been associated with central arterial stiffness parameters in patients with DM type I (Peeters et al., 2017). In the most recent study so far including 206 healthy young adults, MMP-3 levels were significantly associated and independently predicted PWV (Iannarelli et al., 2021).

Association With Cardiovascular Disease

Subsequently, sample data confirm that several MMPs are closely associated with CVD and can predict both CV events and all-cause mortality in various populations including patients with DM, atherosclerosis and the general population (**Table 1**).

Measurement of Matrix Metalloproteinases

Determination of MMPs in biological samples (primarily serum or plasma) can be performed by several analytical methods: ELISA, zymography; optical methods such as near-infrared (IR) optical imaging, fluorescence, and surface plasmon resonance spectroscopy; the use of active-site probes followed by enzymatic digestion of the captured MMPs, and in the last two decades liquid chromatography-mass spectroscopy (LC-MS/MS) (Lopez-Avila et al., 2008). Gelatin zymography is widely used for the detection of the gelatinases MMP-2 and MMP-9 at a level of 10 pg (Kleiner and Stetler-Stevenson, 1994). Casein-, collagen-, and heparin-enhanced substrate- zymography are suitable for the higher quantities of other members of MMPs, while reverse

TABLE 1 | Extracellular matrix biomarkers as predictors of risk in CVD.

Biomarker	Tissue	Clinical context	No. of subjects/type of the study/length of follow-up	Main findings	References
MMP-1	Serum	Atherosclerosis	260/cross-sectional study/–	Serum levels associated with plaque burden	Lehrke et al., 2009
MMP-2	Plasma	Type 1 diabetes	337/cohort/12.3	Association with CVD	Peeters et al., 2017
MMP-8	Serum	CAD, MI	7928/cohort/13	Predictor of mortality	Kormi et al., 2017
MMP-9	Plasma Serum Serum	CVD MI, Stroke CVD	1127/cohort/4.1 1082/cohort/18.1 922/Framingham/9.9	Predictor of cardiovascular mortality Relevant marker of CV mortality Association with mortality	Blakenberg et al., 2003 Hansson et al., 2011 Velagaleti et al., 2010
MMP-10	Serum	PAD	187/cohort/2	Increased levels associated with mortality	Martinez-Aguilar et al., 2015
MMP-12	Plasma	Atherosclerosis, CAD, T2DM	1500/proximity extension assay technology/–	Plaque development	Goncalves et al., 2015
TIMP-1	Plasma	CVD	389/prospective/2	Predictive of all-cause death, MI and cardiac mortality	Cavusoglu et al., 2006

CAD, coronary artery disease; CVD, cardiovascular disease; PAD, peripheral artery disease; MI, myocardial infarction; T2DM, type 2 diabetes mellitus; –, no data.

zymography can be used for the detection of TIMPs (Tunon et al., 2010; Hoefer et al., 2015).

Most of the aforementioned assays for MMPs rely on the biological activity of the enzyme to degrade natural substrates, and are so-called "bioassays." A basic problem in utilizing bioassays in general is that they lack specificity against different substrates, however, they are very sensitive in their level of detection [MMP-9 – 12.5 ng (1.0 nM), MMP-2 – 20 ng (2 nM)]. Given there are a multitude of ways to measure MMPs, each approach presents with its own distinct advantages and disadvantages. For example, zymography as mentioned is perhaps the most routine approach for the detection of particular MMPs based on their activity relative to a relevant substrate, however, a disadvantage of the technique lies in the influence different anticoagulants can have as pre-analytical determinants of plasma MMP activities (this approach should only be used on plasma samples collected in heparin-free collection tubes). In comparison, *in situ* zymography utilizes an antibody raised to target specific MMP species, which upon interaction is captured and immobilized in areas where MMPs are present before subsequently being utilized for detection and quantification processes. This method is quick, and demonstrates good sensitivity for each subtype of MMP as compared to zymography and collagenolysis. However, this mode of analysis has been shown to possibly influence physical tissue parameters of samples. Western blotting (protein blotting or immunoblotting) is a powerful and important procedure for the immunodetection of MMPs post-electrophoresis. Presenting some unique advantages; in that the resultant membranes are pliable and easy to handle, and the proteins which are immobilized on the membrane are readily and equally accessible to different ligands, Western blotting is utilizes antibodies in much the same way as *in situ* zymography does, in being specific to the MMP of interest but is perhaps more versatile in its approach. However, Western Blotting does require knowledge of the MMPs native substrate and the availability of anti-MMPs antibodies. In this way, this approach can be expensive and time-consuming. Owing to these respective limitations, ELISAs have emerged as a popular approach for measuring the abundance of MMPs in a sample, and currently ELISAs are available for a number of MMPs species; MMP-9 and MMP-2 and their specific tissue inhibitors: TIMP-1 and TIMP-2 ELISA kits are commercially available and have a good sensitivity (Cheng et al., 2008).

Growth Differentiation Factor 15

Pathophysiology

Growth differentiation factor 15 is a member of the transforming growth factor-β (TGF-β) cytokine superfamily. Also known as macrophage inhibitory cytokine 1 (MIC-1), under physiological conditions it is found in abundance only in placenta (Fairlie et al., 1999). However, as an autocrine regulator of macrophage activation, its levels increase upon macrophage activation and it is produced under conditions of inflammation, vascular injury, and oxidative stress from human endothelial and vascular smooth muscle cells (Bootcov et al., 1997). Its role in vascular biology is divergent as evidence suggests it can exert either pro- or anti- inflammatory, angiogenetic and apoptotic effects (Unsicker et al., 2013). In this context, GDF-15 is released by macrophages during acute phase responses, and its level is thus influenced by pro-inflammatory cytokines such as IL-1, TNFα, TGF-β and CRP.

Association With Physiological Aging and Vascular Markers

Growth differentiation factor 15 is a molecule directly linked to inflammaging. Recently, in a study investigating the plasma proteomic signature of aging in healthy humans, it was demonstrated that GDF-15 levels rise with aging, and exhibit the strongest positive association with age. Interestingly, in the same study, GDF-15 levels were not associated with other CV risk factors indicating that GDF-15 may specifically represent a biomarker of aging (Tanaka et al., 2018). In addition, it has been shown that GDF-15 is produced by senescent endothelial cells (Ha et al., 2019), and is a constituent of the SASP, which as previously

described is a powerful driver of age-related dysfunction influencing important mediators of inflammaging (Coppé et al., 2010; Fujita et al., 2016). As various SASP circulating components have been shown to be strongly associated with advanced chronological age, the behavior of biomarkers such as GDF-15 thus support the hypothesis that the SASP could become an informative candidate biomarker of biological age, meaning its respective biological levels could be leveraged to predict risk for adverse health outcomes (Schafer et al., 2020).

Relevant to the age-related vascular dysfunction, it has been demonstrated that GDF-15 may play an important role in the initiation and progress of atherosclerosis exerting proinflammatory effects induced by the macrophage-produced monokines. Indeed, evidence has shown that GDF-15 has been identified in human carotid atherosclerotic plaques, and also co-localized in macrophages (Wiklund et al., 2010). In addition, early studies have indicated the association of GDF-15 with endothelial and myocardial dysfunction and atherosclerotic burden in the elderly after adjustment for conventional CV risk factors (Lind et al., 2009).

Association With Cardiovascular Disease

In addition, GDF-15 has shown a strong predictive ability of clinical outcomes across different CV risk populations. More specifically, GDF-15 has shown to predict all-cause and CV mortality in healthy populations free from CVD (Wiklund et al., 2010; Eggers et al., 2013), while in women, (but not men), with carotid atherosclerosis it has been shown to predict secondary CVD events (Gohar et al., 2017). Importantly, GDF-15 holds an established role as a predictor of future CV events and mortality in populations with CHD while it is a predictor of all-cause mortality and major CV events in patients with acute coronary syndromes (Hagström et al., 2016), and chronic heart failure (Kempf et al., 2007).

Measurement of Growth Differentiation Factor 15

Several biochemical approaches such as ELISA which allow for the measurement of plasma levels of GDF-15 in cost-effective ways which are easy to perform positions GDF-15 as a strong potential biomarker for the aging process and many age-related diseases (Barma et al., 2017; Conte M. et al., 2020) though considerations should be made with respect to the analyses obtained. According to a recently published study by Doerstling et al. (2018), a selected group of apparently healthy participants (n = 268), were analyzed for circulating GDF-15 using the generalized additive models for location scale and shape (GAMLSS) in order to develop age-dependent centile values. Unadjusted and adjusted COX proportional hazards models were used to assess the association between the derived GDF-15 reference values (expressed as centiles) and all-cause mortality. Smoothed centile curves showed increasing GDF-15 with age in the apparently healthy participants, while age-dependent GDF-15 centiles remained a significant predictor of all-cause mortality in all subsequent adjusted models.

Epigenetic Based Circulating Biomarkers

Epigenetic regulation refers to modifications influencing gene expression independently of gene sequence. These changes mainly include DNA methylation, histone modifications, chromatin remodeling and non-coding RNA based gene regulation (López-Otín et al., 2013); all of which participate in the process of vascular aging and are closely relate to several CV risk factors including older age, high-salt and fat diet, smoking and sedentariness (Ding et al., 2018). Among all epigenetic mechanisms, DNA methylation is the most extensively studied.

Micro-Ribonucleic Acids

Pathophysiology

Micro-ribonucleic acids (miRNAs) are small, highly conserved non-coding RNA molecules involved in the regulation of gene expression (**Table 2**; Ambros, 2004). More than 2000 miRNAs have been discovered in humans that can regulate one third of the genes in the genome (Hammond, 2015).

Association With Physiological Aging and Vascular Markers

There is growing evidence that vascular aging is associated with a dysregulation in the expression of different microRNAs, which are involved in crucial pathogenetic mechanisms leading to impairment of angiogenic processes (Ungvari et al., 2013), decreased cellular stress resilience (Csiszar et al., 2014) and plaque formation, destabilization and rupture (Menghini et al., 2014; Ungvari et al., 2018). Hence, it has been observed that miRNA expression is decreased during cellular senescence, a hallmark of vascular aging, in human tissue culture cells grown *in vitro* (Brosh et al., 2008). Additionally, it has been shown that several miRNAs have similar expression patterns in both senescent cells and in aging human mononuclear cells and, most importantly, that there is an age-dependent decrease in miRNA expression in peripheral blood mononuclear cells (Hooten et al., 2013). However, existing evidence from larger population studies shows that the expression of particular miRNAs distinctly differs in relation to chronological age, with certain miRNAs showing a positive correlation with age while the majority of them being significantly downregulated in older compared to younger individuals (Meder et al., 2014; Ameling et al., 2015; Huan et al., 2018). Interestingly, while age clearly contributes to expression changes in miRNAs, gender seems to have a rather modest effect. In fact, most miRNAs show a similar behavior over the lifespan in males and females (Fehlmann et al., 2020).

TABLE 2 | Significance of several microRNAs (*miRs*) in vascular aging process (based on a systematic review by Navickas et al., 2016).

Process	Type of microRNAs
Endothelial function and angiogenesis	*miR-1, miR-133*
Vascular smooth muscle cell differentiation	*miR-133, miR-145*
Communication between vascular smooth muscle and endothelial cell to stabilize plaques	*miR-145*
Apoptosis	*miR-1, miR-133, miR-499*
Cardiac myocyte differentiation	*miR-1, miR-133, miR-145, miR-208, miR-499*
Repression of cardiac hypertrophy	*miR-133*

There is increasing evidence confirming that miRNAs are highly influential in various physiological and pathological processes which mediate vascular function. For example, it has been demonstrated that miR-126 and miR-21 can mediate a significantly pro-inflammatory vascular phenotype including but not limited to endothelial cell specific inflammation, in addition to vascular smooth muscle cell proliferation and fibrosis (Lin et al., 2016). Similarly, certain miRNAs are recognized as active contributors to the pathogenesis of vascular calcification (Leopold, 2014) and the progression of atherosclerosis (Toyama et al., 2018). Finally, miRNAs such as miR-34a/b/c, miR-21, and miR-501-3p have been independently associated with established vascular markers of aging including PWV (Parthenakis et al., 2017; Toyama et al., 2018; Gatsiou et al., 2021) whereas miR-132 and miR-1 have been shown to predict carotid artery stiffness (Šatrauskienė et al., 2021).

Association With Cardiovascular Disease

So far, there is currently insufficient evidence to conclusively determine the incremental value and the significance of microRNAs as predictors of clinical outcomes related to vascular aging. However, there are a select number of studies in humans highlighting the significance of several distinct microRNA types in this context. For example, microRNA-208b appears to be an important predictor of mortality, even after adjustment for age and gender, microRNA-133a is related to all-cause mortality, and microRNA-133a, microRNA-499, and microRNA-208a/b are significant diagnostic and/or prognostic markers across different CVD progression stages (Navickas et al., 2016). Moreover, microRNA-199a-3p is a predictor of worsening renal function in acute heart failure patients (Bruno et al., 2016), the complex of five microRNAs (microRNA-106a-5p, -424-5p, let-7g-5p, -144-3p, and -660-5p) is associated with the risk of future myocardial infarction (Bye et al., 2016), and a set of seven microRNAs was recently identified to reliably predict CV death in patients with CHD (Karakas et al., 2017). It is possible that the levels, and respective activities of these particular microRNAs may be dysregulated at different stages of the progression of coronary artery disease (CAD).

According to Šatrauskienė et al. (2021), circulating levels of miR-1 and miR-133 correlated with arterial markers of subclinical atherosclerosis (cardio-ankle vascular index, augmentation index normalized to a heart rate of 75 bpm, aortic pulse wave velocity and carotid artery stiffness).

According to Kumar et al. (2020), circulating miR-21 (as well as miR-133b) were dysregulated in patients with CAD, but without MI. Both of these miRs showed association with CAD severity from subclinical atherosclerosis to acute coronary syndrome. Another study by Cengiz et al. (2015) showed that miR-21 was related to subclinical atherosclerosis in carotid arteries in hypertensive patients.

Moreover, Wang et al. (2019) demonstrated that higher plasma levels of circulating miR-208b and miR-499 were positively associated with the severity of CAD.

Different miRs may be dysregulated in patients without CV risk (at the same time it could be dysregulated in other conditions for example multiple sclerosis, oncological diseases). Considering that CVD are multifactorial diseases, analyses of the profile of miRNA panels may have a more substantial diagnostic or prognostic value than any single miRNA.

Measurements of Micro-Ribonucleic Acids

Plasma and serum miRNAs are the most suitable source for reproducible measurements in everyday clinical practice (Chen et al., 2009; Sato et al., 2009; Wang et al., 2011). MiRNAs are extremely stable and long-term storage or freeze-thaw cycles do not significantly affect them (de Lucia et al., 2017). Reverse transcription quantitative real-time polymerase chain reaction (PCR) is the most widely sensitive method for microRNA profiling (Pritchard et al., 2012), however, it is still unclear which is the best strategy for data normalization (Meyer et al., 2010; Kok et al., 2015; Marabita et al., 2016). Another issue is that cut-off values for miRNAs have not been established yet for almost all miRNAs, except miRNA-133a (Wang et al., 2013).

Human studies on circulating miRNAs represent an active research field, and examples exist in the literature showing their potential use as diagnostic biomarkers. Though several normalization strategies are proposed (Marabita et al., 2016), the provision of uniform procedural guidelines - more than a universal set of normalizers, may assist in obtaining reliable quantifications and comparisons of circulating miRNAs (Schwarzenbach et al., 2015).

DNA Methylation

Pathophysiology

DNA methylation is characterized by the transfer of a methyl group from *S*-adenyl methionine to the 5th carbon atom of cytosine by a DNA methyltransferase (DNMT), resulting in the formation of 5-methylcytosine (5mC). In human DNA, 5mC is found in approximately 1.5% of genomic DNA. The majority of DNA methylation occurs on cytosines that precede a guanine nucleotide or CpG regions that are short, interspersed GC-rich DNA sequences (Jeltsch and Gowher, 2019). Those CpG sites occur with high frequency in genomic regions called CpG islands which contain the majority of promoters located near the transcription start site of a gene. In normal cells, CpG islands are usually unmethylated regardless of their level of expression, however, the presence of multiple methylated CpG sites inside them causes stable silencing of genes, thus influencing gene expression (Schübeler, 2015).

Association With Physiological Aging and Vascular Markers

DNA methylation changes and age seem to be inextricably linked and a rich body of literature confirms that aging has a profound effect on genome-wide DNA methylation levels with almost ∼2% of the CpG sites showing changes in DNA methylation (Unnikrishnan et al., 2019). More specifically, it has been demonstrated that the global DNA methylation levels increase over the first few years of life and then decrease beginning in late adulthood. However, at specific loci a significant increase in variability of DNA methylation levels with age has been reported; either toward hypomethylation or hypermethylation, with a predisposition for the second (Jones et al., 2015). Most importantly, certain changes in the methylation of a few hundred CpG sites which are consistent across individuals, have

been strongly associated with age to the extent that multiple prediction models have been invented to accurately predict the chronological age in humans, commonly termed as epigenetic clocks (Hannum et al., 2013; Horvath, 2013). These models can be nowadays applied across a broad spectrum of tissues and cells although the age prediction accuracy varies depending on the tissue type. Even so, epigenetic clocks represent certain functional age-related epigenetic changes that are common across individuals and are currently considered the best biomarkers for predicting mortality in humans. In addition, epigenetic clocks could help explain why some age-related phenotypes occur. In a prospective study of healthy individuals, it was shown that sites of age-associated-DNA methylation display a greater variability across women who developed cervical cancer within 3 years compared to those who remained healthy (Teschendorff et al., 2012). However, it is uncertain as to how well epigenetic clocks can predict biological age.

So far, no human data regarding the association of DNA methylation with markers of vascular stiffness exist.

Association With Cardiovascular Disease

Evidence of differential DNA methylation patterns has been already observed in various CVD states. For example, enhanced DNMT1 activity has been observed in patients with severe atherosclerotic disease and it correlates with increased levels of inflammatory cytokines (Yu et al., 2016). Similarly, a broad trend toward DNA hypermethylation associated with atherosclerotic plaque progression has been observed (Valencia-Morales et al., 2015; Gallego-Fabrega et al., 2020). In addition, increased DNA methylation levels have been documented in elderly patients with myocardial infarction and CHD and have shown a positive correlation with the degree of coronary atherosclerosis (Jiang et al., 2019).

Finally, DNA methylation changes are claimed to be an independent predictor of mortality similarly to other risk factors, such as hypertension and DM (Martella and Fisher, 2021). In a 10-year follow-up study of 832 participants at the age of 70 years, a strong correlation was observed between DNA methylation status and the incidence of CVD (Lind and Lind, 2018). In addition, in a large meta-analysis including 13,089 individuals, DNA methylation-based measures were found to predict all-cause mortality over and above chronological age and traditional risk factors (Chen et al., 2016).

Measurement of DNA Methylation

DNA methylation is predominantly measured in DNA extracted from peripheral blood cells/whole blood cells samples. In terms of technology, the Illumina 450K array is the current gold standard for DNA methylation measurement, but its genomic coverage may be limited especially concerning regions that may be crucial to aging such as repetitive elements and long non-coding RNAs.

Telomere Length

Pathophysiology

Telomere length has steadily garnered interest as a potential marker of measuring and quantifying vascular aging in recent years. Telomeres are defined as non-coding, repetitive DNA sequences (hexanucleotide TTAGGG) which are found at each end of the chromosomes of eukaryotic cells (Blackburn, 1991), are highly conserved and, in total, amount to an estimated 11 to 15 kilobases (Moyzis et al., 1988; Blasco, 2005, 2007). Functionally, telomeres preserve the genomic integrity by acting as protective caps to the genetic material and preventing attrition (Blackburn, 2001; Blasco, 2005).

Association With Physiological Aging and Vascular Markers

Telomere shortening is a well-known hallmark of organismal aging, and an accelerated rate of telomere attrition is also a common feature of age-related diseases. That said, telomere length is currently recognized as a 'biological clock' of sorts, with a significant number of studies in the literature clearly documenting an inverse correlation with human chronological age (Willeit et al., 2010; Müezzinler et al., 2013).

In addition, short telomere length has been significantly associated with vascular markers of arterial stiffness and aging such as PWV, although these findings are not consistent across different sexes and aging groups (Benetos et al., 2001; Strazhesko et al., 2015). Although not in all (De Meyer et al., 2009), there are quite a few studies demonstrating a significant relationship between carotid atherosclerosis, as a robust marker of subclinical atherosclerosis, and short telomere length (Benetos et al., 2004; Panayiotou et al., 2010; Toupance et al., 2017).

Association With Cardiovascular Disease

Data have shown that short telomere length not only precedes the development of atherosclerotic CVD but may even play a pathogenetic role in the development of the disease later in life (Benetos et al., 2018; Huang et al., 2020). Recent meta-analyses have demonstrated that short telomere length is also significantly and independently associated with the risk of CHD (Haycock et al., 2014), and the presence of stroke and DM type 2 (D'Mello et al., 2014). Importantly, there is evidence that short telomere length is an independent predictor of future CV events namely myocardial infarction and stroke (Willeit et al., 2010). Furthermore, in a meta-analysis including 121,749 individuals, short telomere length was associated with increased all-cause mortality risk in the general population (Wang et al., 2018).

Measurement of Telomeres

Telomere length is predominantly measured in DNA extracted from peripheral blood leukocytes. Currently, there are three main methods for measuring telomere length in said DNA: (a) Southern blot (Lin and Yan, 2005), (b) quantitative polymerase chain reaction (Lin and Yan, 2005), and (c) fluorescent *in situ* hybridization-based methods (Lansdorp et al., 1996; Saldanha et al., 2003). Each method presents its own unique advantages and disadvantages, depending on the type of analyses required, and the scale of study being devised. Overall, the Southern blot remains the gold standard for measuring telomere length. Despite being the first and oldest of the three methods, it remains the most accurate, and thus, it is utilized by those interested in precise measurement of telomere length. However, it is the most time-consuming method of the three, and also does not allow for the analysis of individual chromosomes or even cells

(Saldanha et al., 2003; Aviv et al., 2011). qPCR on the other hand, while less accurate, does allow for single cell/chromosome analyses owing to its sensitivity and dynamic range enabling it to work with minute amounts of material. As such, qPCR is often the most employed method for large population-based studies owing to the nature of analyses available, and the efficiency in doing such (Cawthon, 2002; Saldanha et al., 2003).

CONCLUSION

The term biological marker or biomarker refers to any substance, structure or process that can be measured in the human body, and influences or predicts the incidence of outcomes or diseases (The World Health Organization definition). Many candidate biomarkers have been put forward as viable indicators or vascular aging based on current understanding of vascular pathophysiology, and have been scrutinized accordingly, however, none to date have satisfied all necessary criteria to be translated effectively into clinical practice. While genetic and imaging biomarkers represent some of the current practices, identifying an appropriate circulating biomarker/s, that is/are easily measured in blood or in urine, could be an incredibly useful and direct means of determining different phases of the vascular aging and in turn CV disease susceptibility/progression. While technology and approaches allow for the quick and easy measurement of circulating biomarkers, the acquisition and handling of the body fluids containing them present many limitations; such as sensitivity to temperature, rapid blood coagulation and unstability of urine proteins that are the result of renal filtration.

Our choice of circulating biomarkers which are understood and recognized to see their levels change with respect to indices of vascular aging, was derived from the long list of most frequently mentioned in current literature data (**Supplementary Tables S1, S2**), and includes those associated with oxidative stress, inflammation, the extracellular cell matrix, and epigenetics, amongst others. Based on the data presented in this review, it is unlikely that a single molecule will ever be considered adequate for most conditions. In that regard, the new paradigm is the development of diagnostic panels of biomarkers. In this process, we must progress our understanding of existing biomarkers, in addition to identifying new biomarkers, and evaluate their real clinical relevance in addition to embracing new technologies in the fields of proteomics, genomics, metabolomics, lipidomics and bioinformatics to achieve this.

AUTHOR CONTRIBUTIONS

All authors reviewed the relevant literature and drafted the initial manuscript. KG, DT-P, AŠ, JZ, MB-L, and JN made a choice of biomarkers. EG and AL prepared the figure. EF, KR, ÖA, AL, and PN contributed additional material to the manuscript. DT-P, KG, EG, and JN supervised the study and oversaw preparation, editing, and revision of the manuscript. RC, RB, and KR reviewed the manuscript. All authors have read and approved the final manuscript.

FUNDING

RC was supported by a Postdoctoral Fellowship from the National Heart Foundation of Australia (Award ID: 102484).

ACKNOWLEDGMENTS

This manuscript is based upon work from the European COST ACTION-Network for Research in Vascular Aging CA18216 supported by COST (European Cooperation in Science and Technology).

SUPPLEMENTARY MATERIAL

The Supplementary Material for this article can be found online at: https://www.frontiersin.org/articles/10.3389/fphys.2021.789690/full#supplementary-material

REFERENCES

Ambros, V. (2004). The functions of animal microRNAs. *Nature* 431, 350–355. doi: 10.1038/nature02871

Ameling, S., Kacprowski, T., Chilukoti, R. K., Malsch, C., Liebscher, V., Suhre, K., et al. (2015). Associations of circulating plasma microRNAs with age, body mass index and sex in a population-based study. *BMC Med. Genomics* 8:61. doi: 10.1186/s12920-015-0136-7

Ashor, A. W., Siervo, M., and Mathers, J. C. (2016). "Vitamin C, antioxidant status, and cardiovascular aging," in *Molecular Basis of Nutrition and Aging*, eds M. Malavolta and E. Mocchegiani (Cambridge, MA: Academic Press), 609–619. doi: 10.1016/B978-0-12-801816-3.00043-1

Ashor, A. W., Siervo, M., Lara, J., Oggioni, C., and Mathers, J. C. (2014). Antioxidant vitamin supplementation reduces arterial stiffness in adults: a systematic review and meta-analysis of randomized controlled trials. *J. Nutr.* 144, 1594–1602. doi: 10.3945/jn.114.195826

Aviv, A., Hunt, S. C., Lin, J., Cao, X., Kimura, M., and Blackburn, E. (2011). Impartial comparative analysis of measurement of leaukocyte telomere length/DNA content by Southern blots and qPCR. *Nucleic Acids Res.* 39, e134. doi: 10.1093/nar/gkr634

Barma, M., Khan, F., Price, R. J. G., Donnan, P. T., Messow, C. M., Ford, I., et al. (2017). Association between GDF-15 levels and changes in vascular and physical function in older patients with hypertension. *Aging Clin. Exp. Res.* 29, 1055–1059. doi: 10.1007/s40520-016-0636-0

Basisty, N., Kale, A., Jeon, O. H., Kuehnemann, C., Payne, T., Rao, C., et al. (2020). A proteomic atlas of senescence-associated secretomes for aging biomarker development. *PLoS Biol.* 18:e3000599. doi: 10.1371/journal.pbio.3000599

Batra, G., Lakic, T., Lindbäck, J., Held, C., White, H. D., Stewart, R. A. H., et al. (2021). STABILITY investigators. Interleukin 6 and cardiovascular outcomes in patients with chronic kidney disease and chronic coronary syndrome. *JAMA Cardiol.* 9:e213079. doi: 10.1001/jamacardio.2021.3079

Benetos, A., Jeffrey, P., Gardner, J. P., Zureik, M., Labat, C., Xiaobin, L., et al. (2004). Short telomeres are associated with increased carotid atherosclerosis in hypertensive subjects. *Hypertension* 2004, 182–185. doi: 10.1161/01.HYP.0000113081.42868.f4

Benetos, A., Okuda, K., Lajemi, M., Kimura, M., Thomas, F., Skurnick, J., et al. (2001). Telomere length as an indicator of biological aging. The gender effect and relation with pulse pressure and pulse wave velocity. *Hypertension* 37, 381–385.

Benetos, A., Toupance, S., Gautier, S., Labat, C., Kimura, M., Rossi, P. M., et al. (2018). Short leukocyte telomere length precedes clinical expression of atherosclerosis. The blood-and-muscle model. *Circ. Res.* 122, 616–623.

Biomarkers Definitions Working Group (2001). Biomarkers and surrogate endpoints: preferred definitions and conceptual framework. *Clin. Pharmacol. Ther.* 69, 89–95. doi: 10.1067/mcp.2001.113989

Blackburn, E. H. (1991). Structure and function of telomeres. *Nature* 350, 569–573. doi: 10.1038/350569a0

Blackburn, E. H. (2001). Switching and signalling at the telomere. *Cell* 106, 661–673. doi: 10.1016/S0092-8674(01)00492-5

Blakenberg, S., Rupprecht, H. J., Poirier, O., Bickel, C., Smieja, M., Hafner, G., et al. (2003). Plasma concentrations and genetic variation of matrix metalloproteinase 9 and prognosis of patients with cardiovascular disease. *Circulation* 107, 1579–1585.

Blankenberg, S., Rupprecht, H. J., Bickel, C., Torzewski, M., Hafner, G., Tiret, L., et al. (2003). Glutathione peroxidase 1 activity and cardiovascular events in patients with coronary artery disease. *N. Engl. J. Med.* 349, 1605–1613. doi: 10.1056/NEJMoa030535

Blasco, M. A. (2005). Telomeres and human disease: aging, cancer and beyond. *Nat. Rev. Genet.* 6, 611–622. doi: 10.1038/nrg1656

Blasco, M. A. (2007). Telomere length, stem cells and aging. *Nat. Chem. Biol.* 3, 640–649. doi: 10.1038/nchembio.2007.38

Bonnema, D. D., Webb, C. S., Pennington, W. R., Stroud, R. E., Leonardi, A. E., Clark, L. L., et al. (2007). Effects of age on plasma matrix metalloproteinases (MMPs) and tissue inhibitor of metalloproteinases (TIMPs). *J. Card. Fail.* 13, 530–540. doi: 10.1016/j.cardfail.2007.04.010

Bootcov, M. R., Bauskin, A. R., Valenzuela, S. M., Moore, A. G., Bansal, M., He, X. Y., et al. (1997). MIC-1, a novel macrophage inhibitory cytokine, is a divergent member of the TGF-beta superfamily. *Proc. Natl. Acad. Sci. U.S.A.* 94, 11514–11519. doi: 10.1073/pnas.94.21.11514

Brosh, R., Shalgi, R., Liran, A., Landan, G., Korotayev, K., Nguyen, G. H., et al. (2008). p53-Repressed miRNAs are involved with E2F in a feed-forward loop promoting proliferation. *Mol. Syst. Biol.* 4:229. doi: 10.1038/msb.2008.65

Bruno, N., ter Maaten, J. M., Ovchinnikova, E. S., Vegter, E. L., Valente, M. A., van der Meer, P., et al. (2016). MicroRNAs relate to early worsening of renal function in patients with acute heart failure. *Intern. J. Cardiol.* 203, 564–569. doi: 10.1016/j.ijcard.2015.10.217

Bye, A., Røsjø, H., Nauman, J., Silva, G. J., Follestad, T., Omland, T., et al. (2016). Circulating microRNAs predict future fatal myocardial infarction in healthy individuals – The HUNT study. *J. Mol. Cell. Cardiol.* 97, 162–168. doi: 10.1016/j.yjmcc.2016.05.009

Canugovi, C., Stevenson, M. D., Vendrov, A. E., Hayami, T., Robidoux, J., Xiao, H., et al. (2019). Increased mitochondrial NADPH oxidase 4 (NOX4) expression in aging is a causative factor in aortic stiffening. *Redox Biol.* 26:101288. doi: 10.1016/j.redox.2019.101288

Cavusoglu, E., Ruwende, C., Chopra, V., Yanamadala, S., Eng, C., Clark, L. T., et al. (2006). Tissue inhibitor of metalloproteinase-1 (TIMP-1) is an independent predictor of all-cause mortality, cardiac mortality and myocardial infarction. *Am. Heart J.* 151, 1101.e1-e8. doi: 10.1016/j.ahj.2006.02.029

Cawthon, R. M. (2002). Telomere measurement by quantitative PCR. *Nucleic Acids Res.* 30:e4.

Cengiz, M., Yavuzer, S., Kılıçkıran Avcı, B., and Öngen, Z. (2015). Circulating miR-21 and eNOS in subclinical atherosclerosis in patients with hypertension. *Clin. Exp. Hypertens.* 37, 643–649. doi: 10.3109/10641963.2015.1036064

Chen, B. H., Marioni, R. E., Colicino, E., Peters, M. J., Ward-Caviness, C. K., Tsai, P. C., et al. (2016). DNA methylation-based measures of biological age: meta-analysis predicting time to death. *Aging* 8, 1844–1865. doi: 10.18632/aging.101020

Chen, Q., Wang, Q., Zhu, J., Xiao, Q., and Zhang, L. (2018). II. NITRIC OXIDE GENERATION AND VASCULAR FUNCTION. Reactive oxygen species: key regulators in vascular health and diseases. *Br. J. Pharmacol.* 175, 1279–1292. doi: 10.1111/bph.13828

Chen, Y., Gelfond, J. A., McManus, L. M., and Shireman, P. K. (2009). Reproducibility of quantitative RT-PCR array in miRNA expression profiling and comparison with microarray analysis. *BMC Genomics* 10:407. doi: 10.1186/1471-2164-10-407

Cheng, X.-C., Fang, H., and Xu, W.-F. (2008). Advances in assays of matrix metalloproteinases (MMPs) and their inhibitors. *J. Enzyme Inhib. Med. Chem.* 23, 154–167.

Chi, L., Li, Y., Stehno-Bittel, L., Gao, J., Morrison, D. C., Stechschulte, D. J., et al. (2001). Interleukin-6 production by endothelial cells via stimulation of protease-activated receptors is amplified by endotoxin and tumor necrosis factor-alpha. *J. Interferon Cytokine Res.* 21, 231–240.

Compté, N., Boudjeltia, K. Z., Vanhaeverbeek, M., De Breucker, S., Pepersack, T., Tassignon, J., et al. (2013). Increased basal and alum-induced interleukin-6 levels in geriatric patients are associated with cardiovascular morbidity. *PLoS One* 8:e81911. doi: 10.1371/journal.pone.0081911

Conte, E., Andreini, D., Magnoni, M., Masson, S., Mushtaq, S., Canestrari, M., et al. (2020). Association of high-risk coronary atherosclerosis at CCTA with clinical and circulating biomarkers: insight from CAPIRE study. *J. Cardiovasc. Comput. Tomogr.* 15, 73–80.

Conte, M., Martucci, M., Mosconi, G., Chiariello, A., Cappuccilli, M., Totti, V., et al. (2020). GDF15 plasma level is inversely associated with level of physical activity and correlates with markers of inflammation and muscle weakness. *Front. Immunol.* 11:915. doi: 10.3389/fimmu.2020.00915

Coppé, J.-P., Desprez, P.-Y., Krtolica, A., and Campisi, J. (2010). The senescence-associated secretory phenotype: the dark side of tumor suppression. *Annu. Rev. Pathol. Mech. Dis.* 5, 99–118. doi: 10.1146/annurev-pathol-121808-102144

Crimmins, E., Vasunilashorn, S., Kim, J. K., and Alley, D. (2008). Biomarkers related to aging in human populations. *Adv. Clin. Chem.* 46, 161–216. doi: 10.1016/s0065-2423(08)00405-8

Csiszar, A., Gautam, T., Sosnowska, D., Tarantini, S., Banki, E., Tucsek, Z., et al. (2014). Caloric restriction confers persistent anti-oxidative, pro-angiogenic, and anti-inflammatory effects and promotes anti-aging miRNA expression profile in cerebromicrovascular endothelial cells of aged rats. *Am. J. Physiol. Heart Circ. Physiol.* 307, H292–H306. doi: 10.1152/ajpheart.00307.2014

Cunha, P. G., Boutouyrie, P., Nilsson, P. M., and Laurent, S. (2017). Early vascular aging (EVA): definitions and clinical applicability. *Curr. Hypertens. Rev.* 13, 8–15. doi: 10.2174/1573402113666170413094319

D'Mello, M. J. J., Ross, S. A., Briel, M., Anand, S. S., Gerstein, H., and Paré, G. (2014). Association between shortened leukocyte telomere length and cardiometabolic outcomes systematic review and meta-analysis. *Circul. Cardiovasc. Genet.* 8, 82–90. doi: 10.1161/CIRCGENETICS.113.000485

Danesh, J., Kaptoge, S., Mann, A. G., Sarwar, N., Wood, A. M., Angleman, S. B., et al. (2008). Long-term interleukin-6 levels and subsequent risk of coronary heart disease: two new prospective studies and a systematic review. *PLoS Med.* 5:e78. doi: 10.1371/journal.pmed.0050078

de Lucia, C., Komici, K., Borghetti, G., Femminella, G. D., Bencivenga, L., Cannavo, A., et al. (2017). microRNA in cardiovascular aging and age-related cardiovascular diseases. *Front. Med.* 4:74. doi: 10.3389/fmed.2017.00074

De Meyer, T., Rietzschel, E. R., De Buyzere, M. L., Langlois, M. R., De Bacquer, D., Segers, P., et al. (2009). On behalf of the asklepios study investigators, systemic telomere length and preclinical atherosclerosis: the asklepios study. *Eur. Heart J.* 30, 3074–3081. doi: 10.1093/eurheartj/ehp324

Derhovanessian, E., Larbi, A., and Pawelec, G. (2009). Biomarkers of human immunosenescence: impact of Cytomegalovirus infection. *Curr. Opin. Immunol.* 21, 440–445. doi: 10.1016/j.coi.2009.05.012

Di Micco, R., Krizhanovsky, V., Baker, D., and d'Adda di Fagagna, F. (2021). Cellular senescence in ageing: from mechanisms to therapeutic opportunities. *Nat. Rev. Mol. Cell Biol.* 22, 75–95. doi: 10.1038/s41580-020-00314-w

Ding, Y. N., Tang, X., Chen, H. Z., and Liu, D. P. (2018). Epigenetic regulation of vascular aging and age-related vascular diseases. *Adv. Exp. Med. Biol.* 1086, 55–75. doi: 10.12066/j.issn.1007-2861.2138

Doerstling, S., Hedberg, P., Öhrvik, J., Leppert, J., and Henriksen, E. (2018). Growth differentiation factor 15 in a community-based sample: age-dependent reference limits and prognostic impact. *Ups. J. Med. Sci.* 123, 86–93. doi: 10.1080/03009734.2018.1460427

Donato, A. J., Morgan, R. G., Walker, A. E., and Lesniewski, L. A. (2015). Cellular and molecular biology of aging endothelial cells. *J. Mol. Cell. Cardiol.* 89(Pt. B), 122–135. doi: 10.1016/j.yjmcc.2015.01.021

Eggers, K. M., Kempf, T., Wallentin, L., Wollert, K. C., and Lind, L. (2013). Change in growth differentiation factor 15 concentrations over time independently

predicts mortality in community-dwelling elderly individuals. *Clin. Chem.* 59, 1091–1098.

Fairlie, W. D., Moore, A. G., Bauskin, A. R., Russell, P. K., Zhang, H. P., and Breit, S. N. (1999). MIC-1 is a novel TGF-beta superfamily cytokine associated with macrophage activation. *J. Leukoc. Biol.* 65, 2–5. doi: 10.1002/jlb.65.1.2

Fehlmann, T., Kahraman, M., Ludwig, N., Backes, C., Galata, V., Keller, V., et al. (2020). Evaluating the use of circulating MicroRNA profiles for lung cancer detection in symptomatic patients. *JAMA Oncol.* 6, 714–723. doi: 10.1001/jamaoncol.2020.0001

Ferrini, M. G., Davila, H. H., Valente, E. G., Gonzalez-Cadavid, N. F., and Rajfer, J. A. (2004). Aging-related induction of inducible nitric oxide synthase is vasculo-protective to the arterial media. *Cardiovasc. Res.* 61, 796–805. doi: 10.1016/j.cardiores.2003.12.006

Ferrucci, L., Gonzalez-Freire, M., Fabbri, E., Simonsick, E., Tanaka, T., Moore, Z., et al. (2020). Measuring biological aging in humans: a quest. *Aging Cell* 19:e13080. doi: 10.1111/acel.13080

Franceschi, C. (1989). Cell proliferation and cell death in the aging process. *Aging Clin. Exp. Res.* 1, 3–13. doi: 10.1007/BF03323871

Franceschi, C., and Cossarizza, A. (1995). The reshaping of the immune system with age. *Int. Rev. Immunol.* 12, 1–4. doi: 10.3109/08830189509056697

Franceschi, C., Bonafè, M., Valensin, S., Olivieri, F., De Luca, M., Ottaviani, E., et al. (2000). Inflamm-aging. An evolutionary perspective on immunosenescence. *Ann. N. Y. Acad. Sci.* 908, 244–254. doi: 10.1111/j.1749-6632.2000.tb06651.x

Franceschi, C., Santoro, A., and Capri, M. (2020). The complex relationship between Immunosenescence and Inflammaging: special issue on the New Biomedical Perspectives. *Semin. Immunopathol.* 42, 517–520. doi: 10.1007/s00281-020-00823-y

Freitas-Rodríguez, S., Folgueras, A. R., and López-Otín, C. (2017). The role of matrix metalloproteinases in aging: tissue remodeling and Beyond. *BBA Mol. Cell Res.* 1864, 2015–2025. doi: 10.1016/j.bbamcr.2017.05.007

Fujita, Y., Taniguchi, Y., Shinkai, S., Tanaka, M., and Ito, M. (2016). Secreted growth differentiation factor 15 as a potential biomarker for mitochondrial dysfunctions in aging and age-related disorders. *Geriatr. Gerontol. Int.* 16(Suppl. 1), 17–29. doi: 10.1111/ggi.12724

Gallego-Fabrega, C., Cullell, N., Soriano-Tárraga, C., Carrera, C., Torres-Aguila, N. P., Muiño, E., et al. (2020). DNA methylation of MMPs and TIMPs in atherothrombosis process in carotid plaques and blood tissues. *Oncotarget* 11, 905–912. doi: 10.18632/oncotarget.27469

Gatsiou, A., Georgiopoulos, G., Vlachogiannis, N. I., Pfisterer, L., Fischer, A., Sachse, M., et al. (2021). Additive contribution of microRNA-34a/b/c to human arterial aging and atherosclerosis. *Atherosclerosis* 327, 49–58. doi: 10.1016/j.atherosclerosis.2021.05.005

Gkaliagkousi, E., Doumas, M., Gavriilaki, E., Triantafyllou, A., Vogiatzis, K., Anyfanti, P., et al. (2012). Elevated levels of MMP-9 in untreated patients with stage I essential hypertension. *Clin. Exp. Hypertens.* 34, 561–566. doi: 10.3109/10641963.2012.681726

Gohar, A., Gonçalves, I., Vrijenhoek, J., Haitjema, S., van Koeverden, I., Nilsson, J., et al. (2017). Circulating GDF-15 levels predict future secondary manifestations of cardiovascular disease explicitly in women but not men with atherosclerosis. *Intern. J. Cardiol.* 241, 430–436. doi: 10.1016/j.ijcard.2017.03.101

Goncalves, I., Bengtsson, E., Colhoun, H. M., Shore, A. C., Palombo, C., Natali, A., et al. (2015). SUMMIT consortium elevated plasma levels of MMP-12 are associated with atherosclerotic burden and symptomatic cardiovascular disease in subjects with type 2 diabetes. *Arterioscler. Thromb. Vasc. Biol.* 35, 1723–1731. doi: 10.1161/ATVBAHA.115.305631

Gong, X., Ma, Y., Ruan, Y., Fu, G., and Wu, S. (2014). Long-term atorvastatin improves age-related endothelial dysfunction by ameliorating oxidative stress and normalizing eNOS/iNOS imbalance in rat aorta. *Exp. Gerontol.* 52, 9–17. doi: 10.1016/j.exger.2014.01.015

Gong, Y., Liang, S., Zeng, L., Ni, Y., Zhou, S., and Yuan, X. (2019). Effects of blood sample handling procedures on measurable interleukin 6 in plasma and serum. *J. Clin. Lab. Anal.* 33:e229241.

Gorgoulis, V., Adams, P. D., Alimonti, A., Bennett, D. C., Bischof, O., Bishop, C., et al. (2019). Cellular senescence: defining a path forward. *Cell* 179, 813–827. doi: 10.1016/j.cell.2019.10.005

Graham, C., Chooniedass, R., Stefura, W. P., Lotoski, L., Lopez, P., Befus, A. D., et al. (2017). Stability of pro- and anti-inflammatory immune biomarkers for human cohort studies. *J. Transl. Med.* 15:53. doi: 10.1186/s12967-017-1154-3

Groenwagen, K. A., den Ruijter, H. M., Pasterkamp, D. R., Polak, J. F., Bots, M. L., and Peters Sanne, A. E. (2016). Vascular age to determine cardiovascular disease risk: a systematic review of its concepts, definitions, and clinical applications. *Eur. J. Prev. Cardiol.* 23, 264–274. doi: 10.1177/2047487314566999

Guzik, T. J., and Touyz, R. M. (2017). Oxidative stress, inflammation, and vascular aging in hypertension. *Hypertension* 70, 660–667.

Ha, G., De Torres, F., Arouche, N., Benzoubir, N., Ferratge, S., Hatem, E., et al. (2019). GDF15 secreted by senescent endothelial cells improves vascular progenitor cell function. *PLoS One* 14:e0216602. doi: 10.1371/journal.pone.0216602

Hagström, E., James, S. K., Bertilsson, M., Becker, R. C., Himmelmann, A., Husted, S., et al. (2016). Growth differentiation factor-15 level predicts major bleeding and cardiovascular events in patients with acute coronary syndromes: results from the PLATO study. *Eur. Heart J.* 37, 1325–1333. doi: 10.1093/eurheartj/ehv491

Hammond, S. M. (2015). An overview of microRNAs. *Adv.Drug Deliv. Rev.* 87, 3–14. doi: 10.1016/j.addr.2015.05.001

Hannum, G., Guinney, J., Zhao, L., Zhang, L., Hughes, G., Sadda, S. V., et al. (2013). Genome-wide methylation profiles reveal quantitative views of human aging rates. *Mol. Cell* 49, 359–367. doi: 10.1016/j.molcel.2012.10.016

Hansson, J., Vasan, R. S., Ärnlöv, J., Ingelsson, E., Lind, L., Larsson, A., et al. (2011). Biomarkers of extracellular matrix metabolism (MMP-9 and TIMP-1) and risk of stroke, myocardial infarction and cause-specific mortality:cohort study. *PLoS One* 6:e16185. doi: 10.1371/journal.pone.0016185

Haycock, P. C., Heydon, E. E., Kaptoge, S., Butterworth, A. S., Thompson, A., Willeit, P., et al. (2014). Leucocyte telomere length and risk of cardiovascular disease: systematic review and meta-analysis. *BMJ* 349:g4227. doi: 10.1136/bmj.g4227

He, S., and Sharpless, N. E. (2017). Senescence in health and disease. *Cell* 169, 1000–1011. doi: 10.1016/j.cell.2017.05.015

He, T., Joyner, M. J., and Katusic, Z. S. (2009). Aging decreases expression and activity of glutathione peroxidase-1 in human endothelial progenitor cells. *Microvasc. Res.* 78, 447–452. doi: 10.1016/j.mvr.2009.08.009

Held, C., Harvey, D., White, H. D., Stewart, R. A. H., Budaj, A., Cannon, C. P., et al. (2017). Inflammatory biomarkers interleukin-6 and C-reactive protein and outcomes in stable coronary heart disease: experiences from the STABILITY (Stabilization of Atherosclerotic Plaque by Initiation of Darapladib Therapy) trial and on behalf of the STABILITY Investigators. *J. Am. Heart Assoc.* 6:e005077. doi: 10.1161/JAHA.116.005077

Hirano, T., and Murakami, M. (2020). COVID-19: a new virus, but a familiar receptor and cytokine release syndrome. *Immunity* 52, 731–733. doi: 10.1016/j.immuni.2020.04.003

Hoefer, I. E., Steffens, S., Ala-Korpela, M., Bäck, M., Badimon, L., and Bochaton-Piallat, M.-L. (2015). On behalf of the ESC working group atherosclerosis and vascular biology. novel methodologies for biomarker discovery in atherosclerosis. *Transl. Med. EHJ* 36, 2635–2642. doi: 10.1093/eurheartj/ehv236

Hooten, N. N., Fitzpatrick, M., Wood, W. H., De, S., Ejiogu, N., Zhang, Y., et al. (2013). Age-related changes in microRNA levels in serum. *Aging* 5, 725–740. doi: 10.18632/aging.100603

Horvath, S. (2013). DNA methylation age of human tissues and cell types. *Genome Biol.* 14:3156. doi: 10.1186/gb-2013-14-10-r115

Huan, T., Chen, G., Liu, C., Bhattacharya, A., Rong, J., Chen, B. H., et al. (2018). Age-associated microRNA expression in human peripheral blood is associated with all-cause mortality and age-related traits. *Aging Cell* 17:e12687. doi: 10.1111/acel.12687

Huang, L. C., Lin, R. T., Chen, C. F., Chen, C. H., Juo, S. H., and Lin, H. F. (2016). Predictors of carotid intima-media thickness and plaque progression in a Chinese population. *J. Atheroscler. Thromb.* 23, 940–949. doi: 10.5551/jat.32177

Huang, Y. Q., Jie, L., Chen, Jy, Tang, S. T., Huang, C., and Feng, Y. Q. (2018). The relationship between soluble CD40 ligand level and atherosclerosis in white-coat hypertension. *J. Hum. Hypertens.* 32, 40–45. doi: 10.1038/s41371-017-0016-z

Huang, Y., Liu, L., Lo, K., Huang, J., Zhang, B., and Feng, Y. (2020). The relationship between mean telomere length and blood pressure: results from the National Health and Nutrition Examination Surveys. *Ann. Transl. Med.* 8:535. doi: 10.21037/atm.2020.03.205

Iannarelli, N. J., MacNeil, A. J., Dempster, K. S., Wade, T. J., and O'Leary, D. D. (2021). Serum MMP-3 and its association with central arterial stiffness among young adults is moderated by smoking and BMI. *Physiol. Rep.* 9:e14920. doi: 10.14814/phy2.14920

Ighodaro, O., and Akinloye, O. (2018). First line defence antioxidants-superoxide dismutase (SOD), catalase (CAT) and glutathione peroxidase (GPX): their fundamental role in the entire antioxidant defence grid. *Alex. J. Med.* 54, 287–293. doi: 10.1016/j.ajme.2017.09.001

Iyer, R. P., de Castro Brás, L. E., Patterson, N. L., Bhowmick, M., Flynn, E. R., Asher, M., et al. (2016). Early matrix metalloproteinase-9 inhibition post-myocardial infarction worsens cardiac dysfunction by delaying inflammation resolution. *J. Mol. Cell. Cardiol.* 100, 109–117. doi: 10.1016/j.yjmcc.2016.10.005

Izzo, C., Vitillo, P., Di Pietro, P., Visco, V., Strianese, A., Virtuoso, N., et al. (2021). The role of oxidative stress in cardiovascular aging and cardiovascular diseases. *Life* 11:60. doi: 10.3390/life11010060

Izzo, C., Vitillo, P., Di Pietro, P., Visco, V., Strianese, A., Virtuoso, N., et al. (2016). "Chapter 43 – vitamin C, antioxidant status, and cardiovascular aging," in *Molecular Basis of Nutrition and Aging*, eds M. Malavolta and E. Mocchegiani (Cambridge, MA: Academic Press), 609–619.

Jeltsch, A., and Gowher, H. (2019). Editorial-Role of DNA methyltransferases in the epigenome. *Genes (Basel)* 10, 574–578.

Jiang, S., Kamei, N., Bolton, J. L., Ma, X., Stern, H. S., Baram, T. Z., et al. (2019). Intra-individual methylomics detects the impact of early-life adversity. *Life Sci. Alliance* 2:e201800204. doi: 10.26508/lsa.201800204

Jones, M. J., Goodman, S. J., and Kobor, M. S. (2015). DNA methylation and healthy human aging. *Aging Cell* 14, 924–932. doi: 10.1111/acel.12349

Kaptoge, S., Di Angelantonio, E., Lowe, G., Pepys, M. B., Thompson, S. G., Collins, R., et al. (2009). Emerging Risk Factors Collaboration, C-reactive protein concentration and risk of coronary heart disease, stroke, and mortality: an individual participant meta-analysis. *Lancet* 375, 132–140. doi: 10.1016/S0140-6736(09)61717-7

Kaptoge, S., Seshasai, S. R. K., Pei, G., Freitag, D. F., Butterworth, A. S., Borglykke, A., et al. (2014). Inflammatory cytokines and risk of coronary heart disease: new prospective study and updated meta-analysis. *Eur. Heart J.* 35, 578–589. doi: 10.1093/eurheartj/eht367

Karakas, M., Schulte, C., Appelbaum, S., Ojeda, F., Lackner, K. J., Münzel, T., et al. (2017). Circulating microRNAs strongly predict cardiovascular death in patients with coronary artery disease-results from the large AtheroGene study. *Eur. Heart J.* 38, 516–523. doi: 10.1093/eurheartj/ehw250

Kattoor, A. J., Pothineni, N. V. K., Palagiri, D., and Mehta, J. L. (2017). Oxidative stress in atherosclerosis. *Curr. Atheroscler. Rep.* 19:42. doi: 10.1007/s11883-017-0678-6

Kempf, T., von Haehling, S., Peter, T., Allhoff, T., Cicoira, M., Doehner, W., et al. (2007). Prognostic utility of growth differentiation factor-15 in patients with chronic heart failure. *J.Am. Coll. Cardiol.* 50, 1054–1060. doi: 10.1016/j.jacc.2007.04.091

Kenis, G., Teunissen, C., De Jongh, R., Bosmans, E., Steinbusch, H., and Maes, M. (2002). Stability of interleukin-6, soluble interleukin 6 receptor, interleukin 10 and CC16 in human serum. *Cytokine* 19, 228–235.

Kirkwood, K. L. (2018). Inflammaging. *Immunol. Investig.* 47, 770–773. doi: 10.1080/08820139.2018.1552392

Kleiner, D. E., and Stetler-Stevenson, W. G. (1994). Quantitative zymography: detection of picogram quantities of gelatinases. *Anal. Biochem.* 218, 325–329. doi: 10.1006/abio.1994.1186

Kok, M. G., Halliani, A., Moerland, P. D., Meijers, J. C., Creemers, E. E., and Pinto-Sietsma, S. J. (2015). Normalization panels for the reliable quantification of circulating microRNAs by RT-qPCR. *FASEB J.* 29, 3853–3862. doi: 10.1096/fj.15-271312

Kormi, I., Nieminen, M. T., Havulinna, A. S., Zeller, T., Blankenberg, S., Tervahartiala, T., et al. (2017). Matrix metalloproteinase-8 and tissue inhibitor of matrix metalloproteinase-1 predict incident cardiovascular disease events and all-cause mortality in a population-based cohort. *Eur. J. Prev. Cardiol.* 24, 1136–1144. doi: 10.1177/2047487317706585

Kovacic, J. C., Moreno, P., Hachinski, V., Nabel, E. G., and Fuster, V. (2011). Cellular senescence, vascular disease, and aging: part 1 of a 2-part review. *Circulation* 123, 1650–1660.

Kumar, D., Narang, R., Sreenivas, V., Rastogi, V., Bhatia, J., Saluja, D., et al. (2020). Circulatory miR-133b and miR-21 as novel biomarkers in early prediction and diagnosis of coronary artery disease. *Genes (Basel)* 11:164. doi: 10.3390/genes11020164

Lakatta, E. G. (2007). Central arterial aging and the epidemic of systolic hypertension and atherosclerosis. *J. Am. Soc. Hypertens.* 1, 302–340. doi: 10.1016/j.jash.2007.05.001

Lansdorp, P. M., Verwoerd, N. P., van de Rijke, F. M., Dragowska, V., Little, M. T., Dirks, R. W., et al. (1996). Heterogeneity in telomere length of human chromosomes. *Hum. Mol. Genet.* 5, 685–691. doi: 10.1093/hmg/5.5.685

Lassegue, B., San Martin, A., and Griendling, K. K. (2012). Biochemistry, physiology, and pathophysiology of NADPH oxidases in the cardiovascular system. *Circ. Res.* 110, 1364–1390.

Lee, W. J., Peng, L. N., Loh, C. H., and Chen, L. K. (2020). Sex-different associations between serum homocysteine, high-sensitivity C-reactive protein and sarcopenia: results from I-Lan Longitudinal Aging Study. *Exp. Gerontol.* 132:110832. doi: 10.1016/j.exger.2020.110832

Lehrke, M., Greif, M., Broedl, U. C., Lebherz, C., Laubender, R. P., Becker, A., et al. (2009). MMP-1 serum levels predict coronary atherosclerosis in humans. *Cardiovasc. Diabetol.* 8:50. doi: 10.1186/1475-2840-8-50

Leopold, J. A. (2014). MicroRNAs regulate vascular medial calcification. *Cells* 3, 963–980. doi: 10.3390/cells3040963

Li, R., Jia, Z., and Trush, M. A. (2016). Defining ROS in biology and medicine. *React. Oxyg. Species (Apex)* 1, 9–21. doi: 10.20455/ros.2016.803

Li, Y., Zhong, X., Cheng, G., Zhao, C., Zhang, L., Hong, Y., et al. (2017). Hs-CRP and all-cause, cardiovascular, and cancer mortality risk: a meta-analysis. *Atherosclerosis* 259, 75–82. doi: 10.1016/j.atherosclerosis.2017.02.003

Liao, H., Li, Z., Zheng, D., Liu, J., Liu, Y., Xiao, C., et al. (2014). Increased Hs-CRP/adiponectin ratio is associated with increase carotid intima-media thickness. *Lipids Health Dis.* 13:120. doi: 10.1186/1476-511X-13-120

Libby, P., Ridker, P. M., and Maseri, A. (2002). Inflammation and atherosclerosis. *Circulation* 105, 1135–1143. doi: 10.1161/hc0902.104353

Liguori, I., Russo, G., Curcio, F., Bulli, G., Aran, L., Della-Morte, D., et al. (2018). Oxidative stress, aging, and diseases. *Clin. Interv. Aging* 13, 757–772. doi: 10.2147/CIA.S158513

Lin, K. W., and Yan, J. (2005). The telomere length dynamic and methods of its assessment. *J. Cell. Mol. Med.* 9, 977–989. doi: 10.1111/j.1582-4934.2005.tb00395.x

Lin, X., Zhan, J.-K., Wang, Y.-J., Tan, P., Chen, Y.-Y., Deng, H.-Q., et al. (2016). Function, role, and clinical application of MicroRNAs in vascular aging. *Biomed Res. Int.* 2016:6021394. doi: 10.1155/2016/6021394

Lind, L., Wallentin, L., Kempf, T., Tapken, H., Quint, A., Lindahl, B., et al. (2009). Growth-differentiation factor-15 is an independent marker of cardiovascular dysfunction and disease in the elderly: results from the Prospective Investigation of the Vasculature in Uppsala Seniors (PIVUS) Study. *Eur. Heart J.* 30, 2346–2353. doi: 10.1093/eurheartj/ehp261

Lind, P. M., and Lind, L. (2018). Endocrine-disrupting chemicals and risk of diabetes: an evidence-based review. *Diabetologia* 61, 1495–1502. doi: 10.1007/s00125-018-4621-3

Loperena, R., and Harrison, D. G. (2017). Oxidative stress and hypertensive diseases. *Med. Clin. North Am.* 101, 169–193. doi: 10.1016/j.mcna.2016.08.004

Loperena, R., Van Beusecum, J. P., Itani, H. A., Engel, N., Laroumanie, F., Xiao, L., et al. (2018). Hypertension and increased endothelial mechanical stretch promote monocyte differentiation and activation: roles of STAT3, interleukin 6 and hydrogen peroxide. *Cardiovasc. Res.* 114, 1547–1563. doi: 10.1093/cvr/cvy112

Lopez-Avila, V., Juliet, V., and Spencer, J. V. (2008). Methods for detection of matrix metalloproteinases as biomarkers in cardiovascular disease. *Clin. Med. Cardiol.* 2, 75–87.

López-Otín, C., and Hunter, T. (2010). The regulatory crosstalk between kinases and proteases in cancer. *Nat. Rev. Cancer* 10, 278–292. doi: 10.1038/nrc2823

López-Otín, C., Blasco, M. A., Partridge, L., Serrano, M., and Kroemer, G. (2013). The hallmarks of aging. *Cell* 153, 1194–1217. doi: 10.1016/j.cell.2013.05.039

Loppnow, H., and Libby, P. (1989). Adult human vascular endothelial cells express the IL6 gene differentially in response to LPS or IL1. *Cell Immunol.* 122, 493–503. doi: 10.1016/0008-8749(89)90095-6

Manabe, S., Okura, T., Watanabe, S., Fukuoka, T., and Higaki, J. (2005). Effects of angiotensin II receptor blockade with valsartan on pro-inflammatory cytokines

in patients with essential hypertension. *J. Cardiovasc. Pharmacol.* 46, 735–739. doi: 10.1097/01.fjc.0000185783.00391.60

Marabita, F., de Candia, P., Torri, A., Tegnér, J., Abrignani, S., and Rossi, R. L. (2016). Normalization of circulating microRNA expression data obtained by quantitative real-time RT-PCR. *Brief. Bioinform.* 17, 204–212.

Marin, V., Montero-Julian, F. A., Grès, S., Boulay, V., Bongrand, P., Farnarier, C., et al. (2001). The IL-6-soluble IL-6Ralpha autocrine loop of endothelial activation as an intermediate between acute and chronic inflammation: an experimental model involving thrombin. *J. Immunol.* 167, 3435–3442.

Martella, A., and Fisher, D. I. (2021). Regulation of gene expression and the elucidative role of CRISPR-based epigenetic modifiers and CRISPR-induced chromosome conformational changes. *CRISPR J.* 4, 43–57. doi: 10.1089/crispr.2020.0108

Martinez-Aguilar, E., Gomez-Rodriguez, V., Orbe, J., Rodriguez, J. A., Fernández-Alonso, L., Roncal, C., et al. (2015). Matrix metalloproteinase 10 is associate with disease severity and mortality in patients with peripheral arterial disease. *J. Vasc. Surg.* 61, 428–435. doi: 10.1016/j.jvs.2014.09.002

McNulty, M., Spiers, P., McGovern, E., and Feely, J. (2005). Aging is associated with increased matrix metalloproteinase-2 activity in the human aorta. *Am. J. Hypertens.* 18(4Pt. 1), 504–509. doi: 10.1016/j.amjhyper.2004.11.011

Meder, B., Rühle, F., Weis, T., Homuth, G., Keller, A., Franke, J., et al. (2014). A genome-wide association study identifies 6p21 as novel risk locus for dilated cardiomyopathy. *Eur. Heart J.* 35, 1069–1077. doi: 10.1093/eurheartj/eht251

Menghini, R., Stöhr, R., and Federici, M. (2014). MicroRNAs in vascular aging and atherosclerosis. *Aging Res. Rev.* 17, 68–78. doi: 10.1016/j.arr.2014.03.005

Meyer, S. U., Pfaffl, M. W., and Ulbric, S. E. (2010). Normalization strategies for microRNA profiling experiments: a 'normal' way to a hidden layer of complexity? *Biotechnol. Lett.* 32, 1777–1788. doi: 10.1007/s10529-010-0380-z

Möhlenkamp, S., Lehmann, N., Moebus, S., and Nixdorf, H. (2011). Recall Study Investigators. Quantification of coronary atherosclerosis and inflammation to predict coronary events and all-cause mortality. *J. Am. Coll. Cardiol.* 57, 1455–1464. doi: 10.1016/j.jacc.2010.10.043

Montezano, A. C., and Touyz, R. M. (2014). Reactive oxygen species, vascular Noxs, and hypertension: focus on translational and clinical research. *Antioxid. Redox Signal.* 20, 164–182. doi: 10.1089/ars.2013.5302

Moyzis, R. K., Buckingham, J. M., Cram, L. S., and Wu, J. R. (1988). A highly conserved repetitive DNA sequence, (TTAGGG)n, present at the telomeres of human chromosomes. *Proc. Natl. Acad. Sci. U.S.A.* 85, 6622–6626. doi: 10.1073/pnas.85.18.6622

Mozos, I., Jianu, D., Gug, C., and Stoian, D. (2019). Links between high-sensitivity C-reactive protein and pulse wave analysis in middle-aged patients with hypertension and high normal blood pressure. *Dis. Markers* 2019:2568069. doi: 10.1155/2019/2568069

Müezzinler, A., Zaineddin, A. K., and Brenner, H. (2013). A systematic review of leukocyte telomere length and age in adults. *Aging Res. Rev.* 12, 509–519. doi: 10.1016/j.arr.2013.01.003

Naka, T., Nishimoto, N., and Kishimoto, T. (2002). The paradigm of IL-6: from basic science to medicine. *Arthritis Res.* 4(Suppl. 3), S233–S242. doi: 10.1186/ar565

Nakhai-Pour, H., Grobbee, D., Bots, M., Muller, M., and van der Schouw, Y. T. (2007). C-reactive protein and aortic stiffness and wave reflection in middle-aged and elderly men from the community. *J. Hum. Hypertens.* 21, 949–955. doi: 10.1038/sj.jhh.1002255

Nandi, A., Yan, L. J., Jana, C. K., and Das, N. (2019). Role of catalase in oxidative stress- and age-associated degenerative diseases. *Oxid. Med. Cell. Longev.* 2019:9613090. doi: 10.1155/2019/9613090

Navickas, R., Gal, D., Laucevičius, A., Taparauskaitė, A., Zdanytė, M., and Holvoet, P. (2016). Identifying circulating microRNAs as biomarkers of cardiovascular disease: a systematic review. *Cardiovasc. Res.* 111, 322–337. doi: 10.1093/cvr/cvw174

Nilsson, P. M., Boutouyrie, P., and Laurent, S. (2009). Vascular aging: a tale of EVA and ADAM in cardiovascular risk assessment and prevention. *Hypertension* 54, 3–10.

Nilsson, P. M., Lurbe, E., and Laurent, S. (2008). The early life origins of vascular aging and cardiovascular risk: the EVA syndrome. *J. Hypertens.* 26, 1049–1057.

Nishida, M., Funahashi, T., and Shimomura, I. (2007). Pathophysiological significance of adiponectin. *Med. Mol. Morphol.* 40, 55–67. doi: 10.1007/s00795-007-0366-7

Panayiotou, A. G., Nicolaides, A. N., Griffin, M., Tyllis, T., Georgiou, N., Bond, D., et al. (2010). Leukocyte telomere length is associated with measures of subclinical atherosclerosis. *Atherosclerosis* 211, 176–181.

Papaconstantinou, J. (2019). The role of signaling pathways of inflammation and oxidative stress in development of senescence and aging phenotypes in cardiovascular disease. *Cells* 8:1383. doi: 10.3390/cells8111383

Parthenakis, F., Marketou, M., Kontaraki, J., Patrianakos, A., Nakou, H., Touloupaki, M., et al. (2017). Low levels of MicroRNA-21 are a marker of reduced arterial stiffness in well-controlled hypertension. *J. Clin. Hypertens. (Greenwich)* 19, 235–240. doi: 10.1111/jch.12900

Passacquale, G., Di Giosia, P., and Ferro, A. (2016). The role of inflammatory biomarkers in developing targeted cardiovascular therapies: lessons from the cardiovascular inflammation reduction trials. *Cardiovasc. Res.* 109, 9–23. doi: 10.1093/cvr/cvv227

Peeters, S. A., Engelen, L., Buijs, J., Jorsal, A., Parving, H. H., Tarnow, L., et al. (2017). Plasma matrix metalloproteinases are associated with incident cardiovascular disease and all-cause mortality in patients with type 1 diabetes: a 12-year follow-up study. *Cardiovasc. Diabetol.* 16:55. doi: 10.1186/s12933-017-0539-1

Perk, J., De Backer, G., Gohlke, H., Graham, I., Reiner, Z., Verschuren, M., et al. (2012). European Association for Cardiovascular Prevention & Rehabilitation (EACPR); ESC Committee for Practice Guidelines (CPG). European Guidelines on cardiovascular disease prevention in clinical practice (version 2012). The Fifth Joint Task Force of the European Society of cardiology and other societies on cardiovascular disease prevention in clinical practice (constituted by representatives of nine societies and by invited experts). *Eur. Heart J.* 33, 1635–1701. doi: 10.1093/eurheartj/ehs092

Peyster, E., Chen, J., Feldman, H. I., Go, A. S., Gupta, J., Mitra, N., et al. (2017). On behalf of the CRIC study investigators, inflammation and arterial stiffness in chronic kidney disease: findings from the CRIC study. *Am. J. Hypertens.* 30, 400–408. doi: 10.1093/ajh/hpw164

Pierce, G. L., Donato, A. J., LaRocca, T. J., Eskurza, I., Silver, A. E., and Seals, D. R. (2011). Habitually exercising older men do not demonstrate age-associated vascular endothelial oxidative stress. *Aging Cell* 10, 1032–1037. doi: 10.1111/j.1474-9726.2011.00748.x

Pritchard, C. C., Cheng, H. H., and Tewari, M. (2012). MicroRNA profiling: approaches and considerations. *Nat. Rev. Genet.* 13, 358–369. doi: 10.1038/nrg3198

Puel, A., and Casanova, J. L. (2019). The nature of human IL-6. *J. Exp. Med.* 216, 1969–1971. doi: 10.1084/jem.20191002

Puzianowska-Kuźnicka, M., Owczarz, M., Wieczorowska-Tobis, K., Nadrowski, P., Chudek, J., Slusarczyk, P., et al. (2016). Interleukin-6 and C-reactive protein, successful aging, and mortality: the PolSenior study. *Immun. Aging* 13:21. doi: 10.1186/s12979-016-0076-x

Rao, M., Guo, D., Perianayagam, M. C., Tighiouart, H., Jaber, B. L., Pereira, B. J., et al. (2005). Plasma interleukin-6 predicts cardiovascular mortality in hemodialysis patients. *Am. J. Kidney Dis.* 45, 324–333. doi: 10.1053/j.ajkd.2004.09.018

Rice, K. M., Meduru, S., Kakarla, S. K., Katta, A., Mupparaju, S. P., Kidd, B., et al. (2012). Chronic paracetamol treatment influences indices of reactive oxygen species accumulation in the aging Fischer 344 X Brown Norway rat aorta. *Ann. Clin. Lab. Sci.* 42, 152–161.

Ridker, P. M., Libby, P., MacFadyen, J. G., Thuren, T., Ballantyne, C., Fonseca, F., et al. (2018). Modulation of the interleukin-6 signalling pathway and incidence rates of atherosclerotic events and all-cause mortality: analyses from the Canakinumab Anti-Inflammatory Thrombosis Outcomes Study (CANTOS). *Eur. Heart J.* 39, 3499–3507. doi: 10.1093/eurheartj/ehy310

Roubenoff, R. (2003). Sarcopenia: effects on body composition and function. *J. Gerontol. Ser. A* 58, M1012–M1017.

Said, E. A., Al-Reesi, I., Al-Shizawi, N., Jaju, S., Al-Balushi, M. S., Koh, C. Y., et al. (2021). Defining IL-6 levels in healthy individuals: a meta-analysis. *J. Med. Virol.* 93, 3915–3924.

Saldanha, S. N., Andrews, L. G., and Tollefsbol, T. O. (2003). Assessment of telomere length and factors that contribute to its stability. *Eur. J. Biochem.* 270, 389–403. doi: 10.1046/j.1432-1033.2003.03410.x

Salisbury, D., and Bronas, U. (2015). Reactive oxygen and nitrogen species: impact on endothelial dysfunction. *Nurs. Res.* 64, 53–66. doi: 10.1097/NNR.0000000000000068

Santos, A. L., Sinha, S., and Lindner, A. B. (2018). The good, the bad, and the Ugly of ROS: new insights on aging and aging-related diseases from eukaryotic and prokaryotic model organisms. *Oxid. Med. Cell. Longev.* 2018, 1941285, 23.

Sato, F., Tsuchiya, S., Terasawa, K., and Tsujimoto, G. (2009). Intra-platform repeatability and inter-platform comparability of microRNA microarray technology. *PLoS One* 4:e5540. doi: 10.1371/journal.pone.0005540

Šatrauskienė, A., Navickas, R., Lauceviėius, A., Krilaviėius, T., Užupytė, R., Zdanytė, M., et al. (2021). Mir-1, miR-122, miR-132, and miR-133 are related to subclinical aortic atherosclerosis associated with metabolic syndrome. *Int. J. Environ. Res. Public Health* 18:1483. doi: 10.3390/ijerph18041483

Schafer, M. J., Zhang, X., Kumar, A., Atkinson, E. J., Zhu, X., Jachim, S., et al. (2020). The senescence-associated secretome as an indicator of age and medical risk. *JCI Insight* 5:e133668. doi: 10.1172/jci.insight.133668

Schübeler, D. (2015). Function and information content of DNA methylation. *Nature* 517, 321–326. doi: 10.1038/nature14192

Schwarzenbach, H., da Silva, A. M., Calin, G., and Pantel, K. (2015). Data normalization strategies for MicroRNA quantification. *Clin. Chem.* 61, 1333–1342. doi: 10.1373/clinchem.2015.239459

Sena, C. M., Leandro, A., Azul, L., Seiça, R., and Perry, G. (2018). Vascular oxidative stress: impact and therapeutic approaches. *Front. Physiol.* 9:1668. doi: 10.3389/fphys.2018.01668

Senoner, T., and Dichtl, W. (2019). Oxidative stress in cardiovascular diseases: still a therapeutic target? *Nutrients* 11:2090. doi: 10.3390/nu11092090

Shields, H. J., Traa, A., and Van Raamsdonk, J. M. (2021). Beneficial and detrimental effects of reactive oxygen species on lifespan: a comprehensive review of comparative and experimental studies. *Front. Cell Dev. Biol.* 9:181. doi: 10.3389/fcell.2021.628157

Simard, C., Cloutier, M., and Néron, S. (2014). Rapid determination of IL-6 specific activity by flow cytometry. *J. Immunol. Methods* 415, 63–65. doi: 10.1016/j.jim.2014.09.005

Singh, S. K., Suresh, M. V., Voleti, B., and Agrawal, A. (2008). The connection between C-reactive protein and atherosclerosis. *Ann. Med.* 40, 110–120. doi: 10.1080/07853890701749225

Singh, T., and Newman, A. B. (2011). Inflammatory markers in population studies of aging. *Aging Res. Rev.* 10, 319–329. doi: 10.1016/j.arr.2010.11.002

Stevenson, A. J., McCartney, D. L., Harris, S. E., Taylor, A. M., Redmond, P., Starr, J. M., et al. (2018). Trajectories of inflammatory biomarkers over the eighth decade and their associations with immune cell profiles and epigenetic aging. *Clin. Epigenet.* 10:159. doi: 10.1186/s13148-018-0585-x

Stevenson, A. J., McCartney, D. L., Hillary, R. F., Campbell, A., Morris, S. W., Bermingham, M. L., et al. (2020). Characterisation of an inflammation-related epigenetic score and its association with cognitive ability. *Clin. Epigenet.* 12:113. doi: 10.1186/s13148-020-00903-8

Strazhesko, I., Tkacheva, O., Boytsov, S., Akasheva, D., Dudinskaya, E., Vygodin, V., et al. (2015). Association of insulin resistance, arterial stiffness and telomere length in adults free of cardiovascular diseases. *PLoS One* 10:e0136676. doi: 10.1371/journal.pone.0136676

Stumpf, C., Sheriff, A., Zimmermann, S., Schaefauer, L., Schlundt, C., Raaz, D., et al. (2017). C-reactive protein levels predict systolic heart failure and outcome in patients with first ST-elevation myocardial infarction treated with coronary angioplasty. *Arch. Med. Sci. AMS* 13, 1086–1093. doi: 10.5114/aoms.2017.69327

Sundström, J., Evans, J. C., Benjamin, E. J., Levy, D., Larson, M. G., Sawyer, D. B., et al. (2004). Relations of plasma matrix metalloproteinase-9 to clinical cardiovascular risk factors and echocardiographic left ventricular measures: the Framingham Heart Study. *Circulation* 109, 2850–2856. doi: 10.1161/01.CIR.0000129318.79570.84

Tan, J., Hua, Q., Xing, X., Wen, J., Liu, R., and Yang, Z. (2007). Impact of the metalloproteinase-9/tissue inhibitor of metalloproteinase-1 system on large arterial stiffness in patients with essential hypertension. *Hypertens. Res.* 30, 959–963. doi: 10.1291/hypres.30.959

Tanaka, T., Biancotto, A., Moaddel, R., Moore, A. Z., Gonzalez-Freire, M., Aon, M. A., et al. (2018). Plasma proteomic signature of age in healthy humans. *Aging Cell* 17:e12799. doi: 10.1111/acel.12799

Tang, Y., Fung, E., Xu, A., and Lan, H.-Y. (2017). C-reactive protein and aging. *Clin. Exp. Pharmacol. Physiol.* 44, 9–14. doi: 10.1111/1440-1681.12758

Tanguy, S., Boucher, F., Toufektsian, M.-C., Besse, S., and De Leiris, J. (2000). Aging exacerbates hydrogen peroxide-induced alteration of vascular reactivity in rats. *Antioxid. Redox Signal.* 2, 363–368.

Tayebjee, M. H., Lip, G. Y. H., and MacFadyen, R. J. (2005). What role do extracellular matrix changes contribute to the cardiovascular disease burden of diabetes mellitus? *Diabetic Med.* 22, 1628–1635. doi: 10.1111/j.1464-5491.2005.01675.x

Tegeler, C., O'Sullivan, J. L., Bucholtz, N., Goldeck, D., Pawelec, G., Steinhagen-Thiessen, E., et al. (2016). The inflammatory markers CRP, IL-6, and IL-10 are associated with cognitive function–data from the Berlin Aging Study II. *Neurobiol. Aging* 38, 112–117. doi: 10.1016/j.neurobiolaging.2015.10.039

Tejero, J., Shiva, S., and Gladwin, M. T. (2019). Sources of vascular nitric oxide and reactive oxygen species and their regulation. *Physiol. Rev.* 99, 311–379. doi: 10.1152/physrev.00036.2017)

Teschendorff, A. E., Jones, A., Fiegl, H., Sargent, A., Zhuang, J. J., Kitchener, H. C., et al. (2012). Epigenetic variability in cells of normal cytology is associated with the risk of future morphological transformation. *Genome Med.* 4:24. doi: 10.1186/gm323

Thangaswamy, S., Bridenbaugh, E. A., and Gashev, A. A. (2012). Evidence of increased oxidative stress in aged mesenteric lymphatic vessels. *Lymphat. Res. Biol.* 10, 53–62. doi: 10.1089/lrb.2011.0022

Toupance, S., Labat, C., Temmar, M., Rossignol, P., Kimura, M., Aviv, A., et al. (2017). Short telomeres, but not telomere attrition rates, are associated with carotid atherosclerosis. *Hypertension* 70, 420–425.

Touyz, R. M., Anagnostopoulou, A., Rios, F., Montezano, A. C., and Camargo, L. L. (2019). NOX5: molecular biology and pathophysiology. *Exp. Physiol.* 104, 605–616. doi: 10.1113/EP086204

Touyz, R. M., and Delles, C. (Eds.) (2019). *Textbook of Vascular Medicine*. Cham: Springer.

Toyama, K., Spin, J. M., Deng, A. C., Huang, T.-T., Wei, K., Wagenhäuser, M. U., et al. (2018). MicroRNA-mediated therapy modulating blood–brain barrier disruption improves vascular cognitive impairment. *Arterioscler. Thromb. Vasc. Biol.* 38, 1392–1406. doi: 10.1161/ATVBAHA.118.310822

Tsutamoto, T., Wada, A., Maeda, K., Mabuchi, N., Hayashi, M., Tsutsui, T., et al. (2000). Angiotensin II type 1 receptor antagonist decreases plasma levels of tumor necrosis factor alpha, interleukin-6 and soluble adhesion molecules in patients with chronic heart failure. *J. Am. Coll. Cardiol.* 35, 714–721.

Tunon, J., Martin-Ventura, J. L., Blanco-Colio, L. M., Lorenzo, O., Lopez, J. A., and Egido, J. (2010). Proteomic strategies in the search of new biomarkers in atherothrombosis. *J. Am. Coll. Cardiol.* 55, 2009–2016. doi: 10.1016/j.jacc.2010.01.036

Ungvari, Z., Tarantini, S., Donato, A. J., Galvan, V., and Csiszar, A. (2018). Mechanisms of vascular aging. *Circ. Res.* 123, 849–867.

Ungvari, Z., Tucsek, Z., Sosnowska, D., Toth, P., Gautam, T., Podlutsky, A., et al. (2013). Aging-Induced dysregulation of Dicer1-Dependent MicroRNA expression impairs angiogenic capacity of rat cerebromicrovascular endothelial cells. *J. Gerontol. A Biol. Sci. Med. Sci.* 68, 877–891. doi: 10.1093/gerona/gls242

Unnikrishnan, A., Freeman, W. M., Jackson, J., Wren, J. D., Porter, H., and Richardson, A. (2019). The role of DNA methylation in epigenetics of aging. *Pharmacol. Ther.* 195, 172–185. doi: 10.1016/j.pharmthera.2018.11.001

Unsicker, K., Spittau, B., and Krieglstein, K. (2013). The multiple facets of the TGF-β family cytokine growth/differentiation factor-15/macrophage inhibitory cytokine-1. *Cytokine Growth Factor Rev.* 24, 373–384. doi: 10.1016/j.cytogfr.2013.05.003

Valencia-Morales, M., Zaina, S., Heyn, H., Carmona, F. J., Varol, N., Sayols, S., et al. (2015). The DNA methylation drift of the atherosclerotic aorta increases with lesion progression. *BMC Med. Genomics* 8:7. doi: 10.1186/s12920-015-0085-1

van Wezenbeek, J., Canada, J. M., Ravindra, K., Carbone, S., Trankle, C. R., Kadariya, D., et al. (2018). C-reactive protein and N-terminal pro-brain natriuretic peptide levels correlate with impaired cardiorespiratory fitness in patients with heart failure across a wide range of ejection fraction. *Front. Cardiovasc. Med.* 21:178. doi: 10.3389/fcvm.2018.00178

Vázquez-Oliva, G., Fernández-Real, J., Zamora, A., Vilaseca, M., and Badimón, L. (2005). Lowering of blood pressure leads to decreased circulating interleukin-6 in hypertensive subjects. *J. Hum. Hypertens.* 19, 457–462. doi: 10.1038/sj.jhh.1001845

Velagaleti, R. S., Gona, P., Sundström, J., Larson, M. G., Siwik, D., Colucci, W. S., et al. (2010). Relations of biomarkers of extracellular matrix remodeling to incident cardiovascular events and mortality. *Arterioscler. Thromb. Vasc. Biol.* 30, 2283–2288. doi: 10.1161/ATVBAHA.110.208462

Vlachopoulos, C., Xaplanteris, P., Aboyans, V., Brodmann, M., Cífková, R., Zimlichman, R., et al. (2015). The role of vascular biomarkers for primary and secondary prevention. A position paper from the European Society of Cardiology Working Group on peripheral circulation: endorsed by the Association for Research into Arterial Structure and Physiology (ARTERY) Society. *Atherosclerosis* 241, 507–532. doi: 10.1016/j.atherosclerosis.2015.05.007

Wainstein, M. V., Mossmann, M., Araujo, G. N., Wainstein, M. V., Mossmann, M., Araujo, G. N., et al. (2017). Elevated serum et al interleukin-6 is predictive of coronary artery disease in intermediate risk overweight patients referred for coronary angiography. *Diabetol. Metab. Syndr.* 9:67. doi: 10.1186/s13098-017-0266-5

Walston, J. D., Matteini, A. M., Nievergelt, C., Lange, L. A., Fallin, D. M., and Barzilai, N. (2009). Inflammation and stress-related candidate genes, plasma interleukin-6 levels, and longevity in older adults. *Exp. Gerontol.* 44, 350–355. doi: 10.1016/j.exger.2009.02.004

Wang, B., Howel, P., Bruheim, S., Ju, J., Owen, L. B., Fodstad, O., et al. (2011). Systematic evaluation of three microRNA profiling platforms: microarray, beads array, and quantitative real-time PCR array. *PLoS One* 6:e17167. doi: 10.1371/journal.pone.0017167

Wang, F., Long, G., Zhao, C., Li, H., Chaugai, S., Wang, Y., et al. (2013). Plasma microRNA-133a is a new marker for both acute myocardial infarction and underlying coronary artery stenosis. *J. Transl. Med.* 11:222. doi: 10.1186/1479-5876-11-222

Wang, M., Jiang, L., Monticone, R. E., and Lakatta, E. G. (2014). Proinflammation: the key to arterial aging. *Trends Endocrinol. Metab.* 25, 72–79.

Wang, M., Kim, S. H., Monticone, R. E., and Lakatta, E. G. (2015). Matrix metalloproteinase promote arterial remodeling in aging, hypertension and atherosclerosis. *Hypertension* 65, 698–703.

Wang, Q., Zhan, Y., Pedersen, N. L., Fang, F., and Hägg, S. (2018). Telomere length and all-cause mortality: a meta-analysis. *Aging Res. Rev.* 48, 11–20. doi: 10.1016/j.arr.2018.09.002

Wang, W., Li, T., Gao, L., Li, Y., Sun, Y., and Yao, H. C. (2019). Plasma miR-208b and miR-499: potential biomarkers for severity of coronary artery disease. *Dis. Markers* 2019:9842427. doi: 10.1155/2019/9842427

Wiklund, F. E., Bennet, A. M., Magnusson, P. K., Eriksson, U. K., Lindmark, F., Wu, L., et al. (2010). Macrophage inhibitory cytokine-1 (MIC-1/GDF15): a new marker of all-cause mortality. *Aging Cell* 9, 1057–1064. doi: 10.1111/j.1474-9726.2010.00629.x

Willeit, P., Willeit, J., Brandstätter, A., Ehrlenbach, S., Mayr, A., Gasperi, A., et al. (2010). Cellular aging reflected by leukocyte telomere length predicts advanced atherosclerosis and cardiovascular disease risk. *Arterioscler. Thromb. Vasc. Biol.* 30, 1649–1656. doi: 10.1161/ATVBAHA.110.205492

Wu, J., Xia, S., Kalionis, B., Wan, W., and Sun, T. (2014). The role of oxidative stress and inflammation in cardiovascular aging. *Biomed Res. Int.* 2014:615312. doi: 10.1155/2014/615312

Yasmin, S. W., McEniery, C. M., Dakham, Z., Pusalkar, P., Maki-Petaja, K., Ashby, M. J., et al. (2005). Matrix Metalloproteinase-9 (MMP-9), MMP-2, and Serum Elastase Activity Are Associated With Systolic Hypertension and Arterial Stiffness. *Arterioscler. Thromb. Vasc. Biol.* 25, 372–378. doi: 10.1161/01.ATV.0000151373.33830.41

Yousuf, O., Mohanty, B. D., Martin, S. S., Joshi, P. H., Blaha, M. J., Nasir, K., et al. (2013). Sensitivity C-reactive protein and cardiovascular disease: a resolute belief or an elusive link? *J. Am. Coll. Cardiol.* 62, 397–408.

Yu, V. W. C., Yusuf, R. Z., Oki, T., Wu, J., Saez, B., Wang, X., et al. (2016). Epigenetic memory underlies cell-autonomous heterogeneous behavior of hematopoietic stem cells. *Cell* 167, 1310–1322. doi: 10.1016/j.cell.2017.02.010

Zarzuelo, M. J., López-Sepúlveda, R., Sánchez, M., Romero, M., Gómez-Guzmán, M., Ungvary, Z., et al. (2013). SIRT1 inhibits NADPH oxidase activation and protects endothelial function in the rat aorta: implications for vascular aging. *Biochem. Pharmacol.* 85, 1288–1296. doi: 10.1016/j.bcp.2013.02.015

Conflict of Interest: The authors declare that the research was conducted in the absence of any commercial or financial relationships that could be construed as a potential conflict of interest.

Publisher's Note: All claims expressed in this article are solely those of the authors and do not necessarily represent those of their affiliated organizations, or those of the publisher, the editors and the reviewers. Any product that may be evaluated in this article, or claim that may be made by its manufacturer, is not guaranteed or endorsed by the publisher.

frontiers in Physiology

ORIGINAL RESEARCH
published: 15 December 2021
doi: 10.3389/fphys.2021.774056

Modulation of Arterial Stiffness Gradient by Acute Administration of Nitroglycerin

Catherine Fortier[1,2,3†], Charles-Antoine Garneau[1,2†], Mathilde Paré[1,2], Hasan Obeid[1], Nadège Côté[1,2], Karine Duval[1], Rémi Goupil[3] and Mohsen Agharazii[1,2]*

[1] CHU de Québec Research Center-Université Laval, L'Hôtel-Dieu de Québec Hospital, Québec, QC, Canada, [2] Division of Nephrology, Faculty of Medicine, Université Laval, Québec, QC, Canada, [3] Research Center of the Hôpital du Sacré-Coeur de Montréal, Montréal, QC, Canada

OPEN ACCESS

Edited by:
Bart Spronck,
Maastricht University, Netherlands

Reviewed by:
Alessandro Giudici,
Maastricht University, Netherlands
Carlo Palombo,
University of Pisa, Italy

****Correspondence:***
Mohsen Agharazii
mohsen.agharazii@crchudequebec.ulaval.ca

† These authors have contributed equally to this work and share first authorship

Specialty section:
This article was submitted to Vascular Physiology, a section of the journal Frontiers in Physiology

Received: *10 September 2021*
Accepted: *12 November 2021*
Published: *15 December 2021*

Citation:
Fortier C, Garneau C-A, Paré M, Obeid H, Côté N, Duval K, Goupil R and Agharazii M (2021) Modulation of Arterial Stiffness Gradient by Acute Administration of Nitroglycerin. Front. Physiol. 12:774056. doi: 10.3389/fphys.2021.774056

Background: Physiologically, the aorta is less stiff than peripheral conductive arteries, creating an arterial stiffness gradient, protecting microcirculation from high pulsatile pressure. However, the pharmacological manipulation of arterial stiffness gradient has not been thoroughly investigated. We hypothesized that acute administration of nitroglycerin (NTG) may alter the arterial stiffness gradient through a more significant effect on the regional stiffness of medium-sized muscular arteries, as measured by pulse wave velocity (PWV). The aim of this study was to examine the differential impact of NTG on regional stiffness, and arterial stiffness gradient as measured by the aortic-brachial PWV ratio (AB-PWV ratio) and aortic-femoral PWV ratio (AF-PWV ratio).

Methods: In 93 subjects (age: 61 years, men: 67%, chronic kidney disease [CKD]: 41%), aortic, brachial, and femoral stiffnesses were determined by cf-PWV, carotid-radial (cr-PWV), and femoral-dorsalis pedis artery (fp-PWV) PWVs, respectively. The measurements were repeated 5 min after the sublingual administration of NTG (0.4 mg). The AB-PWV and AF-PWV ratios were obtained by dividing cf-PWV by cr-PWV or fp-PWV, respectively. The central pulse wave profile was determined by radial artery tonometry through the generalized transfer function.

Results: At baseline, cf-PWV, cr-PWV, and fp-PWV were 12.12 ± 3.36, 9.51 ± 1.81, and 9.71 ± 1.89 m/s, respectively. After the administration of NTG, there was a significant reduction in cr-PWV of 0.86 ± 1.27 m/s ($p < 0.001$) and fp-PWV of 1.12 ± 1.74 m/s ($p < 0.001$), without any significant changes in cf-PWV ($p = 0.928$), leading to a significant increase in the AB-PWV ratio (1.30 ± 0.39 vs. 1.42 ± 0.46; $p = 0.001$) and AF-PWV ratio (1.38 ± 0.47 vs. 1.56 ± 0.53; $p = 0.001$). There was a significant correlation between changes in the AF-PWV ratio and changes in the timing of wave reflection ($r = 0.289$; $p = 0.042$) and the amplitude of the heart rate-adjusted augmented pressure ($r = -0.467$; $p < 0.001$).

Conclusion: This study shows that acute administration of NTG reduces PWV of muscular arteries (brachial and femoral) without modifying aortic PWV. This results in an unfavorable profile of AB-PWV and AF-PWV ratios, which could lead to higher pulse pressure transmission into the microcirculation.

Keywords: arterial stiffness gradient, arterial stiffness, aortic stiffness, pulse wave velocity (PWV), nitroglycerin (NTG), pulse wave analysis (PWA), chronic kidney disease (CKD), arterial compliance

INTRODUCTION

Aortic stiffness, determined by aortic pulse wave velocity (PWV), is a hallmark of vascular aging and an independent cardiovascular risk factor in various clinical conditions ranging from hypertension to end-stage kidney disease (Blacher et al., 1999a,b; Laurent et al., 2001; Cruickshank et al., 2002; Karras et al., 2012). The consequences of aortic stiffening on the heart are essentially explained by an increased cardiac workload and a decreased coronary perfusion pressure. However, the peripheral target organ damage may best be explained by the arterial stiffness gradient hypothesis (Mitchell, 2008). Indeed, due to the heterogeneity of vascular wall composition and diameter, there is an increase in arterial stiffness (stiffness gradient) from the heart to the periphery. This gradient in arterial stiffness results in a gradual attenuation of forward pressure wave along the arterial tree down to the microcirculation, where the pulsatility must be minimal. In the process of vascular aging, medium-sized arteries show little changes compared to the aorta, leading to attenuation or even a reversal of the stiffness gradient (Mitchell, 2008; Fortier and Agharazii, 2016). As a consequence, a higher pulse pressure could be transmitted into the microcirculation, causing exaggerated vascular myogenic response, and ultimately hypoperfusion and organ damage (Mitchell, 2008; Fortier and Agharazii, 2016). Indeed, a number of recent studies have underlined the relevance of arterial stiffness gradient on both blood flow and clinical outcomes (Mitchell et al., 2011; Tarumi et al., 2011; Hashimoto and Ito, 2013).

In the context of chronic kidney disease (CKD), we have previously used the PWV ratio between cf-PWV and cr-PWV as a surrogate measure of arterial stiffness gradient and have shown that it was a better prognostic indicator than cf-PWV alone (Fortier et al., 2015). In CKD patients, we have shown that the changes in arterial stiffness gradient are not only guided by an increase in aortic stiffness but also by a decrease in the stiffness of the medium-sized muscular arteries such as the brachial artery (Utescu et al., 2013; Fortier et al., 2015). We have also observed that patients with chronic use of nitroglycerin (NTG), a vasodilatory drug used primarily to treat coronary artery disease and/or heart failure, had a higher PWV ratio. This observation led us to hypothesize that NTG may have a negative impact on arterial stiffness gradient given that it has a more pronounced effect on medium-sized conduit arteries where vascular smooth muscle cells are a major component of the arterial wall (Wilkinson et al., 2002; Pauca et al., 2005; Yamamoto et al., 2017). However, the pharmacological manipulation of arterial stiffness gradient has not been thoroughly studied.

Therefore, we aimed to examine the effect of acute administration of NTG on arterial stiffness gradient. Second, we aimed to study the effect of NTG on local stiffness parameters of the brachial artery and its relation to changes in cr-PWV. Finally, we investigated whether the vascular response to NTG is different in patients with CKD than subjects without a significant decline in renal function.

MATERIALS AND METHODS

Study Design and Population

This is an interventional study designed to examine the acute effects of NTG in a single session of hemodynamic assessment. The inclusion criteria were adult patients with stable blood pressure (BP) medication and without any acute episode of illness (infection or recent cardiovascular events). Patients were excluded if they had a history of adverse reactions to NTG or were on renal replacement therapy. The control group (n = 55) was composed of apparently healthy subjects or hypertensive subjects with an estimated glomerular filtration rate (eGFR) $\geq$ 45 ml/min/1.73 m^2 [CKD-EPI equation (Levey et al., 2009)]. The CKD group (n = 38) was composed of patients with an eGFR $<$ 45 ml/min/1.73 m^2 (i.e., Stage 3B CKD and above) (Kidney Disease Improving Global Outcomes [KDIGO], 2013). This cutoff was used because subjects with an eGFR $\geq$ 45 ml/min/1.73 m^2 are not at substantially higher risk of cardiovascular disease (Padhy et al., 2017). The participants recruited were healthcare workers and patients treated in hypertension or CKD clinics of CHU de Québec-Université Laval hospital. Hypertension was defined as BP $\geq$ 140/90 mmHg or the use of antihypertensive medications in patients with a history of hypertension. Cardiovascular disease was defined as myocardial infarction, coronary artery revascularization, or ischemic heart disease as shown by treadmill, echo, or thallium stress tests; stroke or lower extremity amputation; or revascularization. This protocol had been approved by the *comité d'éthique de la recherche du CHU de Québec* and was conducted in accordance with the Declaration of Helsinki. All procedures followed were in accordance with institutional guidelines, and each patient had provided informed written consent.

Hemodynamic Measurements Sequence

All measurements were performed after 15 min of rest in a supine position. Brachial artery BP was recorded using an automatic oscillometric sphygmomanometer BPM-100 (BP-Tru, Coquitlam, Canada) by an experienced operator who was

present in the room. BP was recorded six times, with a 2-min interval between each measurement, and the average of the last five measurements was used to determine the brachial systolic BP (SBP), diastolic BP (DBP), and brachial artery pulse pressure (*b*PP). Immediately after BP measurements, radial pulse wave profile was recorded using applanation tonometry after calibration with brachial SBP and DBP (SphygmoCor system®, AtCor Medical Pty. Ltd., Sydney, Australia), followed by the determination of PWVs in peripheral (brachial and femoral) and central (aortic) arterial segments using Complior® Analyse (Artech Medical, Pantin, France). Brachial BP, PWVs, and radial pulse wave profile measurements were repeated 5 min after the sublingual administration of 0.4 mg of NTG with the same described procedures except that pulse wave profile has been taken once instead of thrice. Radial pulse wave profile post-NTG was introduced later in the measurement protocol and performed in the last 56 patients. Wall properties of the brachial artery were assessed in 57 subjects by a radiofrequency-based wall-tracking system (ART-LAB, Esaote, Maastricht, Netherlands) before and continuously during 10 min after NTG administration.

Pulse Wave Velocity and Arterial Stiffness Gradients

We determined PWVs by direct measurements of distance and using a maximal upstroke algorithm for pulse transit time. Carotid-radial PWV (cr-PWV, carotid-dorsalis pedis PWV (cp-PWV), and carotid-femoral PWV (cf-PWV were obtained on the same side, in triplicates. Femoral-dorsalis pedis PWV was calculated using the formula (cp distance − cf distance)/(cp transit time − cf transit time). Stiffness gradients from the aorta to the brachial artery (upper limb) and from the aorta to the femoral artery (lower limb) were obtained using the aortic-brachial PWV ratio (AB-PWV ratio = cf-PWV/cr-PWV) and aortic-femoral PWV ratio (AF-PWV ratio = cf-PWV/fp-PWV), respectively.

Local Brachial Stiffness Parameters

With the right arm stabilized in an inflated cushion, pre-NTG end-diastolic diameter (*d*), intima-media thickness (IMT), and distension of the brachial artery (∼3 cm above the elbow crease). The ART-LAB probe (10 MHz linear probe) was fastened by a locking articulating arm mounted on a platform that allowed two-dimensional microadjustments and good stability for a 10 min-period of real-time measurements after sublingual NTG administration. Arterial wall properties were calculated as follows:

- Compliance $= \frac{\triangle A}{\triangle P} = \frac{A_s - A_d}{bPP}$, where A_s and A_d stand for the systolic and diastolic cross-sectional areas; (1)
- Distensibility (DC) $= \frac{1}{A_d} \cdot \frac{\triangle A}{\triangle P}$; (2)
- Luminal cross-sectional area (LCSA) $= \frac{\pi\, d^2}{4}$; (3)
- Mean wall cross-sectional area (WCSA) $= \pi(\frac{d + 2 \times IMT}{2})^2 - \pi\,(\frac{d}{2})^2$; (4)
- Incremental elastic modulus (E_{inc}) $= \frac{3}{DC}(1 + \frac{LCSA}{WCSA})$;(5)
- Wall to lumen ratio (W/Lratio) $= 2\,(\frac{IMT}{d})$; (6)

(Laurent et al., 1994, 2006; Bortolotto et al., 1999; Spronck et al., 2021).

The IMT measurements were not performed after NTG administration, but it was calculated based on the principle of WCSA conservation.

Central Pulse Wave Profile Analysis

Three consecutive recordings were performed on the radial artery to construct a central pulse wave profile using an integrated generalized transfer function. The average of central SBP, central DBP, central pulse pressure (PP), heart rate-adjusted central augmented pressure (AP@75), and augmentation index (AIx@75), as well as end systolic pressure, were measured. Period, ejection duration, diastolic duration, the first peak of pressure height (P1) with the respective time of each peak (T1, T2), time to the reflection of the reflected pressure wave (TR), and subendocardial viability ratio (SEVR) were also obtained (Miyashita, 2012).

Statistical Analysis

The results are expressed as mean ± SD, *n* (%), or median (25th–75th percentiles). Differences between groups were assessed using *t*-test, Mann-Whitney *U*-test, or chi-square accordingly. The effects of NTG on vascular parameters were examined using paired *t*-test. Linear regression was used to examine the relationship between renal function, PWVs, and PWV ratios. We used generalized estimating equations (GEE) to adjust changes in vascular parameters for changes in DBP. Linear regressions were performed to determine the relationship between cr-PWV and brachial artery diameter. GEEs were also used to compare if the vascular response to NTG was different between CKD and the control group. Forward conditional linear regression was used to identify the determinants of changes in cr-PWV after NTG administration. We used the Spearman rank correlation coefficient to assess the association between TR and AP@75 with both AB-PWV and AF-PWV ratios. Finally, as part of sensitivity analysis, we examined if there were any significant interactions between age, sex, and established cardiovascular disease, and the vascular response to NTG (GEE). All statistical analyses were performed using SPSS Statistics for Windows, Version 27.0 (IBM Corp., Armonk, NY, United States). A two-tailed *p*-value <0.05 was considered to be statistically significant.

RESULTS

Patient Population

Table 1 shows the baseline demographic, clinical, pharmacological, and biological characteristics of patients

TABLE 1 | Characteristics of patients for control group, CKD group, and overall.

	Overall	Control	CKD
		eGFR ≥ 45 ml/min/1.73 m^2	eGFR < 45 ml/min/1.73 m^2
Parameters	*n* = 93	*n* = 55	*n* = 38
Male	62 (67)	35 (64)	27 (71)
Age (y)	61.0 [42.8–74.1]	57.1 [39.0–68.0]	72.0 [60.1–79.0]*
Weight (kg)	77.5 ± 15.0	76.2 ± 16.2	79.3 ± 13.0
Body mass index (kg/m^2)	27.1 ± 4.3	26.3 ± 4.5	28.3 ± 3.8*
Hypertension	60 (65)	26 (47)	34 (90)*
Diabetes	15 (16)	5 (9)	10 (26)*
CVD	12 (13)	3 (6)	9 (24)*
eGFR (ml/min/1.73 m^2)	43.0 [21.3–80.0]	80.0 [64.5–96.0]	22.0 [10.0–35.3]*
Medication			
ACEi/ARB	46 (50)	25 (46)	21 (55)
CCB	34 (37)	13 (24)	21 (55)*
β-blockers	20 (21)	10 (18)	10 (26)
ASA	22 (24)	13 (24)	9 (24)
Statins	38 (41)	14 (26)	24 (63)*
Lipid profile			
Total cholesterol (mmol/L)	4.61 ± 1.00	4.43 ± 0.86	4.79 ± 1.09
HDL (mmol/L)	1.37 ± 0.39	1.40 ± 0.32	1.34 ± 0.45
LDL (mmol/L)	2.30 ± 0.80	2.29 ± 0.84	2.30 ± 0.76
TG (mmol/L)	2.02 ± 1.16	1.62 ± 0.69	2.44 ± 1.38*

Results are means ± SD, n (%) or median (25th–75th percentiles). The p-value <0.05 is statistically significant.
ACEi, angiotensin-converting enzyme inhibitor; ARB, angiotensin receptor blockers; ASA, acetylsalicylic acid; CCB, calcium-channel blockers; CVD, cardiovascular disease; eGFR, estimated glomerular filtration rate from CKD-EPI equations; HDL, high-density lipoprotein; LDL, low-density lipoprotein; TG, triglycerides.
**A p-value of <0.05 than control group.*

TABLE 2 | Nitroglycerin-induced changes in brachial pressures and regional arterial stiffness.

	Baseline *n* = 93	NTG *n* = 93	*p*-value	*p*-value (adjusted for DBP)
Peripheral pressure parameters				
SBP (mm Hg)	123.8 ± 18.8	119.2 ± 17.2	<0.001	
DBP (mm Hg)	73.1 ± 9.2	71.9 ± 10.0	0.028	
PP (mm Hg)	50.7 ± 16.1	47.3 ± 13.0	<0.001	
MBP (mm Hg)	92.2 ± 11.5	89.4 ± 12.2	<0.001	
Heart rate (bpm)	65.3 ± 11.1	66.2 ± 10.6	0.025	
Central pressure parameters (*n* = 56)				
SBP (mm Hg)	115.3 ± 20.8	108.3 ± 16.6	<0.001	
DBP (mm Hg)	74.8 ± 8.8	73.5 ± 9.0	0.065	
PP (mm Hg)	41.7 ± 18.4	34.8 ± 14.2	<0.001	
AP@75 (mm Hg)	8.8 ± 7.4	3.6 ± 5.6	<0.001	
Aix@75 (%)	19.7 ± 13.7	7.4 ± 14.8	<0.001	
P1 (mmHg)	29.2 ± 9.1	28.1 ± 7.6	0.160	
T1 (ms)	105.0 ± 9.5	109.9 ± 13.9	0.009	
TR (ms)	139.8 ± 12.1	146.1 ± 14.9	<0.001	
T2 (ms)	228.0 ± 24.7	211.2 ± 27.7	<0.001	
End-systolic pressure (mm Hg)	104.1 ± 16.7	95.8 ± 15.3	<0.001	
Ejection duration (ms)	279.7 ± 59.2	267.5 ± 67.0	<0.001	
Diastolic duration (ms)	634.7 ± 133.9	644.1 ± 137.0	0.228	
Period (ms)	965.1 ± 156.3	968.2 ± 155.9	0.696	
SEVR (%)	156.6 ± 29.0	163.4 ± 31.3	0.004	
PP amplification	1.33 ± 0.20	1.47 ± 0.22	<0.001	
Pulse wave velocities				
cf-PWV (m/s)	12.12 ± 3.36	12.14 ± 3.55	0.928	0.236
cr-PWV (m/s)	9.51 ± 1.81	8.65 ± 1.57	<0.001	<0.001
cp-PWV (m/s)	9.97 ± 1.67	9.02 ± 1.24	<0.001	<0.001
fp-PWV (m/s)	9.71 ± 1.89	8.14 ± 1.62	<0.001	0.032
Aortic-brachial PWV ratio	1.30 ± 0.39	1.42 ± 0.46	0.001	0.001
Aortic-femoral PWV ratio	1.38 ± 0.47	1.56 ± 0.53	0.001	0.005

Results are means ± SD. The p-values were obtained with paired-samples t-test and MBP-adjusted PWVs were obtained with generalized estimating equations. The p-value < 0.05 is statistically significant.
Aix@75, heart rate-adjusted augmentation index; AP@75, heart rate-adjusted augmented pressure; cp-PWV, carotid-dorsalis pedis pulse wave velocity; cr-PWV, carotid-radial pulse wave velocity; DBP, diastolic blood pressure; fp-PWV, femoral-dorsalis pedis pulse wave velocity; MBP, mean blood pressure; NTG, nitroglycerin; P1, first peak of pressure height; PP, pulse pressure; PP amplification, pulse pressure amplification; SBP, systolic blood pressure; SEVR, subendocardial viability ratio; T1, time of peak 1; T2, time of peak 2; TR, time to reflection of the reflected pressure wave.

overall and in control and CKD subjects, respectively. Patients with CKD were older; had a higher BMI and triglyceride levels; had a higher prevalence of hypertension, cardiovascular disease; and diabetes; and were more frequently treated using calcium-channel blockers and statins. At baseline, there were significant correlations between eGFR, cf-PWV ($r = -0.37$, $p < 0.001$), AB-PWV ratio ($r = -0.38$, $p < 0.001$), AF-PWV ratio ($r = -0.27$, $p = 0.024$), but not with cr-PWV ($r = -0.03$, $p = 0.76$), and fp-PWV ($r = -0.12$, $p = 0.33$) in this study population.

As shown in **Table 2**, after NTG administration, there was a slight, but statistically significant, decline in SBP, DBP, and PP. In the 56 subjects who had central pulse wave analysis before and after NTG administration, there was a reduction in AP@75 (8.8 ± 7.4 vs. 3.6 ± 5.6 mmHg; $p < 0.001$) and AIx@75 (19.7 ± 13.7 vs. 7.4 ± 14.8%; $p < 0.001$). The end-systolic pressure decreased despite a reduction in ejection duration, but no changes were observed in the period. Finally, there was an increase in SEVR (156.6 ± 29.0 vs. 163.4 ± 31.3%; $p = 0.004$).

Impact of Nitroglycerin on Regional Stiffness and Arterial Stiffness Gradients

As shown in **Table 2** and **Figures 1A–D**, after NTG administration, there was no significant change in cf-PWV ($p = 0.928$), but there were significant reductions in both cr-PWV (0.86 ± 1.27 m/s; $p < 0.001$) and fp-PWV (1.12 ± 1.74 m/s; $p < 0.001$). The results remained consistent even after adjustment for the small changes in DBP (**Table 2**). Consequently, as shown in **Figures 1E,F**, both AB-PWV and AF-PWV ratios increased

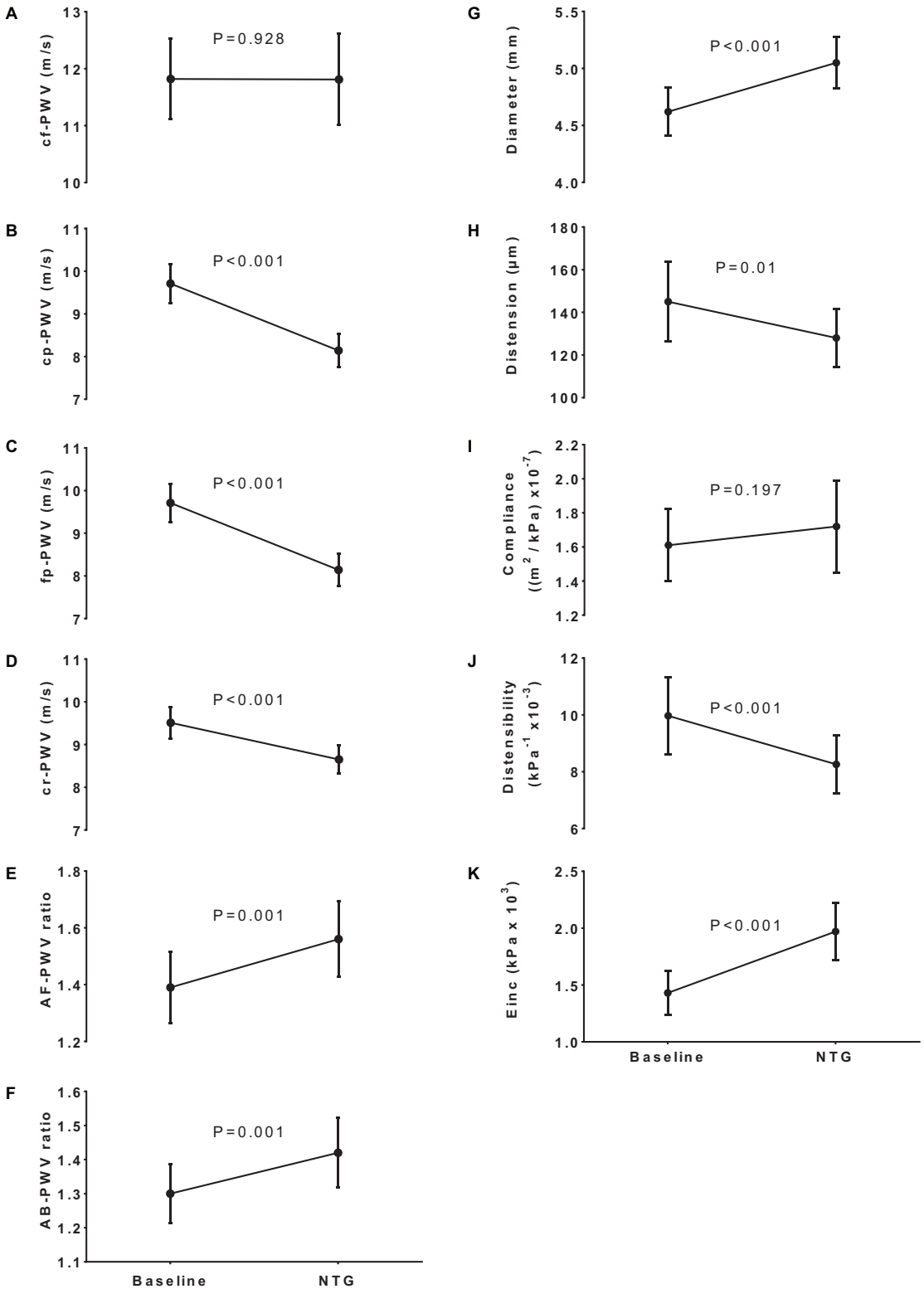

FIGURE 1 | Impact of NTG on regional stiffness, arterial stiffness gradients, and local brachial stiffness parameters. Panels **(A–D)** show the effect of nitroglycerin (NTG) on pulse wave velocity of various territories (PWV). The NTG had no effect on carotid-femoral PWV (cf-PWV) but significantly decreased carotid-pedis PWV (cp-PWV), femoral-pedis PWV (fp-PWV), and carotid-radial PWV (cr-PWV) leading to a corresponding increase in aortic-femoral PWV ratio [AF-PWV ratio **(E)**] and aortic-brachial PWV ratio [AB-PWV ratio **(F)**]. Changes in the brachial artery diameter **(G)**, distention **(H)**, compliance **(I)**, distensibility **(J)**, and incremental elastic modulus [E_{inc},**(K)**] in response to NTG.

significantly after NTG administration and remained significant even after adjustment for changes in DBP.

Table 3 shows the correlation matrix between changes in AB-PWV and AF-PWV ratios and the TR and AP@75.

Local Brachial Stiffness in Response to Nitroglycerin

Table 4 describes the changes in the brachial artery diameter and stiffness parameters in response to NTG. As expected, after NTG, the brachial artery diameter (4.62 ± 0.80 vs. 5.18 ± 0.77 mm; $p < 0.001$) and the luminal cross-sectional area (17.2 ± 5.9 vs. 21.6 ± 6.2 mm^2; $p < 0.001$) increased significantly. However, systolic-diastolic distention (0.145 ± 0.064 vs. 0.128 ± 0.047 mm; $p = 0.010$) and distensibility (9.97 ± 4.67 vs. 8.26 ± 3.56 $kPa^{-1} \times 10^{-3}$; $p < 0.001$) decreased, incremental elastic modulus increased (1.43 ± 0.65 vs. 1.97 ± 0.86 $kPa^{-1} \times 10^{3}$; $p < 0.001$), without any significant changes in brachial artery compliance (1.61 ± 0.72 vs. 1.72 ± 0.92 $m^2 \cdot kPa^{-1} \times 10^{-7}$; $p = 0.197$). These results are summarized in **Figures 1G–K**.

Brachial Pulse Wave Velocity and Brachial Diameter

To examine if the change in cr-PWV was related to brachial artery diameter, we performed a linear regression analysis and found that higher baseline cr-PWV and smaller baseline diameter were significant determinants in the decline of cr-PWV after NTG administration ($R^2 = 0.42$; **Table 5**). Age, CKD, diabetes, and cardiovascular disease were not associated with changes in cr-PWV after NTG. We also examined and found no direct relationship between changes in cr-PWV and changes in brachial diameter or wall-to-lumen ratio in either absolute or relative terms.

Vascular Response to Nitroglycerin by Chronic Kidney Disease Status

Given the clinical heterogeneity of subjects with or without reduction in renal function, we examined if the vascular response to NTG could be affected by the assigned group. To examine this, we built an interaction term into the GEE equations and found no significant interaction between CKD status and changes in PWVs, PWV ratios, and brachial parameters after NTG.

TABLE 3 | Correlations between changes in arterial stiffness gradient and changes in wave reflection parameters.

	Δ AB-PWV ratio		Δ AF-PWV ratio	
	r	*p*-value	*r*	*p*-value
Δ TR	0.203	0.140	0.289	0.042
Δ AP@ 75	−0.288	0.032	−0.467	<0.001

Correlation and p-values were obtained using Spearman rank bivariate correlation. The p-value <0.05 is statistically significant.
AB-PWV, aortic-brachial pulse wave velocity; AF-PWV, aortic-femoral pulse wave velocity; TR, time to the reflection of the reflected pressure wave.

In addition, we examined and found no modifying effect of age (median 61 years old), sex, and established cardiovascular disease on the extent of studied vascular responses to NTG.

DISCUSSION

This study shows that acute administration of NTG reduces brachial and femoral PWVs without affecting aortic PWV, causing an increase in the AB-PWV and AF-PWV ratios. The delay in the timing of the reflected wave and the lowering of the amplitude of the reflection wave after NTG were best correlated with the changes in the AF-PWV ratio.

These observations are in line with previous studies showing that NTG reduces PWV in muscular peripheral arteries but has no effect in attenuating aortic PWV (Pauca et al., 2005; Yamamoto et al., 2017). These changes result in the attenuation or even the reversal of the arterial stiffness gradient. From a cardiac point of view, increasing the AB-PWV and AF-PWV ratios and delaying the arrival and amplitude of the reflection wave in the ascending aorta may seem desirable, especially in the context of heart failure where nitrates and direct vasodilator (hydralazine) have been shown to improve left ventricular ejection fraction, peak oxygen consumption, and mortality (Cohn et al., 1991; Taylor et al., 2004). However, based on the wave propagation model, if there is less wave reflection in the ascending aorta, the forward pressure wave is less attenuated along the arterial tree, leading to a higher pulsatile pressure transmitted to the microcirculation. As stated earlier, given that the microcirculation is not structurally designed to accommodate a high pulse pressure, its chronic exposure to such mechanical stress may lead to microvascular dysfunction and end-organ damage. This is especially problematic for high flow/low resistance organs such as the brain and the kidneys (Mitchell, 2008). Indeed, in type 2 diabetic patients, Pierce et al. (2016) have observed that aortic-brachial stiffness gradient was associated with kidney function independent of aortic stiffness, implying that the arterial stiffness gradient may have a pathophysiological role in kidney disease. In addition, Mitchell et al. (2011) have shown that the loss of aortic-carotid impedance mismatch reduced the carotid reflection coefficient and facilitated the transmission of excessive flow pulsatility into the brain vasculature, which is presumably responsible for structural injuries to the brain microvasculature and the ensuing cognitive decline.

The clinical and biological determinants of a lower cr-PWV remain largely unknown and understudied. However, data are emerging that in certain conditions such as heart failure, kidney disease, or obesity in adolescents, the cr-PWV may be lower, hence contributing to the attenuation of the arterial stiffness gradient beyond the sole increase in aortic PWV (Mitchell et al., 2001; Zhu et al., 2007; Pierce et al., 2013, 2016; Utescu et al., 2013; Fortier et al., 2015; Agbaje et al., 2021). Moreover, the subjects of the African Americans of the atherosclerosis risk in communities (ARIC) study, tended to have a less favorable arterial stiffness gradient, not only due to higher cf-PWV but

TABLE 4 | Brachial artery changes according to nitroglycerin administration.

	Baseline $n = 57$	NTG $n = 57$	*p*-value	Δ NTG-baseline	*p*-value (adjusted for DBP)
Brachial artery					
Diameter (mm)	4.62 ± 0.80	5.18 ± 0.77	<0.001	0.57 (0.50 to 0.64)	<0.001
IMT (mm)	0.385 ± 0.076	0.346 ± 0.072*	–	−0.037 (−0.42 to −0.33)	–
W/L ratio	0.17 ± 0.03	0.14 ± 0.03	<0.001	−0.03 (−0.03 to −0.02)	<0.001
LCSA (mm^2)	17.2 ± 5.9	21.6 ± 6.2	<0.001	4.33 (3.80 to 4.86)	<0.001
WCSA (mm^2)	6.13 ± 1.92	–	–	–	–
Distension (mm)	0.145 ± 0.064	0.128 ± 0.047	0.010	−0.017 (−0.029 to −0.004)	0.012
Compliance ($m^2 \cdot kPa^{-1} \times 10^{-7}$)	1.61 ± 0.72	1.72 ± 0.92	0.197	0.11 (−0.06 to 0.29)	0.254
Distensibility ($kPa^{-1} \times 10^{-3}$)	9.97 ± 4.67	8.26 ± 3.56	<0.001	−1.72 (−2.69 to −0.75)	0.006
Einc ($kPa \times 10^3$)	1.43 ± 0.65	1.97 ± 0.86	<0.001	0.55 (0.37 to 0.72)	<0.001

Results are means ± SD or (95% CI). The p-values and mean changes in parameters with 95% CI were obtained using the paired-samples t-test, and MBP-adjusted p values were obtained using generalized estimating equations. The p-value <0.05 is statistically significant.
E_{inc}, incremental elastic modulus; WCSA, mean wall cross-sectional area; IMT, intima media thickness; LCSA, luminal cross-sectional area; W/L ratio, wall-to-lumen ratio.
**Post-NTG IMT was not measured but calculated based on the conservation of wall cross-sectional area.*

also because they presented with lower femoral-ankle PWV than Caucasians (Meyer et al., 2016).

These findings may suggest that the use of surrogate markers of arterial stiffness gradient may have a superior prognostic value above and beyond aortic stiffness. For example, in the dialysis population, we and others have shown that a higher AB-PWV ratio is associated with the worst survival rate even after adjustments for potential confounding factors (Fortier et al., 2015; Bao et al., 2019). In addition, the AB-PWV ratio was associated with cardiovascular events after kidney transplantation ($p = 0.045$) but not cf-PWV ($p = 0.501$), and only the AB-PWV ratio has been associated with eGFR and albuminuria in a cohort of middle-aged women with increased cardiovascular risk (Laucyte-Cibulskiene et al., 2018, 2019). However, the superiority of the AB-PWV ratio over cf-PWV was not observed in patients at earlier stages of kidney disease (Bai et al., 2019). It is suggested that this is likely because the AB-PWV ratio increases significantly in patients once the eGFR decreases below 45 ml/min/1.73 m^2 (i.e., Stage 3B and above) (Zanoli et al., 2018).

In the ARIC study population, a cross-sectional analysis showed that a low arterial stiffness gradient (femoral-ankle PWV/cf-PWV) was associated with diabetes, coronary heart disease, heart failure, and stroke, whereas a high cf-PWV was only associated with hypertension (Stone et al., 2021). It should be mentioned that this is a relatively older cohort (age of 75 years) with a higher prevalence of hypertension (72%) and diabetes (29%). In contrast, the AB-PWV ratio was not superior to cf-PWV in predicting cardiovascular events in subjects from the Framingham Heart Study, a younger (mean age of 60 years) and healthier cohort (8% diabetes, 31% receiving antihypertensive drugs) (Niiranen et al., 2017).

TABLE 5 | Determinants of change in carotid-radial PWV after NTG.

Parameters	Slope (95% Confidence interval)	*p*-value	R^2
Final model			0.421
Constant	−0.115 (−2.315 to 2.085)	0.917	
Baseline cr-PWV (m/s)	−0.426 (−0.614 to −0.237)	<0.001	
Baseline brachial diameter (mm)	0.708 (0.371 to 1.046)	<0.001	

The final model of a forward conditional regression analysis where excluded variables (e.g., age, CKD, diabetes, and cardiovascular status) are not shown. The p-value <0.05 is statistically significant.

In this study, NTG resulted in vasodilation of the brachial artery (12%), but this increase in diameter was accompanied by a lower degree of distention, showing no significant changes in the brachial artery compliance and even an increase in incremental elastic modulus. This increase in incremental elastic modulus could be explained by the transfer of pressure load from the vascular smooth muscle cells to the stiffer collagens of the extracellular matrix (Roach and Burton, 1957). Therefore, the reduction in cr-PWV could have potentially been explained by a decrease in a wall-to-lumen ratio according to the Moens–Korteweg equation $PWV = \sqrt{\frac{Einc \cdot h}{2r \cdot \rho}}$, where h is the wall thickness and r is the radius of the artery, and ρ is the blood density. However, we found no statistical relationship between measured changes in cr-PWV and changes in either diameter or wall-to-lumen ratio. This discrepancy could be explained by several reasons. First, it could be that our spatial resolution was too limited for a reliable assessment of *in vivo* changes in wall-to-lumen ratio. Second, it could be related to the violation of basic assumptions underlying the equation, i.e., that the arterial wall is isotropic and behaves in an isovolumetric manner in response to pulse pressure (Gosling and Budge, 2003). In addition, since *in vivo* arterial diameter at zero transmural pressure could not be measured, Hooke's law was applied for the determination of E_{inc} (Roark and Young, 1989), therefore implying geometrical assumptions that the arterial segments were considered as uniform thick-walled tubes. However, this assumption does not take into account any geometrical variation along the arterial wall. Finally, this discrepancy can be explained by the heterogeneity of the arterial tree between carotid and radial artery both in terms of diameter, arterial wall thickness, and composition. As such, the measured PWV over an arterial path is the summation of the local vascular responses along with the studied segments (i.e., ignoring potential heterogeneity of the vascular response). This possibility is further supported

by the results from the PWV between the carotid and dorsal pedis artery, which declined after NTG, but this reduction was solely due to the reduction over the vascular bed below the femoral artery.

Besides arterial stiffness gradient, this study underlines the importance of proper assessment of regional vascular stiffness and its response to therapy. Given the nature of translational medicine, we have been eager to take the arterial stiffness assessments out of specialized laboratories and into the large-scale epidemiological studies and clinical practice through simplification of arterial stiffness assessment. For example, our study clearly shows that PWV from the carotid to the dorsal pedis artery declined significantly after NTG, but upon closer look, we saw that this decline was related to the reduction in PWV from the femoral to the dorsal pedis segment and not related to aortic PWV *per se*. This observation is in line with the findings of Yamamoto et al. (2017) using cardio-ankle vascular index (CAVI) and heart-thigh and thigh-ankle B-stiffness indices.

This study has several strengths and limitations. First, it involves a large number of subjects with a detailed evaluation of various regional pulse wave velocities, central pulse wave profile, and brachial stiffness parameters. Second, given the heterogeneity of the subjects, we were able to perform various sensitivity analyses showing the robustness of our findings. Indeed, older subjects may have a more hypotensive response to NTG (Cahalan et al., 1992). However, even if our CKD patients were older and had several other heterogeneities, it did not modify the vascular responses in this study. There are also limitations that should be mentioned. First, we did not examine the smaller arteries of the vascular bed through the assessment of radial-digital PWV (Obeid et al., 2021). Second, it would have also been interesting to assess the local distensibility of both carotid and femoral arteries. However, given that we only had a 5-min window to measure all PWVs in triplicates and brachial distensibility, the addition of local carotid and femoral distensibilities would have pushed us outside the desired window, and besides technical limitations, it would have added uncertainties regarding the potential fading effect of NTG. Third, our interpretation of results is based on the pulse wave propagation model, which does not consider the reservoir function of the arterial tree (Wang et al., 2003; Tyberg et al., 2009; Parker et al., 2012; Mynard and Smolich, 2014). In addition, there are two limitations regarding the use of augmentation index (AIx) as a marker of wave reflection, namely, the reliability of the central AIx estimated *via* transfer function from the radial pressure waveform and the validity of central AIx as a measure of wave reflection (Chen et al., 1996; Millasseau et al., 2003; Segers et al., 2005; Miyashita, 2012; Hughes et al., 2013; Heusinkveld et al., 2019). Indeed, the central AIx derived from the generalized transfer function seems to correlate more strongly with the AIx of the original peripheral waveform rather than the central pressure waveform (Segers et al., 2005). Furthermore, the AIx and the related arrival time may be influenced by other factors, such as myocardial contractility, and hence may not be a proper measure of wave reflection (Hughes et al., 2013; Heusinkveld et al., 2019). Finally, our results are limited to the vascular response to NTG in an acute setting and do not imply similar effects would necessarily occur in a chronic setting.

CONCLUSION

While there are statistical associations between markers of arterial stiffness gradient and certain clinical conditions in both cross-sectional and longitudinal studies, there has not been a systematic focus on the impact of pharmacological interventions on the arterial stiffness gradient. In light of recent evidence supporting the potential usefulness of arterial stiffness gradient assessment, and our present data showing an alteration in arterial stiffness gradient in response to NTG, we would like to underline the importance of assessing regional PWV in order to develop an integrated approach into the arterial tree and its response to therapy. As such, these results are hypothesis generating and their clinical and pharmacological usefulness should be assessed in properly designed studies.

DATA AVAILABILITY STATEMENT

The raw data supporting the conclusions of this article will be made available by the authors, without undue reservation.

ETHICS STATEMENT

The studies involving human participants were reviewed and approved by Comité d'Éthique de la Recherche du CHU de Québec. The patients/participants provided their written informed consent to participate in this study.

AUTHOR CONTRIBUTIONS

MA and CF provided the conception and design of the study. CF, C-AG, MP, HO, NC, KD, and MA recruited participants and collected data. CF, C-AG, and MA performed the statistical analysis and wrote the manuscript. All authors contributed to manuscript revision, read, and approved the submitted version.

FUNDING

This project was supported by a grant from Canadian Institutes of Health Research (CIHR-201903PJT – 419835). C-AG and MP were supported by scholarships from *Fonds de Recherche du Québec-Santé* (FRQ-S), CIHR, and Université Laval. HO was supported by a postdoctoral scholarship from the Société Québécoise d'Hypertension Artérielle and from Fondation de l'Université Laval. RG was supported by a FRQ-S clinician-scientist scholarship.

ACKNOWLEDGMENTS

We are grateful to the clinic personnel of hypertension and CKD and the study subjects for their kind contribution and precious collaboration.

REFERENCES

Agbaje, A. O., Barker, A. R., and Tuomainen, T.-P. (2021). Cardiorespiratory fitness, fat mass, and cardiometabolic health with endothelial function, arterial elasticity, and stiffness. *Med. Sci. Sports Exerc.* doi: 10.1249/MSS.0000000000002757

Bai, Q., Su, C.-Y., Zhang, A.-H., Wang, T., and Tang, W. (2019). Loss of the normal gradient in arterial compliance and outcomes of chronic kidney disease patients. *Cardiorenal. Med.* 9, 297–307. doi: 10.1159/000500479

Bao, W., Wang, F., and Tang, W. (2019). Aortic-brachial stiffness mismatch and mortality in peritoneal dialysis patients. *Kidney Blood Press Res.* 44, 123–132. doi: 10.1159/000498876

Blacher, J., Asmar, R., Djane, S., London, G. M., and Safar, M. E. (1999a). Aortic pulse wave velocity as a marker of cardiovascular risk in hypertensive patients. *Hypertension* 33, 1111–1117. doi: 10.1161/01.hyp.33.5.1111

Blacher, J., Guerin, A. P., Pannier, B., Marchais, S. J., Safar, M. E., and London, G. M. (1999b). Impact of aortic stiffness on survival in end-stage renal disease. *Circulation* 99, 2434–2439. doi: 10.1161/01.cir.99.18.2434

Bortolotto, L. A., Hanon, O., Franconi, G., Boutouyrie, P., Legrain, S., and Girerd, X. (1999). The aging process modifies the distensibility of elastic but not muscular arteries. *Hypertension* 34, 889–892. doi: 10.1161/01.hyp.34.4.889

Cahalan, M. K., Hashimoto, Y., Aizawa, K., Verotta, D., Ionescu, P., Balea, M., et al. (1992). Elderly, conscious patients have an accentuated hypotensive response to nitroglycerin. *Anesthesiology* 77, 646–655. doi: 10.1097/00000542-199210000-00006

Chen, C. H., Ting, C. T., Nussbacher, A., Nevo, E., Kass, D. A., Pak, P., et al. (1996). Validation of carotid artery tonometry as a means of estimating augmentation index of ascending aortic pressure. *Hypertension* 27, 168–175. doi: 10.1161/01.hyp.27.2.168

Cohn, J. N., Johnson, G., Ziesche, S., Cobb, F., Francis, G., Tristani, F., et al. (1991). A comparison of enalapril with hydralazine-isosorbide dinitrate in the treatment of chronic congestive heart failure. *N. Engl. J. Med.* 325, 303–310. doi: 10.1056/NEJM199108013250502

Cruickshank, K., Riste, L., Anderson, S. G., Wright, J. S., Dunn, G., and Gosling, R. G. (2002). Aortic pulse-wave velocity and its relationship to mortality in diabetes and glucose intolerance: an integrated index of vascular function? *Circulation* 106, 2085–2090. doi: 10.1161/01.cir.0000033824.02722.f7

Fortier, C., and Agharazii, M. (2016). Arterial stiffness gradient. *Pulse Basel Switz.* 3, 159–166. doi: 10.1159/000438852

Fortier, C., Mac-Way, F., Desmeules, S., Marquis, K., De Serres, S. A., Lebel, M., et al. (2015). Aortic-brachial stiffness mismatch and mortality in dialysis population. *Hypertension* 65, 378–384. doi: 10.1161/HYPERTENSIONAHA.114.04587

Gosling, R. G., and Budge, M. M. (2003). Terminology for describing the elastic behavior of arteries. *Hypertension* 41, 1180–1182. doi: 10.1161/01.HYP.0000072271.36866.2A

Hashimoto, J., and Ito, S. (2013). Aortic stiffness determines diastolic blood flow reversal in the descending thoracic aorta: potential implication for retrograde embolic stroke in hypertension. *Hypertension* 62, 542–549. doi: 10.1161/HYPERTENSIONAHA.113.01318

Heusinkveld, M. H. G., Delhaas, T., Lumens, J., Huberts, W., Spronck, B., Hughes, A. D., et al. (2019). Augmentation index is not a proxy for wave reflection magnitude: mechanistic analysis using a computational model. *J. Appl. Physiol. Bethesda Md.* 127, 491–500. doi: 10.1152/japplphysiol.00769.2018

Hughes, A. D., Park, C., Davies, J., Francis, D., McG Thom, S. A., Mayet, J., et al. (2013). Limitations of augmentation index in the assessment of wave reflection in normotensive healthy individuals. *PLoS One* 8:e59371. doi: 10.1371/journal.pone.0059371

Karras, A., Haymann, J.-P., Bozec, E., Metzger, M., Jacquot, C., Maruani, G., et al. (2012). Large artery stiffening and remodeling are independently associated with all-cause mortality and cardiovascular events in chronic kidney disease. *Hypertension* 60, 1451–1457. doi: 10.1161/HYPERTENSIONAHA.112.197210

Kidney Disease Improving Global Outcomes [KDIGO] (2013). Chapter 1: definition and classification of CKD. *Kidney Int. Suppl.* 3, 19–62. doi: 10.1038/kisup.2012.64

Laucyte-Cibulskiene, A., Boreikaite, E., Aucina, G., Gudynaite, M., Rudminiene, I., Anisko, S., et al. (2018). Usefulness of pretransplant aortic arch calcification evaluation for kidney transplant outcome prediction in one year follow-up. *Ren. Fail.* 40, 201–208. doi: 10.1080/0886022X.2018.1455588

Laucyte-Cibulskiene, A., Vickiene, A., Ryliskyte, L., Badariene, J., Rimsevicius, L., and Miglinas, M. (2019). Should we calculate arterial stiffness gradient in middle-aged women with increased cardiovascular risk? *Blood Press* 28, 199–205. doi: 10.1080/08037051.2019.1591921

Laurent, S., Boutouyrie, P., Asmar, R., Gautier, I., Laloux, B., Guize, L., et al. (2001). Aortic stiffness is an independent predictor of all-cause and cardiovascular mortality in hypertensive patients. *Hypertension* 37, 1236–1241. doi: 10.1161/01.hyp.37.5.1236

Laurent, S., Cockcroft, J., Van Bortel, L., Boutouyrie, P., Giannattasio, C., Hayoz, D., et al. (2006). Expert consensus document on arterial stiffness: methodological issues and clinical applications. *Eur. Heart J.* 27, 2588–2605. doi: 10.1093/eurheartj/ehl254

Laurent, S., Girerd, X., Mourad, J. J., Lacolley, P., Beck, L., Boutouyrie, P., et al. (1994). Elastic modulus of the radial artery wall material is not increased in patients with essential hypertension. *Arterioscler. Thromb. J. Vasc. Biol.* 14, 1223–1231. doi: 10.1161/01.ATV.14.7.1223

Levey, A. S., Stevens, L. A., Schmid, C. H., Zhang, Y. L., Castro, A. F., Feldman, H. I., et al. (2009). A new equation to estimate glomerular filtration rate. *Ann. Intern. Med.* 150, 604–612. doi: 10.7326/0003-4819-150-9-200905050-00006

Meyer, M. L., Tanaka, H., Palta, P., Cheng, S., Gouskova, N., Aguilar, D., et al. (2016). Correlates of segmental pulse wave velocity in older adults: the Atherosclerosis Risk in Communities (ARIC) study. *Am. J. Hypertens.* 29, 114–122. doi: 10.1093/ajh/hpv079

Millasseau, S. C., Patel, S. J., Redwood, S. R., Ritter, J. M., and Chowienczyk, P. J. (2003). Pressure wave reflection assessed from the peripheral pulse: is a transfer function necessary? *Hypertension* 41, 1016–1020. doi: 10.1161/01.HYP.0000057574.64076.A5

Mitchell, G. F. (2008). Effects of central arterial aging on the structure and function of the peripheral vasculature: implications for end-organ damage. *J. Appl. Physiol. Bethesda Md.* 105, 1652–1660. doi: 10.1152/japplphysiol.90549.2008

Mitchell, G. F., Tardif, J. C., Arnold, J. M., Marchiori, G., O'Brien, T. X., Dunlap, M. E., et al. (2001). Pulsatile hemodynamics in congestive heart failure. *Hypertension* 38, 1433–1439. doi: 10.1161/hy1201.098298

Mitchell, G. F., van Buchem, M. A., Sigurdsson, S., Gotal, J. D., Jonsdottir, M. K., Kjartansson, Ó, et al. (2011). Arterial stiffness, pressure and flow pulsatility and brain structure and function: the Age, Gene/Environment Susceptibility–Reykjavik study. *Brain J. Neurol.* 134, 3398–3407. doi: 10.1093/brain/awr253

Miyashita, H. (2012). Clinical assessment of central blood pressure. *Curr. Hypertens. Rev.* 8, 80–90. doi: 10.2174/157340212800840708

Mynard, J. P., and Smolich, J. J. (2014). Wave potential and the one-dimensional windkessel as a wave-based paradigm of diastolic arterial hemodynamics. *Am. J. Physiol. Heart Circ. Physiol.* 307, H307–H318. doi: 10.1152/ajpheart.00293.2014

Niiranen, T. J., Kalesan, B., Larson, M. G., Hamburg, N. M., Benjamin, E. J., Mitchell, G. F., et al. (2017). Aortic-brachial arterial stiffness gradient and cardiovascular risk in the community: the framingham heart study. *Hypertension* 69, 1022–1028. doi: 10.1161/HYPERTENSIONAHA.116.08917

Obeid, H., Fortier, C., Garneau, C.-A., Pare, M., Boutouyrie, P., Bruno, R. M., et al. (2021). Radial-digital pulse wave velocity: a noninvasive method for assessing stiffness of small conduit arteries. *Am. J. Physiol. Heart Circ. Physiol.* 320, H1361–H1369. doi: 10.1152/ajpheart.00551.2020

Padhy, S., Kar, P., and Ramachandran, G. (2017). Prediction of Major Adverse Cardiovascular and Cerebrovascular Events (MACCE) after thoracic surgery-the role of estimated GFR. *J. Clin. Diagn. Res. JCDR* 11, UC13–UC16. doi: 10.7860/JCDR/2017/27428.10616

Parker, K. H., Alastruey, J., and Stan, G.-B. (2012). Arterial reservoir-excess pressure and ventricular work. *Med. Biol. Eng. Comput.* 50, 419–424. doi: 10.1007/s11517-012-0872-1

Pauca, A. L., Kon, N. D., and O'Rourke, M. F. (2005). Benefit of glyceryl trinitrate on arterial stiffness is directly due to effects on peripheral arteries. *Heart Br. Card. Soc.* 91, 1428–1432. doi: 10.1136/hrt.2004.057356

Pierce, G. L., Pajaniappan, M., DiPietro, A., Darracott-Woei-A-Sack, K., and Kapuku, G. K. (2016). Abnormal central pulsatile hemodynamics in adolescents with obesity: higher aortic forward pressure wave amplitude is independently

associated with greater left ventricular mass. *Hypertension* 68, 1200–1207. doi: 10.1161/HYPERTENSIONAHA.116.07918

Pierce, G. L., Zhu, H., Darracott, K., Edet, I., Bhagatwala, J., Huang, Y., et al. (2013). Arterial stiffness and pulse-pressure amplification in overweight/obese African-American adolescents: relation with higher systolic and pulse pressure. *Am. J. Hypertens.* 26, 20–26. doi: 10.1093/ajh/hps014

Roach, M. R., and Burton, A. C. (1957). The reason for the shape of the distensibility curves of arteries. *Can. J. Biochem. Physiol.* 35, 681–690.

Roark, R. J., and Young, W. C. (1989). *Roark's Formulas for Stress and Strain*, 6th Edn. New York, NY: McGraw-Hill.

Segers, P., Rietzschel, E., Heireman, S., De Buyzere, M., Gillebert, T., Verdonck, P., et al. (2005). Carotid tonometry versus synthesized aorta pressure waves for the estimation of central systolic blood pressure and augmentation index. *Am. J. Hypertens.* 18, 1168–1173. doi: 10.1016/j.amjhyper.2005.04.005

Spronck, B., Tan, I., Reesink, K. D., Georgevsky, D., Delhaas, T., Avolio, A. P., et al. (2021). Heart rate and blood pressure dependence of aortic distensibility in rats: comparison of measured and calculated pulse wave velocity. *J. Hypertens.* 39, 117–126. doi: 10.1097/HJH.0000000000002608

Stone, K., Fryer, S., Meyer, M. L., Kucharska-Newton, A., Faulkner, J., Zieff, G., et al. (2021). The aortic-femoral arterial stiffness gradient: an atherosclerosis risk in communities (ARIC) study. *J. Hypertens.* 39, 1370–1377. doi: 10.1097/HJH.0000000000002808

Tarumi, T., Shah, F., Tanaka, H., and Haley, A. P. (2011). Association between central elastic artery stiffness and cerebral perfusion in deep subcortical gray and white matter. *Am. J. Hypertens.* 24, 1108–1113. doi: 10.1038/ajh.2011.101

Taylor, A. L., Ziesche, S., Yancy, C., Carson, P., D'Agostino, R., Ferdinand, K., et al. (2004). Combination of isosorbide dinitrate and hydralazine in blacks with heart failure. *N. Engl. J. Med.* 351, 2049–2057. doi: 10.1056/NEJMoa042934

Tyberg, J. V., Davies, J. E., Wang, Z., Whitelaw, W. A., Flewitt, J. A., Shrive, N. G., et al. (2009). Wave intensity analysis and the development of the reservoir-wave approach. *Med. Biol. Eng. Comput.* 47, 221–232. doi: 10.1007/s11517-008-0430-z

Utescu, M. S., Couture, V., Mac-Way, F., De Serres, S. A., Marquis, K., Larivière, R., et al. (2013). Determinants of progression of aortic stiffness in hemodialysis patients: a prospective longitudinal study. *Hypertension* 62, 154–160. doi: 10.1161/HYPERTENSIONAHA.113.01200

Wang, J.-J., O'Brien, A. B., Shrive, N. G., Parker, K. H., and Tyberg, J. V. (2003). Time-domain representation of ventricular-arterial coupling as a windkessel and wave system. *Am. J. Physiol. Heart Circ. Physiol.* 284, H1358–H1368. doi: 10.1152/ajpheart.00175.2002

Wilkinson, I. B., Qasem, A., McEniery, C. M., Webb, D. J., Avolio, A. P., and Cockcroft, J. R. (2002). Nitric oxide regulates local arterial distensibility in vivo. *Circulation* 105, 213–217. doi: 10.1161/hc0202.101970

Yamamoto, T., Shimizu, K., Takahashi, M., Tatsuno, I., and Shirai, K. (2017). The effect of nitroglycerin on arterial stiffness of the aorta and the femoral-tibial arteries. *J. Atheroscler. Thromb.* 24, 1048–1057. doi: 10.5551/jat.38646

Zanoli, L., Lentini, P., Boutouyrie, P., Fatuzzo, P., Granata, A., Corrao, S., et al. (2018). Pulse wave velocity differs between ulcerative colitis and chronic kidney disease. *Eur. J. Intern. Med.* 47, 36–42. doi: 10.1016/j.ejim.2017.08.020

Zhu, H., Yan, W., Ge, D., Treiber, F. A., Harshfield, G. A., Kapuku, G., et al. (2007). Cardiovascular characteristics in American youth with prehypertension. *Am. J. Hypertens.* 20, 1051–1057. doi: 10.1016/j.amjhyper.2007.05.009

Conflict of Interest: The authors declare that the research was conducted in the absence of any commercial or financial relationships that could be construed as a potential conflict of interest.

Publisher's Note: All claims expressed in this article are solely those of the authors and do not necessarily represent those of their affiliated organizations, or those of the publisher, the editors and the reviewers. Any product that may be evaluated in this article, or claim that may be made by its manufacturer, is not guaranteed or endorsed by the publisher.

frontiers in Physiology

ORIGINAL RESEARCH
published: 20 December 2021
doi: 10.3389/fphys.2021.787083

Single M-Line Is as Reliable as Multiple M-Line Ultrasound for Carotid Artery Screening

Afrah E. F. Malik[1,2], *Tammo Delhaas*[1,2], *Bart Spronck*[1,2], *Ronald M. A. Henry*[2,3], *Jayaraj Joseph*[4], *Coen D. A. Stehouwer*[2,3], *Werner H. Mess*[5] *and Koen D. Reesink*[1,2*]

[1] *Department of Biomedical Engineering, Maastricht University Medical Center, Maastricht, Netherlands,* [2] *CARIM School for Cardiovascular Diseases, Maastricht University Medical Center, Maastricht, Netherlands,* [3] *Department of Internal Medicine, Maastricht University Medical Center, Maastricht, Netherlands,* [4] *Healthcare Technology Innovation Centre, Indian Institute of Technology Madras, Chennai, India,* [5] *Department of Clinical Neurophysiology, Maastricht University Medical Centre, Maastricht, Netherlands*

Purpose: Carotid artery properties can be evaluated with high accuracy and reproducibility using multiple M-line ultrasound. However, the cost of multiple M-line-based imaging modalities and the extensive operator expertise requirements hamper the large-scale application for arterial properties assessment, particularly in resource-constrained settings. This study is aimed to assess the performance of a single M-line approach as an affordable and easy-to-use alternative to multiple M-line imaging for screening purposes.

Methods: We used triplicate longitudinal common carotid artery (CCA) ultrasound recordings (17 M-lines covering about 16 mm, at 500 frames per second) of 500 subjects from The Maastricht Study to assess the validity and reproducibility of a single against multiple M-line approach. The multiple M-line measures were obtained by averaging over all available 17 lines, whereas the middle M-line was used as a proxy for the single M-line approach.

Results: Diameter, intima-media thickness (IMT), and Young's elastic modulus (YEM) were not significantly different between the single and multiple M-line approaches ($p > 0.07$). Distension and distensibility coefficient (DC) did differ significantly ($p < 0.001$), however, differences were technically irrelevant. Similarly, Bland-Altman analysis revealed good agreement between the two approaches. The single M-line approach, compared to multiple M-line, exhibited an acceptable reproducibility coefficient of variation (CV) for diameter (2.5 vs. 2.2%), IMT (11.9 vs. 7.9%), distension (10 vs. 9.4%), DC (10.9 vs. 10.2%), and YEM (26.5 vs. 20.5%). Furthermore, in our study population, both methods showed a similar capability to detect age-related differences in arterial stiffness.

Conclusion: Single M-line ultrasound appears to be a promising tool to estimate anatomical and functional CCA properties with very acceptable validity and reproducibility. Based on our results, we might infer that image-free, single M-line tools

OPEN ACCESS

Edited by:
Julien Vincent Brugniaux, Université Grenoble Alpes, France

Reviewed by:
Nicola Riccardo Pugliese, University of Pisa, Italy
Carlo Palombo, University of Pisa, Italy

***Correspondence:**
Koen D. Reesink
k.reesink@maastrichtuniversity.nl

Specialty section:
This article was submitted to Vascular Physiology, a section of the journal Frontiers in Physiology

Received: *30 September 2021*
Accepted: *19 November 2021*
Published: *20 December 2021*

Citation:
Malik AEF, Delhaas T, Spronck B, Henry RMA, Joseph J, Stehouwer CDA, Mess WH and Reesink KD (2021) Single M-Line Is as Reliable as Multiple M-Line Ultrasound for Carotid Artery Screening. Front. Physiol. 12:787083. doi: 10.3389/fphys.2021.787083

could be suited for screening and for performing population studies in low-resource settings worldwide. Whether the comparison between single and multiple M-line devices will yield similar findings requires further study.

Keywords: arterial stiffness, common carotid artery, echo tracking, reproducibility, vascular risk management, vascular ultrasound

INTRODUCTION

Cardiovascular (CV) diseases are the leading cause of global mortality. An estimated global CV mortality of 17.9 million was recorded in 2019 (World Health Organization, 2021), with lower- and middle income (LMI) countries accounting for three times more CV cases than high-income countries (Jagannathan et al., 2019). Compared to previous decades, there has been a downward trend in CV mortality in developed countries. However, the rate of CV deaths in LMI countries has remained constant, mainly driven by the low detection rate of early-stage CV diseases in these regions (Jagannathan et al., 2019). Early detection of CV diseases facilitates early intervention and is, hence, necessary to reduce the global burden of CV diseases.

Arterial stiffness is recognized as an important predictor of CV diseases at their early stages. By contributing to elevated systolic blood pressure and increased cardiac afterload, an increased arterial stiffness causes CV diseases (Engelen et al., 2015). Increased arterial stiffness is associated with an enhanced risk of coronary heart disease, cerebrovascular events, and all-cause mortality (Laurent et al., 2001; Mattace-Raso et al., 2006; Karras et al., 2012; Steinbuch et al., 2016).

Carotid-femoral pulse wave velocity is considered to be the gold-standard measurement of arterial stiffness (Laurent et al., 2006). It represents the average stiffness over a long trajectory of the arterial tree. This trajectory, however, involves both central elastic and more muscular arteries (Engelen et al., 2015). The stiffness of these arteries may differently relate to CV diseases (Engelen et al., 2015). In addition, atherosclerotic plaques may result in a local modification of the stiffness, while the rest of the arterial tree remains intact (Hermeling, 2009). Therefore, it might be of particular interest to separately measure the stiffness of different arteries. Common carotid artery (CCA) stiffness, defined as distensibility coefficient (DC), is an independent predictor of CV events and all-cause mortality (Alan et al., 2003; Godia et al., 2007; Yuan et al., 2016; Joseph et al., 2020b).

The common practice of estimating local arterial stiffness involves measuring the instantaneous change in carotid diameter—termed distension—by means of ultrasound echo tracking. Combined with a local pulse pressure (PP) estimate, one obtains DC and Young's elastic modulus (YEM). The evaluation of local carotid stiffness requires accurate and precise tracking of the arterial wall. Conventionally, the tracking is based either on the edges of the arterial wall from a B-mode video recording or on the phase of multiple M-line recording. While scanners based on the former technique are limited by the temporal resolution of B-mode recordings, scanners based on phase tracking are costly and depend on the expertise of the operator. This limits their applicability to a small number of specialized hospitals. Both types of scanners, therefore, do not meet the pressing need for a screening tool in low-resource areas. Devices based on a single M-line (Joseph et al., 2020a) are affordable and accessible tools that are promising for diagnosis and screening in LMI countries.

The question that can be asked is whether carotid properties obtained with single M-line-based scanners are as accurate and reproducible as those obtained with multiple M-line-based scanners. Therefore, the aim of this study was to compare the performance of a single against a multiple M-line approach. For this purpose, we exploited existing multiple M-line image-based recordings and used the middle M-line as a proxy for single M-line-based devices. More specifically, we: (1) assessed the validity and compared the reproducibility of our proxy against a multiple M-line approach, and (2) compared the capacity of both methods to determine age-associated changes in stiffness.

MATERIALS AND METHODS

Study Subjects

In this study, we utilized data from The Maastricht Study, an ongoing, observational, prospective, population-based cohort study. It includes residents of the southern part of the Netherlands aged between 40 and 75 years. Its rationale, methodology, and design have been described in Schram et al. (2014). Briefly, the study focuses on the causation, pathophysiology, complications, and comorbidities of type 2 diabetes. The present study includes 500 participants randomly selected from over 7,000 subjects recruited in the first round of the study. In all selected subjects, three repeated measurements were performed (in accordance with the study protocol). Subject characteristics are presented in **Table 1**. The Maastricht Study has been approved by the institutional medical ethical committee and the Netherlands Health Council. Written informed consent was obtained from all participants prior to the study.

Data Acquisition

All vascular measurements were performed by trained technicians in temperature-controlled rooms (21–23°C) as described in Wijnands et al. (2015) and Zhou et al. (2018). Participants were asked to abstain from smoking and caffeine-containing beverages 3 h prior to the study (Wijnands et al., 2015). Vascular measurements were performed in the supine position after 10 min of rest. Repeated longitudinal ultrasound measurements of the left CCA were performed at least 1 cm proximally from the bifurcation using a Mylab70 scanner (Esaote Europe, Maastricht, The Netherlands) with a 7.5 MHz linear array transducer. During ultrasound measurements, systolic and diastolic pressure of the brachial artery was measured

TABLE 1 | Characteristics of the study population.

N	499
Age (years)	60 ± 8
Men (%)	52
Women (%)	48
BMI (kg/m^2)	26 ± 4
Weight (kg)	78 ± 15
Height (cm)	172 ± 9
Systolic blood pressure (mmHg)	127 ± 14
Diastolic blood pressure (mmHg)	75 ± 7
Pulse pressure (mmHg)	52 ± 10
Heart rate (beats/min)	62 ± 9
History of cardiovascular disease (%)	15.4

Values are presented as mean ± SD or percentage as appropriate.

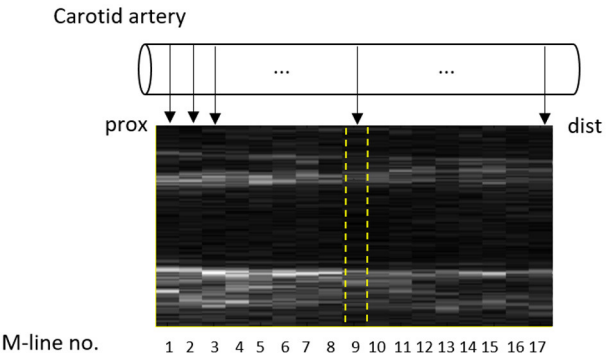

FIGURE 1 | Fast B-mode ultrasound recording of the common carotid artery with the 17 M-lines indicated. The middle M-line (no. 9) was selected as a proxy for a single M-line device and is indicated by dashed (yellow) lines.

with an oscillometric blood pressure monitor (Accutorr Plus, Datascope Inc., Montvale, NJ, USA). Next, PP was calculated as the difference between systolic and diastolic blood pressures. The average of pressure measurements performed at 5-min intervals during the vascular examination (lasting ∼45 min) was considered for further analysis (Geijselaers et al., 2016).

Arterial Wall Tracking

The scanner enabled the recording of radiofrequency (RF) signals in fast B-mode with a frame rate of 498 Hz. Although this very high frame rate enables high precision in wall tracking (Meinders et al., 2003), it comes at the cost of a reduced number of recording positions in the longitudinal plane (17 M-lines, separated by 0.96 mm, covering 16.32 mm). This results in a reduction of the longitudinal resolution while retaining information along the entire length of the imaged vessel. For off-line processing, RF signals were fed into a PC-based acquisition system that was coupled with the scanner (ART.LAB, Esaote Europe B.V. Maastricht, the Netherlands) (Wijnands et al., 2015; Geijselaers et al., 2016). RF signals were sampled at 50 MHz. During measurements, a video was depicted on the screen of the PC and an online tracking algorithm showed real-time instantaneous displacement of the arterial wall to assist the operator in orienting the ultrasound probe and obtaining high-quality RF signals. The RF signals were processed in MATLAB (version 7.5, Mathworks, Natick, MA, USA) using a wall-tracking system (WTS), which follows steps that were previously described in Hoeks et al. (1990, 1997). In brief, intima-media thickness (IMT) is assessed in the far wall by estimating the difference in position between the leading edge of the lumen intima echo and the leading edge of the media-adventitia echo during diastole (Willekes et al., 1999). Diameter is defined as the distance between the trailing edge of the anterior and leading edge of the posterior wall media-adventitia echoes obtained during diastole. The distension waveforms were obtained by tracking the displacement of the media-adventitia transition in the anterior and posterior walls. This was achieved by employing an efficient and commonly used complex cross-correlation model on the phase of the corresponding RF signal (Brands et al., 1997; Meinders et al., 2001; Steinbuch et al., 2016).

The WTS performs the abovementioned procedure and estimates the wall properties for each M-line separately. Conventionally, the average over all individual M-lines is considered for each parameter (Meinders and Hoeks, 2004). We refer to this method as the multiple M-line approach. As described in the introduction, we used the middle M-line as a proxy for an image-free single M-line device, which is referred to as the single M-line approach (**Figure 1**).

The simultaneous assessment of the geometrical parameters, such as diameter, wall thickness, and changes in diameter, in combination with PP, enables the quantification of the local mechanical characteristics of the vessel wall. DC is the relative change in vessel cross-sectional area for a given increase in pressure (Hoeks et al., 1990). YEM reflects the stiffness of a vessel as a function of diastolic diameter, a relative increase in diameter, IMT, and PP (Hoeks et al., 1997). These indices are defined as (Zhou et al., 2018):

$$\mathrm{DC} = \frac{2D\Delta D + \Delta D^2}{\mathrm{PP}^* D^2} \quad (1)$$

$$\mathrm{YEM} = D/(\mathrm{IMT}^*\mathrm{DC}) \quad (2)$$

where D is the diastolic diameter; ΔD is the distension; PP is the brachial pulse pressure; and IMT is the intima-media thickness.

Statistical Analyses

Statistical analyses were performed using SPSS version 27 (SPSS, Chicago, IL, USA). To validate the single M-line against the multiple M-line approach, a comparative analysis was performed. The multiple M-line approach was considered as a reference against which we evaluated the performance of the single M-line approach. This analysis included geometrical parameters and mechanical characteristics of the CCA. The validity of the single M-line approach was evaluated in two ways. First, Bland-Altman analysis was employed to assess the agreement between the two methods. Subsequently, a paired t-test was employed to assess the differences between single and multiple M-line approaches. A two-sided p-value <0.05 was considered statistically significant.

The reproducibility of the single M-line approach was assessed using the intra-subject SD of repeated measurements.

In addition, the coefficient of variation (CV) was calculated as [(intra-subject SD/group mean) × 100%]. The computation of within-subject and between-subject SDs has been described previously in Rodbard (1974). Composite SD (SD_{comp}), which represents the expected between-subject variation for a sample of repeated measurements (n_{rep}), is evaluated using the within-subject SD (SD_w) and between-subject SD (SD_b) using the formula:

$$SD_{comp} = \sqrt{SD_b{}^2 + \frac{SD_w{}^2}{n_{rep}}} \quad (3)$$

Equation (3) estimates the expected composite SD for any number of repetitions, e.g., to be utilized for power calculations in future studies.

We considered the middle M-line of a fast B-mode recording to be representative of a single M-line used in an image-free screening tool. However, with an imageless device, the position and orientation of the single M-line relative to the CCA are less controlled. Therefore, we performed a sensitivity analysis exploring the performance of other single M-lines. Additionally, we explored the influence of averaging different quantiles of M-lines on the validity and reproducibility of carotid properties. This was achieved by employing an averaging window around M-line 9 with increasing width from 1 to 15 M-lines using 2-line steps.

Multiple studies have firmly established an age-associated increase in arterial stiffness (Avolio et al., 1983, 1985; Kawasaki et al., 1987). Hence, we extended our evaluation by assessing the capability of the single M-line approach to detect the stiffness increase with age within our study population. To this end, study subjects were divided into two age groups (<60 and ≥60 years), and an independent sample *t*-test was employed to test for differences in stiffness measures between age groups. A similar procedure was applied to the multiple M-line approach to allow comparison between the two methods. The capability of the two methods to detect the increase in stiffness was compared using repeated-measures ANOVA.

RESULTS

Among the 500 subjects included in the study, one patient was excluded from all statistical analyses due to motion artifacts in the corresponding recording.

Validity and Reproducibility of the Single M-Line Approach

Reproducibility statistics were calculated based on three repeated measurements. These statistics that include the 25–75% CI obtained using bootstrapping are presented in **Table 2**. The composite SD was also computed using the within-subject and between-subject SDs. Although there was a significant difference between the intra-subject SDs obtained by the single and multiple M-line approaches, with the SD for multiple M-line being slightly lower (better), both tracking methods exhibited very low within-subject SD for carotid diameter (0.19 vs. 0.17 mm). The carotid diameter was similar for both single and multiple M-line approaches (7.79 ± 0.91 vs. 7.80 ± 0.90 mm, $p = 0.34$). Moreover, the Bland-Altman analysis shown in **Figure 2A** also revealed a good agreement between the single and multiple M-line approaches for estimating diameter (95% limits of agreement: −0.18 to 0.19 mm).

The single M-line approach yielded a significantly higher intra-subject SD for IMT compared to multiple M-line (0.10 vs. 0.07 mm, $p < 0.001$). However, the Bland-Altman plot shown in **Figure 2B** demonstrates a good agreement between single and multiple M-line approaches for IMT (95% limits of agreement: −0.13 to 0.12 mm), with no significant bias between single and multiple M-line-derived IMT (0.86 ± 0.20 vs. 0.85 ± 0.18 mm, $p = 0.07$).

Compared to when using multiple M-lines, the single M-line approach resulted in a significantly higher intra-subject SD for distension (39 vs. 36 μm, $p < 0.001$) and DC (1.67 vs. 1.55 1/MPa, $p < 0.001$). Similarly, the single M-line method yielded clinically irrelevant but significantly higher distension and DC (389 ± 132 vs. 385 ± 128 μm, and 15.3 ± 5.5 vs. 15.2 ± 5.3 1/MPa, respectively, $p < 0.001$). Nevertheless, the Bland-Altman analysis (**Figures 2C,D**) revealed good agreement between the single and the multiple M-line approach (95% limits of agreement: −42 to 34 μm and −1.8 to 1.5 1/MPa for distension and DC, respectively).

The intra-subject SD of YEM obtained by the single M-line was significantly higher than that achieved with multiple M-lines (0.19 vs. 0.15 MPa, $p < 0.001$). However, the Bland-Altman plot shown in **Figure 2E** reveals good agreement between single and multiple M-line approaches for YEM (95% limits of agreement: −0.22 to 0.22 MPa). This finding is corroborated by their non-significant difference (0.70 ± 0.33 vs. 0.71 ± 0.30 MPa, $p = 0.90$).

Sensitivity Analysis

Figures 3A–C shows how the choice of the single M-line (among the 17 available) affects the 95% limits of agreement between single and multiple M-line approaches for diameter, IMT, and distension, respectively. It is clearly visible that, in comparison with the outermost M-lines, the innermost M-lines showed a better agreement with the multiple M-line approach in terms of limits of agreements derived from Bland-Altman analysis. Moreover, as depicted in **Figures 3D–F**, central M-lines yielded better reproducibility (lower CVs) compared to the outermost M-lines.

Effect of Averaging Multiple M-Lines

The spatial averaging window starts at the middle line and extends toward the edges in steps of 2 lines. It is clearly visible from **Figure 4** that including more M-lines resulted in narrower limits of agreement and lower (better) reproducibility CVs for diameter, IMT, and distension. Reproducibility curves (**Figures 4D–F**) have a higher slope in the first section, indicating a pronounced effect of the innermost lines on the reproducibility of carotid property measurements compared to the outermost lines.

TABLE 2 | Common carotid artery properties as determined by single and multiple M-line approaches.

			Single M-line	Multiple M-line	*p*-value
Carotid diameter	Diameter (mm)		7.79 ± 0.91	7.80 ± 0.90	0.34
	Intra-subject	SD (mm)	0.19 (0.18–0.20)	0.17 (0.16–0.18)	<0.001
		CV (%)	2.5 (2.4–2.6)	2.2 (2.1–2.3)	
	Between subject	SD (mm)	0.90 (0.87–0.92)	0.89 (0.86–0.91)	
		CV (%)	11.5 (11.2–11.8)	11.4 (11.1–11.7)	
	Composite ($n_{rep} = 3$)	SD (mm)	0.90 (0.88–0.93)	0.89 (0.87–0.92)	
		CV (%)	11.6 (11.3–11.9)	11.5 (11.2–11.8)	
Carotid IMT	IMT (mm)		0.86 ± 0.20	0.85 ± 0.18	0.07
	Intra-subject	SD (mm)	0.10 (0.10–11)	0.07 (0.06–0.07)	<0.001
		CV (%)	11.9 (11.6–12.3)	7.9 (7.6–8.2)	
	Between subject	SD (mm)	0.18(0.17–0.19)	0.17 (0.17–0.18)	
		CV (%)	21.2 (20.1–22.0)	20.4 (19.4–21.2)	
	Composite ($n_{rep} = 3$)	SD (μm)	0.19 (0.18–0.20)	0.18 (0.17–0.19)	
		CV (%)	22.3 (21.8–23.5)	20.9 (20.2–21.9)	
Carotid distension	Distension (μm)		389 ± 132	385 ± 128	<0.001
	Intra-subject	SD (μm)	39 (37–40)	36 (35–37)	<0.001
		CV (%)	10.0 (9.6–10.3)	9.4 (9.0–9.7)	
	Between subject	SD (μm)	129 (125–132)	126 (122–129)	
		CV (%)	33.2 (32.3–34.0)	32.7 (31.8–33.5)	
	Composite ($n_{rep} = 3$)	SD (μm)	131 (127–134)	127 (123–131)	
		CV (%)	33.7 (33.0–34.7)	33.1 (32.4–34.1)	
Carotid distensibility coefficient	DC (1/MPa)		15.3 ± 5.5	15.2 ± 5.3	<0.001
	Intra-subject	SD (1/MPa)	1.67 (1.61–1.72)	1.55 (1.49–1.60)	<0.001
		CV (%)	10.9 (10.5–11.2)	10.2 (9.9–10.6)	
	Between subject	SD (1/MPa)	5.32 (5.15–5.47)	5.17 (5.00–5.31)	
		CV (%)	34.8 (33.8–35.6)	34.2 (33.2–35.0)	
	Composite ($n_{rep} = 3$)	SD (1/MPa)	5.41 (5.24–5.55)	5.24 (5.07–5.38)	
		CV (%)	35.4 (34.7–36.5)	34.7 (34.0–35.8)	
Carotid YEM	YEM (MPa)		0.70 ± 0.33	0.71 ± 0.30	0.90
	Intra-subject	SD (MPa)	0.19 (0.18–0.20)	0.15 (0.13–0.16)	<0.001
		CV (%)	26.5 (24.7–27.9)	20.5 (18.7–21.8)	
	Between subject	SD (MPa)	0.32 (0.30–0.33)	0.29 (0.28–0.30)	
		CV (%)	44.4 (41.8–46.3)	41.0 (39.5–42.2)	
	Composite ($n_{rep} = 3$)	SD (MPa)	0.34 (0.32–0.35)	0.30 (0.29–0.32)	
		CV (%)	46.9 (45.6–50.1)	42.6 (41.9–44.7)	

Values are expressed as mean ± SD. p-value based on paired sample t-test. Reproducibility statistics are presented that includes the 25–75% CI (obtained using bootstrapping) between parentheses. SD, standard deviation; CV, coefficient of variation; IMT, intima-media thickness; YEM, young's elastic modulus; DC, distensibility coefficient.

The Capacity of the Single M-Line Approach to Detect an Age-Related Increase in Stiffness

Distensibility coefficient and YEM values for subjects below or above 60 years of age and the inter-group differences are presented in **Table 3**. Both single and multiple M-line approaches showed the ability to detect an increase in stiffness with aging. Both methods revealed a significant reduction in DC as a function of age (single: difference 2.97 1/MPa, *t*-test: $p < 0.001$; multiple: difference 3.00 1/MPa, *t*-test: $p < 0.001$). Similarly, both single and multiple M-line approaches revealed a significant increase of YEM with age (single: difference 0.758 MPa, *t*-test: $p < 0.001$; multiple M-line: difference 0.756 MPa, *t*-test: $p < 0.001$).

The capability to detect the age-associated increase in stiffness was comparable for the single and multiple M-line approaches (DC: 3.00 vs. 2.97 1/MPa, ANOVA, $p = 0.71$; YEM: 0.120 vs. 0.115 MPa, ANOVA, $p = 0.71$).

DISCUSSION

In the present study, we evaluated the performance of single M-line ultrasound for estimating CCA properties taking multiple M-line as reference. Our evaluation showed that, although using a single M-line tends to generate less reproducible measures, the Bland-Altman analysis revealed good agreement between the single and multiple M-line approaches, with no significant

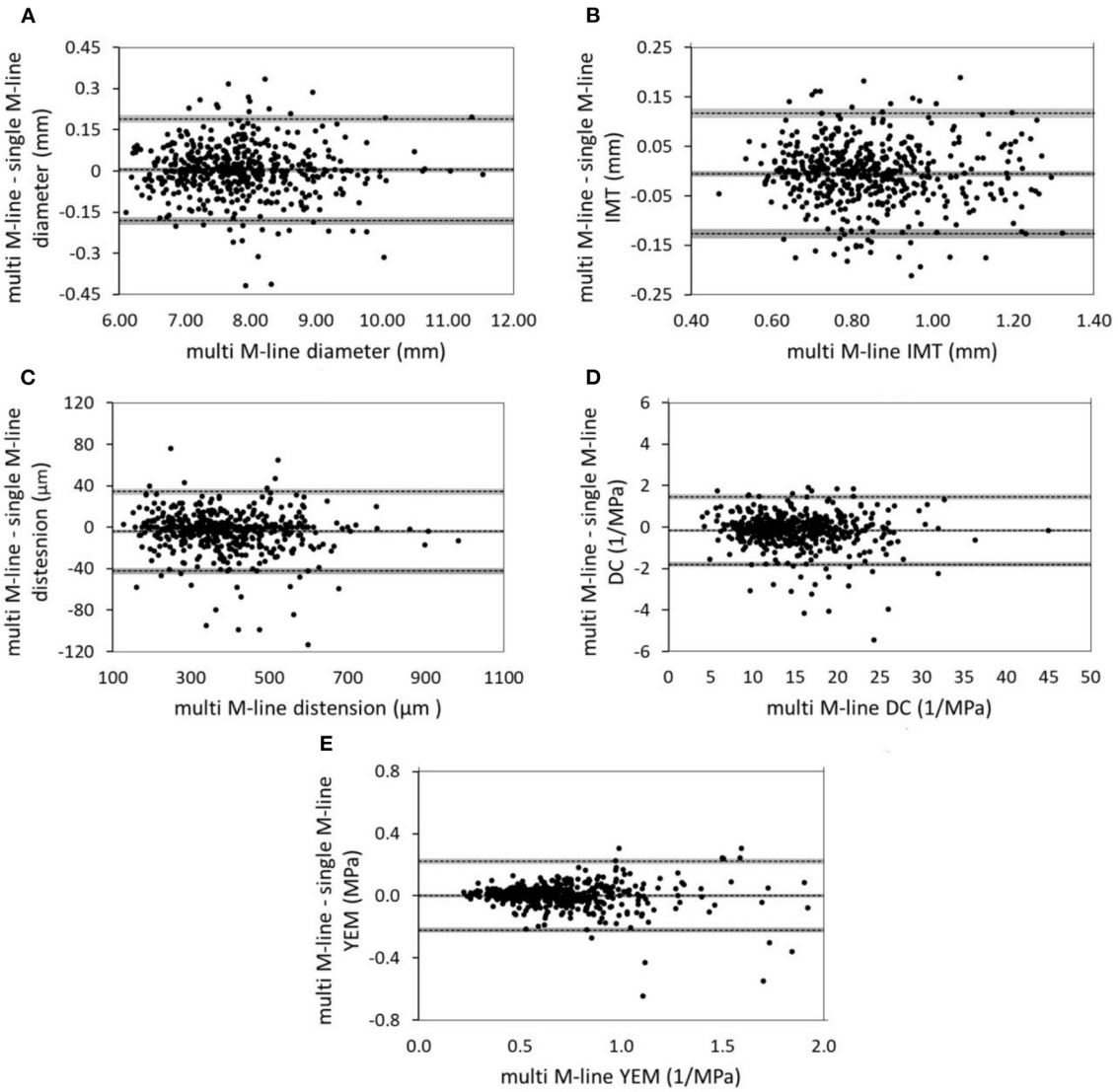

FIGURE 2 | Bland-Altman plots show good agreement between single and multiple-M-line approaches in estimating **(A)** diameter, **(B)** IMT, **(C)** distension, **(D)** DC, and **(E)** YEM. The gray areas indicate the 95% CIs of the bias and the limits of agreement. IMT, intima media thickness; DC, distensibility coefficient; YEM, young's elastic modulus.

bias for diameter, IMT, and YEM. Despite statistically significant biases for distension and DC, these were notably lower than the reproducibility CVs and, hence, practically irrelevant. Our results indicate that a single M-line-based technique evaluates CCA properties with sufficient validity and reproducibility for clinical use and screening purposes.

The cost of WTS, in combination with the required extensive operator expertise, hampers the large-scale application of arterial properties for screening purposes. Although single M-line-based scanners are not a technical novelty (Palombo et al., 2012), their affordability, user-friendliness, and accessibility form a basis for the wider application of arterial property screening in resource-limited settings (Joseph et al., 2020a). However, because single M-line-based scanners are image-free, they miss image-based features present in multiple M-line-based scanners such as plaque detection and characterization.

In principle, using a single M-line ultrasound without an image displayed on the screen implies increased operator dependency compared to that of multiple M-line image-based tools. However, to minimize operator dependency, single M-line tools visualize the RF signal together with real-time tracking of the arterial wall. Moreover, they also provide a signal quality score to ensure that the echos are coming from the carotid walls and that the probe is perpendicular to the walls (Joseph et al., 2020a). These together act as a feedback to guide the operator to orient the probe and reduce operator dependency induced by the lack of image feedback.

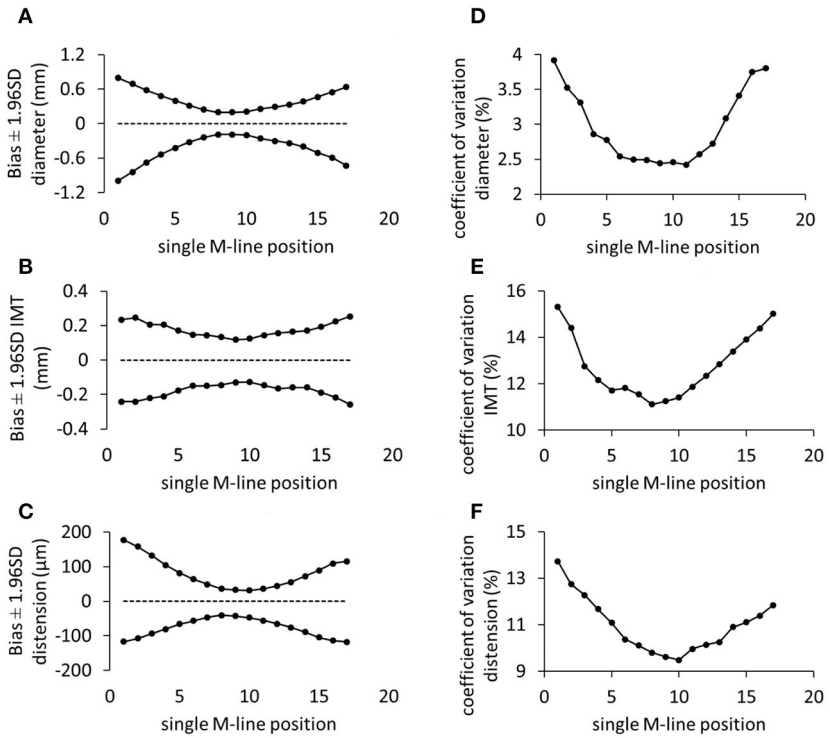

FIGURE 3 | The performance of individual M-lines in terms of the agreement from the Bland-Altman analysis **(A–C)** and reproducibility coefficient of variation **(D–F)** for diameter, intima-media thickness (IMT), and distension, respectively. SD, standard deviation.

This is the first study to compare the performance of a single M-line against a multiple M-line approach in a single recording performed to measure carotid artery characteristics. In an earlier study, Palombo et al. (2012) compared two different image-based devices: one with a single M-line and one with multiple M-lines. The authors reported significant biases for diameter, distension, and beta stiffness index obtained utilizing the two devices. They explained the significant bias in carotid distension by the variance in the placement of the tracking points between the two systems. We did not encounter this issue in our study, since the single and multiple M-line estimates are based on a single recording and tracking was performed on all the M-lines simultaneously with the same tracking points.

Though the differences in distension and DC between single and multiple M-line were statistically significant, the values obtained by single and multiple M-line approaches were highly correlated ($r = 0.99$, $p < 0.001$). Moreover, considering a resolution of about 20 μm of the wall-tracking algorithm (Hoeks et al., 1990), the observed distension bias of 4 μm is technically and practically irrelevant. The observed statistical differences in distension and DC are clearly due to the large sample size and consequently high study power. These differences between single and multiple M-line approaches, however, are smaller than the reproducibility of both methods and, hence, also irrelevant when measuring or monitoring a single subject. The limits of agreement of the single and multiple M-line methods do not exceed 45 μm (about twice the resolution). Despite the absence of a consensus regarding the minimal clinically relevant difference of carotid distension, we regard the limits of the agreement we found as compatible with clinical use and screening purposes.

The single M-line approach yielded comparable reproducibility with the multiple M-line method. When considered in more detail, the reproducibility of diameter, IMT, and distension are in line with previously reported values (CV range: 2.5–11.9%) (Bianchini et al., 2010; Bozec et al., 2020). The YEM obtained using a single M-line showed the most significant difference in CV (poorest reproducibility) compared to that obtained using multiple M-lines. This substantial difference originates from the variability of the IMT measurements, which is commonly reduced by considering the mean over multiple locations along the artery. Therefore, it was expected that IMT and YEM determined with the single M-line approach would have larger variability compared to the other parameters (**Table 2**).

We chose to use the middle M-line of 17 M-line-based recordings as a proxy for a single M-line device. The choice of the middle M-line was arbitrary and, *a priori*, had no specific reason. With an image-free device, however, the position of the single M-line relative to the CCA is unknown. Therefore, we also evaluated the performance of the other M-lines. Clearly, the M-lines on the edges exhibited wider limits of agreement and higher reproducibility CVs compared to middle lines (**Figure 3**). The trend of a worse performance toward the edge can be attributed to the online tracking algorithm. The employed algorithm

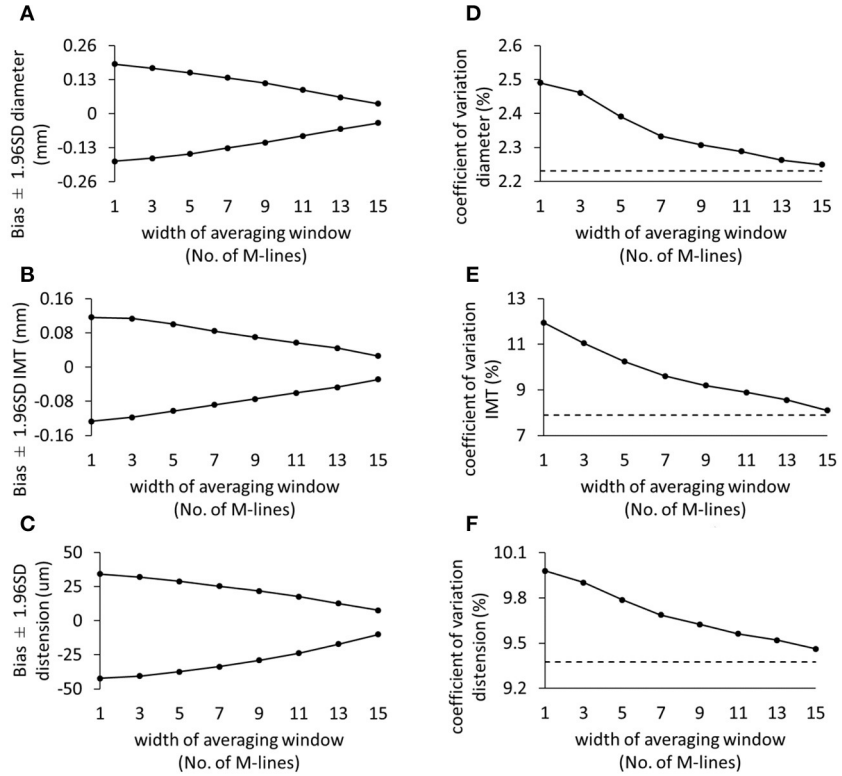

FIGURE 4 | The effect of increasing the spatial averaging window on the validity **(A–C)** and reproducibility coefficient of variation **(D–F)** for diameter, intima-media thickness, and distension, respectively. The dashed lines represent the reproducibility of the multiple M-line method (i.e., including all 17 M-lines). SD, standard deviation; IMT, intima-media thickness.

TABLE 3 | Feasibility of detecting age-related changes in stiffness.

		Single M-line	Multiple M-line	*p*-value
Distensibility coefficient (1/MPa)	<60 y (44%)	17.00	16.82	–
	≥60 y (56%)	14.00	13.85	–
	difference	−3.00	−2.97	0.71
Young's elastic modulus (MPa)	<60 y (44%)	0.638	0.641	–
	≥60 y (56%)	0.758	0.756	–
	difference	+0.120	+0.115	0.64

p-value shown is for the difference between single and multiple M-line approaches.

provides real-time visual feedback on the screen to assist the operator in orienting the probe and optimizing the quality of the M-lines. The tracking feedback entails a criterion forcing the operator to have at least 60% of the M-lines optimized. In this way, the operator may accept a measurement, without a necessity to optimize outermost lines. This technique is beneficial for time-efficient use, yet it does allow for increased noise on the outermost lines. Nevertheless, including more lines in the spatial averaging window resulted in enhanced reproducibility (**Figure 4**).

Our study has several possible limitations. To compare the capability of single and multiple M-line approaches toward the age-associated increase in stiffness, we addressed aging effects by looking into cross-sectional data rather than longitudinal data, although this kind of analysis should ideally consider differences within the same subjects over time.

The evaluation of arterial stiffness requires an accurate assessment of the arterial diameter changes with simultaneous measurement of the PP. Limitations of our study include the use of a single value of PP to evaluate the DC and YEM for both single and multiple M-line approaches, while, in practice, each method will have different values of PP. Nevertheless, this enables a direct comparison between the two methods in the present study. In addition, the caudal-cranial probe orientation was not fully consistent among recordings, affecting line identity (i.e., swap between 1 and 17, and so on). Therefore, probe orientation

was verified by means of the sign of the correlation coefficient of the linear regression line between M-line position and the corresponding dicrotic notch for all M-lines (Hermeling et al., 2009) and, where necessary, images were vertically flipped to make probe orientation consistent prior to sensitivity analysis. In this study, single and multiple M-line estimates were derived from a single scanner and, hence, were based on the same axial and temporal resolutions. In practice, however, separate devices may come with different resolutions. Since resolution largely influences the validity and reproducibility of the estimates obtained using a scanner, it should be taken into account when considering a single M-line device for screening. There exist single M-line tools with temporal and spatial resolution comparable to that of multiple M-line tools (Joseph et al., 2020a).

Another limitation is our selection of study population and setting. First, the characteristics of our population might not be representative of the targeted population. In addition, although our ultimate target is resource-constrained areas, our study context and infrastructure were those of an expert center in a western country with adequately available resources.

Some aspects regarding our study boundaries are worth discussing. First, the current study does not present an evaluation of two systems in the same population; it is instead a retrospective evaluation of two methods based on a single recording obtained using the same scanner. However, using two devices implies the presence of two procedures, so the variance induced by positioning the probe plays a significant role in the comparison. Second, the image and visual feedback are extra information that is not available in an image-free screening tool. In this regard, our proxy may be too near ideal for a single M-line device. Hence, there is a need for a next study to address the boundaries of the present study. Therefore, our next step will be to assess the performance of a single M-line image-free device against multiple M-line scanner in a screening setting.

In conclusion, single M-line ultrasound appears as a promising tool to estimate anatomical and functional common carotid artery properties with very acceptable validity and reproducibility. Based on our results, we might infer that image-free, single M-line tools could be suited for screening and population studies in low-resource settings worldwide. Whether the comparison between single and multiple M-line devices will yield similar findings requires further study.

DATA AVAILABILITY STATEMENT

The data analyzed in this study is subject to the following licenses/restrictions: the data of this study were taken from the Maastricht Study. Data are restricted by ethics and privacy of participants according to the study protocol approved by the Institutional Medical Ethical Committee and the Netherlands Health Council. The Maastricht Study Management Team (research.dms@mumc.nl) may be contacted to request data and access is granted for researchers who follow the guidelines stated in https://www.demaastrichtstudie.nl/research/data-guidelines. Requests to access these datasets should be directed to Anke Wesselius, research.dms@mumc.nl.

ETHICS STATEMENT

The studies involving human participants were reviewed and approved by Medisch Ethische ToetsingsCommissie UM/azM. The patients/participants provided their written informed consent to participate in this study.

AUTHOR CONTRIBUTIONS

AM, KR, and JJ: conceptualization. AM, KR, WM, and TD: methodology. AM, KR, and BS: data analysis. AM: data processing. AM and KR: writing—original draft preparation. AM, TD, BS, RH, JJ, CS, WM, and KR: writing—review and editing. TD, WM, and KR: supervision. All authors contributed to the article and approved the submitted version.

FUNDING

AM was supported by the European Union-funded Horizon 2020 project InSiDe (no. 871547). BS was supported by the European Union's Horizon 2020 research and innovation program (no. 793805).

ACKNOWLEDGMENTS

The authors would like to thank Arnold P. G. Hoeks for making available the Distension software code that was used to re-analyze the carotid ultrasound recordings in the present study.

REFERENCES

Alan, S., Ulgen, M. S., Ozturk, O., Alan, B., Ozdemir, L., and Toprak, N. (2003). Relation between coronary artery disease, risk factors and intima-media thickness of carotid artery, arterial distensibility, and stiffness index. *Angiology* 54, 261–267. doi: 10.1177/000331970305400301

Avolio, A., Chen, S.-G., Wang, R.-P., Zhang, C.-L., Li, M.-F., and O'Rourke, M. (1983). Effects of aging on changing arterial compliance and left ventricular load in a northern Chinese urban community. *Circulation.* 68, 50–58. doi: 10.1161/01.CIR.68.1.50

Avolio, A., Deng, F.-Q., Li, W.-Q., Luo, Y.-F., Huang, Z.-D., and Xing, L. (1985). Effects of aging on arterial distensibility in populations with high and low prevalence of hypertension: comparison between urban and rural communities in China. *Circulation* 71, 202–210. doi: 10.1161/01.CIR.71.2.202

Bianchini, E., Bozec, E., Gemignani, V., Faita, F., Giannarelli, C., and Ghiadoni, L. (2010). Assessment of carotid stiffness and intima-media thickness from ultrasound data: comparison between two methods. *J. Ultrasound Med.* 29, 1169–1175. doi: 10.7863/jum.2010.29.8.1169

Bozec, E., Girerd, N., Ferreira, J. P., Latar, I., Zannad, F., and Rossignol, P. (2020). Reproducibility in echotracking assessment of local carotid stiffness, diameter and thickness in a population-based study (The STANISLAS Cohort Study). *Artery Res.* 26, 5–12. doi: 10.2991/artres.k.200314.001

Brands, P. J., Hoeks, A. P., Ledoux, L. A., and Reneman, R. S. (1997). A radio frequency domain complex cross-correlation model to estimate blood flow velocity and tissue motion by means of ultrasound. *Ultrasound Med. Biol.* 23, 911–20. doi: 10.1016/S0301-5629(97)00021-5

Engelen, L., Bossuyt, J., Ferreira, I., van Bortel, L. M., Reesink, K. D., Segers, P., et al. (2015). Reference values for local arterial stiffness. Part A:

carotid artery. *J. Hypertens.* 33, 1981–1996. doi: 10.1097/HJH.0000000000000654

Geijselaers, S. L., Sep, S. J., Schram, M. T., van Boxtel, M. P., van Sloten, T. T., Henry, R. M., et al. (2016). Carotid stiffness is associated with impairment of cognitive performance in individuals with and without type 2 diabetes. The Maastricht Study. *Atherosclerosis* 253, 186–193. doi: 10.1016/j.atherosclerosis.2016.07.912

Godia, E. C., Madhok, R., Pittman, J., Trocio, S., Ramas, R., Cabral, D., et al. (2007). Carotid artery distensibility: a reliability study. *J. Ultrasound Med.* 26, 1157–1165. doi: 10.7863/jum.2007.26.9.1157

Hermeling, E. (2009). *Local pulse wave velocity determination: the arterial distension waveform from foot to crest* (PhD thesis). Maastricht University.

Hermeling, E., Reesink, K. D., Kornmann, L. M., Reneman, R. S., and Hoeks, A. P. (2009). The dicrotic notch as alternative time-reference point to measure local pulse wave velocity in the carotid artery by means of ultrasonography. *J. Hypertens.* 27, 2028–2035. doi: 10.1097/HJH.0b013e32832f5890

Hoeks, A. P., Brands, P. J., Smeets, F. A., and Reneman, R. S. (1990). Assessment of the distensibility of superficial arteries. *Ultrasound Med. Biol.* 16, 121–8. doi: 10.1016/0301-5629(90)90139-4

Hoeks, A. P., Willekes, C., Boutouyrie, P., Brands, P. J., Willigers, J. M., and Reneman, R. S. (1997). Automated detection of local artery wall thickness based on M-line signal processing. *Ultrasound Med. Biol.* 23, 1017–23. doi: 10.1016/S0301-5629(97)00119-1

Jagannathan, R., Patel, S. A., Ali, M. K., and Narayan, K. V. (2019). Global updates on cardiovascular disease mortality trends and attribution of traditional risk factors. *Curr. Diab. Rep.* 19, 1–12. doi: 10.1007/s11892-019-1161-2

Joseph, J., Kiran, R., Nabeel, P., Shah, M. I., Bhaskar, A., Ganesh, C., et al. (2020a). ARTSENS® Pen—portable easy-to-use device for carotid stiffness measurement: technology validation and clinical-utility assessment. *Biomed. Phys. Eng. Express* 6:025013. doi: 10.1088/2057-1976/ab74ff

Joseph, J., Nabeel, P., Rao, S. R., Venkatachalam, R., Shah, M. I., and Kaur, P. (2020b). Assessment of carotid arterial stiffness in community settings with ARTSENS®. *IEEE J. Transl. Eng. Health Med.* 9, 1–11. doi: 10.1109/JTEHM.2020.3042386

Karras, A., Haymann, J.-P., Bozec, E., Metzger, M., Jacquot, C., Maruani, G., et al. (2012). Large artery stiffening and remodeling are independently associated with all-cause mortality and cardiovascular events in chronic kidney disease. *Hypertension* 60, 1451–1457. doi: 10.1161/HYPERTENSIONAHA.112.197210

Kawasaki, T., Sasayama, S., Yagi, S.-I., Asakawa, T., and Hirai, T. (1987). Non-invasive assessment of the age related changes in stiffness of major branches of the human arteries. *Cardiovasc. Res.* 21, 678–687. doi: 10.1093/cvr/21.9.678

Laurent, S., Boutouyrie, P., Asmar, R., Gautier, I., Laloux, B., Guize, L., et al. (2001). Aortic stiffness is an independent predictor of all-cause and cardiovascular mortality in hypertensive patients. *Hypertension* 37, 1236–1241. doi: 10.1161/01.HYP.37.5.1236

Laurent, S., Cockcroft, J., Van Bortel, L., Boutouyrie, P., Giannattasio, C., Hayoz, D., et al. (2006). Expert consensus document on arterial stiffness: methodological issues and clinical applications. *Eur. Heart J.* 27, 2588–2605. doi: 10.1093/eurheartj/ehl254

Mattace-Raso, F. U., van der Cammen, T. J., Hofman, A., van Popele, N. M., Bos, M. L., Schalekamp, M. A., et al. (2006). Arterial stiffness and risk of coronary heart disease and stroke: the Rotterdam Study. C*irculation* 113, 657–663. doi: 10.1161/CIRCULATIONAHA.105.555235

Meinders, J. M., Brands, P. J., Willigers, J. M., Kornet, L., and Hoeks, A. P. (2001). Assessment of the spatial homogeneity of artery dimension parameters with high frame rate 2-D B-mode. *Ultrasound Med. Biol.* 27, 785–94. doi: 10.1016/S0301-5629(01)00351-9

Meinders, J. M., and Hoeks, A. P. (2004). Simultaneous assessment of diameter and pressure waveforms in the carotid artery. *Ultrasound Med. Biol.* 30, 147–154. doi: 10.1016/j.ultrasmedbio.2003.10.014

Meinders, J. M., Kornet, L., and Hoeks, A. P. (2003). Assessment of spatial inhomogeneities in intima media thickness along an arterial segment using its dynamic behavior. *Am. J. Physiol. Heart Circ. Physiol.* 285, H384–H391. doi: 10.1152/ajpheart.00729.2002

Palombo, C., Kozakova, M., Guraschi, N., Bini, G., Cesana, F., Castoldi, G., et al. (2012). Radiofrequency-based carotid wall tracking: a comparison between two different systems. *J. Hypertens.* 30, 1614–1619. doi: 10.1097/HJH.0b013e328354dd44

Rodbard, D. (1974). Statistical quality control and routine data processing for radioimmunoassays and immunoradiometric assays. *Clin. Chem.* 20, 1255–1270. doi: 10.1093/clinchem/20.10.1255

Schram, M. T., Sep, S. J., van der Kallen, C. J., Dagnelie, P. C., Koster, A., Schaper, N., et al. (2014). The Maastricht Study: an extensive phenotyping study on determinants of type 2 diabetes, its complications and its comorbidities. *Eur. J. Epidemiol.* 29, 439–451. doi: 10.1007/s10654-014-9889-0

Steinbuch, J., Hoeks, A. P., Hermeling, E., Truijman, M. T., Schreuder, F. H., and Mess, W. H. (2016). Standard b-mode ultrasound measures local carotid artery characteristics as reliably as radiofrequency phase tracking in symptomatic carotid artery patients. *Ultrasound Med. Biol.* 42, 586–595. doi: 10.1016/j.ultrasmedbio.2015.07.030

Wijnands, J. M., Boonen, A., van Sloten, T. T., Schram, M. T., Sep, S. J., Koster, A., et al. (2015). Association between serum uric acid, aortic, carotid and femoral stiffness among adults aged 40–75 years without and with type 2 diabetes mellitus: the Maastricht Study. *J. Hypertens.* 33, 1642–1650. doi: 10.1097/HJH.0000000000000593

Willekes, C., Hoeks, A. P., Bots, M. L., Brands, P. J., Willigers, J. M., and Reneman, R. S. (1999). Evaluation of off-line automated intima-media thickness detection of the common carotid artery based on M-line signal processing. *Ultrasound Med. Biol.* 25, 57–64. doi: 10.1016/S0301-5629(98)00138-0

World Health Organization. (2021). *Cardiovascular Diseases (CVDs).* World Health Organization. Available online at: https://www.who.int/news-room/fact-sheets/detail/cardiovascular-diseases-(cvds) (accessed September 22, 2021).

Yuan, C., Wang, J., and Ying, M. (2016). Predictive value of carotid distensibility coefficient for cardiovascular diseases and all-cause mortality: a meta-analysis. *PLoS One* 11:e0152799. doi: 10.1371/journal.pone.0152799

Zhou, T. L., Henry, R. M. A., Stehouwer, C. D. A., van Sloten, T. T., Reesink, K. D., and Kroon, A. A. (2018). Blood pressure variability, arterial stiffness, and arterial remodeling. *Hypertension* 72, 1002–1010. doi: 10.1161/HYPERTENSIONAHA.118.11325

Conflict of Interest: The authors declare that the research was conducted in the absence of any commercial or financial relationships that could be construed as a potential conflict of interest.

Publisher's Note: All claims expressed in this article are solely those of the authors and do not necessarily represent those of their affiliated organizations, or those of the publisher, the editors and the reviewers. Any product that may be evaluated in this article, or claim that may be made by its manufacturer, is not guaranteed or endorsed by the publisher.

frontiers in Physiology

ORIGINAL RESEARCH
published: 11 January 2022
doi: 10.3389/fphys.2021.775052

Template Matching and Matrix Profile for Signal Quality Assessment of Carotid and Femoral Laser Doppler Vibrometer Signals

Silvia Seoni[1†], *Simeon Beeckman*[2,3†], *Yanlu Li*[4], *Soren Aasmul*[5], *Umberto Morbiducci*[6], *Roel Baets*[4], *Pierre Boutouyrie*[7], *Filippo Molinari*[1], *Nilesh Madhu*[3] *and Patrick Segers*[2*]

[1] PoliToBIOMed Lab, Biolab, Politecnico di Torino, Turin, Italy, [2] IBiTech-bioMMeda, Ghent University, Ghent, Belgium, [3] IDLab-imec, Ghent University, Ghent, Belgium, [4] Photonics Research Group, Center for Nano- and Biophotonics, Tech Lane Ghent Science Park/Campus A, Ghent University-imec, Ghent, Belgium, [5] Medtronic Bakken Research Center, Maastricht, Netherlands, [6] Department of Mechanical and Aerospace Engineering, Polytechnic University of Turin, Turin, Italy, [7] INSERM U970, Université de Paris, Assistance Publique Hôpitaux de Paris, Paris, France

OPEN ACCESS

Edited by:
Bart Spronck,
Maastricht University, Netherlands

Reviewed by:
Carlo Palombo,
University of Pisa, Italy
Alessandro Giudici,
Maastricht University, Netherlands

***Correspondence:**
Patrick Segers
patrick.segers@ugent.be

[†]These authors have contributed equally to this work

Specialty section:
This article was submitted to Vascular Physiology, a section of the journal Frontiers in Physiology

Received: *13 September 2021*
Accepted: *06 December 2021*
Published: *11 January 2022*

Citation:
Seoni S, Beeckman S, Li Y, Aasmul S, Morbiducci U, Baets R, Boutouyrie P, Molinari F, Madhu N and Segers P (2022) Template Matching and Matrix Profile for Signal Quality Assessment of Carotid and Femoral Laser Doppler Vibrometer Signals. Front. Physiol. 12:775052. doi: 10.3389/fphys.2021.775052

Background: Laser-Doppler Vibrometry (LDV) is a laser-based technique that allows measuring the motion of moving targets with high spatial and temporal resolution. To demonstrate its use for the measurement of carotid-femoral pulse wave velocity, a prototype system was employed in a clinical feasibility study. Data were acquired for analysis without prior quality control. Real-time application, however, will require a real-time assessment of signal quality. In this study, we (1) use template matching and matrix profile for assessing the quality of these previously acquired signals; (2) analyze the nature and achievable quality of acquired signals at the carotid and femoral measuring site; (3) explore models for automated classification of signal quality.

Methods: Laser-Doppler Vibrometry data were acquired in 100 subjects (50M/50F) and consisted of 4–5 sequences of 20-s recordings of skin displacement, differentiated two times to yield acceleration. Each recording consisted of data from 12 laser beams, yielding 410 carotid-femoral and 407 carotid-carotid recordings. Data quality was visually assessed on a 1–5 scale, and a subset of best quality data was used to construct an acceleration template for both measuring sites. The time-varying cross-correlation of the acceleration signals with the template was computed. A quality metric constructed on several features of this template matching was derived. Next, the matrix-profile technique was applied to identify recurring features in the measured time series and derived a similar quality metric. The statistical distribution of the metrics, and their correlates with basic clinical data were assessed. Finally, logistic-regression-based classifiers were developed and their ability to automatically classify LDV-signal quality was assessed.

Results: Automated quality metrics correlated well with visual scores. Signal quality was negatively correlated with BMI for femoral recordings but not for carotid recordings. Logistic regression models based on both methods yielded an accuracy of minimally 80% for our carotid and femoral recording data, reaching 87% for the femoral data.

Conclusion: Both template matching and matrix profile were found suitable methods for automated grading of LDV signal quality and were able to generate a quality metric that was on par with the signal quality assessment of the expert. The classifiers, developed with both quality metrics, showed their potential for future real-time implementation.

Keywords: laser doppler vibrometry (LDV), matrix profile, template matching, logistic regression, signal quality

1. INTRODUCTION

The aorta and large central arteries fulfill key physiological functions in the circulation, whereby their structure is apt to their function. They consist of complex composite soft tissues, concentrically organized in lamellar units, where sheets of elastin intertwine with layers of vascular smooth-muscle cells in a matrix of collagen and other proteins composing the extra-cellular matrix (Wolinsky and Glagov, 1967). This allows the aorta and large arteries to distend when the heart contracts and blood is ejected into the aorta and store elastic energy in the arterial wall, which is used during the relaxation phase of the heart to maintain blood pressure and drive the perfusion of organs and tissues. This function is also referred to as the windkesseli or buffering function of the large arteries, and ensures that the pulsatile blood flow generated by the heart is transformed into a near steady flow when reaching the smaller arteries (Westerhof et al., 2009). It prevents excessive maximal (systolic) and too low minimal (diastolic) blood pressure. Arterial stiffening leads to a loss of this buffering function with detrimental effects on nearly all organ systems, and especially low resistance organs such as the brain, the kidneys, and the heart itself (Chirinos et al., 2019). Arterial stiffening has received large attention over the past three decades, and there is a consensus that assessment of arterial stiffness is especially relevant in the assessment of an individual's risk for cardiovascular disease and death (Laurent et al., 2006; Vlachopoulos et al., 2010).

Because of the distensible nature of arteries, cardiac contraction generates a wave (detectable as a change in pressure, flow, or arterial diameter). This wave initially propagates from the heart to the periphery, but increases in complexity as it interacts on its way with the branching arterial tree and gets shaped because of wave reflection and transmission (O'Rourke and Kelly, 1993; Mitchell et al., 2004, 2011; Chirinos et al., 2019). The wave speed, or pulse wave velocity (PWV), is directly linked with the distensibility of the arteries (the stiffer the artery, the higher PWV) (Bramwell and Hill, 1922), and the current clinical standard method to measure arterial stiffness is by measuring the pulse wave velocity (Segers et al., 2020). In essence, the method is simple and straightforward: one detects the pulse at two locations a distance dx apart, and from the time delay, dt, between the signals, one gets PWV = dx/dt. Despite the simplicity of the concept, there are still many hurdles in measuring PWV in practice, mainly related to the non-availability of sites to directly measure the pulse along the path of the aorta in a non-invasive way and without the need for clinical scanners (Segers et al., 2020). Accessible sites closest to the aorta are the neck (carotid artery) and groin (femoral artery) and carotid-femoral PWV is considered the best possible proxy for aortic PWV (Laurent et al., 2006).

Several sensors can be used to detect the pulse in the neck and groin (Pereira et al., 2015; Segers et al., 2020), including applanation tonometry, ultrasound (pulsed Doppler recordings), or accelerometers. Motivated by the relatively high cost of equipment, the required level of expertise by the operator, or the contact-based nature of the measurement, we and others have explored the use of Laser-Doppler Vibrometry (LDV) to detect the motion of the skin atop the carotid and/or femoral arteries in response to the passage of the arterial pulse (Morbiducci et al., 2007b; De Melis et al., 2008; Scalise and Morbiducci, 2008; Campo and Dirckx, 2011; Kaplan et al., 2012). To eliminate motion drift and amplify the fast displacements associated with the arrival of the foot of the pulse (Morbiducci et al., 2007b), we have been using skin acceleration as the basic signal from which to derive time delays between the neck and groin for measuring carotid-femoral PWV.

The feasibility of the method has been shown using industrial-type LDV sensors (De Melis et al., 2008), and we have been working on the design and development of a multi-beam handheld device. The core of the device is a silicon photonics chip integrated into a micro-optical system which allows for flexible and compact multi-array designs (Li et al., 2013, 2020). A first prototype (consisting of 2 connected yet separable handheld pieces to measure in the neck and groin with each 6 laser beams) was developed within the context of the H2020-funded project CARDIS and included a clinical feasibility study whereby carotid-femoral PWV was assessed in 100 patients and compared with a reference method based on applanation tonometry (Marais et al., 2019). Measurements were performed with a minimal visual feedback during the measurements and all the analyses were carried out in an off-line modality.

A next generation version of the device is under development and will provide real-time measurement of carotid-femoral PWV. To do so, we need a real-time assessment of the quality of incoming data to decide whether or not data records are of an acceptable quality for subsequent processing. This is, however, not a trivial assessment as there is little reference as to what makes LDV signal recordings appropriate for PWV estimation.

The aim of this study is, therefore, to identify a strategy to objectively and automatically assess the LDV-signal quality and set criteria for future use of this technology in arterial pulse detection. To do that we will use the existing CARDIS database of LDV recordings at the carotid and femoral measurement sites and subject them to two different strategies: the template matching and the matrix profile will be tested for (1) analyzing the nature and achievable quality of the recorded signals,

and (2) exploring models for automated classification of LDV-signal quality.

2. MATERIALS AND METHODS

2.1. The CARDIS Device

Technical details on the optics and overall design of the CARDIS device have been described in Li et al. (2020). Briefly, the device consists of two handpieces (handpiece 1 contains the handgrip of the device, handpiece 2 is the add-on part of the device: we refer to **Figure 1** for an illustration of the device and the positioning of the handpieces), each sending out 6 laser beams (wavelength 1,550 nm), positioned along a line and 5 mm apart. The handpieces can be used separately for measurement of carotid-femoral PWV or attached to measure signals on locations 25–50 mm apart, e.g., to locally measure pulse wave propagation along the carotid artery. A retro-reflective tape is attached to the skin at the measurement location to enhance the reflection of the laser light, and the device is equipped with a spacer to ensure an appropriate optical focus distance and to stabilize measurements.

2.2. Study Population and Available Database

The data used in this study were acquired with a clinical feasibility study in 100 patients, conducted at the Hpital Europen Georges Pompidou (HEGP) in Paris, France, to assess the ability of the CARDIS device to measure signals in a configuration with simultaneous carotid-femoral or carotid-carotid recordings. Patients were in the age range 19–85 and presented with mild to stage 3 hypertension, controlled or not (Marais et al., 2019). For each subject, 4–5 datasets, each consisting of 20 s traces on 12 channels measured with the two handpieces, were acquired. In detail, the analyzed database was made of 410 datasets (4,920 waveforms) from carotid-femoral recordings, and of 407 datasets (4,884 waveforms) from carotid-carotid recordings. Raw IQ (In-phase and quadrature) LDV-data were acquired at a sampling frequency of 100 kHz, and LDV-displacement data were downsampled to 10 kHz upon demodulation. A low-pass filter with a cut-off frequency of 30 Hz was applied to LDV displacement data, which were differentiated two times to yield acceleration. The same low-pass filtering strategy was applied after each differentiation operation.

2.3. Visual Scoring of the Data

A graphical interface displaying all the LDV acceleration signals derived from the six channel recordings per handpiece was implemented in the MATLAB environment (The MathWorks, Naticks MA, US). The acceleration signals were visually scored by an expert operator (Segers P.) on a 5-level grade scale taking values Q_{vis} according to **Table 1**.

Note that the presence of brief artifacts in the 20 s acquired traces was not used as a criterion to score the signal quality. As such, signals qualified as excellent may still demonstrate a brief episode of poor data. Overall, the femoral data were of a markedly lower Q_{vis} "quality" than traces recorded at the carotid artery, which impacted the rating. Therefore, the Q_{vis} quality score of 3 (borderline) was given to femoral traces that appeared to be of a much lesser quality than $Q_{vis} = 3$ rated carotid traces. Such a borderline score was assigned when 5–10 beats were discernible in the signal. Representative carotid and femoral signals receiving the different scores are displayed in **Figure 1**.

2.4. Template Matching

Template matching technique is an effective approach for the automatic detection of *a priori* identified patterns in signal recordings (Jiun-Hung et al., 2003; Won-Du and Chang-Hwan, 2014) and images (Omachi and Omachi, 2007). A good-quality carotid LDV acceleration signal presents two sharp peaks for each heartbeat: the first peak corresponds to the systolic rapid upstroke of pressure and demarcates the foot of the arterial pulse; the second peak denotes the wave that is generated at the moment of closure of the aortic valve (the dicrotic notch). The LDV-femoral recording is devoid of clearly identifiable features related to the dicrotic notch because of the distance of the measurement site from the heart, whose final effect is filtering the recorded LDV pulses, in the femoral artery. An example of displacement, acceleration, and ECG signals together are shown in **Figure 2**.

2.4.1. Constructing the Templates

High-quality carotid and femoral LDV-acceleration traces were adopted for template construction. Traces with visual score values Q_{vis} of 4 and 5 were selected. To avoid subject-specific biasing in template construction, only one 20 s recording (from the acquired channel with the highest Q_{vis}) per subject was selected. Based on these selection criteria, 135 carotid LDV-acceleration traces from 20 different subjects and 40 femoral LDV-acceleration traces from 10 different subjects were identified as suitable for template construction in the CARDIS dataset. The selected carotid LDV-acceleration traces were from both handpieces.

The selected traces, characterized by the presence of sharp and pronounced peaks at the foot (and dicrotic notch for carotid recordings), were then segmented in epochs, each one corresponding to a single heartbeat. LDV-acceleration trace segmentation was carried out using ECG synchronous recordings (available for each subject in the CARDIS dataset, on which automatic R-peak detection was carried out, refer to **Figure 3**). Over each LDV trace, single epochs were then defined within a time interval within the occurrence of two consecutive R peaks in the ECG trace (**Figure 3A**). By construction of the visual inspection classification, some of the identified single epochs might still not be of adequate quality for template construction, because of the presence of short-time artifacts/noise (**Figure 3B**). The lower quality single epochs in an LDV-acceleration trace were identified according to the following strategy: (1) for each LDV segmented trace, a correlation matrix R_{ij} was built up, each element of the matrix being the Pearson-correlation coefficient between epochs i and j, used as a measure of their shape similarity; (2) a threshold value of the correlation coefficient was defined and single epochs with an average correlation coefficient with all the other epochs lower than the threshold was discarded, since they were not sufficiently similar in shape to the other epochs in the recorded trace (**Figure 3C**); (3) for each LDV-acceleration trace, an "individual template" was built

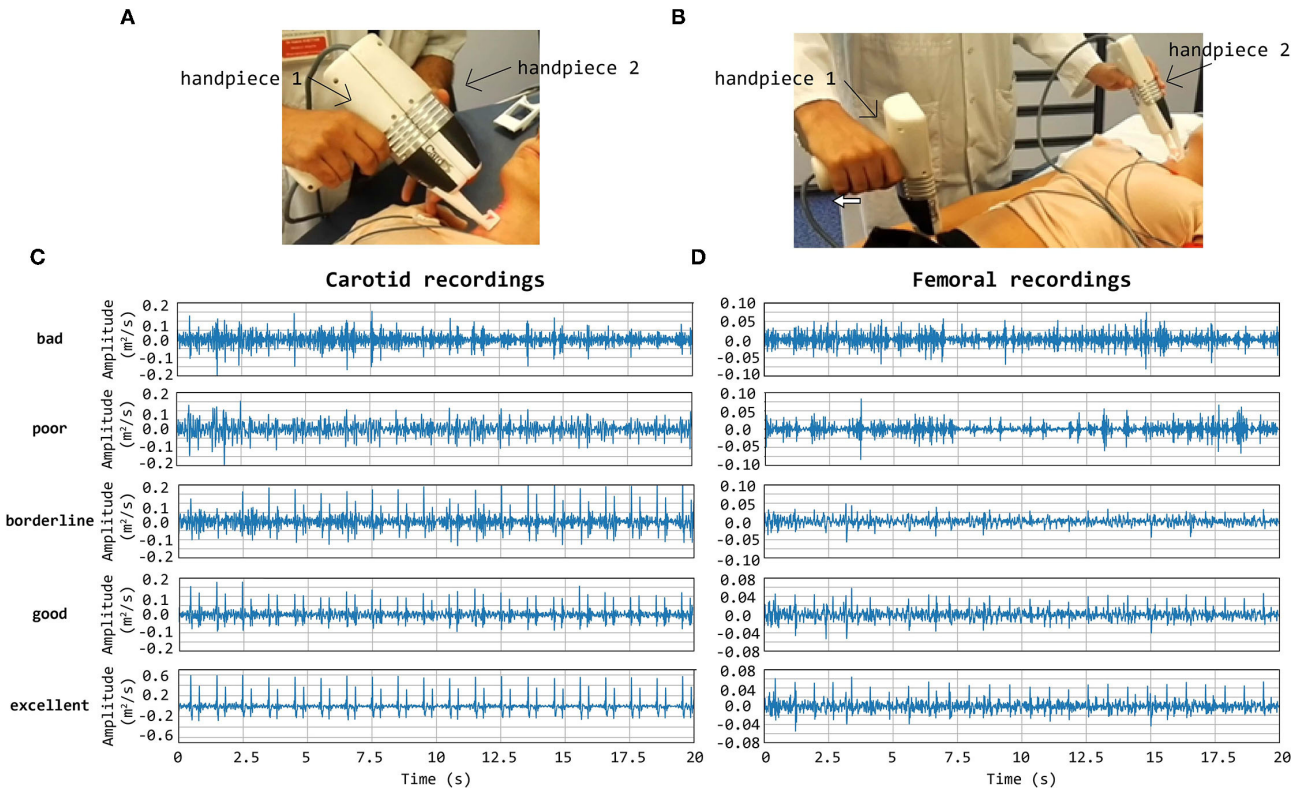

FIGURE 1 | CARDIS device in configuration to measure carotid-femoral **(A)** and local carotid PWV **(B)**. **(C,D)** display representative tracings on the carotid **(C)** and femoral **(D)** measuring site receiving a visual grading score of 1–5. Especially in the excellent tracings, the foot-of-the-wave waveforms are clearly visible, with the same for the dicrotic notch waveforms in the local carotid case.

TABLE 1 | The 5-levels grade scale taking values Q_{vis}.

Quality score Q_{vis}	Quality	Description
Score 1	Bad	Acquisition with no evidence of repeatable features that may be linked to the detection of a pulse
Score 2	Poor	Very noisy acquisition not suitable for analysis, but with identifiable pulses within the noisy trace
Score 3	Bordeline	Acquisition affected by noise but presenting clear repeatable patterns. Advanced signal processing algorithms could remove the noise and allow to detect the foot of the pulse wave with reasonable affordability
Score 4	Good	Acquisition with sharp and pronounced peaks at the foot (and dicrotic notch), with relatively low noise levels between successive pulse peaks
Score 5	Excellent	Acquisition with very sharp and pronounced peaks at the foot (and dicrotic notch), with low noise levels in between the peaks. Signals of textbook quality

up by averaging only the identified highly correlated epochs (**Figure 3D**); (4) by adopting the same approach with the carotid and femoral LDV-acceleration traces, the final carotid and femoral "population templates" were obtained (**Figure 4**).

Template construction is based upon the definition of a strategy to treat the issue of the different time length of single epochs (intra-individual RR variability) (Jensen-Urstad et al., 1997; Zhang, 2007) and the individual templates as well. Hence, the time length of single epochs should be defined on the basis of what the template should represent. In the case under study, the carotid LDV-acceleration template longer than 350 ms will include by construction the foot of the wave (first peak) and the dicrotic notch (second peak). In this study, we speculate that a carotid LDV template incorporating the second peak may degrade in performance, as the distance between the two peaks is (intra-individually and inter-individually) variable. In **Figure 5**, carotid and femoral LDV-acceleration templates constructed for different (predefined) time length are displayed. In detail, time lengths of 300, 400, and 500 ms were considered for the femoral LDV-acceleration template, and time lengths of 200, 400, and 600 ms for the carotid LDV-acceleration template. The impact of the time length in the LDV template performance when used for the automatic assessment of the quality of the CARDIS data was evaluated.

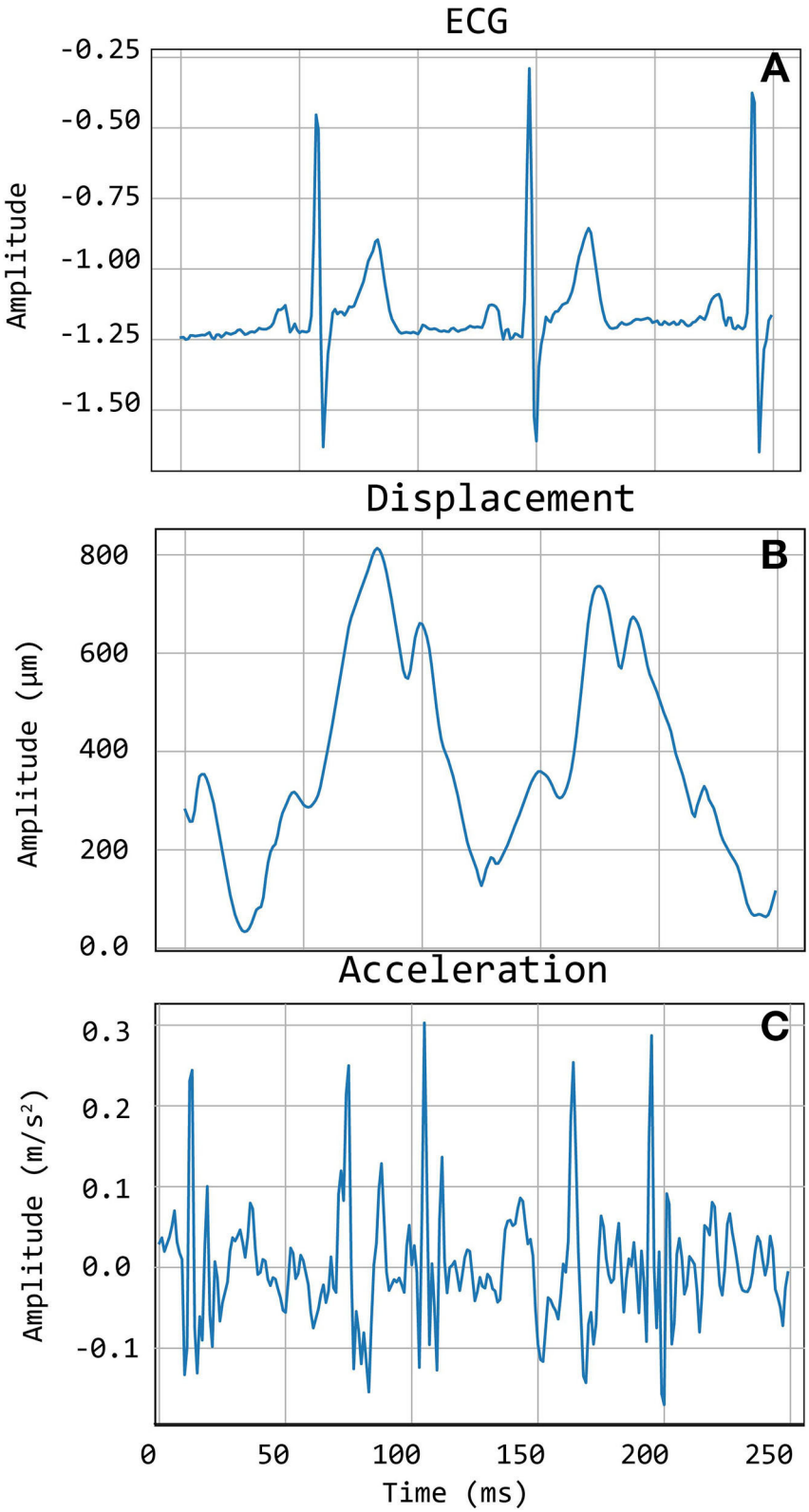

FIGURE 2 | An example of Cardis data. **(A)** shows the ECG signals, **(B)** shows the displacement signal, and **(C)** the corresponding acceleration signal.

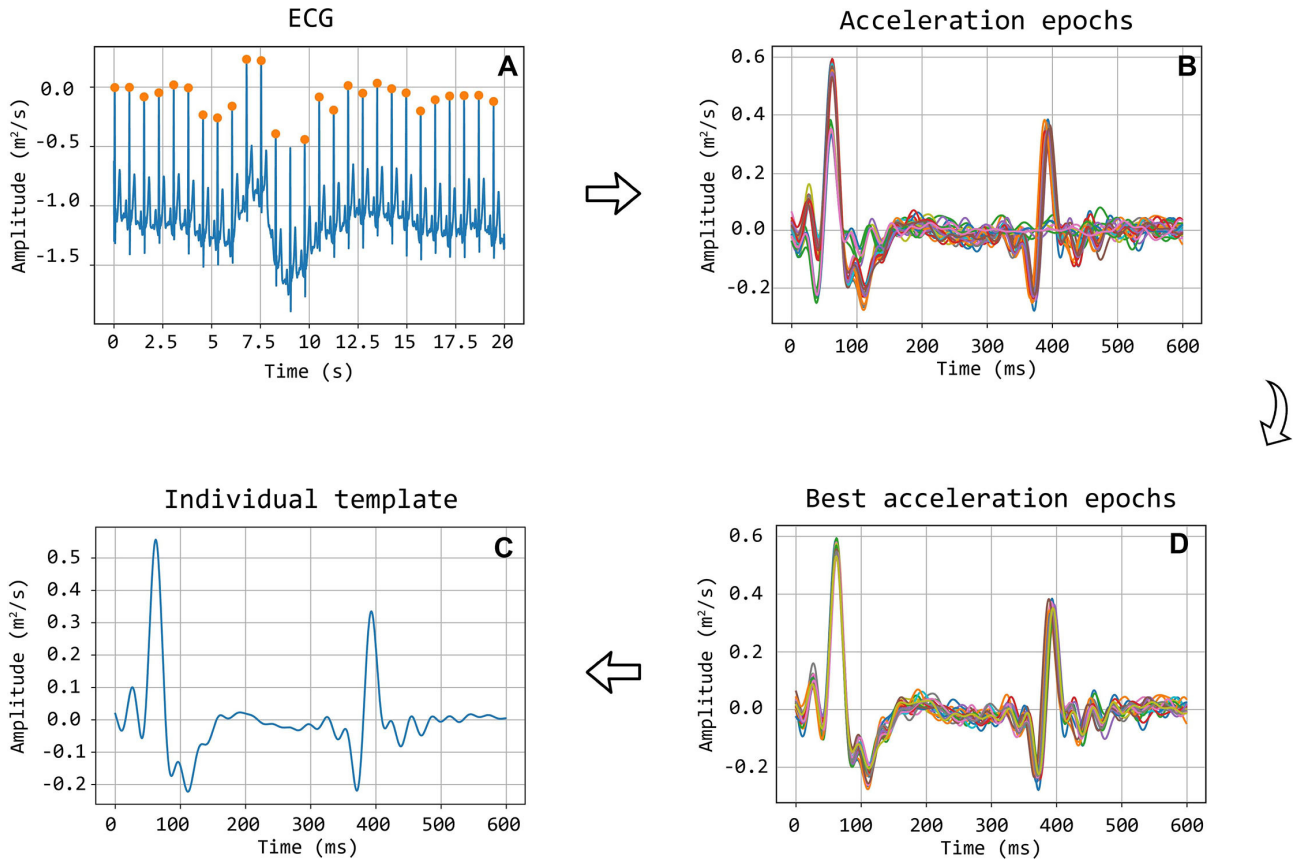

FIGURE 3 | Workflow detailing the construction of the template. Illustration of selection of good quality epochs using the correlation coefficient. **(A)** ECG signal with detected R peaks, which are used to segment the acceleration signal into heartbeat epochs **(B)**. After the correlation matrix analysis, only the good epochs are maintained **(D)**. In **(C)** the final individual template, calculated as the average of the good epochs, is displayed.

2.4.2. Template Matching and Beat Selection

The matching between the templates and the LDV-acceleration traces in the CARDIS dataset was performed by applying a local moving-window function calculating the Pearson's correlation coefficient between the LDV template and the 20 s-long acceleration trace at each time step, as displayed in **Figure 6**. The locations of peaks in the time series resulting from this moving-window cross-correlation operation identify the time instants where the sliding template is similar to a segment of the LDV-acceleration trace.

Setting a threshold for the value of the cross-correlation coefficient then demarcates the correspondence level above which segments of the LDV-acceleration trace can be considered similar to the template. Based on the set threshold value, single segments corresponding to single heartbeats in the LDV trace can be considered of sufficient or not sufficient quality.

To further improve the identification of high-quality heartbeats in the LDV recorded traces, two further selective criteria were added. First, all the LDV-acceleration peaks in the recorded trace with an amplitude lower than 80% of the average peak amplitude were not considered. Then, if two successive peaks were detected within a time window shorter than 500 ms, the second peak was discarded and only the first one was considered. The latter criterion was adopted to avoid the dicrotic notch detection (second peak), especially when the shorter carotid template was used. An explanatory example of peak detection, presenting the LDV-acceleration trace, the moving-window cross-correlation function, and detected peaks are displayed in **Figure 7**.

2.4.3. LDV Traces Classification Based on Template Matching-Finding Threshold Values

The performance of the template matching algorithm in classifying the quality of the CARDIS dataset was evaluated by comparison with visual score classification, according to the following scheme: acceptable heartbeat (label 1), corresponding to Q_{vis} values 4 or 5; not acceptable heartbeat (label 0) corresponding to Q_{vis} values 1 or 2. Signals with Q_{vis}-values of 3 are discarded in this analysis as these signals are difficult to assign an absolute and correct classification (refer to discussion). The template matching-based classification, as also mentioned before, depends upon the threshold value for the moving-window

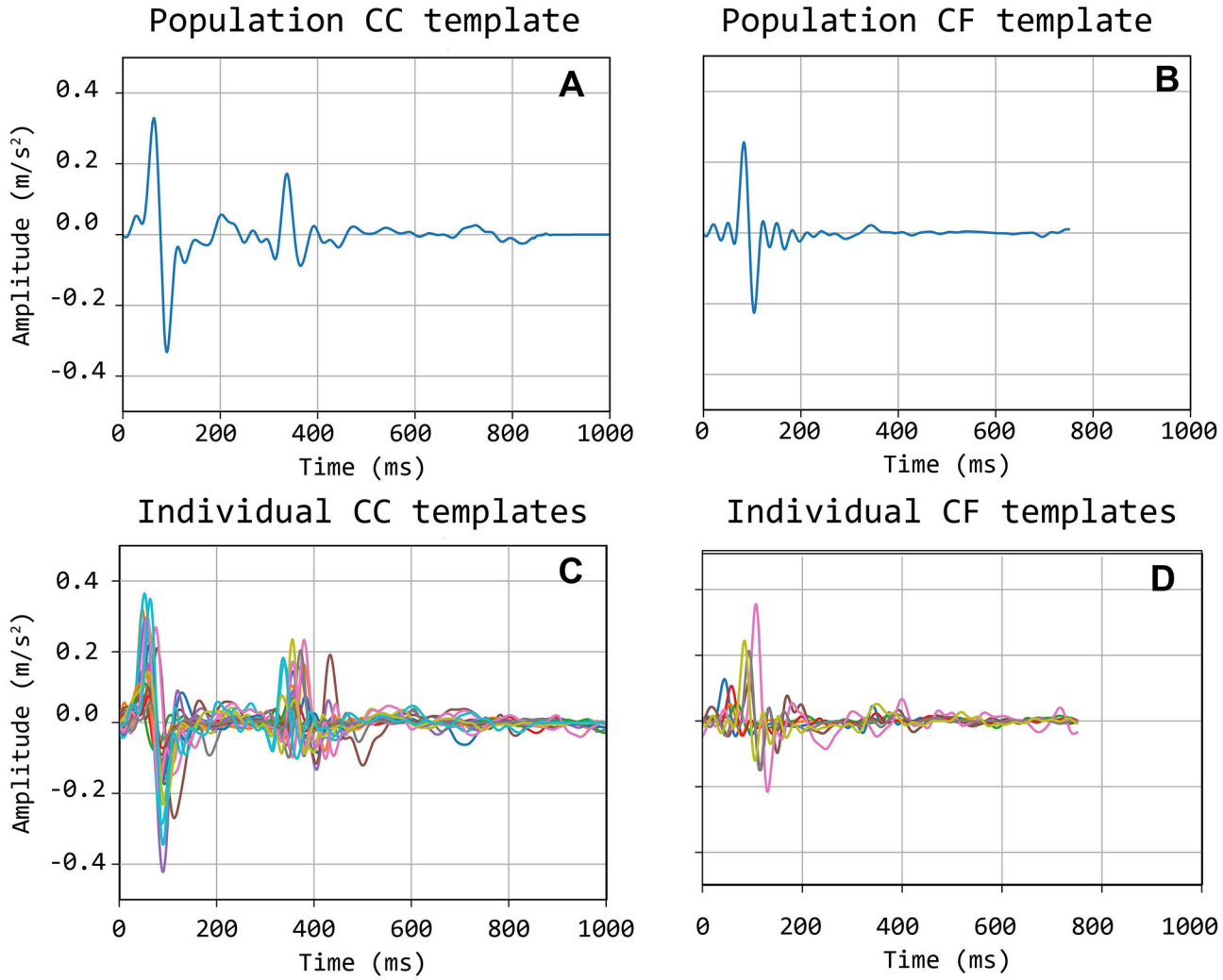

FIGURE 4 | Bottom **(C,D)**: individual carotid (CC) and femoral (CF) templates; Top **(A,B)**: population-average carotid and femoral templates.

correlation function and the number of detected heartbeats in the LDV-acceleration trace, which have to be appropriately set.

In this study, we considered: true positive (TP) an acceptable LDV trace (based on Q_{vis} classified by the template matching as acceptable; false negative (FN) an acceptable LDV trace classified by the template matching as not acceptable; true negative (TN) an unacceptable LDV trace classified by the template matching as not acceptable; false positive (FP) an unacceptable LDV trace classified by the template matching as acceptable. On this basis, sensitivity and specificity values of the classifier are defined as:

$$\text{Sensitivity} = \frac{TP}{TP + FN} \tag{1}$$

and

$$\text{Specificity} = \frac{TN}{TN + FP} \tag{2}$$

Sensitivity and Specificity were then used to build up the Receiver Operating Characteristic (ROC) curves and their area under the curve (AUC) was used to assess the performance of the classifier. Moving-window cross-correlation coefficient threshold values and the number of detected heartbeats yielding the highest AUC were defined on the complete CARDIS dataset and this for each one of the template lengths in time.

2.4.4. LDV Traces Classification Based on Template Matching-Defining Quality Score and Testing on the CARDIS Dataset

Once the best performing carotid and femoral templates time length and the associated moving-window cross-correlation threshold values were identified, a quality score (Q_{TM})was estimated for each 20 s LDV-trace recording, based on two main features.

The first feature (Q_1) is the number of the detected acceleration peaks (n_{peaks}), normalized with the maximum

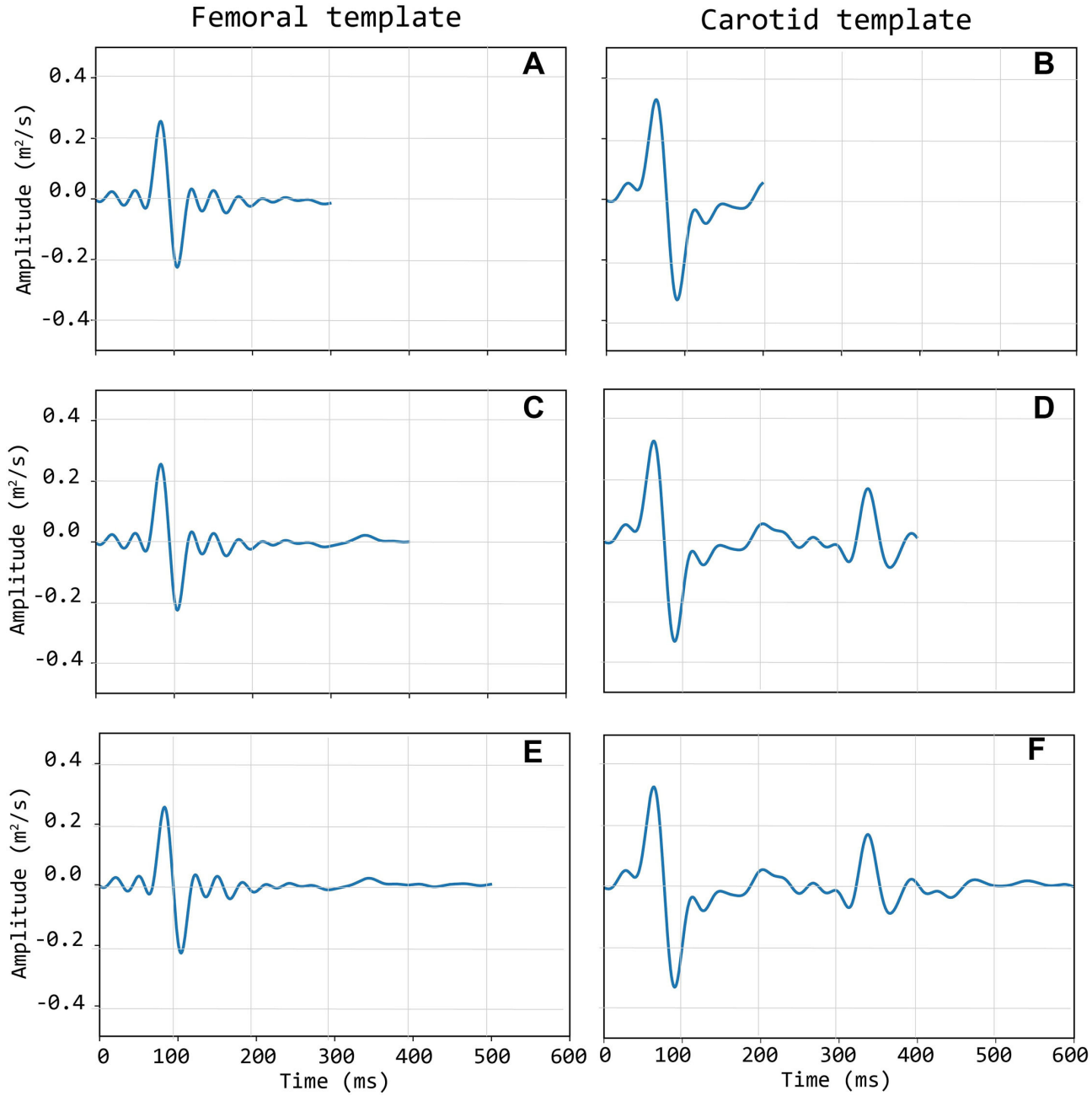

FIGURE 5 | Left column **(A,C,E)**: three different length of the femoral template; Right column **(B,D,F)**: three different lengths of the carotid template.

expected number of peaks or heartbeats in the 20 s LDV-trace recording ($\max_{peaks}$). This value was empirically set equal to 26 to ensure a maximal feature value of 1 in the investigated database:

$$Q_1 = \frac{n_{peaks}}{\max_{peaks}} \tag{3}$$

The second feature (Q_2) is defined as the average time delay between the occurrence of a maximum value of each LDV-acceleration epoch in the recorded trace and the occurrence of the peak value on the template (d_{peak_n}), normalized to the template time length (N):

$$Q_2 = \frac{\sum_{n=1}^{n_{peaks}} (1 - \frac{d\text{peak}_n}{N})}{\max_{peaks}} \tag{4}$$

When the peaks in the template and in each LDV epoch are all perfectly aligned, and when all the peaks in the LDV-trace are detected (i.e., $Q_1 = 1$), feature Q_2 is equal to 1, indicating

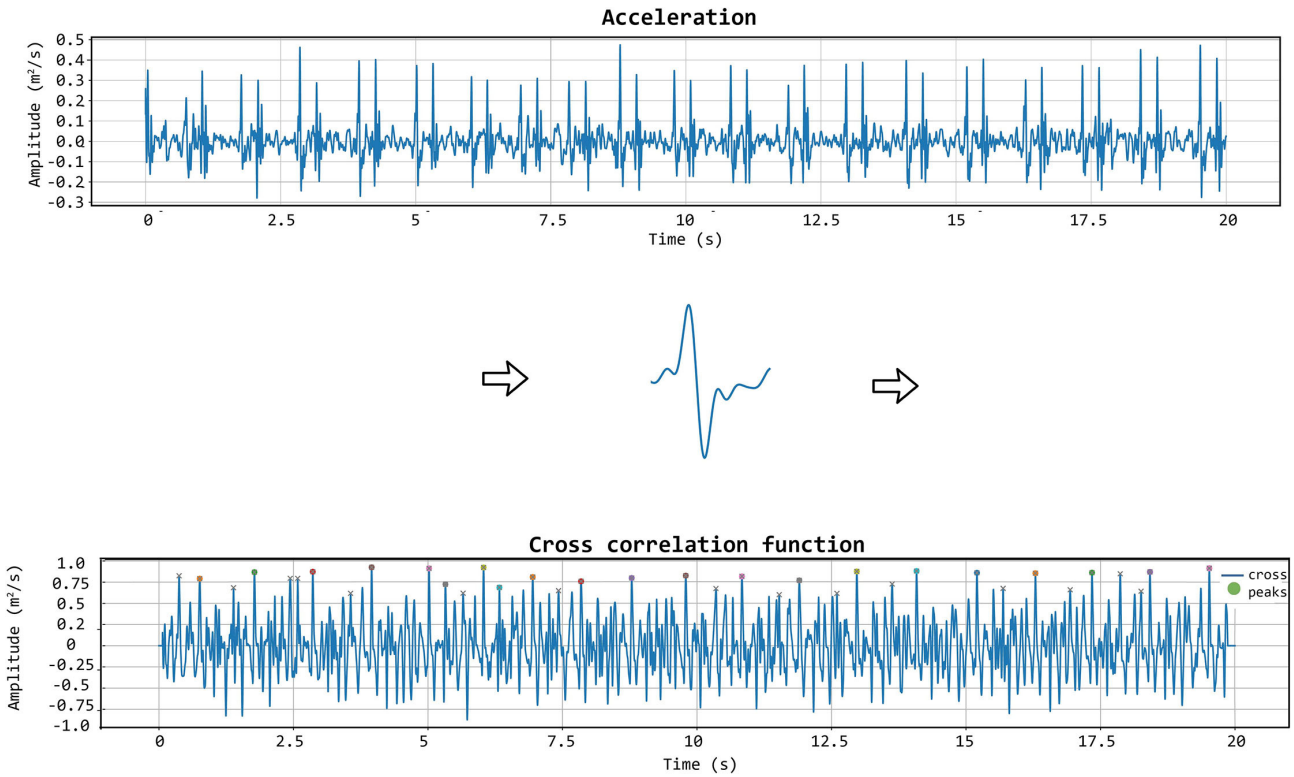

FIGURE 6 | The template matching algorithm is shown. The chosen template (displayed in the middle row of the figure) is iteratively correlated with the acceleration signal to get the cross-correlation function. In that function, the appropriate peaks are then identified.

good quality of the LDV trace recording. The final score based on template matching can be computed as the mean value of the partial scores Q_1 and Q_2:

$$Q_{TM} = \frac{1}{2}(Q_1 + Q_2) \tag{5}$$

By construction, the score Q_{TM} was set up so that the value is within the range $[0, 1]$ (with $Q_{TM} = 0$ representing the worst possible signal quality and $Q_{TM} = 1$ indicating that the signal is of excellent quality). Q_{TM} was calculated for all the traces in the CARDIS database and compared to the corresponding assigned visual score Q_{vis}, which is treated as the ground truth.

2.4.5. A Logistic Regression Model for Signal Classification Based on Template Matching

Q_{TM} Was a heuristically derived quality metric with equal weighting on the sub-components. Now we use logistic regression models to find a better weighting of the contributions of Q_1 and Q_2, and automatically map this to a predicted quality of the signal. Logistic regression models are chosen since they can be well applied to binary classification problems and are typically used in medical research (Domínguez-Almendros et al., 2011; Austin and Steyerberg, 2012; Nick and Campbell, 2012) when a two-class classifier is required. These predictions were then compared to the ground truth labels (given by the visual scores).

Logistic regression models were trained and tested with the two template-matching derived scores (Equations 3 and 4) as features, on both carotid and femoral LDV-acceleration traces. For this purpose, again the LDV traces visually scored with Q_{vis} equal to 1 or 2 were labeled 0, and LDV traces visually scored with Q_{vis} equal to 4 or 5, were labeled 1. Again, signals with a Qvis score of 3 were not included in the analysis.

The data available in the CARDIS database was split such that 80% was used for training the logistic regression model and the remaining 20% used for testing purposes. The training-testing set partition was randomly iterated 1,000 times while storing the model accuracy every iteration, so that the overall accuracy distribution of the logistic regression model approach could be assessed.

Of note, all features used to train logistic regression models were normalized *via* standardization. This allowed the logistic regression-model coefficients to be interpreted as the corresponding feature weights, granting information about which feature was most influential in labeling an LDV trace.

The accuracy distributions of logistic regression models trained on template-matching and the later discussed matrix-profile derived features were evaluated.

2.5. Matrix Profile

The matrix profile is a data structure that annotates a time series (Yeh et al., 2018; Zhu et al., 2020). It allows for exact,

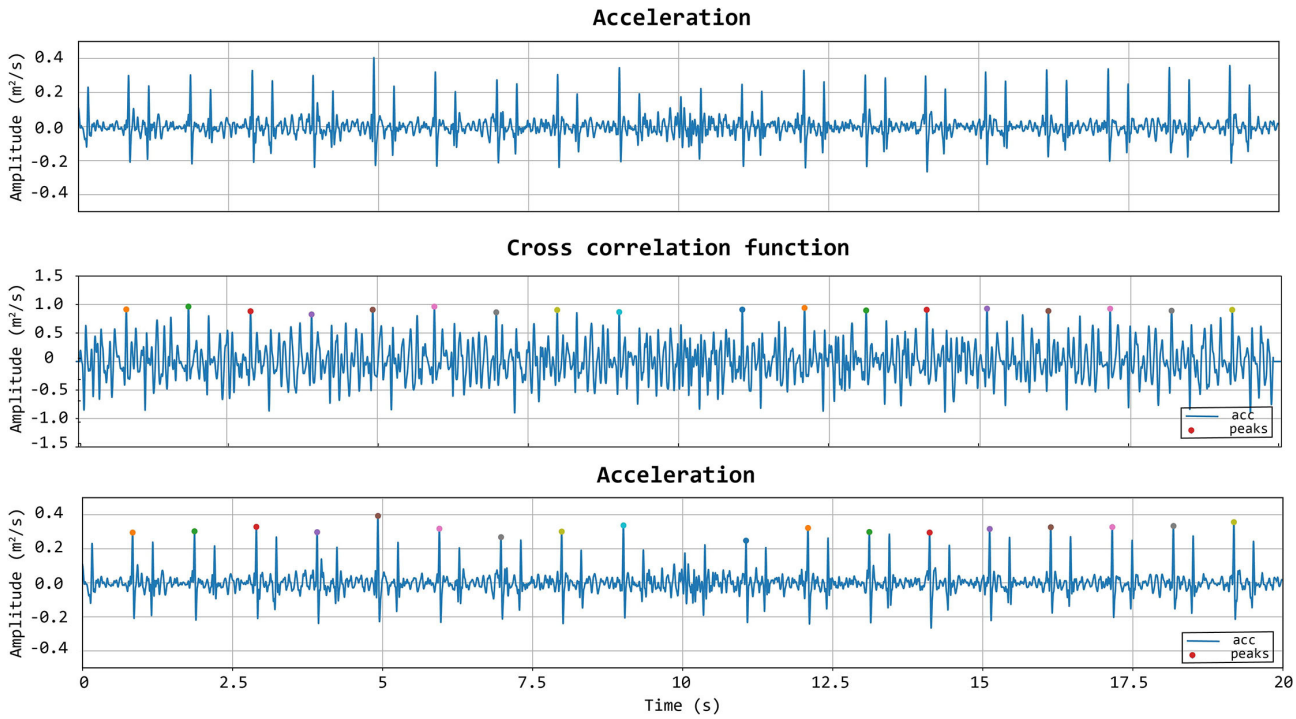

FIGURE 7 | First row: acceleration signal. Second row: normalized cross-correlation function and its maximum values of the acceleration signal with the femoral template of 500 ms. Last row: acceleration signal with the detected peaks using the template matching method.

simple, and fast (Zhu et al., 2017b) similarity search or discord discovery and is among the state-of-the-art techniques in the field of discrete time-series analysis (Zhu et al., 2017a; Madrid et al., 2019). The matrix profile has been used in processing biological signals like EEG (Mueen et al., 2009), ECG, and gait cycles (Zhu et al., 2020). It was applied in this study to accurately identify recurring waveforms in the LDV-acceleration data. Every such waveform is a subsequence of the original sequence or time series. These subsequences, taken together, are collectively called a motif. We gauged the quality of an LDV-measurement *via* several features determined by its best motif. The strength of the matrix profile lies in the fact that it does not require a template or other input parameters except for the length m of the desired motif subsequences. Analogous to the template matching analysis, waveforms were subsampled to 1 kHz. We set m to 200 ms, similar to the optimal length of the template described in previous sections.

2.5.1. Signal Classification Based on the Matrix Profile

A quality metric (Q_{MP}) was constructed based on three features of the matrix profile-generated motif as seen in Equation (6). This metric was constructed so that its possible values lie between 0 and 1.

$$Q_{MP} = A_{MP}\, t_{d,MP}\, n_{MP} \tag{6}$$

The first feature used in calculating (Q_{MP}) is the average relative maximum amplitude of a subsequence in the motif (A_{MP}) computed as in Equation (7). The maximum amplitude of subsequence A was compared with the maximum amplitude of the reference subsequence A_{ref}. This reference is the first subsequence identified by the matrix profile (the minimum of the matrix profile) and subsequently included in the motif. In good quality measurements, most maximum amplitudes of subsequences in the motif were similar.

$$A_{MP} = \frac{1}{n_{mtf}} \sum_{n=1}^{n_{mtf}} \frac{A}{A_{ref}} \tag{7}$$

The second feature, the average relative time-instant of the subsequence peaks in the motif ($t_{d,MP}$), is computed as in Equation (8). The time-instant of the subsequence peak was compared with that of the reference. This value was then normalized over the length of the subsequence m. Ideally, all subsequences in the motif represent the same heartbeat-related waveform with peaks at similar time instants. For poor quality signals, these time instants tended to randomly vary over the length of the subsequence.

$$t_{d,MP} = \frac{1}{n_{mtf}} \sum_{n=1}^{n_{mtf}} \left(1 - \frac{d_{peak}}{m}\right) \tag{8}$$

Finally, the third feature (n_{MP}) was calculated as the expected amount n_{exp} vs. the effective amount n_{mtf} of subsequences in the motif, shown in Equation (9). n_{exp} was estimated based on a

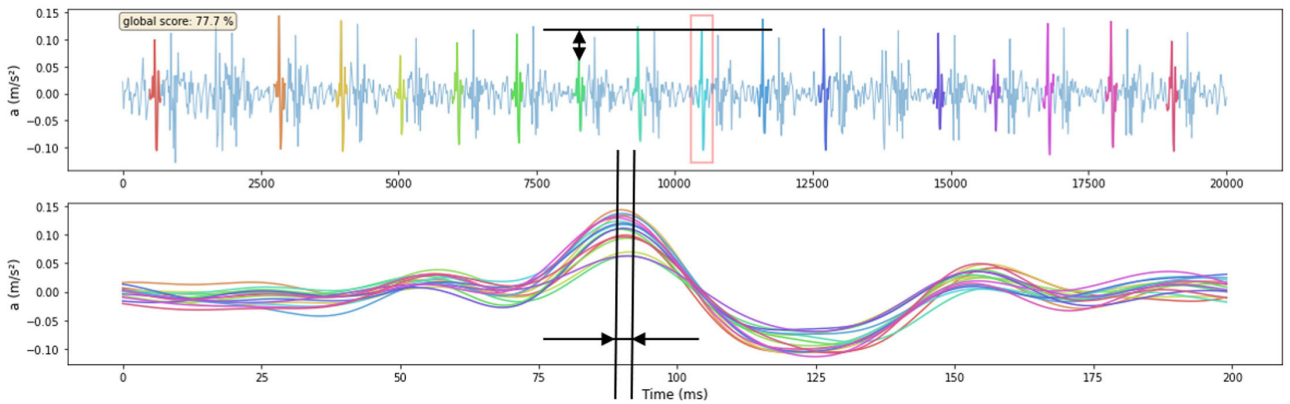

FIGURE 8 | Example of one signal being scored by the features that are derived from the Matrix-Profile-identified motif. The amplitude feature of one subsequence is shown in the upper figure, the reference is indicated with a red square. The time-instant of subsequence peak feature is shown in the lower figure where all subsequences shown in the upper figure are time-aligned. The signal score is shown in the upper left corner of the upper figure. The visual score of this signal is 4.

discrete-Fourier-transform analysis of the entire signal recording. More specifically, the peak corresponding to the heartbeat during the measurement was identified as the most prominent peak in the signal spectrum, in the range 0.5–1.5 Hz. The effective amount of subsequences in the motif n_{mtf} was based on how many heartbeats the matrix-profile technique was able to pick up.

$$n_{\mathrm{MP}} = \frac{n_{\mathrm{mtf}}}{n_{\mathrm{exp}}} \tag{9}$$

Before a subsequence is included in the motif, three criteria decide the inclusion: (1) If a subsequence maximum amplitude was lower than 0.8 times the reference maximum amplitude it was excluded from the motif. (2) If the time instant of the peak deviated 30 ms or more from that of the reference, the subsequence was also removed from the motif. (3) If two subsequences were closer than 0.8 times the expected time delay between two subsequent heartbeats, the one with the lower matrix-profile value (higher similarity to the reference) of the two was preserved, the other was removed. The applied thresholds levels were determined empirically from excellent and poor quality signals.

Figure 8 shows an example of a signal being scored by first finding the motif so that as many heartbeats as possible are present within it, then calculating the features of that motif. Both the relative amplitude and time-instant of subsequence peak features of one subsequence in the motif are indicated in the figure.

The auto-generated matrix-profile-based quality metric was computed for all carotid-carotid and femoral-carotid datasets and results were compared to the visual scores.

2.5.2. A Logistic Regression Model Based on the Matrix Profile

Similar to template matching, we also designed logistic regression models using the previously discussed matrix-profile derived features. These models allow for more freedom in weighting the features to come to a better classification result. Models were trained and tested on the three features mentioned above. Signals were labeled and available data was split into training and testing sets analogous as in the previously discussed template-matching case.

2.6. Relation Between Signal Quality and Physiological Variables

Finally, we investigated the existence of possible associations of quality of the LDV-acceleration traces with age, body mass index (BMI), and systolic blood pressure. The statistical analysis was performed using Q_{MP} as a quality score variable. In detail, the existence of a linear correlation was tested using the Pearson-correlation coefficient on both CC and CF datasets, with data analyzed per handpiece. For all analyzes, significance was assumed for $p < 0.05$.

3. RESULTS

3.1. Visual Scoring

3.1.1. Carotid-Carotid Measurements

By visual inspection, about 12% of all LDV-acceleration traces were qualified as bad and close to 30% as poor (**Figure 9B**). This implies that about 42% of the recorded LDV traces were evaluated to not be of sufficient quality for further analysis. About 22% of all recordings were scored from good to excellent and are deemed suitable for further analysis. About 37% of the traces were visually scored borderline, i.e., these traces might be of sufficient quality for further analysis with advanced processing. The number of LVD traces scored with Q_{vis} 4 or 5 and recorded using handpiece 2 was higher than the number using handpiece 1. For handpiece 1, channel 1 scored almost systematically very low; the best channels were channels 3 and 4. For the second handpiece, the best channels were channels 2 and 3.

3.1.2. Carotid-Femoral Measurements

The bottom row of **Figure 9** illustrates that, concerning femoral LDV-acceleration traces (handpiece 1), 20% of all recordings

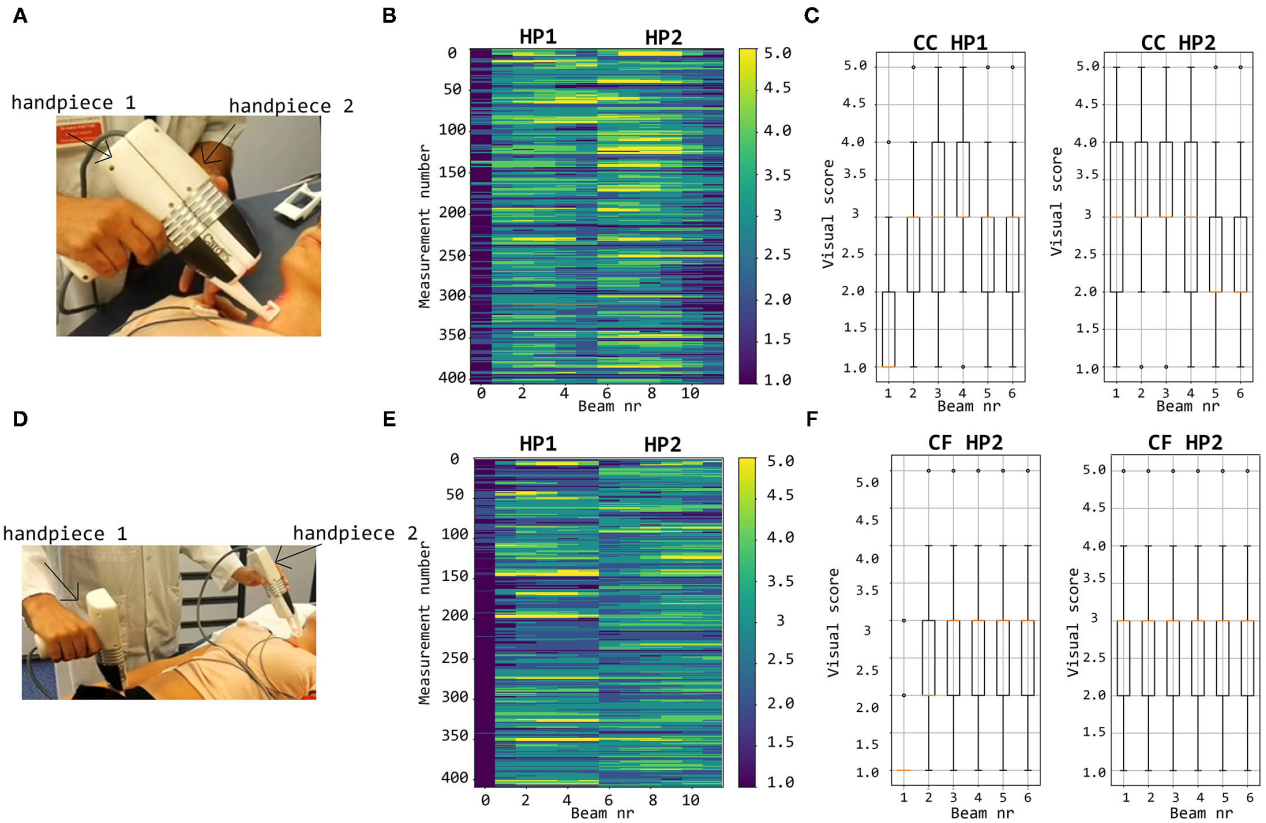

FIGURE 9 | Top row: visual scoring of signals measured with handpieces 1 and 2 during local carotid measurements **(A)** with overall grades shown in **(B)** and box plots and mean values per channel in **(C)**. Bottom row: visual scoring of signals measured during carotid-femoral PWV measurements **(D)** with overall grades shown in **(E)** and box plots and mean values per channel in **(F)**.

TABLE 2 | Confusion matrices of signal classification done by the hand-engineered classification model constructed with template matching.

	Template of 200 ms		Template of 400 ms		Template of 600 ms	
Carotid recordings	**TM score 0(%)**	**TM score 1(%)**	**TM score 0(%)**	**TM score 1(%)**	**TM score 0(%)**	**TM score 1(%)**
Score 1	97	3	97	3	97	3
Score 2	86	14	86	14	82	18
Score 3	58	42	55	45	44	56
Score 4	29	71	30	70	15	85
Score 5	8	92	19	81	6	94

Signals classified in this table were measured at the carotid and the templates used were the carotid population templates.

were qualified as bad, and another 32% as poor, meaning that over 50% of all recordings is not usable for analysis. About 15% of the measured signals get a score good to excellent, deemed immediately suitable for analysis. The best channels are channels 3 and 4 with 21.9% (beam 3) and 19.5% (beam 4) of the recordings good to excellent. For handpiece 2 (carotid recordings), about 20% gets a score good to excellent. This is less than what was obtained for handpiece 2 for the carotid-carotid recordings, where close to 25% of all recordings were rated good to excellent. On the other hand, less signals received grades 1 and 2. The best channels are channels 4 (24.9%) and 5 (24.1% of the recordings scoring good to excellent).

3.2. Template Matching

3.2.1. Carotid-Carotid Measurements

From the analysis carried out on the complete CC dataset, it emerged that using the carotid template of 200 ms length guarantees the best performance in terms of specificity, setting the cross-correlation threshold to 0.74 and the minimum number of detected heartbeats per trace to 15 (AUC = 0.89, sensitivity

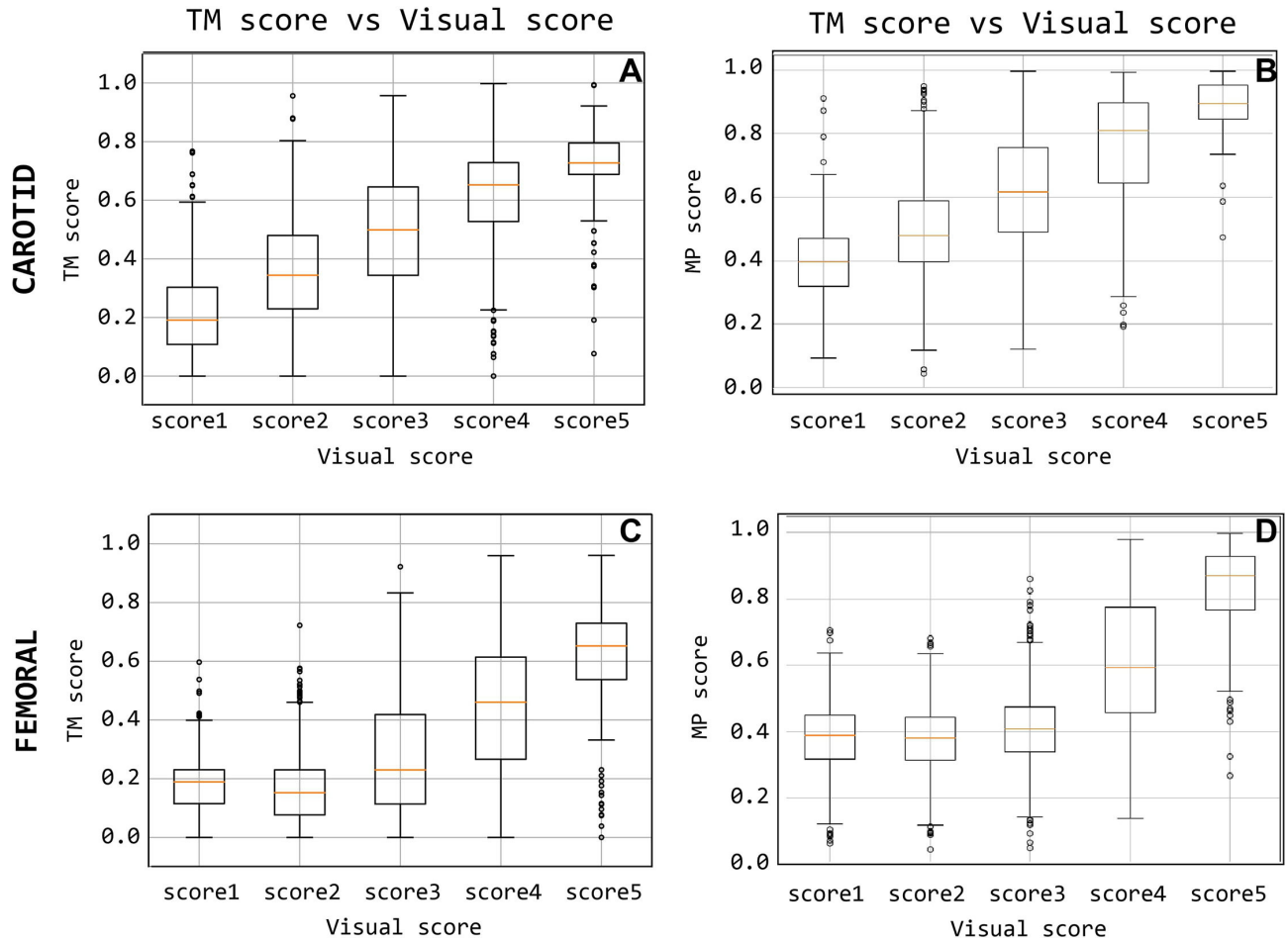

FIGURE 10 | Quality score comparison between visual score and the template-matching-derived and matrix-profile-derived. Subfigures **(A,C)** display the score based on the template matching and **(B,D)** quality score based on the matrix profile.

74%, specificity 89%; template of 400 ms length: AUC = 0.89, sensitivity 81%, specificity of 83%; template of 600 ms length: AUC = 0.92, sensitivity 87%, specificity 86%). For each template length, the corresponding confusion matrix is presented in **Table 2**. The adoption of specificity for the evaluation of the performance of the template matching strategy was dictated by the need of maximizing the removal of LDV traces with inadequate quality. More in detail, it emerged that in general, the template matching performed excellently in correctly classifying visual scores 1 and 5, while accuracy decreased for visual scores 2 and 4 (**Table 2**). Interestingly, using the shorter template length of 200 ms led to a score of 42% of the LDV acceleration traces visually scored 3 (borderline) as acceptable data.

The level of agreement obtained between Q_{TM} and Q_{vis} on the CC recordings dataset, with template matching adopting a 200 ms template length, is presented in **Figure 10**. This suggests that the median of the Q_{TM} values, computed on traces that have a $Q_{vis} = 3$, could be adopted as a threshold value for the automatic quality checking of an LDV trace (i.e., in the case under study, traces with a $Q_{TM} > 0.5$ could be considered of adequate quality; note that, manually setting these thresholds is not required for the logistic regression models since this is implicitly learned in the training).

The accuracy distributions of logistic regression models trained on quality scores derived from template-matching are displayed in **Figure 11**. On average, the accuracy on traces acquired using handpiece 2 is higher than handpiece 1 (85 $\pm$ 1.6% and 80 $\pm$ 1.70%, respectively; the results are summarized in **Table 4**).

3.2.2. Carotid-Femoral Measurements

From the analysis carried out on the complete CF dataset, it emerged that using the carotid template of 500 ms length guarantees the best performance in terms of specificity, setting the cross-correlation threshold to 0.56 and the minimum number of detected heartbeats per trace to 10 (AUC = 0.89, sensitivity 77%, specificity 92%; template of 400 ms length: AUC = 0.88, sensitivity 76%, specificity of 91%; template of 300 ms length: AUC = 0.87, sensitivity 72%, specificity 92%). The confusion matrices are shown in **Table 3** for each template.

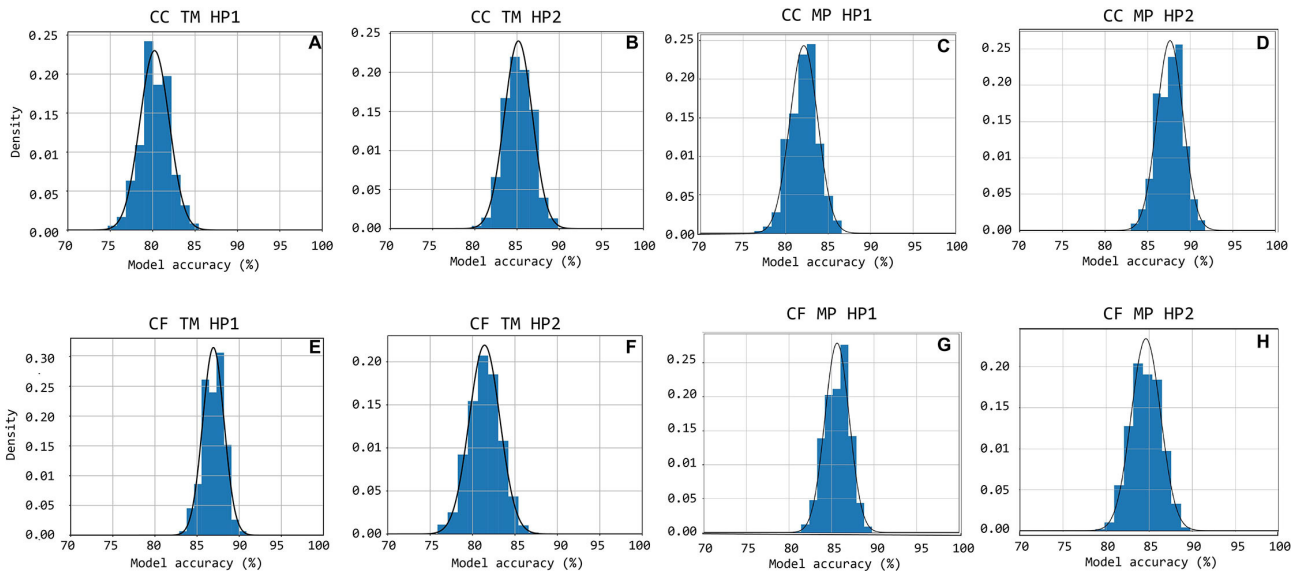

FIGURE 11 | Accuracy distributions for 1,000 random train-test set partitions and subsequent logistic regression models trained. The accuracy distribution is shown cumulatively through bar-charts with the equivalent Gauss-curve plotted on top of it. Subfigures **(A–H)** show this for CC HP1, CC HP2, CF HP1, and CF HP2 cases, respectively.

TABLE 3 | Confusion matrices of signal classification done by the hand-engineered classification model constructed with template matching.

	Template of 300 ms		Template of 400 ms		Template of 500 ms	
Femoral recordings	**TM score 0(%)**	**TM score 1(%)**	**TM score 0(%)**	**TM score 1(%)**	**TM score 0(%)**	**TM score 1(%)**
Score 1	96	4	96	4	96	4
Score 2	91	9	89	11	91	9
Score 3	68	32	64	36	65	35
Score 4	33	67	28	72	27	73
Score 5	8	92	6	94	7	93

Signals classified in this table were measured at the femoral and the templates used were the femoral population templates.

As for the carotid traces, the performance of the template matching algorithm was based on the specificity values, in order to remove the bad quality signals. More in detail, the template matching strategy shows excellent performance for the classification of visual scores 1 and 5 (accuracy of 96 and 93%, respectively), while the accuracy decreases for class 2 and class 4 (91 and 72%, respectively). In the femoral case, the method classified a majority of LDV traces with a visual score of 3 (borderline) as inadequate. Indeed, considering the template of 500 ms, the template matching method classified 65% of score 3 as inadequate signals and the other 35% (borderline)as adequate.

The level of agreement obtained between Q_{TM} and Q_{vis} on the CF recordings dataset, using the 500 ms template length, is shown in **Figure 10C**. The results indicate that from the median Q_{TM} values scored Q_{vis} = 3, a threshold value could be adopted for the automatic quality checking of the LDV trace (i.e., in the case under study, traces with a $Q_{TM} > 0.23$ could be considered of adequate quality; again, this threshold is not required when working with the logistic regression models.)

The accuracy distributions of logistic regression models trained on quality scores derived from template-matching are displayed in **Figure 11**. On average, the accuracy on traces acquired using handpiece 1 is higher than handpiece 2 (87 $\pm$ 1.3% and 81 $\pm$ 1.9%, respectively; the results are summarized in **Table 4**).

3.3. Matrix Profile

On good quality data, i.e., those visually scored at 4 or 5, the matrix profile technique was able to include nearly all heartbeats in the motif. On poor quality data, the matrix profile was unable to identify most heartbeats because of noise or artifacts in the measurement. On some measurements that contain pure noise, the matrix profile picked up random noisy waveforms that were less prevalent and differed much compared to the desired foot-of-the-wave waveform.

TABLE 4 | The table contains the average performance of the logistic regression models trained on features derived by both template matching and matrix profile methods.

	Template matching		Matrix profile	
Accuracy	**Average(%)**	**Std(%)**	**Average(%)**	**Std(%)**
Carotid-carotid hp1	80	1.75	82	1.64
Carotid-carotid hp2	85	1.63	88	1.53
Femoral-carotid hp1	87	1.31	86	1.43
Femoral-carotid hp2	81	1.96	85	1.71

Results are shown per handpiece of the measuring device. Average classification accuracy and its SD are given.

3.3.1. Quality Metric Results

The signals measured at the carotid measuring site were given a matrix profile-derived quality score that is compared with their visual scores in **Figure 10B**. A positive, linear relation between the two scoring methods is observed for the carotid-carotid database. The same information is shown for the femoral measuring site in **Figure 10D**. The difference between poor and good quality signals is apparent. Signals with visual scores 1, 2, or 3 have significantly lower Q_{MP} than those with visual scores 4 or 5.

3.3.2. Logistic Regression Models Performance

Figures 10C,D,H show the accuracy distributions of the repeated logistic regression model-training experiment for signals measured in the neck with the different handpieces. All accuracy averages are above 80 with 82% (±1.64%) and 88% (±1.53%) for carotid-carotid recordings with handpieces 1 and 2, respectively. For carotid-femoral recordings, carotid data recorded with handpiece 2 yielded an accuracy of 85%± 1.71%. The distributions were assumed to be normally-distributed after a Shapiro-Wilk test and thus the Gauss-curves are drawn onto the subfigures of **Figure 11**.

The same data for the femoral data (measured with handpiece 1 during carotid-femoral recordings), is shown in **Figure 11G**. Average accuracy of 86% with a SD of 1.43% is observed. All accuracy statistics of the different measurement situations are summarized in **Table 4**.

3.4. Signal Quality vs. Physiological Variables

The results from the correlation analysis between Q_MP and age, BMI, and systolic blood pressure are shown in **Figure 12** for the femoral data (carotid-femoral recording, handpiece 1; CF hp1) and the carotid-carotid recordings with handpiece 2 (CC hp2) showing the strongest trends. Significant negative correlations were found between age and Q_{MP} for CF hp1 ($r = -0.253$, $P < 0.05$) and CC hp2 ($r = -0.365$, $P < 0.001$). The correlation with BMI (**Figure 11B**) was significant only for the femoral recording ($r = -0.304$, $P < 0.01$) while the correlation with systolic blood pressure was significant only for CC hp2 ($r = -0.206$, $P < 0.05$)(**Figure 11C**). In a multivariate regression model including both age and systolic blood pressure, the correlation between carotid signal quality and systolic blood pressure was no longer significant (due to the correlation between age and systolic blood pressure). In contrast, in a multivariate model of femoral signal quality, both age and BMI remained significantly correlated with signal quality. The same relations are found when repeating the analysis with Q_{vis} or Q_{MP} (data not shown).

4. DISCUSSION

The potential of LDV for non-contact measurement of physiological (cardiovascular) signals has been reported since about 2000 in explorative studies (Pinotti et al., 1998; Morbiducci et al., 2007a; Kaplan et al., 2012; Rohrbaugh et al., 2013) making use of bulky industry-time devices, and the technique has been suggested for measurement of carotid-femoral PWV by De Melis et al. (2008). An important technological breakthrough to enable LDV-based measurements in a clinical setting is the use of silicon photonics to miniaturize and integrate the optical components onto chips (Li et al., 2013) that are easily built-in into hand-held devices as the CARDIS prototype used in this study. That prototype was used in a clinical feasibility study where measurements were performed on the carotid and femoral artery, and we previously reported on the agreement of LDV-based carotid-femoral PWV with a reference method (Marais et al., 2019). In that article, data were processed off-line and algorithms for foot detection relied on the ECG and gating was applied on carotid and femoral tracings to ensure identification of the correct characteristic points on the waveforms. Further developments aim for ECG-independent measurements and will require a more stringent quality assessment in real-time application to ensure that data is captured from which transit times can be derived. Unlike the CARDIS device, future versions of the device will provide real-time feedback on signal quality and valid measurements will only be accepted after a minimal number of data samples have been retrieved from signals passing predefined quality criteria. In this study, we explored two possible strategies for such quality assessment, template matching and matrix profile, and benchmarked them using visual scoring as reference.

The visual grading was done by what we considered an expert observer but is inherently subjective. The graphical user interface that was developed showed all data within one single window for reasons of efficiency but inevitably leads to a weighed appreciation where data from different channels do get, to some extent, a degree of relative scoring. This mainly applies to the scores good (4)-excellent (5) where recordings of certain channels could have likely received different rankings if they had been individually assessed without the knowledge of the signal on the other channels. This remark may also pertain to the grade borderline. As future use of the device will target acquiring the best possible signals in a given subject, we particularly focused on signals graded 4 or 5. **Figure 9** provides a visual overview of observed quality across the complete database. Each handpiece of the device is equipped with 6 channels in line, spanning 2.5 cm with the aim to have minimally one channel that detects a strong signal. It is clear that channel 1 on handpiece 1

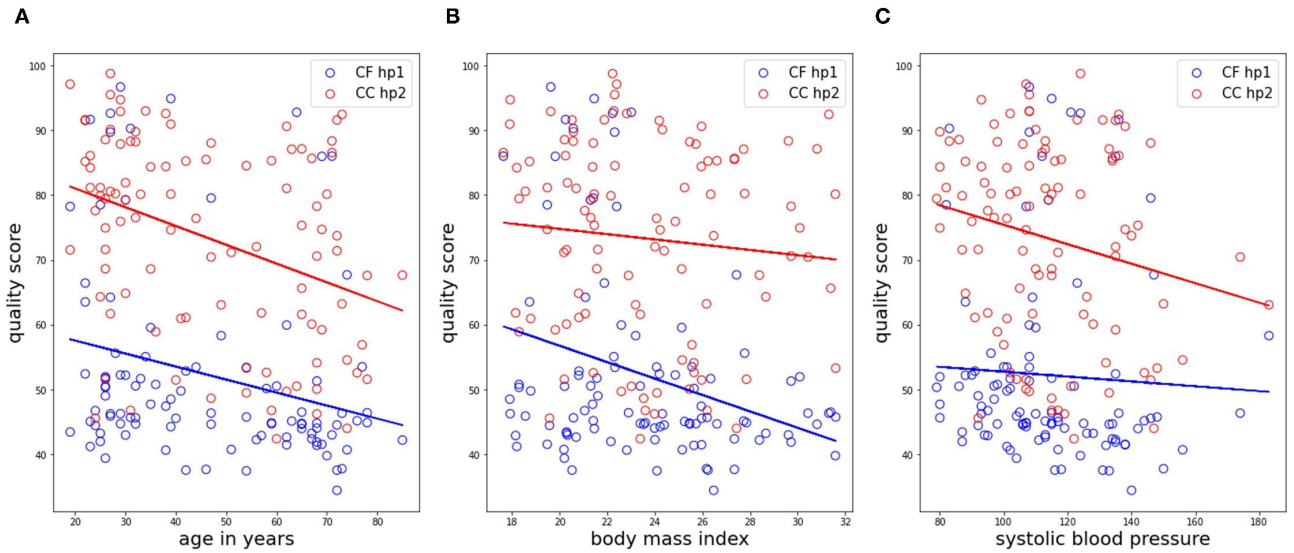

FIGURE 12 | Correlation analyses of the matrix profile-based quality score with age, BMI and systolic blood pressure, shown in subfigures **(A–C)**, respectively. Only data in the CC HP2 and CF HP1 cases is shown. Trendlines of the data are also drawn.

systematically yields very low scores, which was attributed to a hardware problem with the inadequate alignment of the optical components during device assembly. For carotid measurements, the middle channels 3 and 4 yielded the highest quality signals (as expected), but this shifted to channels 2 and 3 for handpiece 2. Also, the overall signal quality was slightly higher for handpiece 2. We speculate that the use of the spacer underneath handpiece 1 may contribute to the difference in signal quality between both handpieces. These data can be compared to the data from handpiece 2 during carotid-femoral measurement, where handpiece 2 is now equipped with a spacer (refer to **Figure 9** for the measuring configurations). The mean signal quality is now in the same range as it was for handpiece 1 on the local carotid measurements. An extra factor, however, is the fact that carotid-femoral measurements are technically more demanding, requiring the simultaneous acquisition of signals at 2 distinct locations. The same conclusions can be drawn on the basis of the automatically calculated sores Q_{TM} and Q_{MP}.

In essence, one very good to excellent channel recording on each of the handpieces should guarantee a reliable transit time estimation from one handpiece to the other. This was achieved in 27% of the local carotid datasets and in 13% of the carotid-femoral datasets mainly due to the suboptimal femoral recording that is more challenging due to the fact that the operators have to manipulate two sensors on two distinct locations as well as the deeper positioning of the femoral artery leading to weaker signals. That does not imply that the remaining datasets cannot be processed (especially when the ECG is available; refer to Marais et al., 2019) or that LDV would not be suitable as a measuring technique; we just speculate that these results can be drastically improved with real-time feedback on the signal quality upon measurement.

The main objective of this study was to explore different methods for an automated signal quality assessment, where we first explored template matching. The template should minimally contain the foot fingerprint of the wave, apparent on both the carotid and femoral measuring locations. That pattern turned out to be fairly robust across the tested population. Even though the amplitude of acceleration signals was lower at the femoral measuring site, the pattern of the foot is quite similar on both measuring locations. A practical choice that has to be made is the length of the template. For carotid signals, it may be relevant to extend the template such that it also encompasses the dicrotic notch. We preferred the shorter template of 200 ms (which does not extend beyond the dicrotic notch) as the time delay between the wave's foot and the dicrotic notch is not constant but varies in between subjects and also within one subject from cycle to cycle due to physiological variations in blood pressure and heart rate. The shorter template was found to result in a somewhat higher specificity in correctly classifying poor signals, but overall, the performance of the carotid templates with different lengths was not very different, as can be observed from the confusion matrix (**Table 2**). On the other hand, for the femoral artery, we preferred the longest template of 500 ms which should detect epochs characterized by one prominent peak, the foot of the wave, followed by a long tail of low amplitude signals.

We then determined optimal thresholds levels for the magnitude of the cross-correlation and the number of detected beats using ROC analysis, whereby we maximized the classification performance of a binary classifier on the basis of Q_{TM}. In this exploratory study, that analysis was done on the complete database and further optimizations should be done on the used features and repeating the analysis with separate training and testing data set. Using the resulting thresholds,

the agreement between Q_{TM} and Q_{vis} was overall satisfactory. The logistic regression model analyses learned that a template matching approach is a valuable option to automatically classify signal quality as acceptable or not acceptable with an accuracy of over 80%.

As a second method, we considered the matrix profile as a technique to identify recurring patterns in the LDV-measurements in an automatic manner (Zimmerman et al., 2019), with very few control parameters. The potential advantage of a matrix profile approach over template matching is that no prior knowledge is required on the shape of the signal feature that one is looking for. Also, using the matrix profile allows the generation of a "user-dependent" template *in situ*. Signal quality was quantifiable using features of the motifs found by the matrix profile and combined into the quality metric Q_{TM}, which showed a good agreement with the ground truth of visual scores as can be observed from **Figure 10**.

As for the template matching approach, the average accuracy of a logistic regression model trained and tested on features derived from motifs provided by the matrix profile technique is in all cases higher than 80%. Overall, only relatively small differences are observed between the two techniques. Both techniques perform similarly well which suggests that both, or a combination of the two, can be used for classifying new, future data into "bad, unusable" or "good, usable." This allows us to state that a logistic regression model suffices, along with the signal features and techniques that are considered, to accurately assess incoming data in future real-time applications.

In our logistic model training, we purposely discarded datasets visually labeled "borderline" (score 3) as these data were simply hard to classify visually in an unequivocal way. That difficulty is relatively well reflected in the values of the quantitative metrics for these signals (**Figure 10**) and the performance of the classifiers as quantified by the confusion matrix (**Tables 2**, **3**). Especially for the carotid artery, automated classification leads to a close to fifty-fifty percent labeling of data as acceptable or not acceptable. For the femoral recordings, there is a larger tendency to classify signals with a visual score of 3 as not acceptable. This is in line with our own perception that femoral data may have received higher scores than carotid data of similar quality and underlines the need for objective tools to score signal quality.

Interestingly, the quality score, exemplified by Q_{MP}, correlates negatively with age and especially with BMI when signals are measured in the groin on the femoral artery. This observation supports the operators impression that measuring good quality LDV-signals on more obese subjects is consistently more challenging. The deeper the positioning of the artery and the more surrounding tissue, the stronger the signal attenuation. Such relation with BMI was absent for neck recordings. Also, skin inelasticity or thickness is expected to play a role in the transmission of intra-arterial vibrations and likely contributed to the observed negative correlation between and signal quality at the carotid and femoral locations in the study populations. The negative correlations between signal quality and age for carotid-carotid recordings with handpiece 2 were less strong, and were not found for the other carotid recordings (carotid-carotid handpiece 1 or carotid-femoral handpiece 2 recordings). A possible explanation may be the use of the spacer for these latter measurements, which may mechanically interfere with the transmission of the vibrations from within the artery to the skin and exert an effect on the recordings. Overall, this effect is considered minor, but it may nonetheless be a factor contributing to observed differences in the recordings.

The CARDIS prototype has a laser wavelength of 1,550 nm which is insufficiently reflected by the skin. We, therefore, attached retroreflective patches to the skin at the measurement locations to enhance reflection. The next-generation prototype aims for measurements without the retroreflective patch to facilitate practical use. A wavelength of 1,300 nm, for which there is a relative peak in skin reflectance (Rockwell and Goldman, 1974), will be used but the impact of skin pigmentation or sweating on data quality will have to be investigated.

In this study, signal quality was assessed off-line on 20 s recordings. Future developments will focus on real-time assessment of data quality as data is being captured and where the considered techniques will be used for epoch detection and subsequent quality quantification. Although a template-matching approach has the benefit that prior knowledge can be used to assess incoming data from the start, we assume that both techniques provide similarly useful features and that both are suitable for real-time implementation. It may be an option to hybridize the two techniques to come to a stronger, even more robust algorithm when implementing them into the device.

5. CONCLUSION

In conclusion, template matching and matrix profiling are methods suitable for the automated assessment of the signal quality of acceleration data measured from the skin in the neck and groin using laser Doppler velocimetry. Both methods allow to identify epochs in a data stream and provide quantifiable features that can be combined into a quality score or be used as input for logistic regression models for automated classification of signals as acceptable or not acceptable. Models based on both methods yielded an accuracy of minimally 80% in our CARDIS database of carotid and femoral recordings, reaching as high as 87% for the femoral data.

DATA AVAILABILITY STATEMENT

The original contributions presented in the study are included in the article/supplementary files, further inquiries can be directed to the corresponding author.

ETHICS STATEMENT

The studies involving human participants were reviewed and approved by HEGP Ethics Committee. The patients/participants

provided their written informed consent to participate in this study.

AUTHOR CONTRIBUTIONS

The manuscript was written by SS, SB, PS, and NM, as they performed the analysis that is documented. SS and SB contributed equally to the analysis and writing of the text. All authors are included as they provided invaluable work regarding the design of the device and conducting the measurements.

FUNDING

The research was funded by the European Union's Horizon 2020 Research and Innovation Programme under grant agreement nos. 644798 (CARDIS) and 871547 (INSIDE).

ACKNOWLEDGMENTS

We acknowledge the key contributions of Louise Marais, Hakim Khettab, and Michael Vanslembrouck in setting up the CARDIS data and acquiring the data.

REFERENCES

Austin, P. C., and Steyerberg, E. W. (2012). Interpreting the concordance statistic of a logistic regression model: Relation to the variance and odds ratio of a continuous explanatory variable. *BMC Med. Res. Methodol.* 12:82. doi: 10.1186/1471-2288-12-82

Bramwell, J. C., and Hill, A. V. (1922). The velocity of pulse wave in man. *Proc. R. Soc. Lond. B* 93, 298–306. doi: 10.1098/rspb.1922.0022

Campo, A., and Dirckx, J. (2011). "Dual-beam laser doppler vibrometer for measurement of pulse wave velocity in elastic vessels," in *22nd Congress of the International Commission for Optics: Light for the Development of the World, Vol. 8011* (Puebla: International Society for Optics and Photonics), 80118Y.

Chirinos, J. A., Segers, P., Hughes, T., and Townsend, R. (2019). Large-artery stiffness in health and disease: Jacc state-of-the-art review. *J. Am. Coll. Cardiol.* 74, 1237–1263. doi: 10.1016/j.jacc.2019.07.012

De Melis, M., Morbiducci, U., Scalise, L., Tomasini, E. P., Delbeke, D., Baets, R., et al. (2008). A noncontact approach for the evaluation of large artery stiffness: a preliminary study. *Am. J. Hypertens* 21, 1280–1283. doi: 10.1038/ajh.2008.280

Domínguez-Almendros, S., Benítez-Parejo, N., and Gonzalez-Ramirez, A. R. (2011). Logistic regression models. *Allergol. Immunopathol.* 39, 295–305. doi: 10.1016/j.aller.2011.05.002

Jensen-Urstad, K., Storck, N., Bouvier, F., Ericson, M., and Lindblad, L. E. (1997). Heart rate variability in healthy subjects is related to age and gender. *Acta Physiol. Scand.* 60, 235–241. doi: 10.1046/j.1365-201X.1997.00142.x

Jiun-Hung, C., Chu-Song, C., and Yong-Sheng, C. (2003). Fast algorithm for robust template matching with M-Estimators. *IEEE Trans. Signal Proc.* 51, 230–243. doi: 10.1109/TSP.2002.806551

Kaplan, A. D., OrSullivan, J. A., Sirevaag, E. J., Lai, P.-H., and Rohrbaugh, J. W. (2012). Hidden state models for noncontact measurements of the carotid pulse using a laser doppler vibrometer. *IEEE Trans. Biomed. Eng.* 59, 744–753. doi: 10.1109/TBME.2011.2179297

Laurent, S., Cockcroft, J., Van Bortel, L., Boutouyrie, P., Giannattasio, C., Hayoz, D., et al. (2006). Expert consensus document on arterial stiffness: methodological issues and clinical applications. *Eur. Heart J.* 27, 2588–2605. doi: 10.1093/eurheartj/ehl254

Li, Y., Marais, L., Khettab, H., Quan, Z., Aasmul, S., Leinders, R., et al. (2020). Silicon photonics-based laser doppler vibrometer array for carotid-femoral pulse wave velocity (pwv) measurement. *Biomed. Opt. Express.* 11, 3913–3926. doi: 10.1364/BOE.394921

Li, Y., Segers, P., Dirckx, J., and Baets, R. (2013). On-chip laser doppler vibrometer for arterial pulse wave velocity measurement. *Biomed. Opt. Express.* 4, 1229–1235. doi: 10.1364/BOE.4.001229

Madrid, F., Imani, S., Mercer, R., Zimmerman, Z., Shakibay, N., and Keogh, E. (2019). "Matrix profile XX: finding and visualizing time series motifs of all lengths using the matrix profile," in *Proceedings-10th IEEE International Conference on Big Knowledge, ICBK 2019* (Beijing: IEEE), 175–182.

Marais, L., Khettab, H., Li, Y., Segers, P., Baets, R., Reesink, K., et al. (2019). Measurement of aortic stiffness by laser doppler vibrometry: the cardis study. *J. Hypertens* 37:e88. doi: 10.1097/01.hjh.0000570292.62996.dd

Mitchell, G. F., Parise, H., Benjamin, E. J., Larson, M. G., Keyes, M. J., Vita, J. A., et al. (2004). Changes in arterial stiffness and wave reflection with advancing age in healthy men and women: the framingham heart study. *Hypertension* 43, 1239–1245. doi: 10.1161/01.HYP.0000128420.01881.aa

Mitchell, G. F., van Buchem, M. A., Sigurdsson, S., Gotal, J. D., Jonsdottir, M. K., Kjartansson, Ó., et al. (2011). Arterial stiffness, pressure and flow pulsatility and brain structure and function: the Age, Gene/Environment Susceptibility-Reykjavik study. *Brain* 134(Pt 11), 3398–3407. doi: 10.1093/brain/awr253

Morbiducci, U., Scalise, L., De Melis, M., and Grigioni, M. (2007a). Optical vibrocardiography: a novel tool for the optical monitoring of cardiac activity. *Ann. Biomed. Eng.* 35, 45–58.

Morbiducci, U., Scalise, L., Melis, M. D., and Grigioni, M. (2007b). Optical vibrocardiography: a novel tool for the optical monitoring of cardiac activity. *Ann. Biomed. Eng.* 35, 45–58. doi: 10.1007/s10439-006-9202-9

Mueen, A., Keogh, E., Zhu, Q., Cash, S., and Westover, B. (2009). "Exact discovery of time series motifs," in *Society for Industrial and Applied Mathematics-9th SIAM International Conference on Data Mining 2009, Proceedings in Applied Mathematics, Vol. 1* (Puebla), 469–480.

Nick, T., and Campbell, K. (2012). Logistic regression. *Discov. Stat. Using SPSS* 404, 731–735. doi: 10.1007/978-1-59745-530-5_14

Omachi, S., and Omachi, M. (2007). Fast template matching with polynomials. *IEEE Trans. Image Proc.* 16, 2139–2149. doi: 10.1109/TIP.2007.901243

O'Rourke, M., and Kelly, R. (1993). Wave reflection in the systemic circulation and its implications in ventricular-function. *J. Hypertens* 11, 327–337. doi: 10.1097/00004872-199304000-00001

Pereira, T., Correia, C., and Cardoso, J. (2015). Novel methods for pulse wave velocity measurement. *J. Med. Biol. Eng.* 35, 555–565. doi: 10.1007/s40846-015-0086-8

Pinotti, M., Paone, N., Santos, F. A., and Tomasini, E. P. (1998). "Carotid artery pulse wave measured by a laser vibrometer," in *Third International Conference on Vibration Measurements by Laser Techniques: Advances and Applications, Vol. 3411* (Puebla: International Society for Optics and Photonics), 611–616.

Rockwell, R., and Goldman, L. (1974). *Research on human skin laser damage thresholds*. Report DERM-LL-74-1003, USAF School of Aerospace Medicine, Brooks Air Force Base TX.

Rohrbaugh, J. W., Sirevaag, E. J., and Richter, E. J. (2013). Laser doppler vibrometry measurement of the mechanical myogram. *Rev. Sci. Instruments* 84, 121706. doi: 10.1063/1.4845435

Scalise, L., and Morbiducci, U. (2008). Non-contact cardiac monitoring from carotid artery using optical vibrocardiography. *Med. Eng. Phys.* 30, 490–497. doi: 10.1016/j.medengphy.2007.05.008

Segers, P., Rietzschel, E. R., and Chirinos, J. A. (2020). How to measure arterial stiffness in humans. *Arterioscler. Thromb. Vasc Biol.* 40, 1034–1043. doi: 10.1161/ATVBAHA.119.313132

Vlachopoulos, C., Aznaouridis, K., and Stefanadis, C. (2010). Prediction of cardiovascular events and all-cause mortality with arterial stiffness: a systematic review and meta-analysis. *J. Am. Coll. Cardiol.* 55, 1318–1327. doi: 10.1016/j.jacc.2009.10.061

Westerhof, N., Lankhaar, J.-W., and Westerhof, B. E. (2009). The arterial windkessel. *Med. Biol. Eng. Comput.* 47, 131–141. doi: 10.1007/s11517-008-0359-2

Wolinsky, H., and Glagov, S. (1967). A lamellar unit of aortic medial structure and function in mammals. *Circ. Res.* 20, 99–111. doi: 10.1161/01.RES.20.1.99

Won-Du, C., and Chang-Hwan, I. (2014). Enhanced template matching using dynamic positional warping for identification of specific patterns in electroencephalogram. *J. Appl. Math*. 2014:528071. doi: 10.1155/2014/528071

Yeh, C.-C. M., Zhu, Y., Ulanova, L., Begum, N., Ding, Y., Dau, H. A., et al. (2018). Time series joins, motifs, discords and shapelets: a unifying view that exploits the matrix profile. *Data Min. Knowl. Discov*. 32, 83–123. doi: 10.1007/s10618-017-0519-9

Zhang, J. (2007). Effect OF age and sex on heart rate variability in healthy subjects. *J. Manipulative Physiol. Ther*. 30, 374–379. doi: 10.1016/j.jmpt.2007.04.001

Zhu, Y., Gharghabi, S., Silva, D. F., Dau, H. A., Yeh, C.-C. M., Shakibay Senobari, N., et al. (2020). The Swiss army knife of time series data mining: ten useful things you can do with the matrix profile and ten lines of code. *Data Min. Knowl. Discov*. 34, 949–979. doi: 10.1007/s10618-019-00668-6

Zhu, Y., Imamura, M., Nikovski, D., and Keogh, E. (2017a). "Matrix profile VII: time series chains: a new primitive for time series data mining," *2017 IEEE International Conference on Data Mining (ICDM)* (New Orleans, LA: IEEE).

Zhu, Y., Zimmerman, Z., Senobari, N. S., Yeh, C. C. M., Funning, G., Mueen, A., et al. (2017b). "Matrix profile II: Exploiting a novel algorithm and GPUs to break the one hundred million barrier for time series motifs and joins," in *Proceedings-IEEE International Conference on Data Mining, ICDM* (Barcelona: IEEE), 739–748.

Zimmerman, Z., Shakibay Senobari, N., Funning, G., Papalexakis, E., Oymak, S., Brisk, P., et al. (2019). "Matrix profile XVIII: time series mining in the face of fast moving streams using a learned approximate matrix profile," in *Proceedings-IEEE International Conference on Data Mining, ICDM 2019* (Beijing: IEEE), 936–945.

Conflict of Interest: The authors declare that the research was conducted in the absence of any commercial or financial relationships that could be construed as a potential conflict of interest.

Publisher's Note: All claims expressed in this article are solely those of the authors and do not necessarily represent those of their affiliated organizations, or those of the publisher, the editors and the reviewers. Any product that may be evaluated in this article, or claim that may be made by its manufacturer, is not guaranteed or endorsed by the publisher.

frontiers in Physiology

ORIGINAL RESEARCH
published: 20 January 2022
doi: 10.3389/fphys.2021.774390

Central Pressure Waveform-Derived Indexes Obtained From Carotid and Radial Tonometry and Brachial Oscillometry in Healthy Subjects (2–84 Y): Age-, Height-, and Sex-Related Profiles and Analysis of Indexes Agreement

Yanina Zócalo and Daniel Bia*

Departamento de Fisiología, Facultad de Medicina, Centro Universitario de Investigación, Innovación y Diagnóstico Arterial (CUiiDARTE), Universidad de la República, Montevideo, Uruguay

OPEN ACCESS

Edited by:
Andrea Guala, Vall d'Hebron Research Institute (VHIR), Spain

Reviewed by:
Alun Hughes, University College London, United Kingdom
Chloe May Park, University College London, United Kingdom

***Correspondence:**
Yanina Zócalo
yana@fmed.edu.uy; yaninazocalo@gmail.com

Specialty section:
This article was submitted to Vascular Physiology, a section of the journal Frontiers in Physiology

Received: *11 September 2021*
Accepted: *22 December 2021*
Published: *20 January 2022*

Citation:
Zócalo Y and Bia D (2022) Central Pressure Waveform-Derived Indexes Obtained From Carotid and Radial Tonometry and Brachial Oscillometry in Healthy Subjects (2–84 Y): Age-, Height-, and Sex-Related Profiles and Analysis of Indexes Agreement. Front. Physiol. 12:774390. doi: 10.3389/fphys.2021.774390

Aortic blood pressure (aoBP) waveform-derived indexes could provide valuable (prognostic) information over and above cardiovascular risk factors (CRFs). To obtain aoBP waveform-characteristics, several (i) techniques, (ii) recording sites, (iii) pressure-only waveform analysis mathematical approaches [e.g., pulse wave analysis (PWA), wave separation analysis (WSA)], and (iv) indexes [augmentation pressure and index (AP and AIx), forward (Pf) and backward (Pb) components of aoBP, reflection magnitude (RM), and reflection index (Rix)], were proposed. An accurate clinical use of these indexes requires knowing their physiological age-related profiles and the expected values for a specific subject. There are no works that have characterized waveform-derived indexes profiles in large populations considering: (i) as a continuous, data from different age stages (childhood, adolescence, and adulthood), (ii) complementary indexes, (iii) data obtained from different techniques and approaches, and (iv) analyzing potential sex- and body height (BH)-related differences. In addition, (v) there is a lack of normative data (reference intervals, RIs) for waveform-derived indexes.

Aims: (1) to evaluate the association and agreement between PWA- and/or WSA-derived indexes obtained with different techniques and approaches; (2) to determine the need for sex-, BH-, and/or age-specific RIs; (3) to define RIs for PWA- and WSA-derived indexes in a large cohort of healthy children, adolescents, and adults.

Methods: 3619 subjects (3–90 y) were included; 1688 healthy (2–84 y). AP, AIx, AIx@75, Pf, Pb, RM, and RIx were obtained (carotid and radial tonometry, brachial oscillometry/plethysmography). The association and agreement between indexes were analyzed (Concordance correlation coefficients, Bland–Altman analysis). Mean and SD equations and sex-specific BH- and age-related profiles were obtained (regression methods; fractional polynomials).

Results: Waveform-derived indexes were not equivalent; for a specific index, there were systematic and proportional differences associated with the recording site (e.g., carotid *vs.* radial) and technique (e.g., tonometry *vs.* oscillometry). The need for sex-, BH-, or age-specific RIs was dependent on the index and/or age considered. RIs were defined for each index considering differences between recording sites and techniques. Equations for waveform-derived indexes age-related profiles were included, enabling to determine for a specific subject, the expected values and potential data deviations.

Keywords: adolescents, adults, applanation tonometry, children, oscillometry, pulse wave analysis, wave separation analysis, normative data

INTRODUCTION

Central aortic blood pressure (aoBP) waveform contains valuable (e.g., prognostic) information beyond and in addition to the obtained from its corresponding systolic, diastolic, and pulse pressure levels (aoSBP, aoDBP, aoPP) (Mynard et al., 2020). Several techniques (e.g., applanation tonometry, oscillometry/plethysmography) and mathematical methods (e.g., direct carotid or distal-arteries recordings associated to a general transfer function) have been proposed to perform waveform analyses (Hametner and Wassertheurer, 2017). In addition, different pressure-only approaches for waveform analysis [e.g., pulse wave analysis (PWA), wave separation analysis (WSA)] are available (Westerhof et al., 2006; Wang et al., 2010; Chirinos et al., 2012; Weber et al., 2012; Zamani et al., 2014; Hametner et al., 2015; Sluyter et al., 2017; Mynard et al., 2020). Augmentation pressure (AP), augmentation index (AIx), and AIx corrected for heart rate (AIx@75) are the PWA-derived indexes most commonly used. The concept or basic idea underlying PWA is that forward waves traveling from the ventricle toward the periphery are distally reflected. Reflected waves augment (central) pressure. AP represents the augmentation level (a positive AP indicates "additional" pressure arising from reflections) (Baksi et al., 2009; Sugawara et al., 2010). It is calculated from the inflection point in the pressure waveform (systolic phase) that "signalizes or identifies" the reflected component's arrival to the aortic root (Kelly et al., 1989). AIx, calculated as AP/aoPP, is considered as a surrogate index of wave reflection (although it is known that it also depends on factors like heart rate or ventricle function) (Hametner and Wassertheurer, 2017). In WSA, the aoBP waveform is decomposed into single forward (Pf) and backward (Pb) components, which actually integrate different forward and backward propagating waves. Furthermore, it is to note that the Pf represents the integration of forward wave arising from the ventricle and re-reflections of backward propagating waves at the ventricular-aorta interface. From Pf and Pb, the reflection magnitude (RM; RM = Pb/Pf) and index {RIx; RIx = [Pb/(Pf + Pb)]} were determined. However, taking into account the above stated (and despite the names), they cannot be considered as simple measures or indicators of the reflections (Westerhof and Westerhof, 2013; Zamani et al., 2014).

In the last decade, several clinical studies have shown that waveform analysis could provide valuable information (even exceeding the information obtained from the analysis of the exposure to cardiovascular risk factors [CRFs]) (Zamani et al., 2014; Hametner and Wassertheurer, 2017; Mynard et al., 2020). However, to optimize their value and to ensure a proper use of waveform-derived indexes, some issues should be assessed and clarified. First, it is unknown whether the different techniques and methods used to quantify waveform-derived indexes provide equivalent information that would allow the use of similar normative data (reference intervals, [RIs]) regardless of the approach considered. Second, there is limited information concerning age and/or sex-related RIs for PWA- and WSA-derived indexes obtained at the same time in large healthy populations (including children, adolescents, and adults). This is true, even more so if data from South American populations are considered. In this regard, it is to note that ethnicity may be an independent determinant of wave reflections (both in adults and children) (Chirinos et al., 2011; Heffernan et al., 2020). In addition, an accurate use of waveform-derived indexes requires knowing the expected physiological age-related profiles and the predicted value for a specific subject. However, in our knowledge, there are no works assessing waveform-derived indexes' variations (as a continuous) considering data from different age-stages and their transitions (childhood-adolescence-adulthood). It is to note that studies that aimed at analyzing age-related differences do not allow for their adequate and comprehensive characterization, as they (i) considered small numbers of subjects [e.g., $n = 65$ (Hughes et al., 2013), $n = 267$ (Yu et al., 2020)], (ii) did not exclude subjects with cardiovascular disease or exposed to CRFs [e.g., cardiology outpatients (Namasivayam et al., 2016), unhealthy or diseased subjects (Torjesen et al., 2014; Hodson et al., 2016; Li et al., 2019), and subjects with CRFs (Mitchell et al., 2004; Hughes et al., 2013; Hickson et al., 2016; Wilenius et al., 2016; Gómez-Sánchez et al., 2020; Yu et al., 2020)]; (iii) compared "mean values" of groups comprising subjects of wide age ranges (e.g.,

Abbreviations: AIx, augmentation index; AIx@75, augmentation index corrected for heart rate 75 beats/minute; aoBP, central aortic blood pressure; aoDBP, central aortic diastolic blood pressure; aoPP, central aortic pulse pressure; aoSBP, central aortic systolic blood pressure; AP, augmentation pressure; baDBP, brachial artery diastolic blood pressure; baMBP, brachial artery mean blood pressure; baPP, brachial artery pulse pressure; baSBP, brachial artery systolic blood pressure; BH, body height; BMI, body mass index; BP, blood pressure; CRFs, cardiovascular risk factors; MOG, Mobil-O-Graph PWA-monitor system; Pb, backward (reflected) component of pressure waveform; Pf, forward (incident) component of pressure waveform; PWA, pulse wave analysis; RIs, reference intervals; RIx, reflection index; RM, reflection magnitude; SCOR, SphygmoCor-CvMS system; WSA, wave separation analysis; y, years.

5–7 years (y) (Segers et al., 2007; Janner et al., 2010; Hodson et al., 2016) or 10 y (Kelly et al., 1989; Mitchell et al., 2004; McEniery et al., 2005; Torjesen et al., 2014; Hickson et al., 2016; Namasivayam et al., 2016; Solanki et al., 2018; Li et al., 2019; Yu et al., 2020) of difference in the age of subjects belonging to the same group); (iv) considered only adults within a limited age range (e.g., 40–70 y, grouped by decades) (Li et al., 2019), and (v) in general, did not consider subjects under 18–20 years of age. In this context, it should be noted that the need for RIs for vascular parameters in children and adolescents is now well-recognized and is considered necessary to extend their use in clinical practice (Climie et al., 2021).

In this context, this work's aims were: (1) to evaluate the association and/or agreement between PWA- and/or WSA-derived indexes obtained with different techniques and approaches, (2) to determine the need for sex-, body height (BH)-, and/or age-specific RIs, (3) to define RIs for PWA- and WSA-derived indexes in a large cohort of healthy children, adolescents, and adults from South America. As a secondary aim, non-linear equations for sex-, BH-, and/or age-specific percentiles were determined and included (text and spreadsheet formats); the information given enables to determine the expected value for a particular subject (and to assess any possible deviation from the anticipated).

MATERIALS AND METHODS

Study Population and Clinical and Anthropometric Evaluation

The study was carried out in the context of the CUiiDARTE project (Bia et al., 2011; Santana et al., 2012a,b; Zócalo et al., 2020; Bia and Zócalo, 2021), a population-based study developed in Uruguay. In this work, we considered data from 3619 subjects included in CUiiDARTE database. This contains data on demographic and anthropometric variables, exposure to CRFs, personal and family history of cardiovascular disease and data on hemodynamic, and on structural and functional vascular parameters (Bia et al., 2011; Santana et al., 2012a,b; Zócalo et al., 2020; Bia and Zócalo, 2021; Zócalo and Bia, 2021a,b). In this work, the analysis was focused on PWA- and WSA-derived indexes.

All procedures agree with the Declaration of Helsinki (1975 and reviewed in 1983). The study protocol was reviewed and approved by the Ethics Committee of Centro Hospitalario Pereira Rossell, Universidad de la República. Prior to the evaluation, the participants provided their written informed consent to participate in the study. In subjects under 18 y, parents' written consent and children's assent were obtained before the evaluations. Subjects or parents (in case of subjects aged < 18 y) provided informed written consent to have data from their medical records used in research.

Before cardiovascular evaluation, a brief clinical interview together with the anthropometric and blood test results evaluation enabled to assess exposure to CRFs. Body weight and BH were measured with the participant wearing light clothing and no shoes. Standing BH was measured using a portable stadiometer and recorded to the nearest 0.1 cm. Body weight was measured with an electronic scale (841/843, Seca Inc., Hamburg, Germany; model HBF-514C, Omron Inc., Chicago, IL, United States) and recorded to the nearest 0.1 kg. Body mass index (BMI) was calculated as body weight-to-squared BH ratio. In children and adolescents, z-scores for BMI were calculated using the WHO software (Anthro-v.3.2.2; Anthro-Plus-v.1.0.4) (Castro et al., 2019).

Obesity was defined as z-score for BMI $\geq$ 2.0 (for subjects < 18 y) or BMI > 30 Kg/m^2 (for subjects ≥ 18 y). Arterial hypertension was considered to be present, if it had been previously diagnosed in agreement with reference guidelines and/or use of blood pressure-lowering drugs was reported. Cut-off values were: brachial systolic blood pressure (baSBP) ≥ 140 mmHg and/or diastolic blood pressure (baDBP) ≥ 90 mmHg (for subjects ≥ 18 y) and baSBP and baDBP $>$ 95th percentile for sex, age, and BH (for subjects < 18 y). Personal and family histories of cardiovascular disease (i.e., presence of cerebral, coronary, aortic, or peripheral arterial disease) were assessed. A family history of cardiovascular disease was defined by the presence of first-degree (for all the subjects) and/or second-degree (for subjects ≤ 18 y) relatives with early (< 55 y in males, < 65 y in females) cardiovascular disease. History of dyslipidemia and diabetes were considered to be present if they had been previously diagnosed in agreement with reference guidelines and/or the use of lipid- or glucose-lowering drugs (respectively) was reported. Dyslipidemia was defined as total cholesterol > 240 mg/dL or high-density lipoprotein cholesterol for men < 40 mg/dL and for women < 46 mg/dL. In turn, diabetes diagnosis was based on plasma glucose levels (fasting plasma glucose ≥ 126 mg/dl). Regular (current) smokers, defined as usually smoking at least one cigarette/week, were identified.

Cardiovascular Evaluation

The participants were asked to avoid exercise, tobacco, alcohol, caffeine, and food-intake 4 h before the evaluation. All hemodynamic measurements were performed in a temperature-controlled environment (21–23°C), with the subject in supine position and after resting for at least 10–15 min, which enabled reaching steady hemodynamic conditions. Using a validated oscillometric device (HEM-433INT; Omron Healthcare Inc., IL, United States), heart rate, baSBP, and baDBP were recorded in supine position simultaneously and/or immediately before or after each non-invasive arterial recording. Then, brachial artery pulse pressure (baPP; baPP = baSBP-baDBP) and mean BP (baMBP, baMBP = baDBP + baPP/3) were calculated.

Structural and Functional Markers of Subclinical Atherosclerosis

Left and right common, internal, and external carotid arteries, vertebral artery, common femoral artery, and left brachial artery were examined (B-Mode and Doppler ultrasound, 7–13 MHz, linear transducer, M-Turbo, SonoSite Inc., Bothell, WA, United States). Transverse and longitudinal arterial views were obtained to assess the presence of atherosclerotic plaques (defined

as focal wall thickening at least 50% greater than the adjacent segment, focal thickening protruding ≥0.5 mm into the lumen, or an intima-media thickness ≥1.5 mm) (Zócalo and Bia, 2016; Marin et al., 2020).

Left and right brachial and tibial systolic and diastolic blood pressure levels were obtained (no fixed order) at 5 min intervals (Hem-4030, Omron Inc., IL, United States). At least five measurements were obtained from each recording site. The Ankle Brachial Index, an index of arterial permeability and central-peripheral blood pressure amplification, was calculated as tibial systolic blood pressure/baSBP (Zócalo and Bia, 2016). Right and left Ankle-Brachial Index values < 0.9 were used to define and rule out stenosis of at least 50% distal to common femoral artery (Zócalo and Bia, 2016). After applying the exclusion criteria related to exposure to CRFs, there were no subjects with Ankle-Brachial Index < 0.9 in the group of RIs.

Central Blood Pressure Levels and Waveform Analysis-Derived Indexes

Central aoBP levels and waveforms were obtained (random order) using commercially available devices: SphygmoCor-CvMS ([SCOR]; v.9, AtCor-Medical, Sydney, NSW, Australia) and Mobil-O-Graph PWA-monitor system ([MOG]; I.E.M.-GmbH, Stolberg, Germany).

Using SCOR, aoBP waveforms were derived from, (i) radial artery (applying a general transfer function) and (ii) carotid artery (directly) manual tonometric recordings (**Figure 1**). Carotid pulse waveforms were assumed to be identical to the aortic ones (due to the proximity of the arterial sites) (Karamanoglu and Feneley, 1996). Thus, a transfer function was not applied to obtain central waveforms from carotid recordings. Only accurate waveforms on visual inspection and high-quality recordings (in-device quality control (operator) index > 75%) were considered. The operator index is an indicator of recorded signals' overall reproducibility. It is calculated by assesing weighted quality control parameters and adding them to give a number as a percentage. Quality index assessment includes: (i) average height of individual records above 100 units, (ii) pulse height variation (accepted values: <5%), (iii) diastolic variation (indicates constancy of the basal level of the wave, accepted value: <5%), (iv) shape variation (difference in the shape of the recorded waves, accepted values <5%), and (v) maximum dP/dt (maximum value of the first derivative or maximal rate of

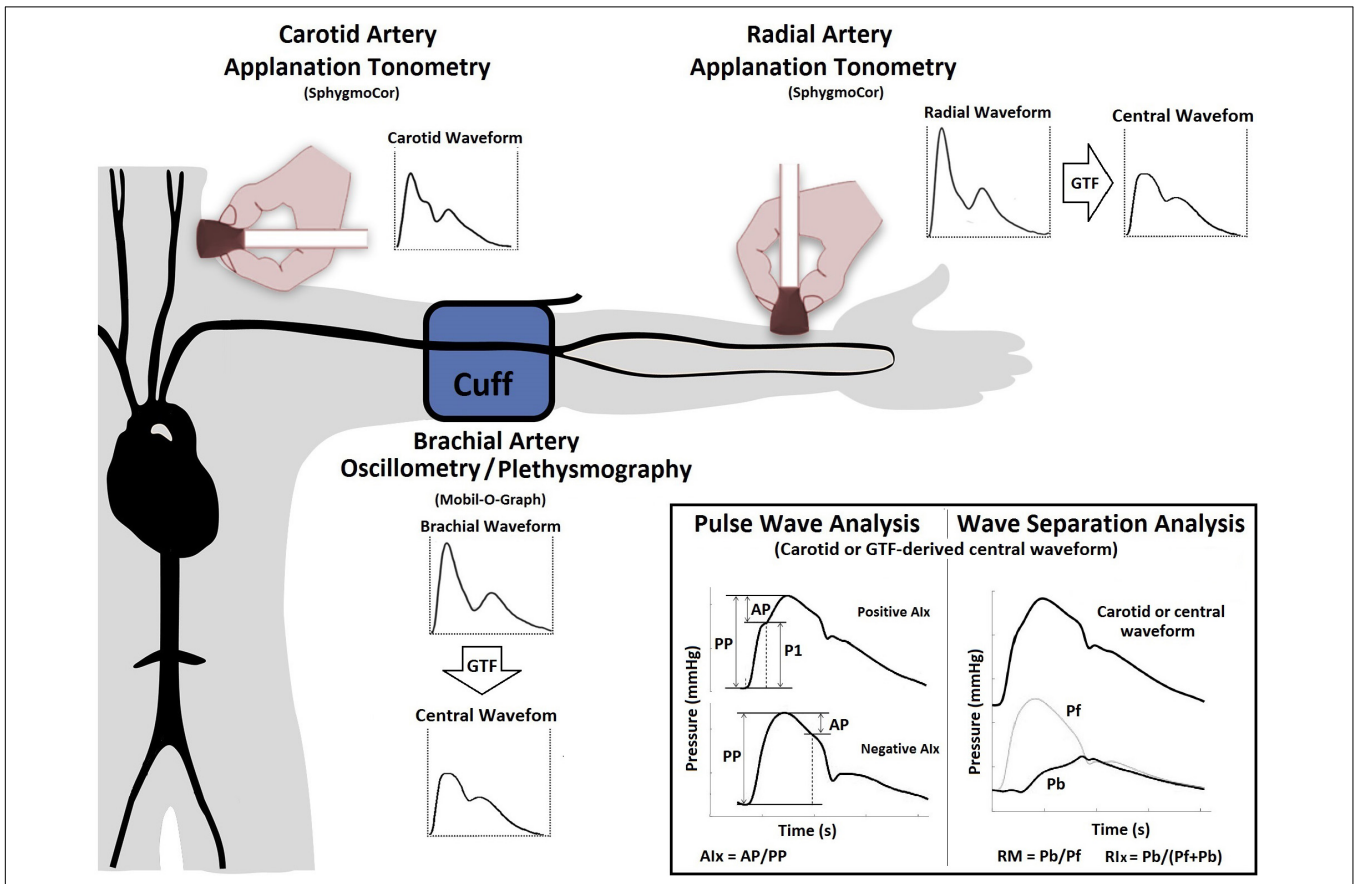

FIGURE 1 | Instrumental approach employed to obtain central blood pressure waves and waveform-derived indexes. Examples of positive and negative AIx. Aix, Augmentation index; AP, augmentation pressure; GTF, general transfer function; Pf and Pb, forward and backward central blood pressure components; PP, pulse pressure; SphygmoCor, SphygmoCor device; v.9, AtCor-Medical, Sydney, NSW, Australia. Mobil-O-Graph, Mobil-O-Graph PWA-monitor system, I.E.M.-GmbH, Stolberg, Germany.

TABLE 1 | Subjects demographic, anthropometric, and clinical characteristics.

	All (n = 3619)							Reference Intervals (n = 1688)						
Variable	**MV**	**SD**	**Min**	**p25th**	**p50th**	**p75th**	**Max**	**MV**	**SD**	**Min**	**p25th**	**p50th**	**p75th**	**Max**
Age [years]	33.87	24.20	2.80	11.50	23.65	56.40	89.00	20.12	16.93	2.80	6.29	17.60	21.80	84.20
Body weight [Kg.]	61.13	25.28	12.30	45.60	63.20	78.10	150.60	47.91	22.83	12.30	22.60	52.80	65.20	105.00
Body height [m]	1.55	0.23	0.90	1.46	1.62	1.71	1.97	1.47	0.26	0.90	1.17	1.58	1.69	1.94
BMI [Kg./m^2]	24.06	6.02	11.53	19.70	23.63	27.84	71.34	20.36	4.22	11.53	16.59	20.00	23.56	29.95
z-BMI [SD]	0.94	1.45	−4.63	−0.05	0.74	1.77	8.03	0.34	0.92	−4.63	−0.27	0.41	1.00	1.98
TC [mg/dl]	200.26	44.27	94.30	170.00	196.00	227.00	379.00	194.87	25.85	99.00	179.00	198.00	214.00	238.00
HDL [mg/dl]	51.18	15.09	17.00	41.00	49.00	60.00	122.00	57.73	12.03	41.00	49.00	55.00	64.00	100.00
LDL [mg/dl]	123.39	39.83	28.00	95.00	119.00	146.00	323.00	117.96	25.51	31.00	101.00	120.60	134.00	180.00
Triglycerides [mg/dl]	133.21	85.94	24.00	80.00	111.00	158.00	783.00	93.30	38.85	24.00	65.00	86.00	113.00	272.00
Glicaemia [mg/dl]	94.35	18.68	40.00	85.00	92.00	100.00	307.00	88.23	9.48	40.00	83.00	88.00	93.00	121.00
baSBP [mmHg]	119.02	16.81	64.25	107.00	118.44	128.76	235.00	112.02	13.35	80.00	101.35	111.63	121.25	171.00
baDBP [mmHg]	68.84	10.36	41.25	60.78	67.73	75.80	129.18	64.79	8.36	46.70	58.92	63.29	70.00	97.44
TC ≥ 240 mg/dl [%]				7.2							0			
HDL < 40 mg/dl [%]				8.9							0			
Glicamia ≥ 126 mg/dl [%]				0.9							0			
Current Smoke [%]				11.4							0			
Hypertension [%]				26.4							0			
Diabetes [%]				5.7							0			
History of CVD [%]				8.8							0			
Obesity [%]				21.9							0			
Familiar CVD [%]				13.5							7.6			
Antihypertensive drugs				21.7							0			
Antihyperlipidemic agent [%]				13.5							0			
Antidiabetic agents [%]				4.1							0			
Atherosclerotic plaques (%)				22.2							6.6			

MV, mean value; Min. and Max., minimal and maximal value. p25th, p50th (median), and p75th: 25, 50 and 75 percentiles; BMI, body mass index; baSBP, baDBP, brachial artery systolic and diastolic blood pressure; CVD, cardiovascular disease; TC, total cholesterol; HDL, HDL Cholesterol; LDL, LDL Cholesterol; Familiar CVD, Familiar history of premature CVD [%].

wave rise). Based on the described variables, the operator index (recordings quality/reproducibility) was automatically assessed by the recording device. Brachial artery blood pressure levels and waveforms were automatically obtained using the MOG system (brachial cuff-based oscillometric device) (Zinoveev et al., 2019). The device determined aoBP levels and waveforms from peripheral recordings using a validated general transfer function. Only high-quality records (index equal to 1 or 2) and satisfactory waveforms (visual inspection) were considered.

Both devices (SCOR and MOG) enable PWA and WSA. A detailed (step-by-step) explanation of the method used for WSA based on recorded (carotid waveforms, SCOR) and mathematically derived aortic waveforms (SCOR and MOG) was included as **Supplementary Material** in a previous work (Zinoveev et al., 2019). As was previously published, absolute and relative intra- (repeatability) and interobserver (reproducibility) variability of aoBP levels and waveform-derived indices were analyzed (considering different methodological approaches: radial tonometry, carotid tonometry, and brachial oscillometric records) (Zinoveev et al., 2019). No significant differences were observed in aoSBP, aoPP, and waveform derived-indexes levels either within each visit, between two records [obtained by a single investigator (Y.Z.)], or between records obtained by two investigators (Y.Z., D.B.); indicating adequate repeatability, as well as reproducibility. In all cases, relative inter- and intraobserver variability was <6%.

Using both devices (SCOR and MOG) and the three recording sites (carotid and radial with SCOR and brachial with MOG), we quantified: (i) AP, AIx, AIx@75 and (ii) Pf, Pb, RM, and RIx (**Figure 1**). Recorded waveforms were calibrated using baDBP and baMBP (Zinoveev et al., 2019). AIx, AIx@75, RM, and RIx are "attractive" biomarkers because they are dimensionless and, therefore, do not depend on waveform calibration.

The variables were named based on the (i) waveform-derived index, (ii) recording site, and (iii) device (e.g., Pf_Radial_SCOR *vs.* Pf_Carotid_SCOR *vs.* Pf_Brachial_MOG).

Data Analysis

A step-wise analysis was performed. First, after descriptive statistics were computed and checked (**Tables 1**, **2** and **Supplementary Tables 1, 2**), it was analyzed whether the studied variables showed the expected trend in terms of age-related variations. **Figure 2** exemplifies the results obtained for AIx@75_SCOR_Radial.

Second, it was defined as a reference subgroup to determine RIs. This subgroup included subjects (n = 1688, 864 females) without any of the following (Engelen et al., 2013, 2015; Bossuyt et al., 2015): (i) cardiovascular disease; (ii) use of blood pressure-, lipid-, and/or glucose-lowering drugs; (iii) arterial hypertension; (iv) tobacco use; (v) diabetes; (vi) dyslipidemia; and (vii) obesity. In this subgroup, the atherosclerotic plaques presence was not associated with the waveform-derived indexes. Then, the

TABLE 2 | Central and peripheral blood pressure and central waveform-derived indexes.

	All (*n* = 3619)							Reference Intervals (*n* = 1688)						
Variable	**MV**	**SD**	**Min**	**p25th**	**p50th**	**p75th**	**Max**	**MV**	**SD**	**Min**	**p25th**	**p50th**	**p75th**	**Max**
Brachial Artery Oscillometry/Plethysmography (MOG device)														
baSBP [mmHg]	116.66	14.20	81.00	107.00	114.55	125.00	199.27	111.85	11.68	81.00	103.75	110.50	120.07	157.67
baDBP [mmHg]	68.31	11.25	36.00	60.40	66.87	74.75	131.43	64.76	8.89	38.67	58.40	63.71	70.25	106.00
aoSBP [mmHg]	104.89	16.99	71.00	92.00	103.78	115.63	185.09	99.13	14.93	71.00	86.73	97.50	108.53	168.50
aoDBP [mmHg]	69.63	11.25	38.00	61.83	68.47	76.00	133.14	66.08	8.93	39.33	59.50	65.00	71.61	109.00
HR [b.p.m]	75.68	15.47	33.40	64.00	73.47	85.67	135.25	78.60	16.29	41.00	66.75	76.75	88.83	135.25
AP [mmHg]	7.22	5.38	1.00	3.76	5.39	8.63	37.60	5.93	3.77	1.00	3.62	5.00	7.00	32.00
AIx [%]	19.33	10.49	−7.00	11.57	16.74	24.39	60.82	17.55	8.41	−7.00	11.24	16.17	22.36	60.00
AIx@75 [%]	19.67	11.95	−7.33	10.42	19.00	28.33	65.00	19.57	12.31	−7.00	10.00	19.15	28.42	65.00
Pf [mmHg]	23.37	7.54	10.30	18.13	21.94	26.80	65.55	22.27	7.68	10.30	17.06	20.60	25.25	65.55
Pb [mmHg]	13.91	5.17	4.20	10.13	13.10	16.58	38.15	12.79	5.10	4.20	9.15	11.65	15.23	38.15
RM	0.59	0.1	0.18	0.53	0.6	0.66	0.81	0.57	0.09	0.18	0.52	0.58	0.63	0.8
RIx	0.37	0.04	0.15	0.35	0.37	0.4	0.45	0.36	0.04	0.15	0.34	0.37	0.39	0.44
Radial Artery Applanation Tonometry (SCOR device)														
baSBP [mmHg]	120	16.48	77	109	120	130	235	114.24	13.55	78	105	114	124	160
baDBP [mmHg]	69	10.86	37	61	69	76	130	65.17	9.29	42	59	64	71	95
aoSBP [mmHg]	105	16.3	64	94	105	115	208	98.57	13.35	64	88	99	108	140
aoDBP [mmHg]	70	10.96	17	62	70	77	131	66.47	9.27	43	60	65	73	97
HR [b.p.m]	72	14.05	35	63	71	82	151	75.56	15.32	38	65	74	85	151
AP [mmHg]	4.93	6.76	−21	1	4	9	50	2.2	4.87	−21	−1	2	5	26
AIx [%]	13.2	15.3	−36	2	13	25	54	7.71	13.57	−36	−2	7	17	46
AIx@75 [%]	12.08	14.56	−37	1	13	23	49	7.78	14.27	−37	−3	8	18	49
Pf [mmHg]	29.13	9.13	7	23	28	34	89	28.57	9.66	7	21	27	34	71
Pb [mmHg]	15.47	5.75	3	12	14	18	78	13.45	4.31	3	11	13	16	78
RM	0.55	0.17	0.17	0.42	0.52	0.65	2.05	0.49	0.15	0.17	0.4	0.47	0.56	2.05
RIx	0.35	0.07	0.14	0.3	0.34	0.4	0.67	0.33	0.06	0.14	0.28	0.32	0.36	0.67
Carotid Artery Applanation Tonometry (SCOR device)														
baSBP [mmHg]	120.94	17.55	78	109	120	131	239	114.35	15.29	78	104	114	124	217
baDBP [mmHg]	68.84	10.98	38	60	68	76	127	64.47	9.31	38	58	63	70	100
aoSBP [mmHg]	112.6	18.17	69	100	111	124	216	105.48	16	69	94	105	116	216
aoDBP [mmHg]	68.84	10.98	38	60	68	76	127	64.47	9.31	38	58	63	70	100
HR [b.p.m]	71.75	14.15	32	61	70	80	145	75.11	15.44	40	64	74	84	145
AP [mmHg]	−1	11.69	−64	−8	−2	7	49	−5.38	9.6	−64	−10	−5	0	25
AIx [%]	−2.51	22.95	−63	−21	−5	17	56	−11.82	19.02	−55	−25	−14	0	44
AIx@75 [%]	−4.02	20.91	−60	−20	−5	12	53	−11.81	18.04	−56	−24	−12	−1	43
Pf [mmHg]	39.78	13.26	8	31	37	47	114	40.06	13.83	8	30	38	47	114
Pb [mmHg]	18.75	6.89	5	14	18	23	53	16.03	5.42	5	12	15	19	39
RM	0.5	0.18	0.11	0.36	0.47	0.63	1	0.43	0.15	0.11	0.33	0.41	0.5	0.97
RIx	0.32	0.08	0.1	0.27	0.32	0.38	0.5	0.29	0.07	0.1	0.25	0.29	0.33	0.49

MV, mean value; Min. and Max., minimal and maximal value; p25th, p50th (median) and p75th, 25, 50 and 75 percentiles; BMI, body mass index; HR, heart rate; baSBP, baDBP, brachial systolic and diastolic pressure; aoSBP, aoDBP, aortic systolic and diastolic pressure; CVD, cardiovascular disease; AP, Augmentation Pressure; AIx, Augmentation Index. AIx@75, AIx adjusted by HR equal 75 beats/minute (b.p.m.); Pf, forward pressure; Pb, backward pressure; RM and RIx, reflection magnitude and index, respectively.

subjects with plaques were not excluded from the RIs subgroup (**Supplementary Table 3**).

Third, in order to determine whether specific RIs were necessary for the same waveform-derived parameter obtained with different approaches (e.g., Pf_Radial_SCOR *vs.* Pf_Carotid_SCOR *vs.* Pf_Brachial_MOG), we analyzed the degree of association and agreement between data by assessing: (i) concordance correlation coefficients and (ii) mean and proportional differences (Bland–Altman analysis) (**Table 3** and **Supplementary Table 4**). **Figure 2** exemplifies the results obtained when comparing AIx@75_SCOR_Radial and AIx@75_SCOR_Carotid. Specific RIs for all waveform-derived indexes obtained with the different approaches were defined as necessary.

Fourth, we evaluated whether age-, BH-, and/or sex-specific RIs were necessary using multiple linear regression models that included interaction analysis (Sex*Age; Sex*BH) with Johnson-Neyman significance regions definition (**Supplementary Tables 5–10**). Variables "y," "x," and "w" (moderating variable) were assigned to the waveform-derived

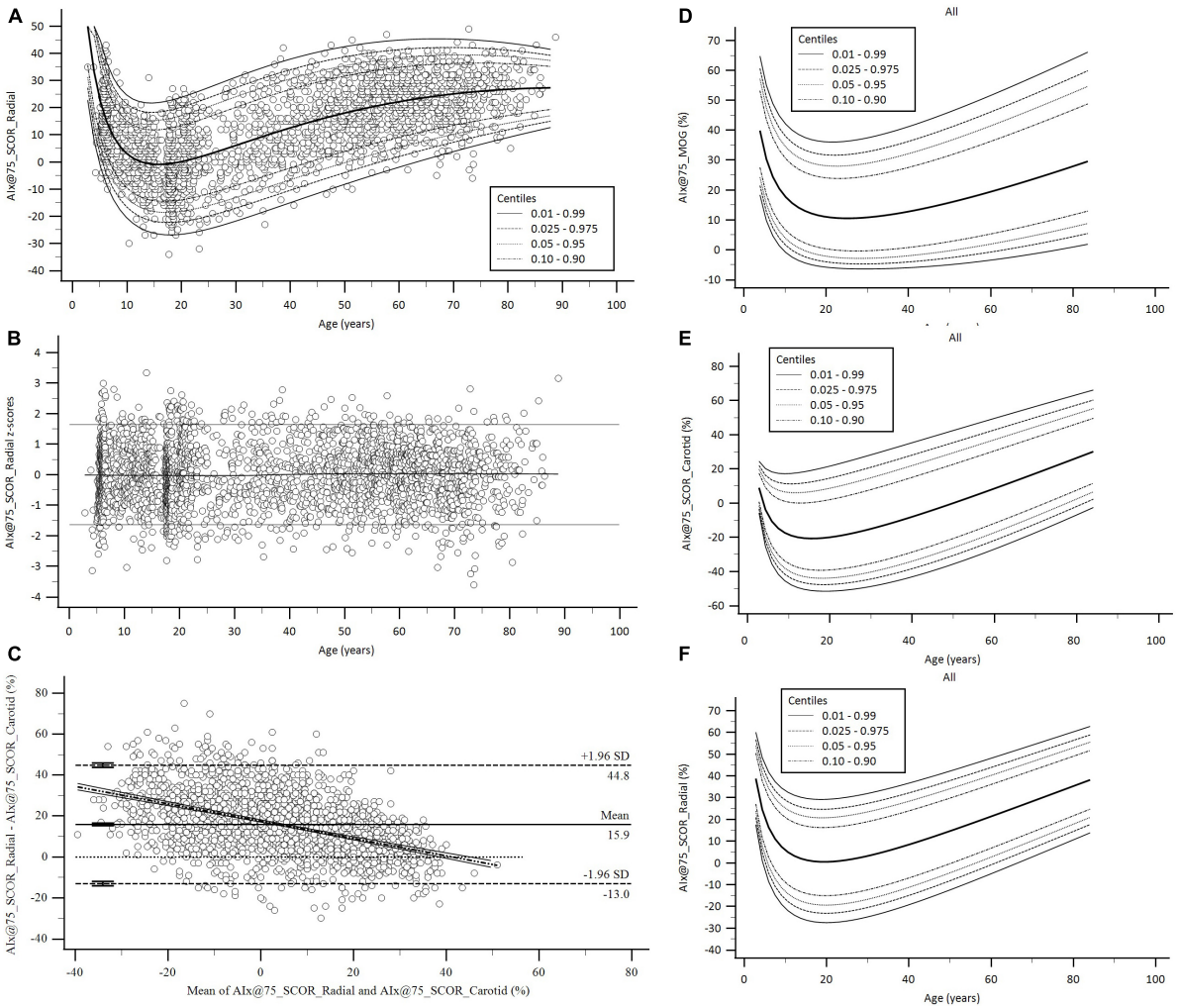

FIGURE 2 | Age-related profiles and Bland–Altman analysis for AIx@75. **(A,B)** Age-related profiles (1th, 2.5th, 5th, 10th, 50th, 90th, 95th, 97.5th, and 99th percentiles) for AIx@75_SCOR_Radial and z-score diagram used to verify model fit. **(C)** Bland–Altman diagram for AIx@75_SCOR_Radial and AIx@75_SCOR_Carotid comparison. There were significant mean (15.9, 95% CI.; 15.28 to 16.53%, $p < 0.001$) and proportional errors (slope coefficient: –0.4234, 95% CI.: –0.4571 to –0.3897, $p < 0.001$). **(D–F)** Age-related percentile curves for AIx@75 obtained with three different methods. Age-related percentile curves (1th, 2.5th, 5th, 10th, 50th, 90th, 95th, 97.5th, and 99th percentiles) for AIx@75_MOG, AIx@75_SCOR_Radial, and AIx@75_SCOR_Carotid.

indexes (y), sex (x), and age or BH (w). We identified indexes that: (i) required sex-specific RIs only from a certain age or BH, (ii) required sex-specific RIs regardless of age or BH, (iii) did not require sex-specific RIs, (iv) did not require age-, BH-, and/or sex-specific RIs (**Supplementary Table 11**). To enable comparisons with other authors and, at the same time, to minimize type 1 error associated with the development of several multiple regression models ($n = 42$), even in the case that sex-variable was significant, we defined RIs for the whole group (males and females).

Fifth, age- and BH-related percentile curves and RIs were obtained. To obtain age- and BH-related equations for mean values and SD, we used parametric regression methods based on fractional polynomials (Royston and Wright, 1998; Díaz et al., 2018; Zócalo et al., 2020; Bia and Zócalo, 2021; Zócalo and Bia, 2021a,b). Briefly, fitting fractional polynomials, age-specific (and BH-specific) mean value and SD regression curves were defined for the different variables (e.g., AIx@75_SCOR_Radial) using an iterative procedure (generalized least squares). Then, age-specific (and BH-specific) equations were obtained for the different indexes. For instance, AIx@75_SCOR_Radial equation would be: "AIx@75_SCOR_Radial mean value = $a + b^*Age^p + c^*Age^q + .$," where a, b, c, are the coefficients, and p and q are the powers, with numbers selected from the set [−2, −1, −0.5, 0, 0.5, 1, 2, 3] estimated from the regression for mean AIx@75_SCOR_Radial curve, and likewise from the regression for SD curve. Fractional polynomials with powers [1,2], that is, with p = 1 and q = 2, illustrate an equation with the form $a + b^*Age + c^*Age^2$ (Royston and Wright, 1998). Residuals were used to assess the model fit, which was deemed appropriate if the scores were normally distributed, with a mean of 0 and a SD of 1,

TABLE 3 | Agreement between central waveform-derived indexes obtained with carotid and radial applanation tonometry and brachial oscillometry: Concordance Correlation and Bland–Altman analysis.

Method A	**MOG_Brachial**	**MOG_Brachial**	**SCOR_Radial**	**MOG_Brachial**	**MOG_Brachial**	**SCOR_Radial**
Method B	**SCOR_Radial**	**SCOR_Carotid**	**SCOR_Carotid**	**SCOR_Radial**	**SCOR_Carotid**	**SCOR_Carotid**
	Augmentation Pressure (AP; mmHg)			**AIx@75 (%)**		
Concordance Correlation Coefficient						
CCC	0.4246	0.2139	0.5521	0.3316	0.1163	0.4771
95% C.I. CCC	0.38 to 0.46	0.18 to 0.24	0.53 to 0.57	0.29 to 0.37	0.09 to 0.13	0.45 to 0.49
Pearson ρ (precision)	0.5198	0.4587	0.7675	0.4218	0.3184	0.709
Bias correction factor (accuracy)	0.8169	0.4662	0.7193	0.7862	0.3653	0.6729
Bland–Altman						
Mean Error (Method A–B)	3.8533	10.5921	5.9383	8.8828	26.7975	15.9068
Mean Error, 95% C.I.	3.53 to 4.17	9.99 to 11.18	5.60 to 6.26	8.07 to 9.68	25.63 to 27.96	15.28 to 16.53
P (H_0: Mean Error = 0)	<1.0E-14	<1.0E-14	<1.0E-14	<1.0E-14	<1.0E-14	<1.0E-14
Lower limit, Mean Error	−7.3202	−9.352	−9.4158	−18.8699	−12.0174	−13.0218
Upper limit, Mean Error	15.0267	30.5362	21.2924	36.6355	65.6124	44.8354
Regression Equation	y = 4.42-0.10×	y = 12.55-0.90×	y = 7.15-0.61×	y = 13.82-0.34×	y = 31.07-0.82×	y = 17.58-0.42×
Intercept, *p* value	<1.0E-14	<1.0E-14	<1.0E-14	<1.0E-14	<1.0E-14	<1.0E-14
Slope, *p* value	0.0014	<1.0E-14	<1.0E-14	<1.0E-14	<1.0E-14	<1.0E-14
	Forward pressure (Pf; mmHg)			**Backward pressure (Pb; mmHg)**		
Concordance Correlation Coefficient						
CCC	0.2859	0.08184	0.367	0.4306	0.3032	0.6187
95% C.I. CCC	0.24 to 0.32	0.05 to 0.10	0.34 to 0.39	0.38 to 0.47	0.25 to 0.35	0.59 to 0.64
Pearson ρ (precision)	0.3501	0.2197	0.572	0.4329	0.3688	0.7155
Bias correction factor (accuracy)	0.8166	0.3725	0.6417	0.9947	0.8222	0.8647
Bland–Altman						
Mean Error (Method A–B)	−5.3221	−17.7235	−10.5389	−0.113	−3.5821	−2.9946
Mean Error, 95% C.I.	−5.88 to −4.76	−18.62 to −16.81	−11.03 to −10.04	−0.41 to 0.18	−4.01 to −3.14	−3.21 to −2.77
P (H_0: Mean Error = 0)	<1.0E-14	<1.0E-14	<1.0E-14	0.4614	<1.0E-14	<1.0E-14
Lower limit, Mean Error	−24.5978	−45.6596	−31.9075	−10.4926	−17.0728	−12.4717
Upper limit, Mean Error	13.9536	10.2126	10.8296	10.2665	9.9087	6.4826
Regression Equation	y = 3.52-0.33×	y = 12.00-0.90×	y = 6.64-0.49×	y = −2.11 + 0.14×	y = 2.66-0.38×	y = 2.21-0.30×
Intercept, *p* value	0.0011	<1.0E-14	<1.0E-14	0.0001	0.000291	7.39E-11
Slope, *p* value	<1.0E-14	<1.0E-14	<1.0E-14	0.000124	<1.0E-14	<1.0E-14
	Reflection Magnitude (RM; Pb/Pf)			**Reflection Index {RIx; [Pb/(Pf + Pb)]}**		
Concordance Correlation Coefficient						
CCC	0.307	0.2321	0.6592	0.2759	0.2016	0.6286
95% C.I. CCC	0.26 to 0.34	0.19 to 0.26	0.63 to 0.68	0.23 to 0.31	0.17 to 0.23	0.60 to 0.65
Pearson ρ (precision)	0.413	0.4322	0.7014	0.3872	0.4164	0.6852
Bias correction factor (accuracy)	0.7432	0.537	0.9397	0.7125	0.484	0.9175
Bland–Altman						
Mean Error (Method A–B)	0.08005	0.148	0.06211	0.03757	0.06985	0.02883
Mean Error, 95% C.I.	0.071 to 0.088	0.13 to 0.15	0.055 to 0.068	0.034 to 0.041	0.065 to 0.074	0.026to 0.031
P (H_0: Mean Error = 0)	<1.0E-14	<1.0E-14	<1.0E-14	<1.0E-14	<1.0E-14	<1.0E-14
Lower limit, Mean Error	−0.2138	−0.1578	−0.2067	−0.08566	−0.06858	−0.08882
Upper limit, Mean Error	0.3739	0.4539	0.331	0.1608	0.2083	0.1465
Regression Equation (y=)	0.472-0.701×	0.566-0.785×	0.105-0.0811×	0.287-0.707×	0.376-0.899×	0.095-0.198×
Intercept, *p* value	<1.0E-14	<1.0E-14	<1.0E-14	<1.0E-14	<1.0E-14	<1.0E-14
Slope, *p* value	<1.0E-14	<1.0E-14	0.0000321	<1.0E-14	<1.0E-14	<1.0E-14

CCC, Concordance correlation coefficient; SCOR, SphygmoCor device; MOG, Mobil-O-Graph device; Bland–Altman test: (y: Method A–Method B; x: Mean of both Methods). AIx@75, Augmentation Index adjusted by HR equal 75 beats/minute.

randomly scattered above and below 0 when plotted against age (or BH). Best-fit curves, according to visual and mathematical criteria (Kurtosis and Skewness coefficients), were selected. From the equations obtained, age- and BH-specific percentiles were defined using the standard normal distribution (Z) (**Supplementary Tables 12, 13**).

Detailed age- and BH-related RIs and percentile curves data can be found in **Supplementary Tables 14–76** (for age) and 77–139 (for BH) and in **Supplementary Material 2** (**Supplementary Figures 1–21**; for age) and 3 (**Supplementary Figures 22–42**; for BH). **Figure 2** exemplifies age-related percentile curves for AIx@75_MOG, AIx@75_SCOR_Radial and AIx@75_SCOR_Carotid. **Table 4** shows a summary (5 y intervals) of the age-related RIs (p50th, p75th, p90th, p95th, p97.5th, p99th) for each waveform-derived index. **Table 5** shows a summary (10 cm intervals) of BH-related RIs (p50th, p75th, p90th, p95th, p97.5th, p99th) for each waveform-derived index.

TABLE 4 | Age-related reference intervals for central waveform-derived indexes (All: Females and Males).

	Brachial Oscillometry (MOG)						Radial Artery Tonometry (SCOR)						Carotid Artery Tonometry (SCOR)					
Age [y]	**50th**	**75th**	**90th**	**95th**	**97.5th**	**99th**	**50th**	**75th**	**90th**	**95th**	**97.5th**	**99th**	**50th**	**75th**	**90th**	**95th**	**97.5th**	**99th**
Augmentation Pressure (AP; mmHg)																		
3	4.51	5.83	7.42	8.62	9.85	11.56	5.93	6.96	7.89	8.45	8.93	9.50	0.18	1.86	3.35	4.23	5.00	5.88
5	4.41	5.90	7.78	9.23	10.77	12.94	2.79	4.40	5.86	6.75	7.52	8.42	−4.73	−1.72	0.94	2.51	3.86	5.41
10	4.55	6.36	8.76	10.71	12.84	15.97	0.29	2.54	4.60	5.84	6.93	8.21	−8.72	−4.16	−0.19	2.14	4.13	6.42
15	4.82	6.92	9.78	12.17	14.83	18.82	0.01	2.55	4.87	6.28	7.51	8.95	−9.05	−3.85	0.66	3.30	5.56	8.14
20	5.14	7.52	10.83	13.65	16.83	21.68	0.46	3.16	5.63	7.13	8.44	9.98	−8.14	−2.65	2.11	4.89	7.26	9.98
25	5.49	8.15	11.92	15.18	18.88	24.62	1.25	4.04	6.60	8.15	9.51	11.11	−6.68	−1.08	3.78	6.61	9.04	11.82
30	5.87	8.81	13.05	16.76	21.02	27.69	2.22	5.07	7.68	9.26	10.65	12.28	−4.95	0.66	5.53	8.38	10.81	13.60
35	6.27	9.51	14.24	18.41	23.25	30.90	3.29	6.18	8.81	10.42	11.82	13.46	−3.10	2.46	7.30	10.13	12.55	15.32
40	6.69	10.24	15.48	20.15	25.59	34.28	4.43	7.33	9.98	11.59	12.99	14.64	−1.19	4.29	9.06	11.85	14.24	16.98
45	7.13	11.01	16.78	21.97	28.07	37.86	5.61	8.51	11.16	12.76	14.16	15.81	0.74	6.11	10.79	13.54	15.89	18.58
50	7.59	11.81	18.15	23.89	30.68	41.66	6.82	9.71	12.34	13.94	15.33	16.97	2.66	7.91	12.49	15.18	17.48	20.13
55	8.08	12.66	19.59	25.92	33.44	45.69	8.04	10.91	13.52	15.11	16.49	18.11	4.57	9.69	14.16	16.78	19.03	21.62
60	8.59	13.55	21.11	28.05	36.36	49.97	9.27	12.11	14.70	16.27	17.64	19.24	6.45	11.43	15.78	18.35	20.54	23.06
65	9.13	14.48	22.71	30.32	39.46	54.53	10.50	13.31	15.87	17.42	18.78	20.36	8.31	13.14	17.37	19.87	22.00	24.46
70	9.69	15.46	24.40	32.71	42.75	59.38	11.74	14.51	17.04	18.57	19.90	21.46	10.13	14.82	18.93	21.35	23.43	25.82
75	10.28	16.50	26.18	35.24	46.24	64.56	12.97	15.71	18.20	19.70	21.01	22.55	11.92	16.46	20.45	22.80	24.82	27.14
80	10.90	17.58	28.07	37.92	49.94	70.07	14.21	16.90	19.34	20.82	22.11	23.62	13.67	18.07	21.93	24.21	26.17	28.42
84	11.42	18.49	29.65	40.18	53.07	74.74	15.19	17.85	20.26	21.71	22.98	24.47	15.05	19.33	23.09	25.32	27.23	29.43
Augmentation Index (AIx; %)																		
3	27.09	33.61	39.96	44.01	47.66	52.07	22.90	29.39	35.33	38.95	42.11	45.82	−8.86	−2.81	2.88	6.41	9.53	13.25
5	20.53	25.82	30.99	34.27	37.24	40.82	12.03	19.07	25.56	29.52	32.99	37.07	−16.25	−8.24	−0.53	4.32	8.67	13.89
10	15.21	19.73	24.16	26.99	29.55	32.65	2.95	10.49	17.48	21.76	25.53	29.97	−20.98	−11.00	−1.17	5.12	10.81	17.68
15	14.02	18.60	23.11	26.00	28.61	31.79	1.21	8.94	16.11	20.52	24.39	28.96	−20.49	−9.60	1.21	8.14	14.42	22.03
20	14.13	19.02	23.87	26.98	29.81	33.25	1.91	9.73	16.99	21.45	25.37	29.99	−18.32	−6.85	4.51	11.80	18.40	26.39
25	14.85	20.19	25.50	28.92	32.03	35.82	3.75	11.62	18.91	23.38	27.32	31.96	−15.33	−3.49	8.21	15.70	22.47	30.66
30	15.93	21.78	27.63	31.42	34.86	39.07	6.22	14.10	21.39	25.86	29.79	34.43	−11.87	0.23	12.12	19.70	26.55	34.82
35	17.23	23.67	30.12	34.30	38.11	42.77	9.07	16.94	24.22	28.67	32.58	37.19	−8.10	4.15	16.13	23.75	30.61	38.89
40	18.71	25.77	32.86	37.47	41.68	46.83	12.17	20.02	27.26	31.68	35.57	40.14	−4.09	8.23	20.21	27.81	34.63	42.86
45	20.32	28.03	35.81	40.87	45.50	51.16	15.45	23.25	30.44	34.83	38.67	43.20	0.09	12.41	24.33	31.86	38.62	46.74
50	22.03	30.43	38.93	44.46	49.53	55.74	18.85	26.60	33.72	38.06	41.87	46.34	4.41	16.67	28.48	35.91	42.56	50.55
55	23.83	32.95	42.19	48.22	53.75	60.52	22.34	30.01	37.06	41.35	45.11	49.53	8.85	21.00	32.63	39.94	46.47	54.28
60	25.70	35.57	45.59	52.13	58.13	65.48	25.89	33.49	40.45	44.68	48.40	52.75	13.38	25.37	36.80	43.95	50.33	57.96
65	27.65	38.28	49.10	56.16	62.65	70.62	29.49	37.00	43.86	48.04	51.70	55.99	18.00	29.78	40.96	47.94	54.16	61.57
70	29.66	41.08	52.71	60.32	67.32	75.90	33.13	40.53	47.30	51.42	55.02	59.24	22.70	34.23	45.13	51.91	57.95	65.13
75	31.72	43.95	56.43	64.60	72.11	81.33	36.79	44.08	50.75	54.80	58.34	62.49	27.45	38.70	49.29	55.87	61.70	68.64
80	33.83	46.89	60.23	68.97	77.01	86.89	40.46	47.65	54.20	58.18	61.66	65.74	32.27	43.20	53.45	59.80	65.43	72.11
84	35.56	49.29	63.34	72.55	81.02	91.43	43.41	50.50	56.97	60.89	64.31	68.33	36.16	46.81	56.77	62.93	68.39	74.85
Augmentation Index adjusted by heart rate 75 beats/minute (AIx@75; %)																		
3	48.03	55.03	61.52	65.50	69.00	73.14	35.65	41.99	47.68	51.11	54.08	57.54	6.08	11.03	15.54	18.27	20.67	23.47
5	32.39	39.21	45.58	49.52	53.00	57.12	20.36	27.48	33.88	37.73	41.08	44.97	−7.39	0.03	6.88	11.08	14.77	19.12
10	17.82	24.39	30.66	34.57	38.05	42.19	5.70	13.61	20.73	25.02	28.74	33.08	−18.53	−8.74	0.49	6.20	11.25	17.24
15	12.87	19.41	25.71	29.67	33.21	37.45	1.30	9.48	16.87	21.31	25.17	29.67	−20.73	−9.95	0.25	6.60	12.23	18.91
20	10.99	17.61	24.04	28.10	31.73	36.08	0.48	8.77	16.25	20.76	24.67	29.23	−20.00	−8.69	2.04	8.71	14.63	21.67
25	10.52	17.30	23.91	28.09	31.83	36.32	1.37	9.69	17.19	21.71	25.63	30.20	−17.90	−6.27	4.74	11.59	17.66	24.88
30	10.83	17.82	24.64	28.95	32.81	37.45	3.22	11.51	18.99	23.49	27.40	31.96	−15.03	−3.22	7.94	14.87	21.01	28.30
35	11.64	18.87	25.91	30.36	34.35	39.14	5.65	13.88	21.31	25.78	29.66	34.18	−11.67	0.22	11.43	18.37	24.52	31.82
40	12.79	20.28	27.56	32.16	36.28	41.21	8.44	16.60	23.96	28.38	32.22	36.70	−7.99	3.92	15.10	22.02	28.13	35.38
45	14.19	21.95	29.48	34.22	38.47	43.56	11.48	19.55	26.82	31.19	34.99	39.41	−4.07	7.78	18.88	25.74	31.79	38.96
50	15.79	23.82	31.60	36.49	40.87	46.12	14.69	22.65	29.83	34.14	37.89	42.26	0.02	11.77	22.75	29.51	35.47	42.53
55	17.55	25.86	33.88	38.92	43.43	48.83	18.01	25.87	32.94	37.19	40.88	45.18	4.24	15.85	26.66	33.30	39.16	46.09
60	19.44	28.02	36.29	41.48	46.12	51.67	21.41	29.15	36.11	40.30	43.93	48.17	8.57	19.99	30.60	37.11	42.85	49.62
65	21.44	30.29	38.81	44.14	48.91	54.60	24.86	32.47	39.33	43.45	47.02	51.19	12.97	24.17	34.56	40.92	46.52	53.13
70	23.53	32.66	41.41	46.89	51.78	57.62	28.35	35.83	42.57	46.62	50.13	54.23	17.43	28.39	38.52	44.73	50.18	56.61
75	25.70	35.10	44.09	49.71	54.73	60.71	31.85	39.21	45.83	49.81	53.26	57.28	21.94	32.63	42.50	48.52	53.82	60.06
80	27.94	37.60	46.83	52.59	57.73	63.86	35.37	42.59	49.09	53.00	56.39	60.33	26.49	36.89	46.47	52.31	57.44	63.48
84	29.78	39.65	49.06	54.94	60.17	66.41	38.18	45.30	51.70	55.55	58.89	62.78	30.15	40.30	49.64	55.33	60.32	66.19

(Continued)

TABLE 4 | (Continued)

	Brachial Oscillometry (MOG)						Radial Artery Tonometry (SCOR)						Carotid Artery Tonometry (SCOR)					
Age [y]	**50th**	**75th**	**90th**	**95th**	**97.5th**	**99th**	**50th**	**75th**	**90th**	**95th**	**97.5th**	**99th**	**50th**	**75th**	**90th**	**95th**	**97.5th**	**99th**
Forward pressure (Pf; mmHg)																		
3	12.39	13.66	14.90	15.69	16.42	17.31	12.94	15.40	17.98	19.73	21.37	23.44	17.45	21.43	25.77	28.78	31.68	35.41
5	14.98	16.90	18.82	20.08	21.23	22.66	18.40	22.05	25.92	28.54	31.02	34.16	22.91	28.00	33.53	37.35	41.01	45.73
10	22.33	26.47	30.84	33.80	36.59	40.13	26.39	31.87	37.71	41.69	45.47	50.27	39.72	48.62	58.29	64.98	71.41	79.68
15	24.60	29.55	34.83	38.44	41.87	46.24	30.14	36.51	43.32	47.97	52.38	58.01	43.00	52.98	63.89	71.48	78.79	88.23
20	24.94	30.02	35.44	39.15	42.68	47.18	31.73	38.49	45.72	50.66	55.36	61.35	42.92	53.14	64.36	72.20	79.76	89.55
25	24.59	29.52	34.77	38.36	41.78	46.13	32.10	38.96	46.30	51.32	56.09	62.18	41.65	51.71	62.78	70.52	78.01	87.71
30	24.04	28.74	33.73	37.13	40.36	44.46	31.74	38.53	45.79	50.76	55.48	61.51	40.07	49.78	60.46	67.94	75.17	84.55
35	23.50	27.97	32.69	35.89	38.93	42.78	30.94	37.55	44.63	49.46	54.06	59.93	38.54	47.80	58.00	65.12	72.01	80.93
40	23.08	27.33	31.81	34.84	37.70	41.32	29.89	36.26	43.07	47.73	52.16	57.80	37.19	45.99	55.64	62.38	68.88	77.29
45	22.79	26.88	31.16	34.04	36.76	40.19	28.68	34.78	41.29	45.74	49.98	55.37	36.07	44.41	53.51	59.85	65.94	73.81
50	22.67	26.62	30.75	33.52	36.13	39.42	27.40	33.20	39.40	43.63	47.65	52.78	35.20	43.09	51.65	57.58	63.27	70.60
55	22.70	26.56	30.59	33.28	35.81	39.00	26.09	31.59	37.46	41.47	45.28	50.13	34.58	42.02	50.06	55.59	60.89	67.68
60	22.89	26.71	30.67	33.33	35.81	38.93	24.78	29.98	35.53	39.31	42.91	47.49	34.19	41.21	48.73	53.88	58.79	65.06
65	23.25	27.06	31.01	33.65	36.11	39.21	23.49	28.40	33.63	37.20	40.58	44.90	34.01	40.63	47.65	52.44	56.97	62.74
70	23.77	27.62	31.59	34.24	36.73	39.84	22.24	26.86	31.79	35.14	38.33	42.38	34.05	40.27	46.81	51.23	55.40	60.68
75	24.46	28.38	32.43	35.13	37.65	40.81	21.03	25.38	30.01	33.17	36.16	39.96	34.29	40.12	46.19	50.25	54.07	58.87
80	25.33	29.36	33.53	36.30	38.90	42.14	19.87	23.96	28.31	31.27	34.08	37.65	34.74	40.17	45.76	49.48	52.96	57.30
84	26.15	30.31	34.61	37.47	40.14	43.48	18.99	22.88	27.01	29.83	32.49	35.88	35.23	40.35	45.57	49.01	52.21	56.20
Backward pressure (Pb; mmHg)																		
3	6.67	7.46	8.24	8.75	9.22	9.80	6.97	8.03	9.12	9.84	10.52	11.36	8.17	9.91	11.78	13.06	14.29	15.87
5	7.99	9.20	10.44	11.26	12.03	12.99	8.25	9.56	10.92	11.82	12.66	13.72	9.47	11.42	13.52	14.95	16.32	18.07
10	12.05	14.75	17.70	19.74	21.69	24.22	11.96	14.03	16.20	17.65	19.02	20.74	13.53	16.25	19.16	21.14	23.02	25.43
15	13.76	17.08	20.73	23.29	25.76	28.97	13.02	15.31	17.71	19.32	20.84	22.76	15.01	18.08	21.37	23.62	25.76	28.49
20	14.47	17.94	21.77	24.44	27.02	30.37	13.53	15.91	18.40	20.08	21.66	23.65	15.89	19.20	22.75	25.19	27.51	30.49
25	14.74	18.17	21.91	24.52	27.02	30.27	13.84	16.26	18.80	20.51	22.11	24.13	16.50	19.99	23.74	26.32	28.78	31.93
30	14.84	18.13	21.69	24.16	26.52	29.56	14.09	16.54	19.10	20.82	22.44	24.48	17.00	20.62	24.52	27.20	29.77	33.05
35	14.88	18.00	21.36	23.66	25.87	28.68	14.36	16.83	19.41	21.15	22.78	24.83	17.45	21.17	25.19	27.96	30.60	33.99
40	14.91	17.88	21.03	23.18	25.23	27.84	14.67	17.17	19.78	21.53	23.17	25.23	17.88	21.70	25.81	28.64	31.35	34.81
45	14.99	17.80	20.77	22.79	24.69	27.11	15.04	17.58	20.22	21.99	23.65	25.74	18.34	22.23	26.42	29.29	32.05	35.57
50	15.11	17.80	20.61	22.50	24.29	26.54	15.48	18.07	20.75	22.55	24.24	26.36	18.82	22.77	27.02	29.94	32.72	36.29
55	15.30	17.88	20.55	22.35	24.03	26.14	16.00	18.65	21.39	23.23	24.95	27.11	19.34	23.35	27.64	30.59	33.40	36.99
60	15.56	18.04	20.61	22.33	23.93	25.93	16.61	19.33	22.15	24.03	25.79	28.00	19.90	23.96	28.29	31.26	34.08	37.69
65	15.89	18.31	20.79	22.44	23.98	25.90	17.31	20.12	23.02	24.96	26.77	29.04	20.52	24.62	28.98	31.96	34.79	38.40
70	16.30	18.67	21.10	22.70	24.19	26.04	18.12	21.02	24.03	26.03	27.90	30.25	21.19	25.32	29.71	32.69	35.52	39.12
75	16.79	19.14	21.52	23.10	24.55	26.36	19.03	22.06	25.18	27.26	29.20	31.63	21.93	26.08	30.48	33.46	36.28	39.86
80	17.36	19.71	22.08	23.64	25.08	26.86	20.06	23.22	26.48	28.65	30.67	33.20	22.73	26.90	31.30	34.27	37.07	40.62
84	17.89	20.25	22.63	24.18	25.62	27.40	20.98	24.26	27.64	29.89	31.98	34.61	23.42	27.60	31.99	34.95	37.74	41.26
Reflection Magnitude (RM)																		
3	0.54	0.59	0.63	0.66	0.68	0.70	0.65	0.73	0.80	0.85	0.89	0.95	0.42	0.49	0.56	0.61	0.65	0.70
5	0.54	0.59	0.64	0.66	0.68	0.70	0.53	0.59	0.67	0.71	0.76	0.81	0.38	0.45	0.52	0.56	0.60	0.66
10	0.56	0.61	0.65	0.67	0.69	0.72	0.44	0.50	0.57	0.62	0.67	0.72	0.35	0.42	0.50	0.54	0.59	0.64
15	0.58	0.62	0.67	0.69	0.71	0.73	0.42	0.49	0.56	0.61	0.66	0.72	0.36	0.43	0.51	0.56	0.61	0.66
20	0.59	0.64	0.68	0.70	0.72	0.74	0.42	0.50	0.58	0.63	0.68	0.74	0.37	0.45	0.53	0.59	0.63	0.70
25	0.61	0.65	0.69	0.72	0.73	0.76	0.44	0.52	0.60	0.66	0.71	0.78	0.39	0.48	0.56	0.62	0.67	0.73
30	0.62	0.67	0.71	0.73	0.75	0.77	0.46	0.54	0.63	0.69	0.75	0.83	0.42	0.51	0.59	0.65	0.71	0.78
35	0.63	0.68	0.72	0.74	0.76	0.78	0.49	0.57	0.67	0.74	0.80	0.88	0.44	0.54	0.63	0.69	0.75	0.82
40	0.64	0.69	0.73	0.75	0.77	0.79	0.51	0.61	0.71	0.78	0.85	0.94	0.47	0.57	0.67	0.73	0.79	0.86
45	0.66	0.70	0.74	0.76	0.78	0.80	0.55	0.65	0.76	0.84	0.91	1.01	0.50	0.60	0.70	0.77	0.83	0.91
50	0.67	0.71	0.75	0.77	0.79	0.81	0.58	0.69	0.81	0.90	0.98	1.08	0.53	0.64	0.74	0.81	0.88	0.96
55	0.68	0.72	0.76	0.78	0.80	0.82	0.62	0.74	0.87	0.96	1.05	1.16	0.56	0.67	0.78	0.86	0.93	1.01
60	0.69	0.73	0.77	0.79	0.80	0.82	0.67	0.79	0.93	1.03	1.12	1.24	0.59	0.71	0.83	0.90	0.97	1.06
65	0.69	0.74	0.77	0.79	0.81	0.83	0.71	0.85	1.00	1.10	1.20	1.34	0.62	0.75	0.87	0.95	1.02	1.11
70	0.70	0.74	0.78	0.80	0.82	0.84	0.76	0.91	1.07	1.18	1.29	1.43	0.66	0.78	0.91	0.99	1.07	1.16
75	0.71	0.75	0.79	0.81	0.83	0.85	0.82	0.98	1.15	1.27	1.39	1.54	0.69	0.82	0.95	1.04	1.12	1.22
80	0.72	0.76	0.80	0.82	0.83	0.85	0.87	1.05	1.23	1.36	1.49	1.65	0.73	0.86	1.00	1.09	1.17	1.27
84	0.73	0.77	0.80	0.82	0.84	0.86	0.92	1.11	1.30	1.44	1.58	1.75	0.76	0.90	1.04	1.13	1.21	1.32

(Continued)

TABLE 4 | (Continued)

	Brachial Oscillometry (MOG)						Radial Artery Tonometry (SCOR)						Carotid Artery Tonometry (SCOR)					
Age [y]	**50th**	**75th**	**90th**	**95th**	**97.5th**	**99th**	**50th**	**75th**	**90th**	**95th**	**97.5th**	**99th**	**50th**	**75th**	**90th**	**95th**	**97.5th**	**99th**
Reflection Index (RIx)																		
3	0.35	0.37	0.39	0.40	0.40	0.41	0.39	0.42	0.44	0.46	0.47	0.49	0.30	0.33	0.36	0.38	0.39	0.41
5	0.35	0.37	0.39	0.40	0.41	0.41	0.34	0.37	0.40	0.42	0.43	0.45	0.27	0.31	0.34	0.36	0.38	0.40
10	0.36	0.38	0.39	0.40	0.41	0.42	0.30	0.34	0.36	0.38	0.40	0.42	0.26	0.30	0.33	0.35	0.37	0.39
15	0.37	0.38	0.40	0.41	0.42	0.42	0.30	0.33	0.36	0.38	0.40	0.42	0.26	0.30	0.34	0.36	0.38	0.40
20	0.37	0.39	0.40	0.41	0.42	0.43	0.30	0.33	0.37	0.39	0.40	0.43	0.27	0.31	0.35	0.37	0.39	0.41
25	0.38	0.40	0.41	0.42	0.42	0.43	0.31	0.34	0.37	0.40	0.42	0.44	0.28	0.32	0.36	0.38	0.40	0.42
30	0.38	0.40	0.41	0.42	0.43	0.44	0.32	0.35	0.39	0.41	0.43	0.45	0.29	0.34	0.37	0.40	0.42	0.44
35	0.39	0.40	0.42	0.43	0.43	0.44	0.33	0.36	0.40	0.42	0.44	0.47	0.31	0.35	0.39	0.41	0.43	0.45
40	0.39	0.41	0.42	0.43	0.44	0.44	0.34	0.38	0.42	0.44	0.46	0.49	0.32	0.36	0.40	0.42	0.44	0.47
45	0.40	0.41	0.42	0.43	0.44	0.45	0.35	0.39	0.43	0.46	0.48	0.50	0.33	0.37	0.41	0.44	0.46	0.48
50	0.40	0.42	0.43	0.44	0.44	0.45	0.37	0.41	0.45	0.47	0.50	0.52	0.34	0.39	0.43	0.45	0.47	0.50
55	0.40	0.42	0.43	0.44	0.44	0.45	0.38	0.43	0.47	0.49	0.51	0.54	0.36	0.40	0.44	0.46	0.49	0.51
60	0.41	0.42	0.43	0.44	0.45	0.45	0.40	0.44	0.48	0.51	0.53	0.56	0.37	0.41	0.45	0.48	0.50	0.52
65	0.41	0.42	0.44	0.44	0.45	0.46	0.42	0.46	0.50	0.53	0.55	0.58	0.38	0.43	0.47	0.49	0.51	0.54
70	0.41	0.43	0.44	0.45	0.45	0.46	0.43	0.48	0.52	0.55	0.57	0.60	0.40	0.44	0.48	0.50	0.53	0.55
75	0.42	0.43	0.44	0.45	0.45	0.46	0.45	0.50	0.54	0.57	0.59	0.62	0.41	0.45	0.49	0.52	0.54	0.56
80	0.42	0.43	0.44	0.45	0.46	0.46	0.47	0.51	0.56	0.59	0.61	0.64	0.42	0.47	0.51	0.53	0.55	0.58
84	0.42	0.43	0.45	0.45	0.46	0.46	0.48	0.53	0.58	0.60	0.63	0.66	0.43	0.48	0.52	0.54	0.56	0.59

SCOR, SphygmoCor device; MOG, Mobil-O-Graph device; Percentiles, 50th, 75th, 90th, 95th, 97.5th, and 99th; y, years old.

The minimum sample size required was 377 (Bellera and Hanley, 2007). Like in previous works and according to the central limit theorem, normal distribution was considered (considering Kurtosis and Skewness coefficients distribution and sample size >30) (Lumley et al., 2002). Data analysis was done using MedCalc-Statistical software (v.18.5, MedCalc Inc., Ostend, Belgium) and IBM-statistical package for the social sciences (SPSS) software (v.26, SPSS Inc., IL, United States). PROCESS v.3.5 (SPSS extension) was used for moderation (interaction) analysis (Hayes, 2020). A $p < 0.05$ was considered statistically significant.

RESULTS

Agreement of Waveform-Derived Indices Obtained From Carotid, Radial, and Brachial Recordings

Table 3 (**Supplementary Table 4**) shows correlation coefficients and Bland–Altman analyses carried out to determine the agreement between data of a "similar waveform-derived index" obtained with different devices and/or approaches. Although the associations between indexes (e.g., Pb obtained with different approaches) were significant (95% CI did not cross zero), they were "weak" or "moderate." Then, regardless of whether AP, AIx@75, Pf, Pb, RM, or RIx were considered: (i) the levels of association were always statistically significant and (ii) in all cases, concordance correlation coefficients showed low agreement between data (values were always <0.66). For instance, concordance correlation coefficients [95% CI] were 0.43 [0.38–0.47], 0.30 [0.25–0.35], and 0.62 [0.59–0.64] for the association between (i) Pb_MOG and Pb_SCOR_Radial, (ii) Pb_MOG and Pb_SCOR_Carotid and (iii) Pb_SCOR_Radial and Pb_SCOR_Carotid, respectively. It is to note that the highest levels of association were obtained when analyzing carotid and radial tonometry data (SCOR_Radial and SCOR_Carotid), whereas data from brachial oscillometry (MOG) and carotid tonometry (SCOR_Carotid) showed the lowest levels of association (**Table 3** and **Supplementary Table 4**).

Bland–Altman tests showed not only significant systematic, but also proportional differences (errors). Then the differences varied in magnitude depending on the index values (**Table 3** and **Supplementary Table 4**). The highest systematic (mean) errors were obtained when analyzing agreement between MOG and carotid tonometry (SCOR_Carotid). As a result, specific RIs for all the waveform-derived indexes obtained were defined as necessary.

Age-, Sex-, and/or Body Height-Related Differences

Age, BH, and/or sex-specific RIs for a given waveform-derived index (e.g., AIx@75) may (or may not) be required, depending on the approach used for its measurement (MOG *vs.* SCOR_Carotid *vs.* SCOR_Radial). For instance, Pb_MOG was independently associated with sex and BH, but not with age. In turn, Pb_Radial_SCOR and Pb_Carotid_SCOR showed independent associations with age and BH (but not with sex). AIx@75_MOG was independently associated with sex and age (and BH), without age-dependent changes in the association with sex (non-significant Johnson-Neyman regions).

On the other hand, AIx@75_SCOR_Radial and AIx@75_SCOR_Carotid were associated with age, but not with sex, but in subjects aged 7–8 y and older, sex

TABLE 5 | Body height-related reference intervals for central waveform-derived indexes (All: Females and Males).

	Brachial Oscillometry (MOG)						Radial Artery Tonometry (SCOR)						Carotid Artery Tonometry (SCOR)					
BH [m]	**50th**	**75th**	**90th**	**95th**	**97.5th**	**99th**	**50th**	**75th**	**90th**	**95th**	**97.5th**	**99th**	**50th**	**75th**	**90th**	**95th**	**97.5th**	**99th**
Augmentation Pressure (AP; mmHg)																		
1.0	4.42	6.28	8.78	10.85	13.12	16.51	2.31	3.65	4.86	5.59	6.22	6.97	−5.89	−3.03	−0.50	0.99	2.27	3.75
1.1	4.42	6.02	8.06	9.67	11.39	13.87	2.28	3.95	5.46	6.37	7.17	8.10	−5.73	−2.29	0.74	2.52	4.05	5.81
1.2	4.49	5.99	7.88	9.34	10.89	13.07	2.25	4.24	6.06	7.16	8.12	9.24	−5.58	−1.55	1.97	4.04	5.81	7.86
1.3	4.60	6.16	8.10	9.62	11.21	13.48	2.21	4.54	6.67	7.95	9.08	10.39	−5.42	−0.82	3.19	5.54	7.56	9.87
1.4	4.76	6.48	8.69	10.43	12.29	14.97	2.18	4.84	7.27	8.75	10.04	11.55	−5.27	−0.10	4.40	7.03	9.28	11.87
1.5	4.97	6.98	9.66	11.84	14.22	17.75	2.15	5.14	7.88	9.55	11.01	12.71	−5.11	0.63	5.60	8.51	10.99	13.84
1.6	5.22	7.66	11.08	14.01	17.30	22.37	2.12	5.45	8.50	10.35	11.98	13.88	−4.96	1.35	6.79	9.97	12.69	15.79
1.7	5.51	8.55	13.10	17.22	22.08	29.92	2.09	5.75	9.11	11.16	12.95	15.06	−4.81	2.06	7.98	11.43	14.37	17.73
1.8	5.85	9.69	15.94	21.99	29.54	42.54	2.05	6.05	9.73	11.97	13.94	16.25	−4.65	2.78	9.15	12.87	16.03	19.64
1.9	6.23	11.15	19.93	29.17	41.52	64.58	2.02	6.35	10.35	12.78	14.92	17.44	−4.50	3.49	10.32	14.30	17.68	21.53
Augmentation Index (AIx; %)																		
1.0	20.29	25.18	29.92	32.92	35.63	38.89	12.66	19.00	24.83	28.37	31.48	35.13	−18.65	−10.64	−2.90	1.98	6.36	11.62
1.1	19.16	23.95	28.62	31.58	34.25	37.47	10.69	17.96	24.65	28.74	32.34	36.56	−17.70	−8.71	0.03	5.57	10.55	16.55
1.2	18.21	23.04	27.75	30.74	33.45	36.71	9.18	17.19	24.60	29.13	33.11	37.81	−16.75	−6.74	3.04	9.26	14.87	21.63
1.3	17.41	22.36	27.21	30.30	33.10	36.49	8.04	16.65	24.63	29.52	33.83	38.90	−15.78	−4.74	6.11	13.04	19.29	26.85
1.4	16.73	21.87	26.94	30.18	33.12	36.69	7.23	16.31	24.75	29.93	34.49	39.87	−14.81	−2.71	9.25	16.90	23.83	32.21
1.5	16.15	21.55	26.89	30.33	33.45	37.25	6.69	16.14	24.94	30.34	35.10	40.72	−13.83	−0.64	12.45	20.86	28.48	37.71
1.6	15.66	21.35	27.04	30.70	34.04	38.12	6.38	16.12	25.19	30.76	35.68	41.48	−12.83	1.46	15.72	24.90	33.23	43.35
1.7	15.24	21.27	27.34	31.27	34.86	39.25	6.29	16.23	25.49	31.19	36.21	42.14	−11.83	3.59	19.05	29.03	38.10	49.13
1.8	14.87	21.28	27.77	32.00	35.88	40.63	6.37	16.45	25.84	31.62	36.72	42.74	−10.82	5.76	22.45	33.24	43.08	55.05
1.9	14.56	21.38	28.34	32.89	37.08	42.22	6.61	16.77	26.23	32.06	37.19	43.26	−9.80	7.95	25.90	37.54	48.16	61.10
Augmentation Index adjusted by heart rate 75 beats/minute (AIx@75; %)																		
1.0	32.40	36.84	40.93	43.44	45.64	48.24	18.41	23.51	28.09	30.84	33.23	36.01	−8.09	−2.10	3.41	6.77	9.72	13.19
1.1	29.06	34.82	40.19	43.50	46.42	49.87	16.88	23.73	29.91	33.61	36.84	40.59	−10.17	−1.88	5.83	10.56	14.73	19.66
1.2	25.81	32.43	38.67	42.53	45.95	50.02	15.13	23.30	30.66	35.09	38.93	43.41	−11.70	−1.59	7.87	13.71	18.87	24.98
1.3	22.66	29.79	36.55	40.76	44.50	48.95	13.21	22.30	30.49	35.42	39.70	44.69	−12.78	−1.27	9.58	16.30	22.25	29.31
1.4	19.63	26.97	33.98	38.36	42.26	46.92	11.12	20.78	29.50	34.74	39.30	44.61	−13.48	−0.90	11.01	18.41	24.97	32.76
1.5	16.73	24.04	31.07	35.48	39.41	44.11	8.88	18.81	27.77	33.16	37.85	43.30	−13.86	−0.49	12.20	20.09	27.10	35.43
1.6	13.94	21.05	27.91	32.23	36.09	40.71	6.52	16.44	25.38	30.76	35.44	40.90	−13.97	−0.06	13.16	21.40	28.71	37.41
1.7	11.29	18.04	24.58	28.71	32.41	36.84	4.04	13.69	22.39	27.63	32.19	37.49	−13.82	0.40	13.94	22.37	29.87	38.78
1.8	8.77	15.04	21.15	25.01	28.48	32.63	1.46	10.61	18.86	23.83	28.15	33.19	−13.46	0.88	14.54	23.05	30.61	39.60
1.9	6.39	12.09	17.67	21.20	24.38	28.19	−1.21	7.23	14.84	19.42	23.41	28.05	−12.91	1.39	14.99	23.46	30.98	39.93
Forward pressure (Pf; mmHg)																		
1.0	15.29	17.09	19.04	20.39	21.69	23.40	17.03	19.76	22.55	24.40	26.13	28.28	27.84	32.96	38.29	41.85	45.18	49.36
1.1	16.39	18.57	20.98	22.69	24.36	26.58	19.42	23.02	26.78	29.32	31.70	34.70	30.51	36.87	43.60	48.15	52.45	57.89
1.2	17.57	20.16	23.07	25.16	27.25	30.07	21.71	26.12	30.80	33.98	36.99	40.82	32.94	40.37	48.33	53.77	58.94	65.52
1.3	18.85	21.86	25.32	27.85	30.41	33.92	23.87	28.99	34.48	38.23	41.80	46.36	35.10	43.43	52.42	58.60	64.49	72.03
1.4	20.22	23.70	27.75	30.77	33.86	38.16	25.87	31.58	37.73	41.95	45.98	51.12	37.00	46.03	55.81	62.56	69.01	77.28
1.5	21.72	25.68	30.39	33.95	37.64	42.85	27.70	33.87	40.50	45.06	49.41	54.97	38.64	48.16	58.50	65.63	72.46	81.22
1.6	23.34	27.85	33.28	37.44	41.80	48.04	29.36	35.81	42.75	47.50	52.04	57.83	40.04	49.85	60.49	67.83	74.85	83.85
1.7	25.12	30.21	36.43	41.26	46.38	53.80	30.83	37.42	44.46	49.28	53.86	59.70	41.20	51.10	61.81	69.19	76.23	85.24
1.8	27.07	32.80	39.89	45.47	51.44	60.22	32.12	38.68	45.65	50.39	54.89	60.59	42.13	51.95	62.51	69.76	76.66	85.47
1.9	29.23	35.65	43.71	50.12	57.06	67.38	33.22	39.61	46.34	50.88	55.17	60.59	42.85	52.42	62.64	69.62	76.24	84.66
Backward pressure (Pb; mmHg)																		
1.0	8.37	9.54	10.77	11.61	12.40	13.40	9.02	10.35	11.69	12.55	13.34	14.31	10.25	12.29	14.42	15.83	17.16	18.81
1.1	8.82	10.29	11.89	12.99	14.06	15.44	9.95	11.57	13.20	14.26	15.23	16.44	11.29	13.61	16.03	17.64	19.16	21.06
1.2	9.41	11.19	13.15	14.53	15.88	17.66	10.82	12.69	14.59	15.83	16.97	18.39	12.30	14.89	17.58	19.39	21.09	23.21
1.3	10.16	12.24	14.57	16.24	17.88	20.07	11.64	13.73	15.85	17.24	18.53	20.13	13.30	16.13	19.09	21.07	22.94	25.28
1.4	11.08	13.46	16.18	18.14	20.08	22.69	12.40	14.67	16.98	18.50	19.91	21.65	14.27	17.33	20.53	22.68	24.70	27.24
1.5	12.17	14.89	17.99	20.25	22.50	25.53	13.11	15.52	17.97	19.59	21.09	22.94	15.22	18.49	21.92	24.22	26.38	29.10
1.6	13.48	16.54	20.05	22.61	25.17	28.61	13.76	16.27	18.84	20.52	22.08	24.01	16.15	19.61	23.25	25.69	27.98	30.86
1.7	15.04	18.46	22.38	25.24	28.10	31.96	14.36	16.94	19.57	21.29	22.89	24.86	17.05	20.70	24.52	27.08	29.48	32.51
1.8	16.90	20.69	25.03	28.19	31.34	35.58	14.91	17.53	20.18	21.92	23.52	25.50	17.94	21.75	25.73	28.40	30.90	34.05

(Continued)

TABLE 5 | (Continued)

	Brachial Oscillometry (MOG)						Radial Artery Tonometry (SCOR)						Carotid Artery Tonometry (SCOR)					
BH [m]	**50th**	**75th**	**90th**	**95th**	**97.5th**	**99th**	**50th**	**75th**	**90th**	**95th**	**97.5th**	**99th**	**50th**	**75th**	**90th**	**95th**	**97.5th**	**99th**
1.9	19.11	23.29	28.05	31.49	34.91	39.50	15.41	18.03	20.67	22.39	23.98	25.95	18.80	22.75	26.88	29.65	32.24	35.49
Reflection Magnitude (RM)																		
1.0	0.55	0.59	0.62	0.64	0.65	0.67	0.52	0.58	0.64	0.69	0.72	0.77	0.38	0.44	0.49	0.53	0.56	0.60
1.1	0.55	0.60	0.63	0.66	0.68	0.70	0.51	0.58	0.65	0.70	0.74	0.80	0.38	0.45	0.52	0.56	0.60	0.65
1.2	0.55	0.60	0.65	0.67	0.70	0.72	0.50	0.57	0.65	0.71	0.76	0.83	0.38	0.46	0.54	0.59	0.64	0.70
1.3	0.56	0.61	0.66	0.69	0.71	0.74	0.49	0.57	0.66	0.72	0.78	0.85	0.38	0.47	0.56	0.62	0.68	0.75
1.4	0.56	0.62	0.67	0.70	0.72	0.75	0.48	0.57	0.66	0.73	0.79	0.87	0.39	0.48	0.58	0.65	0.71	0.79
1.5	0.58	0.64	0.68	0.71	0.73	0.76	0.47	0.56	0.67	0.74	0.81	0.90	0.40	0.50	0.60	0.67	0.74	0.82
1.6	0.59	0.65	0.69	0.72	0.74	0.77	0.47	0.56	0.67	0.75	0.82	0.92	0.41	0.51	0.62	0.69	0.76	0.85
1.7	0.60	0.66	0.70	0.73	0.75	0.77	0.46	0.56	0.67	0.75	0.83	0.94	0.42	0.53	0.64	0.71	0.78	0.87
1.8	0.62	0.67	0.71	0.74	0.75	0.78	0.46	0.56	0.68	0.76	0.85	0.95	0.44	0.55	0.66	0.73	0.80	0.89
1.9	0.64	0.68	0.72	0.74	0.76	0.78	0.45	0.56	0.68	0.77	0.86	0.97	0.45	0.56	0.68	0.75	0.82	0.91
Reflection Index (RIx)																		
1.0	0.36	0.37	0.38	0.39	0.40	0.40	0.34	0.37	0.39	0.41	0.42	0.44	0.28	0.30	0.33	0.35	0.36	0.38
1.1	0.35	0.37	0.39	0.40	0.40	0.41	0.34	0.37	0.39	0.41	0.43	0.44	0.27	0.31	0.34	0.36	0.38	0.40
1.2	0.35	0.38	0.39	0.40	0.41	0.42	0.33	0.36	0.39	0.41	0.43	0.45	0.27	0.31	0.35	0.37	0.39	0.41
1.3	0.36	0.38	0.40	0.41	0.42	0.42	0.33	0.36	0.40	0.42	0.43	0.46	0.28	0.32	0.36	0.38	0.40	0.43
1.4	0.36	0.38	0.40	0.41	0.42	0.43	0.32	0.36	0.40	0.42	0.44	0.46	0.28	0.32	0.37	0.39	0.42	0.44
1.5	0.37	0.39	0.41	0.42	0.42	0.43	0.32	0.36	0.40	0.42	0.44	0.47	0.28	0.33	0.37	0.40	0.43	0.45
1.6	0.37	0.39	0.41	0.42	0.43	0.44	0.32	0.36	0.40	0.43	0.45	0.47	0.29	0.34	0.38	0.41	0.43	0.46
1.7	0.38	0.40	0.41	0.42	0.43	0.44	0.32	0.36	0.40	0.43	0.45	0.48	0.30	0.34	0.39	0.42	0.44	0.47
1.8	0.38	0.40	0.42	0.42	0.43	0.44	0.32	0.36	0.40	0.43	0.46	0.49	0.30	0.35	0.40	0.42	0.45	0.48
1.9	0.39	0.41	0.42	0.43	0.43	0.44	0.31	0.36	0.41	0.43	0.46	0.49	0.31	0.36	0.40	0.43	0.45	0.48

BH, body height in meters.

moderated the "AIx@75-age" association. Regardless of the method (MOG or SCOR) considered, RM and RIx were not independently associated with sex. However, for SCOR_Radial and SCOR_Carotid records, in subjects aged 17 years and older, sex moderated the relationship with age.

Regardless of the measurement method, almost all waveform-derived indexes showed an independent association with age and BH (and/or an association through their interaction with sex). Consequently, both age- and BH-related RIs were necessary. In contrast, we identified waveform-derived indexes that: (i) required sex-specific RIs only from a certain age (e.g., AP_SCOR_Radial) or BH (e.g., Pf_SCOR_Radial), (ii) required sex-specific RIs regardless of age or BH (e.g., Pf_MOG, Pb_MOG), (iii) did not require sex-specific RIs (e.g., Pb_SCOR_Radial), or (iv) did not require sex-specific and/or BH-related RIs (e.g., RI_MOG) (**Supplementary Tables 5–11**).

Age-, Sex-, and/or Body Height-Related Reference Intervals

Year-by-year (for age) and decimeter-by-decimeter (for BH) RIs data can be found in **Supplementary Tables 14–139**. **Supplementary Materials 2 and 3** show age-related (**Supplementary Figures 1–21**) and BH-related (**Supplementary Figures 22–42**) percentile curves for waveform-derived indexes. **Tables 4**, **5** show a summary (5 y and 1 decimeter intervals) of age- and BH-related RIs data for each waveform-derived index.

Comparisons of data from this study (p50th for all subjects), with data obtained by other authors (p50th or mean value), are shown in **Figures 3–6**.

DISCUSSION

Main Findings

Considering their demonstrated value (e.g., as prognostic tool), there is growing interest in assessing central BP waveform-derived indexes in clinical practice. Their accurate clinical use requires knowing their physiological age-related profiles and the expected values for a specific subject. To our knowledge, this is the first time RIs for different waveform-derived indexes (obtained from different widely used measurement approaches) were defined (at the same time) in large population of healthy children, adolescents, and adults (2–84 y). The main findings can be summarized as follows:

First, methods used to quantify aoBP waveform-derived indexes (brachial oscillometry; carotid and radial tonometry) showed mostly little (statistically significant) association with each other. Furthermore, in no case, the association was very strong ($r \geq 0.80$) (**Table 3**). Methodological approaches used to quantify similar waveform-derived indexes (e.g., Pb) were not equivalent, but showed systematic and proportional errors (**Table 3**).

Second, the need for sex-specific RIs relied on both physiological (e.g., age and/or waveform-derived index) and

non-physiological factors (e.g., methodological approach used) (**Supplementary Table 11**). Then, the associations of a given arterial propagate property (e.g., reflection coefficient) with subjects' characteristics (e.g., sex, age) could vary depending on the approach used in the evaluation.

Third, the population-based RIs for waveform-derived indexes were defined from data obtained in the same group of healthy children, adolescents, and adults (**Tables 4**, **5** and **Supplementary Tables 14–139**). Defining RIs is an important step when considering the use of waveform-derived indexes in laboratory and clinical practice, for example, as a tool to identify conditions associated with data deviation from anticipated values in physiological settings and/or to detect subclinical target organ (vascular) damage.

Fourth, aiming at contributing with other groups and/or researchers, sex-specific BH- and age-related equations for mean value, SD, and percentile values were included in text and spreadsheet formats (**Supplementary Material 1**). Thus, the expected values for a given subject could be calculated.

Wave Separation Analysis-Derived Indexes: Forward Pressure, Backward Pressure, Reflection Magnitude, and Reflection Index

Age-Related Profiles

The age-related profiles obtained for WSA-derived indexes showed similarities and differences with data reported by other authors (**Figures 3**, **4**). However, it is to note that although some articles showed age-related changes in waveform-derived indexes, data from large populations of healthy subjects, with minimized exposure to traditional CRFs, are scarce, limiting the possibility of comparing our findings with those of other authors. Moreover, we found no work including children, adolescents, and adults.

Regardless of the methodological approach considered, the Pf increased in childhood and adolescence, reaching a maximum at ∼20 y. Thereafter, it remained stable and finally showed a tendency to increase after 60–70 y (**Figure 3**). At least in theory, the significant increase in Pf during childhood and adolescence could be related to (explained by) changes in stroke volume. In this regard, it was previously described that early in life, there is a rapid increase in stroke volume, reaching a peak at ∼20 y, followed by a slow decline from the beginning of the third decade of life (Cattermole et al., 2017; Zócalo et al., 2020). The (relative) Pf stability observed within the range of 30 and 60 y of age is in agreement with previous findings in subjects with controlled and uncontrolled blood pressure (Hodson et al., 2016), in healthy and unhealthy subjects (Li et al., 2019) and in subjects with cardiovascular disease (Namasivayam et al., 2016). On the other hand, whereas in this work, the increase in Pf after 70 y of age was discrete, works that included subjects with cardiovascular disease and/or exposed to CRFs described a greater (steeper) increase (**Figure 3**). At least in theory, the dissimilar findings could be explained by a cumulative effect of cardiovascular disease and/or CRFs on Pf determinants (e.g., aortic root impedance). In this regard, in Hodson et al. work, it was observed that compared with subjects with controlled blood pressure, those with uncontrolled pressure showed almost identical Pf (and Pb) levels at early ages (e.g., <21, 21–25, and 30–37 y). Subsequently, the Pf levels were gradually higher in subjects with uncontrolled blood pressure (with the differences being statistically significant from ∼45 y) (**Figure 3**; Hodson et al., 2016). In addition, since the Pf component actually integrates forward wave and re-reflections of backward waves at the ventricular-aorta interface, the increase in Pf could also be explained by increased reflections (and the subsequent increase in re-reflections). In this regard, it should be noted that aging has been associated with arterial stiffening and increased wave reflections. Finally, it is worth noting that despite of the differences in Pf values, the different methodological approaches considered enabled to obtain similar age-related profiles.

Taking into account the above mentioned, the differences in Pf values among studies could be explained (at least partially) by differences in the calibration methods, methodological approaches, and/or subjects considered.

Similarly, Pb showed a significant rate of increase in the first decade of life, and then it continued to increase steadily throughout life. The age-related profiles obtained for adults are in agreement with data from other works. However, the age-related increase in Pb observed in this work was (apparently) smaller compared with data from other works. Furthermore, for young subjects (e.g., 20–30 y), data from this and other works overlapped, but the maximum values reported by other authors for old subjects (e.g., 80–90 y) were almost always higher than the observed in this work (**Figure 3**). The differences could be ascribed to differences in the populations studied (**Figure 3**). In this regard, it is to note that this work was carried out in healthy subjects with minimized exposure to risk factors.

Jointly considering the above factors, it could be said that more flattened curves would be expected for both Pf and Pb in adults without cardiovascular disease and minimally exposed to traditional CRFs. Finally, the differences in the rate of Pf and Pb change observed in adults in this work are consistent with data from other studies (Cecelja et al., 2009; Namasivayam et al., 2009, 2016).

The age-related changes in RM (Pb/Pf) and RIx [Pb/(Pf + Pb)] showed great heterogeneity (**Figure 4**). Both RM and RIx tend to increase in adult life, but the rate of increase differed depending on the methodological approach considered (MOG or SCOR). In addition, while RM and RIx obtained with tonometry (SCOR) showed a reduction in the first years of life and started to increase after the age of 10 y, the data obtained from MOG increased through all the age-range considered (**Figure 4**). The finding of an age-related increase in RM and RIx is in agreement with other authors (Segers et al., 2007; Hodson et al., 2016; Namasivayam et al., 2016). On the other hand, Torjesen et al. (2014) and Li et al. (2019) reported a slight increase in RM and RIx until ∼60 y, followed by a subsequent reduction. In turn, Hughes et al. (2013) (in a small sample of subjects exposed to CRFs) found an age-associated decrease in RM. Finally, there were differences in RM and RIx data among works, even at ages in which neither the cardiovascular disease presence nor the exposure to CRFs could contribute to explain them (e.g., RM values equal to ∼1.0 [Yu et al., 2020], 0.55 [Hodson et al., 2016], 0.45 [Namasivayam et al., 2016], 0.35 [Li et al., 2019],

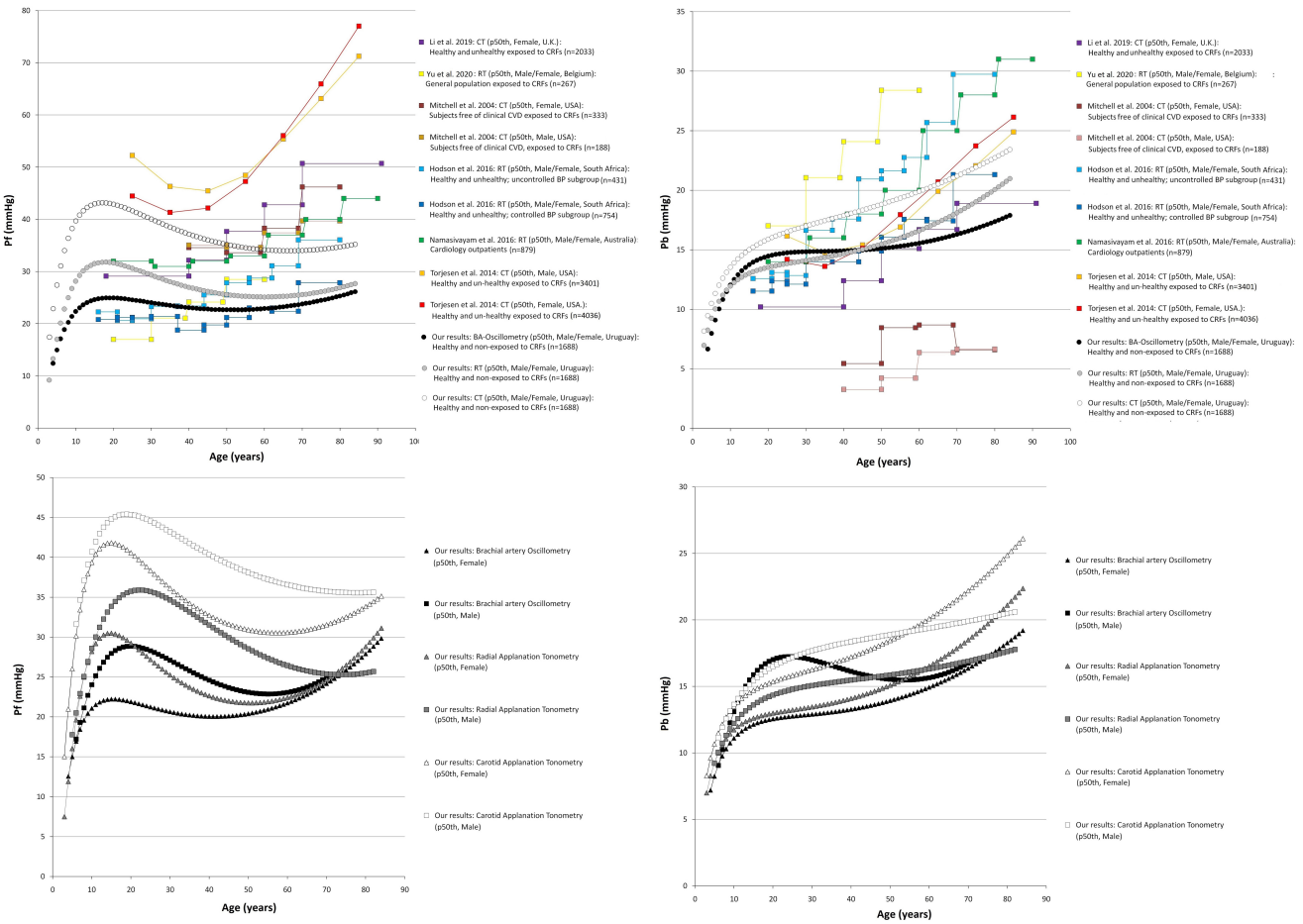

FIGURE 3 | Forward pressure (Pf) and backward pressure (Pb) age-related profiles. Top: Comparison between curves obtained in our study (p50th) and mean values or p50th obtained by other authors. CT, carotid applanation tonometry; CRFs, cardiovascular risk factors; RT, radial applanation tonometry; U.K., United Kingdom; United States, United States of America; BP, blood pressure; BA, brachial artery; Bottom: Age-related profiles (p50th) for males and females.

and 0.15 [Hughes et al., 2013] were observed in subjects aged ∼20 y) (**Figure 4**).

Sex-Related Differences

Data from multiple linear regression models (**Supplementary Table 11**) and age-related profiles (**Figures 3–5**) showed that the association between waveform-derived indexes (Pf, Pb, RM, and RIx) and sex differed depending on the approach considered.

Figure 3 shows that after approximately 10–15 y, the p50th for Pf and Pb was higher in males than in females, but Pf values tend to be similar at ages over 70 y. In turn, for subjects over 50–60 y, the Pb values were higher in females than in males (**Figure 3**). In regression analysis, adjusted by BH, the Pf and Pb remained associated with sex only when considering data from MOG. This is in agreement with other authors (Lieber et al., 2010; Liao et al., 2011; Hughes et al., 2013).

The above data should be carefully analyzed. Whereas we (and other authors) analyzed Pf and Pb and absolute values, and other authors analyzed waveform components in terms relative to aoPP. In subjects younger than 60 y of age, Namasivayam et al. found that both incident and reflected waves showed a greater contribution to the age-related increase in aortic pressure in females than in males (Namasivayam et al., 2009; Torjesen et al., 2014; Hodson et al., 2017). Our curves for RM and RIx (indexes that allow relativizing Pb amplitude) tended to be higher in females from ∼20 y; except for MOG-derived data (**Figure 4**). Opposite to the described levels for Pf and Pb, RM and RIx levels obtained with SCOR showed sex-related differences (higher values in females), from 13.5 to 12.6 y for SCOR_Radial and from 17.1 to 17.2 y for SCOR_Carotid. Our findings add to those reported by Namasivayam et al. (2009). These authors found that the higher relative contribution of Pb in females would be observed from ∼12 to ∼17 y for radial and carotid recordings, respectively. Additionally, the authors described that the sex-related differences remained thorough adult life.

The similarity observed in girls and boys agrees with previous works that reported no sex-related differences in structural and functional arterial parameters at prepubertal ages (4–8 y), but showed sex-related differences in adolescents (∼15 y) (Curcio et al., 2016).

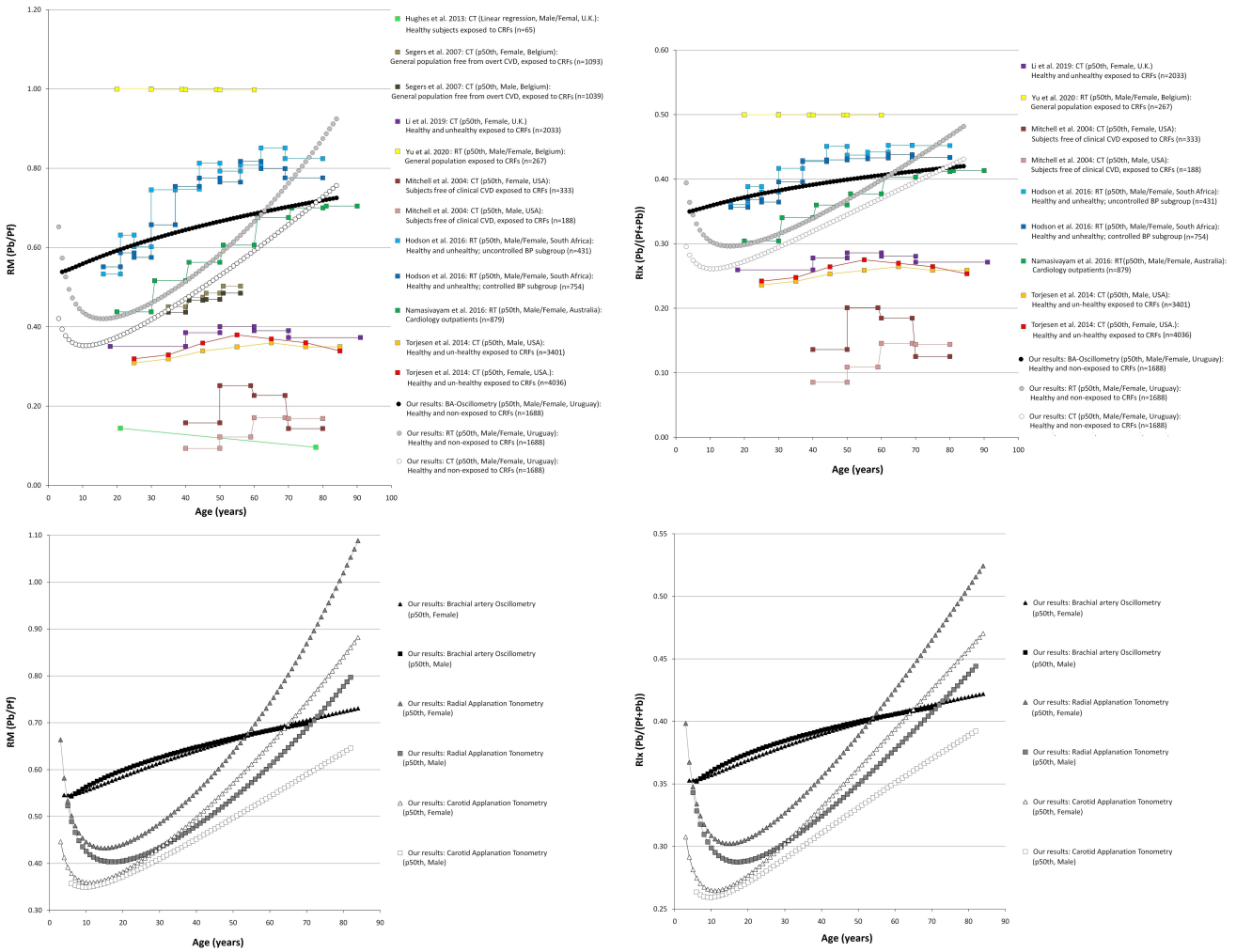

FIGURE 4 | Reflection magnitude (RM) and Reflection index (RIx) age-related profiles. Top: Comparison between curves obtained in our study (p50th) and mean values or p50th obtained by other authors. Pb and Pf, backward and forward pressure; CT, carotid applanation tonometry; CVD, cardiovascular disease; CRFs, cardiovascular risk factors; RT, radial applanation tonometry; U.K., United Kingdom; United States, United States of America; BP, blood pressure; BA, brachial artery. Bottom: Age-related profiles (p50th) for males and females.

Body Height-Related Profiles

Regardless of the methodological approach considered, and with independence of sex and age, Pf and Pb were positively associated with BH (**Figure 6** and **Supplementary Table 11**). In turn, RM and RIx data obtained with MOG did not show an independent association with BH, whereas SCOR-derived RM and RIx data were independently associated with BH (higher BH, lower RM and RIx) (**Supplementary Tables 9, 10**). The negative association of BH with RM and RIx could be explained (at least partially) by the well-known inverse relationship between the magnitude of reflections measured at the central aorta and the distance between the site of wave generation (heart) and reflection (which move away as BH increases).

Our findings could be considered opposite to that reported by Hughes et al. (2013) who did not find association between RM and BH in healthy normotensive subjects (n = 65; 21–78 y; 43 male) evaluated with carotid tonometry. However, the results were alike when considering the association of BH with RM and RIx data obtained with SCOR_Carotid without adjusting for cofactors (**Figure 6**; note the flattened profiles).

Pulse Wave Analysis-Derived Indexes: Augmentation Pressure, Augmentation Index, and Augmentation Index Corrected for Heart Rate 75 Beats/Minute

Age-Related Profiles

Like in previous works, the AP showed an age-related increase in adults (**Figure 5**). When considering SCOR data, it was observed as a decrease in AP during childhood and adolescence and an increase from the age of ∼15 onward. The AP levels obtained with MOG showed an increase from childhood onward.

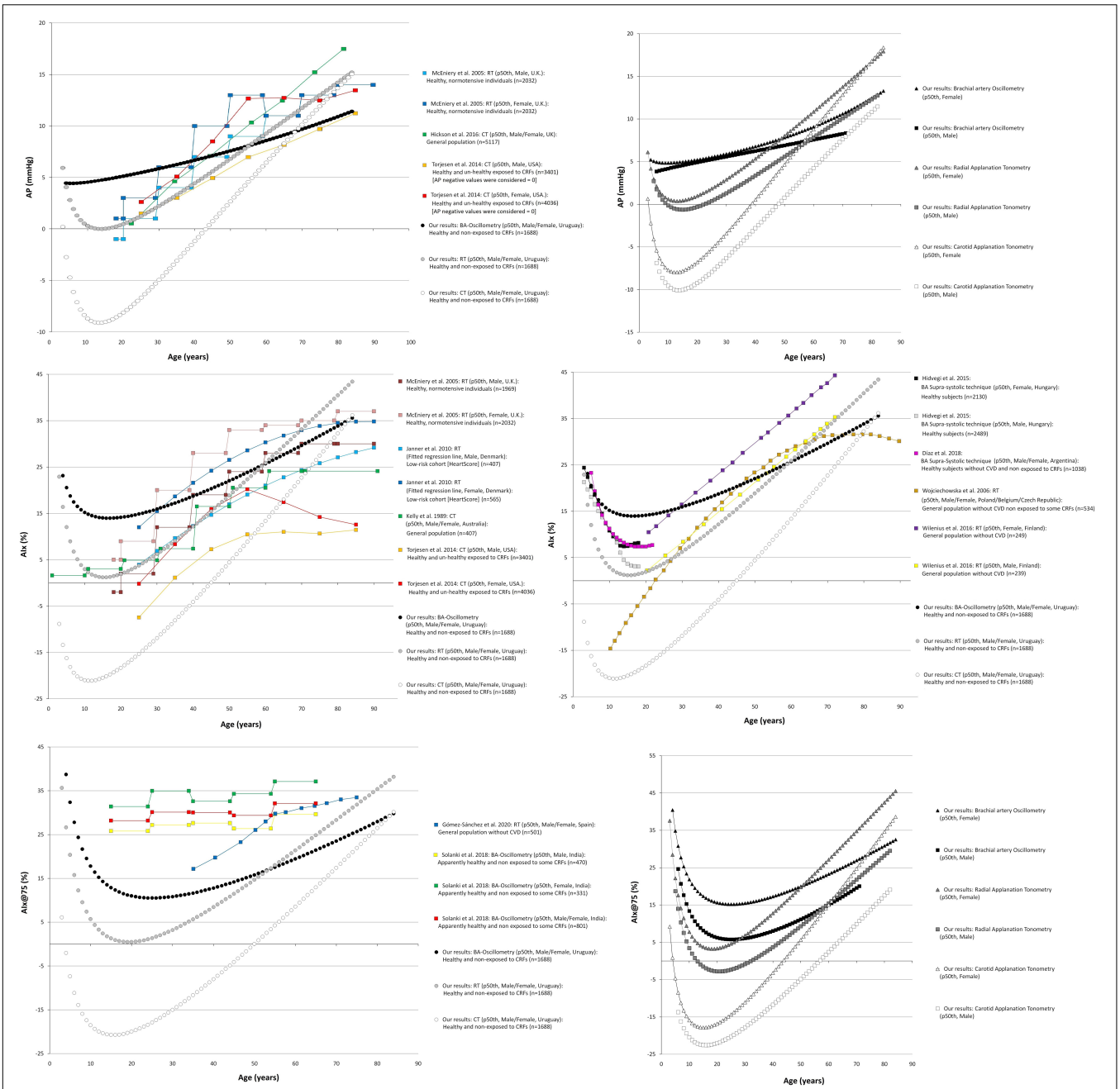

FIGURE 5 | Augmentation pressure (AP), Augmentation Index (AIx), and heart rate-corrected AIx (AIx@75) age-related profiles. Left and right middle panel: Comparison between curves obtained in our study (p50th) and mean values or p50th obtained by other authors. CT, carotid applanation tonometry; CVD, cardiovascular disease; CRFs, cardiovascular risk factors; RT, radial applanation tonometry; U.K., United Kingdom; United States, United States of America; BP, blood pressure; BA, brachial artery. Right top and bottom panel: Age-related profiles (p50th) for males and females.

Additionally, there were differences in the AP levels obtained with the different methodological approaches (**Figure 5**).

Regardless of the methodological approach considered, the AIx and AIx@75 showed a reduction in childhood and adolescence, but they increased from ∼10–15 y onward (**Figure 5**). This is in agreement with previous findings in children and adolescents (Hidvégi et al., 2015; Díaz et al., 2018), and in adults (McEniery et al., 2005). We found a linear relationship with age that did not become non-linear in subjects aged 70 y and older as was described by other authors (McEniery et al., 2005). The dissimilar findings could be explained by differences in studied subjects' characteristics (e.g., we evaluated healthy subjects minimally exposed to traditional CRFs, whereas other authors included subjects with extensive

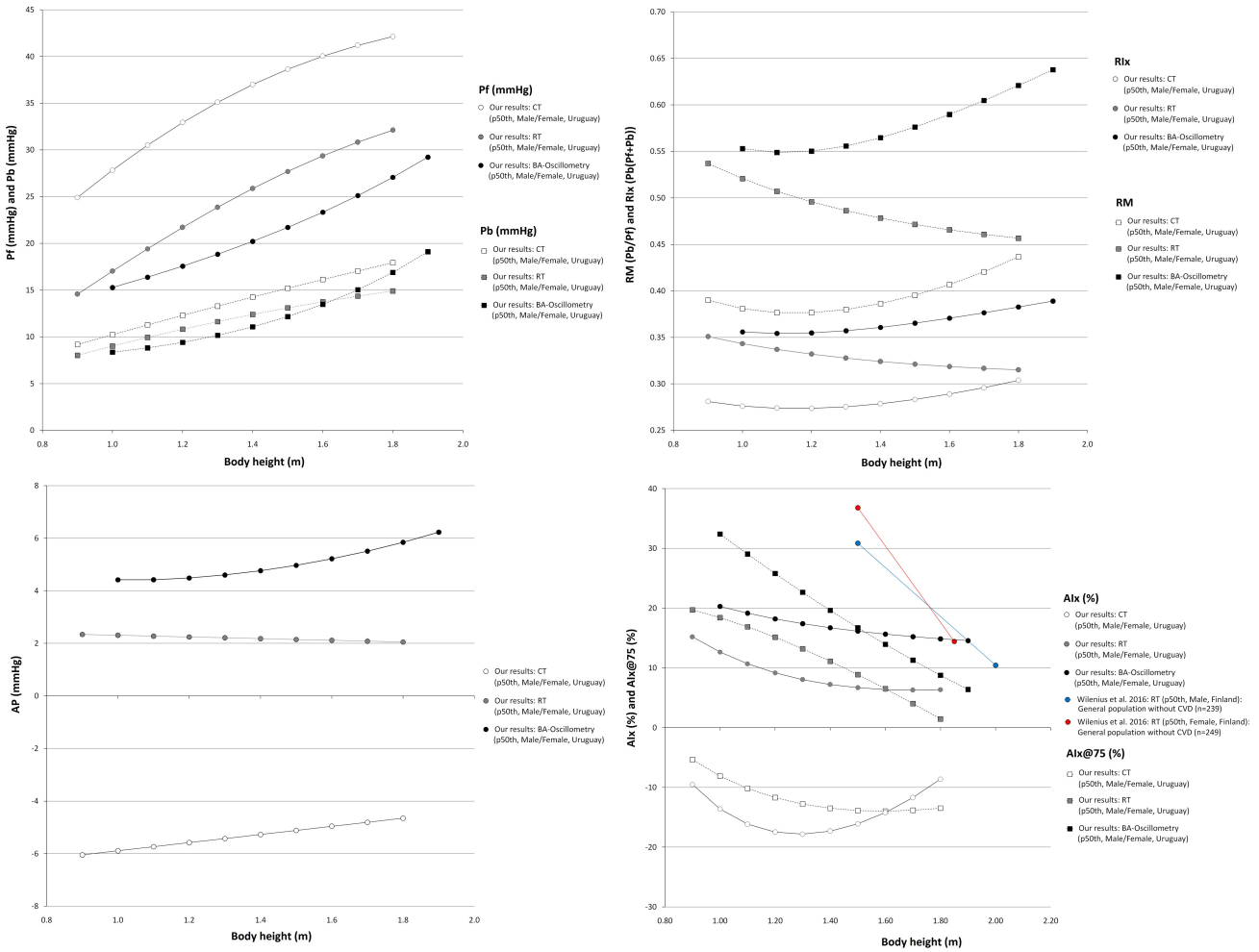

FIGURE 6 | Waveform-derived indexes body height-related profiles. Comparison between curves for waveform derived indexes obtained in our study (p50th) using three different approaches. Pf, Forward pressure; Pb, Backward pressure; RM, Reflection magnitude; RIx, Reflection index; AP, Augmentation pressure; AIx and AIx@75, Augmentation index and heart rate-corrected AIx; CT, carotid applanation tonometry; CVD, cardiovascular disease; RT, radial applanation tonometry; BA, brachial artery.

exposure to CRFs) and/or by demographics differences between the populations considered. About this, Janner et al. (2010) found that the association between AIx and age became progressively less linear (above 60–70 y) when considering subjects with increased cardiovascular risk (associated with exposure to CRFs). Other hypotheses have been proposed to explain the findings. Namasivayam et al. suggested that the ratio of two linear relationships, such as AP *vs.* age and aoPP *vs.* age, resulted in a curvilinear trend (AIx *vs.* age). This mathematical phenomenon could contribute to the "flattening" of age-AIx curve (described by other authors) (Hickson et al., 2016).

Finally, it is to note that only few authors reported reference data or age-related profiles for AIx@75. The available works described an age-related increase, but whereas Gómez-Sánchez et al. showed a significant constant increase in AIx@75 with aging (like in this work), and Solanki et al. found a slight age-related increase (**Figure 5**; Solanki et al., 2018; Gómez-Sánchez et al., 2020).

Sex-Related Differences

The augmentation pressure levels tended to be higher in females than in males (**Figure 5**), but the differences were statistically significant only in case of SCOR_Radial data from subjects aged > 12.9 y (**Supplementary Table 11**). This is in agreement with data from other authors (adult subjects) (Mitchell et al., 2004; McEniery et al., 2005; Segers et al., 2007; Torjesen et al., 2014).

Regardless of BH, compared to males, females showed higher AIx and AIx@75 (**Figure 5**): (i) for all ages when considering MOG records, (ii) from 9.5 and 7.8 y when considering SCOR_Radial records, and (iii) from 2.8 and 7.0 y when considering SCOR_Carotid records (**Supplementary Table 11**). The finding of higher AIx and AIX@75 in females than in males is in agreement with data from previous works (Mitchell et al., 2004; McEniery et al., 2005; Wojciechowska et al., 2006; Segers et al., 2007; Janner et al., 2010; Hughes et al., 2013; Torjesen et al., 2014; Wilenius et al., 2016; Solanki et al., 2018).

Body Height-Related Profiles

When analyzing the (simple) association between AP and BH data, no clear trend was observed (**Figure 6**). However, in multivariate analysis, it was observed a negative association between BH and AP. The association was independent of age and sex in case of SCOR and of age for MOG records (**Supplementary Tables 8–11**). In turn, the AIx and AIx@75 showed a negative association with BH, regardless of sex and age (**Supplementary Tables 8–11**). This is in agreement with Wilenius et al. (2016).

Strengths and Limitations

Our results should be analyzed in the context of the work's strengths and limitations. First, since this is a cross-sectional study, it provides no data on longitudinal age-related variations in waveform-derived indexes. Although useful for quantifying RIs, our data do not allow to determine with certainty the true impact of aging on arterial system properties (Campos-Arias et al., 2021). Second, the outcome data were not considered. Thus, cutoff points (e.g., p90th, p95th) could not be selected based on the association with increased cardiovascular risk, but on data distribution in the RIs group. Whether or not the RIs values should be used as cutoff values for central hemodynamic alterations diagnose and/or treatment is not known. Third, in this work, the concept of "waveform-derived index" was mainly presented as "static or unchanged," rather than the composite of (i) "fixed or stable" (e.g., age-dependent arterial pulse propagation and reflection capabilities) and (ii) "variable or adjustable" (e.g., vascular smooth muscle capability to temporally adjust arterial pulse propagation or reflection properties) (Bia et al., 2003, 2008). Fourth, the RIs subgroup consisted of people whose CRFs levels did not exceed accepted thresholds for abnormality (e.g., hypertensive subjects were excluded). Given that the prevalence of many CRFs increases with age (e.g., arterial hypertension), by definition (older), "superhealthy" individuals would have had a greater possibility of being included in the RIs group. Consequently, at least for adults, this work's data probably describe an "optimal," rather than a "typical" aging trajectory.

Fifth, as a strength, in this study, waveform-derived indexes were obtained in a large population sample (of children, adolescents, and adults) that included subjects within a wide age-range (almost the whole range of life expectancy), as a continuum. This would contribute to understand the arterial pulse propagations and their impact on waveform-derived indexes throughout life, providing important information for clinical diagnosis and cardiovascular research. To our knowledge, this is the first study of its sort in South Americans. Sixth, despite we previously demonstrated that aoBP and some waveform-derived indexes could vary depending on the calibration schema considered (Zinoveev et al., 2019), in this work, we opted for the schema most used in the literature (use of baDBP and baMBP). In this regard, it is to note that whereas some indexes do not depend on the calibration schema (e.g., AIx), others are highly dependent on the methodological approach used (e.g., Pf and Pb). Hence, data should be analyzed/used being aware of this. Seventh, it is to note that an accurate optimal analysis of wave reflections would require pressure and flow measurement, rather than BP waveform recording and analysis alone. However, the simultaneous measurement of pressure and flow might not always be feasible. On the other hand, the different approaches used to quantify waveform-reflection indexes may differ in the obtained data (e.g., differences in the algorithms used to analyze the waveform and to identify the "inflection point" may yield different indexes values). In this context, we opted for working with widely used devices and algorithms of analysis (SphygmoCor and Mobil-O-Graph). Finally, it should be noted that while in this work we focused on the most frequently used waveform-derived indexes, we recognize (i) the existence of other indexes and (ii) the limitations of the quantified indexes. For instance, the AIx reflects both cardiac and vascular properties. Hence, it has limitations as a measure of wave reflection (Hughes et al., 2013; Heusinkveld et al., 2019).

CONCLUSION

This study adds to the knowledge of the physiological variations in waveform-derived indexes and arterial pulse propagative properties that would be expected during growth and aging, analyzing at the same time (and comparatively) the behavior of different indexes, obtained with three different approaches. Our data showed that the methods used to quantify aoBP waveform-derived indexes (brachial oscillometry, carotid, and radial tonometry) showed little association with each other. Waveform-derived data from different approaches were not equivalent, but showed systematic and proportional errors. These results evidenced that the non-invasive methodological approach used is an important determinant of the results (e.g., RIs levels). Our study strongly emphasizes the need for consensus on non-invasive assessment of waveform-derived indexes.

There were not uniform behaviors that standardize the need for sex-related RIs (normative data), but the need for sex-specific waveform-derived indexes RIs relied on the index and/or age considered. Population-based RIs for waveform-derived indexes were defined from data obtained in the same group of healthy children, adolescents, and adults. Aiming at contributing with other groups and/or researchers, sex-specific BH- and age-related equations for mean value, SD, and percentiles values were included in text and spreadsheet formats. Thus, the expected values for a given subject could be calculated for clinical and/or research purposes.

DATA AVAILABILITY STATEMENT

The original contributions presented in the study are included in the article/**Supplementary Material**, further inquiries can be directed to the corresponding author/s.

ETHICS STATEMENT

The studies involving human participants were reviewed and approved by Comité de Ética de Investigación, Centro Hospitalario Pereira Rossell, ASSE, Universidad de la República.

Written informed consent to participate in this study was provided by the participants' legal guardian/next of kin.

AUTHOR CONTRIBUTIONS

YZ and DB contributed to conception and design of the study, performed the cardiovascular recordings, constructed and organized the database, performed the statistical analysis, wrote the first draft and final version of the manuscript, contributed to manuscript revision, read, and approved the submitted version. Both authors contributed to the article and approved the submitted version.

FUNDING

This research was funded by Agencia Nacional de Investigación e Innovación (ANII), grant number PRSCT–008–020; and extra budgetary funds provided by DB and YZ and CUiiDARTE Center.

ACKNOWLEDGMENTS

We thank the children, adolescents and adults, and their families for their participation in the study. To colleagues who integrated the CUiiDARTE Project in different stages, as part of their final degree, master and/or doctoral projects.

SUPPLEMENTARY MATERIAL

The Supplementary Material for this article can be found online at: https://www.frontiersin.org/articles/10.3389/fphys.2021.774390/full#supplementary-material

REFERENCES

Baksi, A. J., Treibel, T. A., Davies, J. E., Hadjiloizou, N., Foale, R. A., Parker, K. H., et al. (2009). A meta-analysis of the mechanism of blood pressure change with aging. *J. Am. Coll. Cardiol.* 54, 2087–2092. doi: 10.1016/j.jacc.2009.06.049

Bellera, C. A., and Hanley, J. A. (2007). A method is presented to plan the required sample size when estimating regression-based reference limits. *J. Clin. Epidemiol.* 60, 610–615. doi: 10.1016/j.jclinepi.2006.09.004

Bia, D., and Zócalo, Y. (2021). Physiological age- and sex-related profiles for local (aortic) and regional (carotid-femoral, carotid-radial) pulse wave velocity and center-to-periphery stiffness gradient, with and without blood pressure adjustments: reference intervals and agreement between methods in healthy subjects (3-84 years). *J. Cardiovasc. Dev. Dis.* 8:3. doi: 10.3390/jcdd8010003

Bia, D., Armentano, R. L., Grignola, J. C., Craiem, D., Zócalo, Y. A., Ginés, F. F., et al. (2003). The vascular smooth muscle of great arteries: local control site of arterial buffering function? *Rev. Esp. Cardiol.* 56, 1202–1209. doi: 10.1016/s0300-8932(03)77039-0

Bia, D., Zócalo, Y., Armentano, R., Camus, J., De Forteza, E., and Cabrera-Fischer, E. (2008). Increased reversal and oscillatory shear stress cause smooth muscle contraction-dependent changes in sheep aortic dynamics: role in aortic balloon pump circulatory support. *Acta Physiol. (Oxf.)* 192, 487–503. doi: 10.1111/j.1748-1716.2007.01765.x

Bia, D., Zócalo, Y., Farro, I., Torrado, J., Farro, F., Florio, L., et al. (2011). Integrated evaluation of age-related changes in structural and functional vascular parameters used to assess arterial aging, subclinical atherosclerosis, and cardiovascular risk in Uruguayan adults: CUiiDARTE Project. *Int. J. Hypertens.* 2011:587303. doi: 10.4061/2011/587303

Bossuyt, J., Engelen, L., Ferreira, I., Stehouwer, C. D., Boutouyrie, P., Laurent, S., et al. (2015). Reference values for arterial measurements collaboration. Reference values for local arterial stiffness. Part B: femoral artery. *J. Hypertens.* 33, 1997–2009. doi: 10.1097/HJH.0000000000000655

Campos-Arias, D., De Buyzere, M. L., Chirinos, J. A., Rietzschel, E. R., and Segers, P. (2021). Longitudinal changes of input impedance, pulse wave velocity, and wave reflection in a middle-aged population: the Asklepios study. *Hypertension* 77, 1154–1165. doi: 10.1161/HYPERTENSIONAHA.120.16149

Castro, J. M., García-Espinosa, V., Zinoveev, A., Marin, M., Severi, C., Chiesa, P., et al. (2019). Arterial structural and functional characteristics at end of early childhood and beginning of adulthood: impact of body size gain during early, intermediate, late and global growth. *J. Cardiovasc. Dev. Dis.* 6:33. doi: 10.3390/jcdd6030033

Cattermole, G. N., Leung, P. Y., Ho, G. Y., Lau, P. W., Chan, C. P., Chan, S. S., et al. (2017). The normal ranges of cardiovascular parameters measured using the ultrasonic cardiac output monitor. *Physiol. Rep.* 5:e13195. doi: 10.14814/phy2.13195

Cecelja, M., Jiang, B., McNeill, K., Kato, B., Ritter, J., Spector, T., et al. (2009). Increased wave reflection rather than central arterial stiffness is the main determinant of raised pulse pressure in women and relates to mismatch in arterial dimensions: a twin study. *J. Am. Coll. Cardiol.* 54, 695–703. doi: 10.1016/j.jacc.2009.04.068

Chirinos, J. A., Kips, J. G., Jacobs, D. R. Jr., Brumback, L., Duprez, D. A., Kronmal, R., et al. (2012). Arterial wave reflections and incident cardiovascular events and heart failure: MESA (Multiethnic Study of Atherosclerosis). *J. Am. Coll. Cardiol.* 60, 2170–2177. doi: 10.1016/j.jacc.2012.07.054

Chirinos, J. A., Kips, J. G., Roman, M. J., Medina-Lezama, J., Li, Y., Woodiwiss, A. J., et al. (2011). Ethnic differences in arterial wave reflections and normative equations for augmentation index. *Hypertension* 57, 1108–1116. doi: 10.1161/HYPERTENSIONAHA.110.166348

Climie, R. E., Park, C., Avolio, A., Mynard, J. P., Kruger, R., and Bruno, R. M. (2021). Vascular ageing in youth: a call to action. *Heart Lung Circ.* 30, 1613–1626. doi: 10.1016/j.hlc.2021.06.516

Curcio, S., García-Espinosa, V., Arana, M., Farro, I., Chiesa, P., Giachetto, G., et al. (2016). Growing-Related changes in arterial properties of healthy children, adolescents, and young adults nonexposed to cardiovascular risk factors: analysis of gender-related differences. *Int. J. Hypertens.* 2016:4982676. doi: 10.1155/2016/4982676

Díaz, A., Zócalo, Y., Bia, D., and Cabrera Fischer, E. (2018). Reference intervals of central aortic blood pressure and augmentation index assessed with an oscillometric device in healthy children, adolescents, and young adults from Argentina. *Int. J. Hypertens.* 2018:1469651. doi: 10.1155/2018/1469651

Engelen, L., Bossuyt, J., Ferreira, I., van Bortel, L. M., Reesink, K. D., Segers, P., et al. (2015). Reference values for arterial measurements collaboration. Reference values for local arterial stiffness. Part A: carotid artery. *J. Hypertens.* 33, 1981–1996. doi: 10.1097/HJH.0000000000000654

Engelen, L., Ferreira, I., Stehouwer, C. D., Boutouyrie, P., and Laurent, S. (2013). Reference Values for Arterial Measurements Collaboration. Reference intervals for common carotid intima-media thickness measured with echotracking: relation with risk factors. *Eur. Heart J.* 34, 2368–2380. doi: 10.1093/eurheartj/ehs380

Gómez-Sánchez, M., Patino-Alonso, M. C., Gómez-Sánchez, L., Recio-Rodríguez, J. I., Rodríguez-Sánchez, E., Maderuelo-Fernández, J. A., et al. (2020). Reference values of arterial stiffness parameters and their association with cardiovascular risk factors in the Spanish population. The EVA Study. *Rev. Esp. Cardiol. (Engl. Ed.)* 73, 43–52. doi: 10.1016/j.rec.2019.04.016

Hametner, B., and Wassertheurer, S. (2017). Pulse waveform analysis: is it ready for prime time? *Curr. Hypertens. Rep.* 19:73. doi: 10.1007/s11906-017-0769-3

Hametner, B., Parragh, S., Mayer, C., Weber, T., Van Bortel, L., De Buyzere, M., et al. (2015). Assessment of model based (input) impedance, pulse wave velocity, and wave reflection in the Asklepios cohort. *PLoS One* 10:e0141656. doi: 10.1371/journal.pone.0141656

Hayes, A. F. (2020). *Introduction to Mediation, Moderation, and Conditional Process Analysis*, 2nd Edn. Available online at: http://www.guilford.com/p/hayes3 (accessed November 13, 2020).

Heffernan, K. S., Lefferts, W. K., Atallah-Yunes, N. H., Glasgow, A. C., and Gump, B. B. (2020). Racial differences in left ventricular mass and wave reflection intensity in children. *Front. Pediatr.* 8:132. doi: 10.3389/fped.2020.00132

Heusinkveld, M. H. G., Delhaas, T., Lumens, J., Huberts, W., Spronck, B., Hughes, A. D., et al. (2019). Augmentation index is not a proxy for wave reflection magnitude: mechanistic analysis using a computational model. *J. Appl. Physiol. (1985)* 127, 491–500. doi: 10.1152/japplphysiol.00769.2018

Hickson, S. S., Nichols, W. W., Yasmin, McDonnell, B. J., Cockcroft, J. R., Wilkinson, I. B., et al. (2016). Influence of the central-to-peripheral arterial stiffness gradient on the timing and amplitude of wave reflections. *Hypertens. Res.* 39, 723–729. doi: 10.1038/hr.2016.64

Hidvégi, E. V., Illyés, M., Molnár, F. T., and Cziráki, A. (2015). Influence of body height on aortic systolic pressure augmentation and wave reflection in childhood. *J. Hum. Hypertens.* 29, 495–501. doi: 10.1038/jhh.2014.118

Hodson, B., Norton, G. R., Ballim, I., Sareli, P., and Woodiwiss, A. J. (2017). Contribution of backward and forward wave pressures to age-related increases in aortic pressure in a community sample not receiving antihypertensive therapy. *J. Am. Soc. Hypertens.* 11, 616–626.e2. doi: 10.1016/j.jash.2017.08.003

Hodson, B., Norton, G. R., Booysen, H. L., Sibiya, M. J., Raymond, A., Maseko, M. J., et al. (2016). Brachial pressure control fails to account for most distending pressure-independent, age-related aortic hemodynamic changes in adults. *Am. J. Hypertens.* 29, 605–613. doi: 10.1093/ajh/hpv140

Hughes, A. D., Park, C., Davies, J., Francis, D., McG Thom, S. A., Mayet, J., et al. (2013). Limitations of augmentation index in the assessment of wave reflection in normotensive healthy individuals. *PLoS One* 8:e59371. doi: 10.1371/journal.pone.0059371

Janner, J. H., Godtfredsen, N. S., Ladelund, S., Vestbo, J., and Prescott, E. (2010). Aortic augmentation index: reference values in a large unselected population by means of the SphygmoCor device. *Am. J. Hypertens.* 23, 180–185. doi: 10.1038/ajh.2009.234

Karamanoglu, M., and Feneley, M. P. (1996). Derivation of the ascending aortic-carotid pressure transfer function with an arterial model. *Am. J. Physiol.* 271(6 Pt. 2), H2399–H2404. doi: 10.1152/ajpheart.1996.271.6.H2399

Kelly, R., Hayward, C., Avolio, A., and O'Rourke, M. (1989). Noninvasive determination of age-related changes in the human arterial pulse. *Circulation* 80, 1652–1659. doi: 10.1161/01.cir.80.6.1652

Li, Y., Jiang, B., Keehn, L., Gu, H., Boguslavskyi, A., Cecelja, M., et al. (2019). Hemodynamic mechanism of the age-related increase in pulse pressure in women. *Hypertension* 73, 1018–1024. doi: 10.1161/HYPERTENSIONAHA.118.12402

Liao, C. F., Cheng, H. M., Sung, S. H., Yu, W. C., and Chen, C. H. (2011). Determinants of pressure wave reflection: characterization by the transit time-independent reflected wave amplitude. *J. Hum. Hypertens.* 25, 665–671. doi: 10.1038/jhh.2010.106

Lieber, A., Millasseau, S., Bourhis, L., Blacher, J., Protogerou, A., Levy, B. I., et al. (2010). Aortic wave reflection in women and men. *Am. J. Physiol. Heart Circ. Physiol.* 299, H236–H242. doi: 10.1152/ajpheart.00985.2009

Lumley, T., Diehr, P., Emerson, S., and Chen, L. (2002). The importance of the normality assumption in large public health data sets. *Annu. Rev. Public Health* 23, 151–169. doi: 10.1146/annurev.publhealth.23.100901.140546

Marin, M., Bia, D., and Zócalo, Y. (2020). Carotid and femoral atherosclerotic plaques in asymptomatic and non-treated subjects: cardiovascular risk factors, 10-years risk scores, and lipid ratios' capability to detect plaque presence, burden, fibro-lipid composition and geometry. *J. Cardiovasc. Dev. Dis.* 7:11. doi: 10.3390/jcdd7010011

McEniery, C. M., Yasmin, Hall, I. R., Qasem, A., Wilkinson, I. B., Cockcroft, J. R., et al. (2005). Normal vascular aging: differential effects on wave reflection and aortic pulse wave velocity: the Anglo-Cardiff Collaborative Trial (ACCT). *J. Am. Coll. Cardiol.* 46, 1753–1760. doi: 10.1016/j.jacc.2005.07.037

Mitchell, G. F., Parise, H., Benjamin, E. J., Larson, M. G., Keyes, M. J., Vita, J. A., et al. (2004). Changes in arterial stiffness and wave reflection with advancing age in healthy men and women: the Framingham Heart Study. *Hypertension* 43, 1239–1245. doi: 10.1161/01.HYP.0000128420.01881.aa

Mynard, J. P., Kondiboyina, A., Kowalski, R., Cheung, M., and Smolich, J. J. (2020). Measurement, analysis and interpretation of pressure/flow waves in blood vessels. *Front. Physiol.* 11:1085. doi: 10.3389/fphys.2020.01085

Namasivayam, M., Adji, A., and O'Rourke, M. F. (2016). Evaluating the hemodynamic basis of age-related central blood pressure change using aortic flow triangulation. *Am. J. Hypertens.* 29, 178–184. doi: 10.1093/ajh/hpv080

Namasivayam, M., McDonnell, B. J., McEniery, C. M., O'Rourke, M. F., and Anglo-Cardiff Collaborative Trial Study Investigators (2009). Does wave reflection dominate age-related change in aortic blood pressure across the human life span? *Hypertension* 53, 979–985. doi: 10.1161/HYPERTENSIONAHA.108.125179

Royston, P., and Wright, E. (1998). A method for estimating age-specific reference intervals ('normal ranges') based on fractional polynomials and exponential transformation. *J. R. Stat. Soc. Ser. A Stat. Soc.* 161, 79–101.

Santana, D. B., Zócalo, Y. A., and Armentano, R. L. (2012a). Integrated e-Health approach based on vascular ultrasound and pulse wave analysis for asymptomatic atherosclerosis detection and cardiovascular risk stratification in the community. *IEEE Trans. Inf. Technol. Biomed.* 16, 287–294. doi: 10.1109/TITB.2011.2169977

Santana, D. B., Zócalo, Y. A., Ventura, I. F., Arrosa, J. F., Florio, L., Lluberas, R., et al. (2012b). Health informatics design for assisted diagnosis of subclinical atherosclerosis, structural, and functional arterial age calculus and patient-specific cardiovascular risk evaluation. *IEEE Trans. Inf. Technol. Biomed.* 16, 943–951. doi: 10.1109/TITB.2012.2190990

Segers, P., Rietzschel, E. R., De Buyzere, M. L., Vermeersch, S. J., De Bacquer, D., Van Bortel, L. M., et al. (2007). Noninvasive (input) impedance, pulse wave velocity, and wave reflection in healthy middle-aged men and women. *Hypertension* 49, 1248–1255. doi: 10.1161/HYPERTENSIONAHA.106.085480

Sluyter, J. D., Camargo, C. A. Jr., Stewart, A. W., Waayer, D., Lawes, C. M. M., Toop, L., et al. (2017). Effect of monthly, high-dose, long-term vitamin d supplementation on central blood pressure parameters: a randomized controlled trial substudy. *J. Am. Heart Assoc.* 6:e006802. doi: 10.1161/JAHA.117.006802

Solanki, J. D., Mehta, H. B., and Shah, C. J. (2018). Aortic pulse wave velocity and augmentation index@75 measured by oscillometric pulse wave analysis in Gujarati nonhypertensives. *Vasc. Invest. Ther.* 1, 50–55.

Sugawara, J., Hayashi, K., and Tanaka, H. (2010). Distal shift of arterial pressure wave reflection sites with aging. *Hypertension* 56, 920–925. doi: 10.1161/HYPERTENSIONAHA.110.160549

Torjesen, A. A., Wang, N., Larson, M. G., Hamburg, N. M., Vita, J. A., Levy, D., et al. (2014). Forward and backward wave morphology and central pressure augmentation in men and women in the Framingham Heart Study. *Hypertension* 64, 259–265. doi: 10.1161/HYPERTENSIONAHA.114.03371

Wang, K. L., Cheng, H. M., Sung, S. H., Chuang, S. Y., Li, C. H., Spurgeon, H. A., et al. (2010). Wave reflection and arterial stiffness in the prediction of 15-year all-cause and cardiovascular mortalities: a community-based study. *Hypertension* 55, 799–805. doi: 10.1161/HYPERTENSIONAHA.109.139964

Weber, T., Wassertheurer, S., Rammer, M., Haiden, A., Hametner, B., and Eber, B. (2012). Wave reflections, assessed with a novel method for pulse wave separation, are associated with end-organ damage and clinical outcomes / novelty and significance. *Hypertension* 60, 534–541. doi: 10.1161/HYPERTENSIONAHA.112.194571

Westerhof, B. E., Guelen, I., Westerhof, N., Karemaker, J. M., and Avolio, A. (2006). Quantification of wave reflection in the human aorta from pressure alone: a proof of principle. *Hypertension* 48, 595–601. doi: 10.1161/01.HYP.0000238330.08894.17

Westerhof, N., and Westerhof, B. E. (2013). A review of methods to determine the functional arterial parameters stiffness and resistance. *J. Hypertens.* 31, 1769–1775. doi: 10.1097/HJH.0b013e3283633589

Wilenius, M., Tikkakoski, A. J., Tahvanainen, A. M., Haring, A., Koskela, J., Huhtala, H., et al. (2016). Central wave reflection is associated with peripheral arterial resistance in addition to arterial stiffness in subjects without antihypertensive medication. *BMC Cardiovasc. Disord.* 16:131. doi: 10.1186/s12872-016-0303-6

Wojciechowska, W., Staessen, J. A., Nawrot, T., Cwynar, M., Seidlerová, J., Stolarz, K., et al. (2006). Reference values in white Europeans for the arterial pulse wave recorded by means of the SphygmoCor device. *Hypertens. Res.* 29, 475–483. doi: 10.1291/hypres.29.475

Yu, C. G., Wei, F. F., Zhang, Z. Y., Thijs, L., Yang, W. Y., Mujaj, B., et al. (2020). Central hemodynamics in relation to low-level environmental lead exposure. *Blood Press.* 29, 157–167. doi: 10.1080/08037051.2019.1658518

Zamani, P., Jacobs, D. R. Jr., Segers, P., Duprez, D. A., Brumback, L., Kronmal, R. A., et al. (2014). Reflection magnitude as a predictor of mortality: the Multi-Ethnic Study of Atherosclerosis. *Hypertension* 64, 958–964. doi: 10.1161/HYPERTENSIONAHA.114.03855

Zinoveev, A., Castro, J. M., García-Espinosa, V., Marin, M., Chiesa, P., Bia, D., et al. (2019). Aortic pressure and forward and backward wave components in children, adolescents and young-adults: agreement between brachial oscillometry, radial and carotid tonometry data and analysis of factors associated with their differences. *PLoS One* 14:e0226709. doi: 10.1371/journal.pone.0226709

Zócalo, Y., and Bia, D. (2016). Ultrasonografía carotídea para detección de placas de ateroma y medición del espesor íntima-media; índice tobillo-brazo: evaluación no invasiva en la práctica clínica: importancia clínica y análisis de las bases metodológicas para su evaluación. *Rev. Urug. Cardiol.* 31, 47–60. doi: 10.3989/mc.1960.v10.i099.1916

Zócalo, Y., and Bia, D. (2021a). Age- and sex-related profiles for macro, macro/micro and microvascular reactivity indexes: association between indexes and normative data from 2609 healthy subjects (3-85 years). *PLoS One* 16:e0254869. doi: 10.1371/journal.pone.0254869

Zócalo, Y., and Bia, D. (2021b). Sex-and age-related physiological profiles for brachial, vertebral, carotid and femoral arteries blood flow velocity parameters during growth and aging (4-76 y): comparison with clinical cut-off levels. *Front. Physiol.* 12:729309. doi: 10.3389/fphys.2021.729309

Zócalo, Y., García-Espinosa, V., Castro, J. M., Zinoveev, A., Marin, M., Chiesa, P., et al. (2020). Stroke volume and cardiac output non-invasive monitoring based on brachial oscillometry-derived pulse contour analysis: explanatory variables and reference intervals throughout life (3–88 years). *Cardiol. J.* 28, 864–878. doi: 10.5603/CJ.a2020.0031

Conflict of Interest: The authors declare that the research was conducted in the absence of any commercial or financial relationships that could be construed as a potential conflict of interest.

Publisher's Note: All claims expressed in this article are solely those of the authors and do not necessarily represent those of their affiliated organizations, or those of the publisher, the editors and the reviewers. Any product that may be evaluated in this article, or claim that may be made by its manufacturer, is not guaranteed or endorsed by the publisher.

frontiers in Physiology

ORIGINAL RESEARCH
published: 15 February 2022
doi: 10.3389/fphys.2021.783457

Subject-Specific Pressure Normalization of Local Pulse Wave Velocity: Separating Intrinsic From Acute Load-Dependent Stiffening in Hypertensive Patients

*Alessandro Giudici[1], Carlo Palombo[2], Michaela Kozakova[3], Carmela Morizzo[2], J. Kennedy Cruickshank[4] and Ashraf W. Khir[1]**

[1] Brunel Institute for Bioengineering, Brunel University London, Uxbridge, United Kingdom, [2] Department of Surgical, Medical, Molecular Pathology and Critical Area Medicine, University of Pisa, Pisa, Italy, [3] Department of Clinical and Experimental Medicine, University of Pisa, Pisa, Italy, [4] School of Life-Course/Nutritional Sciences, King's College, St. Thomas' and Guy's Hospitals, London, United Kingdom

Pulse wave velocity (PWV) is a powerful predictor of cardiovascular events. However, its intrinsic blood pressure (BP)-dependency complicates distinguishing between acute and chronic effects of increased BP on arterial stiffness. Based on the assumption that arteries exhibit a nearly exponential pressure-area (*P-A*) relationship, this study proposes a method to assess intersubject differences in local PWV independently from BP. The method was then used to analyze differences in local carotid PWV (cPWV) between hypertensive and healthy normotensive people before and after BP-normalization. Pressure (*P*) and diameter (*D*) waveforms were simultaneously acquired *via* tonometer at the left and ultrasound scanning at right common carotid artery (CCA), respectively, in 22 patients with Grade 1 or 2 hypertension and 22 age- and sex-matched controls. cPWV was determined using the D^2P-loop method. Then, the exponential modeling of the *P*-area ($A = \pi D^2/4$) relationships allowed defining a mathematical formulation to compute subject-specific changes in cPWV associated with BP changes, thus enabling the normalization of cPWV against intersubject differences in BP at the time of measurement. Carotid systolic BP (SBP) and diastolic BP (DBP) were, on average, 17.7 ($p < 0.001$) and 8.9 mmHg ($p < 0.01$) higher in hypertensives than controls, respectively. cPWV was 5.56 ± 0.86 m/s in controls and 6.24 ± 1.22 m/s in hypertensives. BP alone accounted for 68% of the cPWV difference between the two groups: 5.80 ± 0.84 vs. 6.03 ± 1.07 m/s after BP-normalization ($p = 0.47$). The mechanistic normalization of cPWV was in agreement with that estimated by analysis of covariance (ANCOVA). In conclusion, the proposed method, which could be easily implemented in the clinical setting, allows to assess the intersubject differences in PWV independently of BP. Our results suggested that mild hypertension in middle-aged subjects without target organ damage does not significantly alter the stiffness of the CCA wall independently of acute differences in BP. The results warrant further clinical investigations to establish the potential clinical utility of the method.

Keywords: pressure-independent PWV, hypertension, arterial stiffness, common carotid arteries, blood pressure

OPEN ACCESS

Edited by:
Dimitrios Terentes-Printzios, University of Oxford, United Kingdom

Reviewed by:
Zhe Sun, University of Missouri, United States
Spyretta Golemati, National and Kapodistrian University of Athens, Greece

***Correspondence:**
Ashraf W. Khir
ashraf.w.khir@durham.ac.uk

Specialty section:
This article was submitted to Vascular Physiology, a section of the journal Frontiers in Physiology

Received: *26 September 2021*
Accepted: *14 December 2021*
Published: *15 February 2022*

Citation:
Giudici A, Palombo C, Kozakova M, Morizzo C, Cruickshank JK and Khir AW (2022) Subject-Specific Pressure Normalization of Local Pulse Wave Velocity: Separating Intrinsic From Acute Load-Dependent Stiffening in Hypertensive Patients. Front. Physiol. 12:783457. doi: 10.3389/fphys.2021.783457

INTRODUCTION

Arterial stiffness as pulse wave velocity (PWV) is a powerful predictor of mortality and cardiovascular events in hypertensive patients, above and beyond traditional risk factors (Boutouyrie et al., 2002; Laurent et al., 2003; Cardoso et al., 2019). The arterial wall, however, presents a complex microstructure where different wall constituents, mainly collagen, elastin, and smooth muscle, play different but equally important roles in arterial function (Boutouyrie et al., 1998; Cruickshank et al., 2002; Krasny et al., 2017; Giudici et al., 2021e). The heterogeneous microstructure of the arterial wall makes its behavior highly nonlinear (Giudici et al., 2021b) so that arterial stiffness and, consequently, PWV are intrinsically blood pressure (BP)-dependent (Spronck et al., 2015b). This fact complicates distinguishing between chronic (i.e., actual BP-induced wall remodeling) and acute effects (i.e., transitional shift to a different working point in the nonlinear behavior of the arterial wall) of increased BP on arterial structure and mechanics. Most clinical studies address the issue of the BP-dependency of PWV *via* statistical methods, using BP as a confounding factor for PWV (Desamericq et al., 2015; Diaz et al., 2018; Valbusa et al., 2019). However, statistical methods suffer some limitations: (1) they lack subject specificity and, hence, are less likely to be used in clinical practice, (2) they may fail to discriminate between acute and chronic effects of increased BP on the wall stiffness (Spronck, 2021), and (3) the choice of the normalizing pressure, i.e., the subject-specific pressure level to be used as the confounder in multivariate analysis, is not trivial and largely affects the size of the correction itself (Giudici et al., 2021a). While, in clinical investigations, statistical adjustments for systolic BP (SBP) (Valbusa et al., 2019), mean BP (MBP) (Desamericq et al., 2015), and pulse pressure (PP) (Brandts et al., 2012) are often made, most regional PWV metrics (e.g., carotid-femoral and brachial-ankle PWV), use the foot of arterial waves as the fiducial point, suggesting that diastolic BP (DBP) likely represent a more appropriate choice for their pressure-normalization (Spronck et al., 2017b). As intergroup differences in SBP are typically larger than those in DBP, widely used SBP- and MBP-statistical adjustments likely lead to overcorrections of PWV and potentially limit our understanding of pressure-induced chronic vascular damage (Spronck et al., 2017b).

In the past two decades, researchers have attempted to address the BP-dependency of PWV using mechanistic approaches that rely chiefly on the assumption that, in the physiological pressure range, the pressure (P)-area (A)/diameter (D) relationship of arteries resembles an exponential function (Gavish and Izzo, 2016). If the fitting exponential function is opportunely formulated, its constant can be used as a BP-normalized index of arterial stiffness (Spronck et al., 2017a; Giudici et al., 2021a). In 2006, Shirai et al. introduced the cardio-ankle vascular index (CAVI) that uses the heart-to-ankle PWV (haPWV), a regional PWV metric quantifying the average properties of the entire heart-to-ankle arterial pathway, to estimate Kawasaki's stiffness index β, defining the exponential relationship between P and D. A decade later, however, Spronck et al. (2017a) raised concerns related to the actual (in)dependency of CAVI from BP at the time of measurement, due to the inherent dependency of β from the subject-specific DBP. They proposed a revised metric $CAVI_0$ that relies on Hayashi's stiffness index β_0, which, unlike β, is defined with respect to a standardized reference pressure (P_{ref}). Furthermore, CAVI and $CAVI_0$ differ also in the normalizing pressure used to estimate β from haPWV, raising once more the question of which is the most appropriate pressure level for the normalization of PWV metrics (Giudici et al., 2021a).

Similar methods have been devised to correct local PWV estimates, which, unlike regional PWVs, provide information on the stiffness of a specific location of the arterial tree. Spronck et al. (2015a) used the exponential *P-A* relationship proposed by Meinders and Hoeks (2004) to effectively predict the changes in local carotid PWV (cPWV), estimated *via* a linearized Bramwell-Hill equation (Bramwell et al., 1923), associated with the BP lowering achieved with 3-months of antihypertensive treatment in hypertensive patients. A considerably more complex approach was proposed by Ma et al. (2018) who used Fung's exponential hyperelastic strain energy function to define the relationship between BP and local PWV. While undoubtedly elegant, this approach is unlikely to be used in clinical practice due to the difficulty in estimating subject-specific parameters for the mathematical model describing the artery behavior.

Using a similar mechanistic approach based on the exponential modeling of the *P-A* relationship of arteries (Spronck et al., 2015b, 2017a), our current study analyzed differences in local cPWV between healthy controls and patients with hypertension, aiming to distinguish between acute and chronic effects of high BP on carotid function. We also aimed to compare mechanistic and statistical correction of cPWV, analyzing the impact of the choice of the normalizing pressure on the size of the correction and on inter-group differences.

MATERIALS AND METHODS

Theoretical Background

Tube laws mathematically define the relationship between P and A in flexible tubes. The pressure-normalization method adopted in this study is based on the tube law proposed by Meinders and Hoeks (2004):

$$P(D) = P_{ref} e^{\gamma_0 \left(\frac{D^2}{D_{ref}^2} - 1 \right)}, \quad (1)$$

where D is the luminal diameter (A is assumed to be circular, $A = \pi D^2/4$), P_{ref} is a reference pressure, D_{ref} is the diameter at P_{ref}, and γ_0 is an index of arterial stiffness defining the exponential relationship between P and D^2. Note that identical P-D^2 relationships can be obtained with opportunely different combinations of P_{ref}, D_{ref}, and γ_0 (Giudici et al., 2021a). Eq. 1 represents a generalized form of the tube law proposed by Meinders and Hoeks who chose P_{ref} = DBP. While P_{ref} does not have any physiological meaning and its choice is arbitrary, fixing P_{ref} to a constant value makes γ_0 a pressure-normalized index of arterial stiffness. Following previous studies (Giudici et al., 2021a; van der Bruggen et al., 2021), we chose P_{ref} = 100 mmHg. This value represents the most commonly established value for

mean pressure of healthy adults and allows direct comparison with previous studies.

The Bramwell-Hill equation (Bramwell et al., 1923), defining the relationship between arterial distensibility and local PWV, suggests that PWV at a given pressure level P_c can be expressed as a function of the slope of the tangent to the P-D^2 relationship at P_c.

$$\mathrm{PWV}\,(P_c) \;=\; \sqrt{\frac{D^2}{\rho}\,\frac{\mathrm{d}P}{\mathrm{d}D^2}\Big|_{P_c}}, \tag{2}$$

where ρ is the blood density, here assumed as 1,060 kg/m^3. Using Eq. 1 to determine the derivative term in Eq. 2 and rearranging using Eq. 1 leads to the following relationship between PWV and γ_0, as previously demonstrated (Giudici et al., 2021d) (refer to Eqs A1–A7 in **Appendix** for the detailed calculations):

$$\mathrm{PWV}(P_c)^2 \;=\; \frac{P_c\gamma_0}{\rho} + \frac{P_c}{\rho}\ln\left(\frac{P_c}{P_{\mathrm{ref}}}\right). \tag{3}$$

Eq. 3 indicates that PWV at any P_c can be directly estimated using γ_0 and P_{ref}.

Let us define a target pressure P_T as the pressure level to which normalization is required. Given that PWV was measured at the pressure P_c [i.e., PWV(P_c)], the pressure change used to normalize PWV(P_c) is determined as the difference between the two pressure levels: P_T–P_c. Following from Eq. 3, PWV at P_T can be determined as follows:

$$\mathrm{PWV}(P_\mathrm{T})^2 \;=\; \frac{P_\mathrm{T}\,\gamma_0}{\rho} + \frac{P_\mathrm{T}}{\rho}\ln\left(\frac{P_\mathrm{T}}{P_{\mathrm{ref}}}\right). \tag{4}$$

By combining Eq. 3 and 4, we obtain as follows:

$$\mathrm{PWV}\,(P_\mathrm{T}) \;=\; \sqrt{\mathrm{PWV}(P_c)^2\,\frac{P_\mathrm{T}}{P_c} + \frac{P_\mathrm{T}}{\rho}\ln\left(\frac{P_\mathrm{T}}{P_c}\right)}. \tag{5}$$

Eq. 5 allows us to convert PWV at pressure P_c to the desired target pressure P_T. We noted that P_c is generally unknown and depends on the choice of the method used to estimate PWV. However, if γ_0 is known, P_c for any PWV estimation method can be numerically estimated by solving Eq. 3.

Study Population and Data Acquisition

The study sample came from individuals undergoing standard outpatient cardiovascular risk assessment at the Pisa University Hospital (Pisa, Italy), omitting anyone with carotid atherosclerotic plaque, diabetes, and history of major cardiovascular events, atrial fibrillation, malignancy, or chronic inflammatory disease. Hypertension was defined as brachial SBP ($\mathrm{SBP_b}$) > 140 mmHg and/or DBP > 90 mmHg or based on active antihypertensive treatment. The final study population included n = 22 healthy normotensive controls and n = 22 patients with mild-to-moderate (or Grade 1–2) hypertension (Williams et al., 2018), of which 41% (n = 9) were treated (treatment duration < 1 year). The protocol of the study followed the principles of the Declaration of Helsinki and was approved by the institutional ethics committee "Comitato Etico di Area Vasta Nord Ovest" (reference number: 3146/2010). All subjects gave their informed consent to participate.

Both $\mathrm{SBP_b}$ and DBP were measured using a digital Omron device (model 705cp, Kyoto, Japan) after subjects had rested for at least 15 min in the supine position. Then, the pressure waveform of the left common carotid artery (CCA) and the diameter waveform of the right CCA were simultaneously acquired by tonometry (PulsePen, DiaTecne, Milan, Italy; sampling frequency = 1 kHz) and ultrasound scanning (Aloka Prosound 10, Hitachi Ltd., Japan), respectively. A similar coupling of waveforms acquired at the contralateral CCAs has been performed previously to achieve correspondence in heartbeats between the pressure and diameter signals, under the assumption that hemodynamic features are similar in the two CCAs due to their similar geometrical characteristics and downstream branching (Giannattasio et al., 2008). The ultrasound machine was equipped with a 10.0 MHz linear array probe with radiofrequency data output at the frequency of 1 kHz. In the longitudinal right CCA view, a single scan line was aligned perpendicularly to the vessel walls, approximately 1.5 cm proximal to the carotid bulb, as reported previously (Uejima et al., 2019). The cursors were then placed by the experienced operator at the anterior and posterior carotid walls to enable wall tracking. PulsePen recordings were calibrated assuming constant DBP and MBP along the arterial tree. Brachial MBP was estimated from $\mathrm{SBP_b}$ and DBP assuming a form factor of 0.43: MBP = DBP+0.43 ($\mathrm{SBP_b}$–DBP) (Segers et al., 2009). Both acquisitions lasted for approximately 10 s, yielding 7–10 overlapping pressure and diameter cardiac cycles to be used in the analysis. The two main peaks of the second derivatives (i.e., acceleration) of the pressure and diameter signals (identifying the foot of the wave and dicrotic notch, respectively) were used as fiducial points for the alignment of the two waveforms, as previously described (Giudici et al., 2021c). **Figures 1A,B** provide examples of aligned left CCA pressure and right CCA diameter waveforms in a representative normotensive and hypertensive person, respectively.

Data Analysis

cPWV was estimated using the D^2P-loop method (Alastruey, 2011), a linearization of the Bramwell-Hill equation (Eq. 2) over the late diastolic part of the P-D^2 relationship (i.e., the diastolic decay spanning from the pressure at the dicrotic notch, P_{notch}, to DBP), as described previously (Giudici et al., 2021c).

$$\mathrm{cPWV} \;=\; \sqrt{\frac{D_\mathrm{d}^2}{\rho}\,\frac{\mathrm{d}P}{\mathrm{d}D^2}} \tag{6}$$

where D_d is the diameter at DBP, and the derivative term $\mathrm{d}P/\mathrm{d}D^2$ indicates the slope of the linear regression of the late diastolic part of the P-D^2 relationship.

As detailed in the theoretical background section, the accurate BP-normalization of cPWV requires knowledge of the pressure, P_c, that drives the BP-dependency of cPWV estimated with the D^2P-loop method. As indicated above, the D^2P-loop method estimates cPWV over the pressure range between P_{notch} and DBP. Therefore, the representative P_c is expected to fall within these two pressure levels. To estimate the most suitable P_c for the D^2P-loop method, the beat-to-beat relationships between left CCA P and right CCA D^2 were fitted using Eq. 1, as shown in **Figure 1C**,

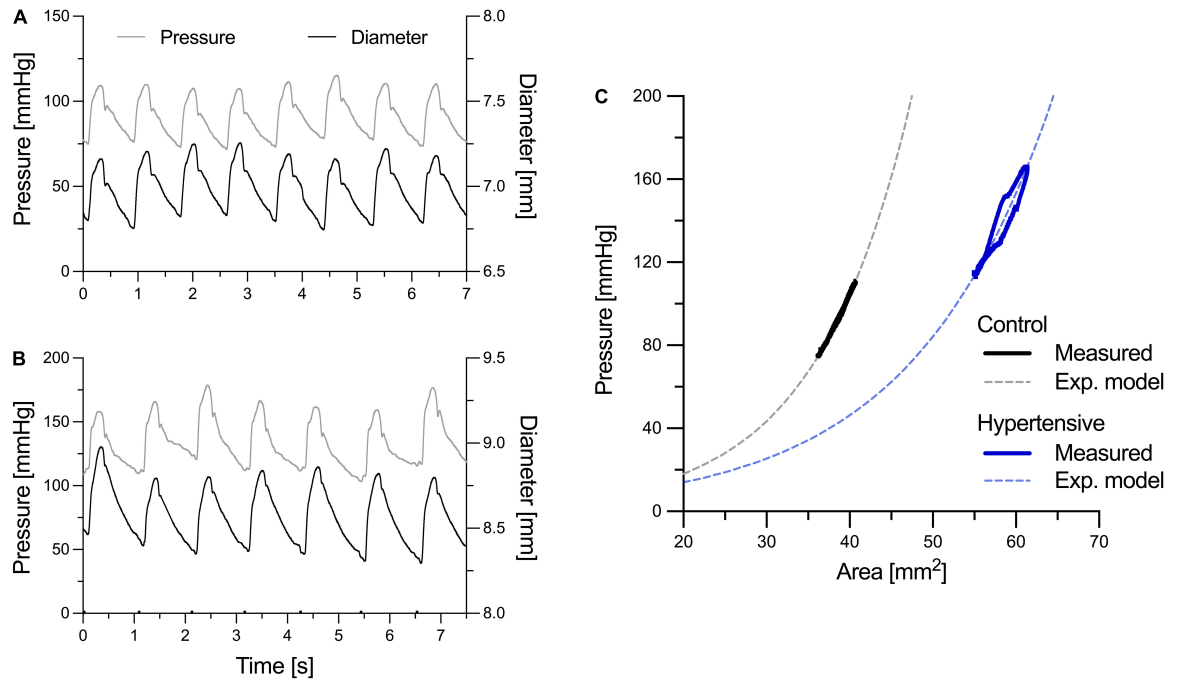

FIGURE 1 | Examples of left common carotid artery (CCA) pressure and right CCA diameter distension waveforms of a representative normotensive (control) person **(A)** and hypertensive patient **(B)**. Pressure and diameter waveforms were aligned using the two major peaks of their second derivative, representing the foot of the wave and the dicrotic notch, as fiducial points. In **(C)**, representative pressure-area (*P-A*) relationships were obtained by ensemble averaging pressure and diameter heartbeats [the luminal area (*A*) was calculated from the diameter *(D)* assuming a circular luminal area: $A = \pi D^2/4$]. **(C)** Illustrates how the exponential relationship in Eq. 1 was fitted on the measured subject-specific *P-A* relationships to estimate the stiffness index γ_0 (notably, in reality, this was performed on a beat-to-beat basis rather than on the ensemble-averaged curves).

to estimate γ_0. For each heartbeat, this step entailed determining the combination of γ_0 and D_{ref} that minimizes the difference between the measured *P* waveform and that estimated using Eq. 1, given the *D* waveform as input. Then, the most suitable P_c was numerically determined by solving Eq. 3, given γ_0 and cPWV. Notably, for each patient, the used γ_0 and cPWV were the mean values of the 7–10 simultaneously recorded heartbeats. Finally, cPWV was pressure-normalized using Eq. 5.

Statistical Analysis

Statistical analysis was performed using SPSS 23 (SPSS, IBM Corp., Chicago, IL, United States). Comparison of variables between the two groups was first performed using Student's *t*-test and then adjusting for potential confounders using analysis of covariance (ANCOVA). The BP-normalization of cPWV was performed using both mechanistic (Eq. 5) and statistical (ANCOVA) methods and considering four different pressure levels as normalizing pressure: (1) P_c, determined numerically by solving Eq. 3, (2) DBP, (3) MBP, and (4) SBP. The latter three pressure levels were chosen because often used as normalizing pressures in clinical studies. For each pressure level, P_T in Eq. 5 was set to the average P_c, DBP, MBP, or SBP across groups. Data are generally presented as average ± standard deviation (SD). ANCOVA estimates are presented as average (95% CI). The *p*-value < 0.05 was considered statistically significant.

RESULTS

Group Characteristics

Group characteristics are presented in **Table 1**. Hypertensive and control groups were matched in age and gender, but not heart rate (HR) that was on average 6 bpm higher in hypertensives ($p = 0.021$). Carotid SBP was, on average 17.7 mmHg higher in hypertensives than controls ($p < 0.001$), while the difference in DBP was approximately half ($p < 0.01$). As a result, PP was also 8.7 mmHg higher in hypertensives than controls. Average CCA diameters at SBP and DBP were slightly higher in hypertensives than controls, but differences were not significant and were reduced further after appropriate SBP and DBP adjustments [7.62 (7.23–8.02) vs. 7.76 (7.37–8.16) mm and 7.15 (6.77–7.53) vs. 7.33 (6.95–7.71) mm]. Conversely, carotid IMT and IMT/D_d were higher in hypertensives than controls ($p = 0.005$ and $p = 0.058$, respectively).

As expected, before accounting for BP differences, cPWV, calculated using Eq. 6, was on average 12% higher in hypertensives than controls (6.24 ± 1.22 vs. 5.56 ± 0.86 m/s, $p < 0.05$) (**Figure 2**, left, and **Table 2**), even after HR adjustments ($p < 0.05$). However, the pressure-normalized stiffness index γ_0 did not differ significantly (3.48 ± 1.04 vs. 3.77 ± 1.27, $p = 0.41$), suggesting that increased cPWV in hypertensives was likely mainly related to BP differences between groups. In fact, the average estimated *P-A* relationships of the two groups (**Figure 3**)

TABLE 1 | Characteristics and carotid artery dimensions of control and hypertension groups.

	Controls	Hypertensives	
Age [years]	55 ± 6	56 ± 9	$p = 0.77$
Male : Females	13 : 9	13 : 9	$p = 0.77$
HR [bpm]	60 ± 7	66 ± 9	$p = 0.021$
SBP_b [mmHg]	116.6 ± 12.2	133.7 ± 17.9	$p < 0.001$
SBP [mmHg]	113.9 ± 11.4	131.6 ± 17.9	$p < 0.001$
DBP [mmHg]	74.9 ± 8.7	83.8 ± 9.8	$p = 0.003$
MBP [mmHg]	92.7 ± 9.5	105.1 ± 12.2	$p < 0.001$
PP [mmHg]	39.0 ± 7.4	47.7 ± 12.6	$p = 0.009$
P_{notch} [mmHg]	100.0 ± 9.9	114.6 ± 14.6	$p < 0.001$
D_s [mm]	7.54 ± 0.84	7.85 ± 0.82	$p = 0.23$
D_d [mm]	7.08 ± 0.83	7.40 ± 0.81	$p = 0.21$
IMT [μm]	711 ± 145	819 ± 138	$p = 0.005$
IMT/D_d [–]	0.101 ± 0.017	0.111 ± 0.015	$p = 0.058$

The p-values are the results of the independent Student's t-test.
D_d, diastolic diameter; D_s, systolic diameter; DBP, diastolic blood pressure; HR, heart rate; IMT, intima-media thickness; MBP, mean blood pressure; P_{notch}, pressure at the dicrotic notch; PP, pulse pressure; SBP, carotid systolic blood pressure; SBP_b, brachial systolic blood pressure. Data are presented as mean ± standard deviation (SD).

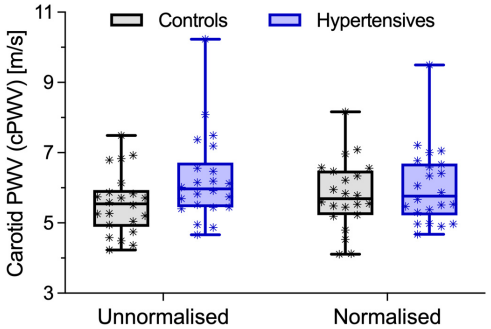

FIGURE 2 | Local carotid pulse wave velocity (cPWV) in control and hypertensive people before and after pressure-normalization using Eq. 5. Bars indicate minimum and maximum.

TABLE 2 | Comparison between mechanistic and statistical blood pressure adjustment of the local carotid pulse wave velocity (cPWV) using different normalizing pressures.

	Controls		Hypertensives	
	Mechanistic	Statistical	Mechanistic	Statistical
Uncorrected	5.56 ± 0.86		6.24 ± 1.22	
SBP	5.88 ± 0.84	5.85 (5.40–6.30)	5.95 ± 0.98	5.95 (5.50–6.40)
MBP	5.82 ± 0.89	5.80 (5.34–6.26)	6.00 ± 1.00	6.00 (5.54–6.46)
P_c	5.80 ± 0.95	5.77 (5.33–6.20)	6.04 ± 1.07	6.03 (5.54–6.46)
DBP	5.80 ± 0.94	5.69 (5.21–6.17)	6.03 ± 1.05	6.11 (5.59–6.47)

DBP, diastolic blood pressure; MBP, mean blood pressure; P_c, numerically determined local carotid PWV relevant pressure level; SBP, systolic blood pressure. Uncorrected and mechanistically corrected cPWV data are presented as mean ± standard deviation (SD). Statistically corrected cPWV data are presented as mean (95% confidence interval).

run almost parallel to each other and are largely superimposed, suggesting that the mechanical response of the carotid arteries in the two groups was similar.

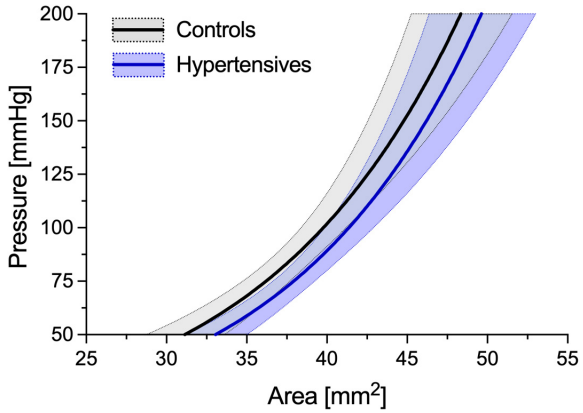

FIGURE 3 | Average estimated *P-A* relationships of the control and hypertensive groups. Average curves have been built by estimating γ_0 for all the subjects included in the two groups. Then, the subject-specific estimated *P-A* relationship was built using Eq. 1 and assuming a circular luminal area (i.e., $A = \pi D^2/4$, where D is the diameter). Finally, ensemble averaging was performed between all people in each group. Solid lines indicate the average relationship, and areas delimited by dotted lines indicate ± standard deviation (SD).

Pressure-Normalized Carotid PWV

P_c, estimated from cPWV and γ_0 by numerically solving Eq. 3, was 87.5 ± 10.3 in hypertensives and 78.4 ± 10.3 in controls, corresponding approximately to DBP + 0.085 (SBP–DBP) for both groups (**Figure 3**). Notably, in both groups, P_{notch} (**Table 1**) was, on average, (0.65 ± 0.10) PP above DBP. In a first BP-normalization, P_T was set to the average P_c across groups: 83.1 mmHg. After the BP-normalization, the difference in cPWV between the two groups reduced by 68%: 5.80 ± 0.94 m/s in controls and 6.03 ± 1.05 m/s in hypertensives ($p = 0.47$) (**Figure 2**, right). In fact, except for a single hypertensive subject whose cPWV largely exceeded those of controls both before and after the pressure-normalization, all other hypertensives had normalized cPWV within the control range. Similar results were obtained when normalizing using ANCOVA with P_c as a confounder: 5.77 (5.33–6.20) vs. 6.03 (5.59–6.47) m/s ($p = 0.41$) (62% of the total cPWV difference).

Table 2 reports the comparison between the BP-normalization using Eq. 5 and ANCOVA and using P_c, SBP, MBP, and DBP as normalizing pressures. As expected, the corrections of cPWV were stronger when using higher values of normalizing pressure and, except when the normalizing pressure was set to DBP, showed good agreement between statistical and mechanistic methods. BP accounted for 90 (mechanistic) and 84% (statistical) with SBP as confounder, 75 and 69% with MBP, and 65 and 39% with DBP.

DISCUSSION

The BP-dependency of arterial stiffness limits the ability of PWV to define changes in the mechanical properties of the arterial wall in response to cardiovascular pathologies and wall remodeling and damage (Spronck, 2021). This fact assumes particular

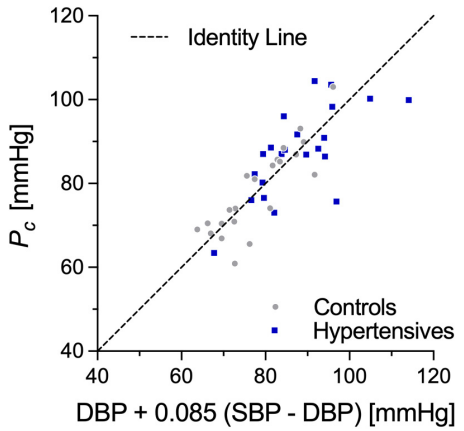

FIGURE 4 | Correlation between P_c, the pressure value linking cPWV to γ_0, and DBP + 0.085 (SBP-DBP). SBP, systolic blood pressure; DBP, diastolic blood pressure.

relevance when evaluating changes in arterial mechanics in response to hypertension since elevated BP drives the short-term increase in PWV and potentially the long-term damage to the wall microstructure that, in turn, could result in a chronic increase in PWV. The BP-dependency of PWV has been typically addressed *via* statistical methods (Desamericq et al., 2015; Valbusa et al., 2019). More recently, methods that rely on the exponential modeling of the wall behavior have allowed to mathematically predict subject-specific changes in PWV in response to acute changes in BP (Shirai et al., 2006; Spronck et al., 2017a). Using a similar approach, we aimed to characterize differences in CCA stiffness between healthy controls and hypertensive patients, providing subject-specific BP-normalization of cPWV. Furthermore, we aimed to compare the mechanistic BP-normalization with that obtained using statistical methods, as well as investigate the impact of the choice of the normalizing pressure on the obtained correction. Our results indicated that BP alone accounted for 68% of the cPWV difference between groups.

The association between hypertension and increased PWV has long been known (The Reference Values for Arterial Stiffness' Collaboration, 2010). However, understanding the causal relationships between the two is less trivial; on the one hand, studies have shown that PWV is an independent predictor of the longitudinal increase in SBP (Najjar et al., 2008), so that increased PWV drives the development of hypertension. On the other hand, PWV intrinsically depends on the BP level at the time of the data acquisition, and the subject-specific PWV can vary considerably in response to BP changes (Spronck et al., 2015b). This two-way relationship between PWV and BP complicates investigating the consequences of increased BP on arterial mechanics. Methods for the BP-normalization of PWV aim to address this issue, providing stiffness metrics that refer to a predefined reference pressure level and are, hence, independent from the BP level at the time of the measurement (Spronck et al., 2017a; Giudici et al., 2021a).

In this study, we analyzed differences in CCA PWV between normotensive and Grade 1–2 hypertensive individuals. In agreement with previous studies (Maritz et al., 2016; Park et al., 2020), our results indicated that the cPWV was, in fact, higher in hypertensives than in controls at their relative working pressure: 12% difference with a 13 and 12% difference in SBP and DBP, respectively. Notably, while age and sex are key determinants of arterial stiffness (The Reference Values for Arterial Stiffness' Collaboration, 2010), our studied groups were well-matched, so that these factors unlikely played a role in inter-group differences in cPWV. Our finding is in agreement with previous work (Laurent et al., 1994) where distensibility of the CCA at MBP was reduced by ∼33% in hypertensive people compared to healthy controls but with a ∼30% difference in SBP/DBP. Similar results have also been reported for regional carotid-femoral PWV (The Reference Values for Arterial Stiffness' Collaboration, 2010). However, the pressure-normalization of cPWV proposed here indicated that more than two-thirds of this difference had to be imputed to BP differences between the two groups (**Figure 2**) and that, in absolute terms, the CCA of hypertensive patients was not intrinsically stiffer than that of healthy people. Notably, as suggested by the Moens-Kortweg equation (Moens, 1878; Li et al., 2021), PWV quantifies the structural stiffness of an artery as a whole (i.e., including both wall material stiffness and geometrical features). As hypertensives here had a higher IMT and IMT/D_d ratio than controls, residual differences in PWV after pressure-normalization may, at least in part, be attributable to these structural differences, rather than pure differences in wall material properties. This finding was further confirmed by the exponential modeling of the *P-A* relationships, with the average hypertensive curve running almost parallel to that of controls, independently of pressure. Our findings are in agreement with seminal works of Laurent et al. (1994) and Armentano et al. (1995), who showed that CCA distensibility-pressure relationships of controls and hypertensives are almost superimposed. These results suggest that wall stiffening in response to increased BP is mild at the CCA. It is worth considering, however, that patients in our study presented only mild-to-moderate hypertension with a relatively short time between the diagnosis of the condition and the time of the examination (< 1 year). Therefore, it is possible that longer exposure to severely increased BP might trigger intensive remodeling and, consequently, intrinsic stiffening (i.e., BP-independent) of the carotid wall.

Whether accounting for the BP-dependency of PWV with statistical or mechanistic methods, the choice of the normalizing pressure has an important quantitative impact on the size of the correction. While the most widely adopted choices in clinical studies are SBP or MBP (Desamericq et al., 2015; Valbusa et al., 2019), it has been previously argued that the BP-dependency of most metrics pertaining to PWV, especially those relying on the foot-to-foot detection technique, is likely governed by DBP (i.e., the pressure at the foot of the wave) rather than either SBP or MBP (Spronck et al., 2015b, 2017a; Giudici et al., 2021a). In this study, cPWV was estimated *via* linear regression of the P-D^2 relationship in late diastole, i.e., the diastolic decay after the dicrotic notch (Giudici et al., 2021c). Although this phase of the cardiac cycle spanned between DBP and ∼65% of the PP,

our results indicated that, on average, P_c was determined for its 91.5% by DBP and only for its 8.5% by SBP (**Figure 4**). We obtained similar results when estimating cPWV *via* the ln*DU*-loop method, a linear regression between blood velocity (U) and the natural logarithm of the diameter distension (ln$D$) in early systole (Giudici et al., 2021d). These findings suggest that, as regional PWV, loop methods provide nearly diastolic measures of PWV and that DBP should be regarded as the main driver of their BP-dependency. Notably, however, in this study, DBP-adjustment provided the largest difference between statistical and mechanistic methods for the cPWV correction. This result warrants caution when performing statistical DBP-adjustment of all arterial stiffness metrics that are notably *purely* diastolic.

As other local techniques (Rabben et al., 2004; Khir and Parker, 2005; Feng and Khir, 2010; Campos Arias et al., 2019), the D^2P-loop method (Alastruey, 2011) is based on the coupling of two arterial waveforms to provide an estimate of the wave speed at a single location of the arterial tree (i.e., local wave speed). In contrast, regional PWVs, such as the carotid-femoral PWV (Laurent et al., 2006), provide insights into the average arterial stiffness along a given wave path, which inevitably includes arteries with different wall structures. This is particularly relevant when considering that elastic and muscular arteries have shown to be affected differently by aging and disease (Borlotti et al., 2012). Furthermore, local methods are not affected by known limitations of regional PWVs, such as the possible inaccuracies in the estimation of the true arterial pathway length (Huybrechts et al., 2011; Giudici et al., 2021a). Finally, local arterial properties can be useful to predict damage of target organs located in the vicinity of the measurement site; for example, carotid stiffening and function have been associated with cognitive decline (Chiesa et al., 2019). For the aforementioned reasons, results reported here on differences in arterial wall stiffness between normotensives and hypertensives concern the carotid artery and should not be generalized to other locations or regions of the arterial tree.

LIMITATIONS

In this study, we assumed the existence of an exponential *P-A* relationship for the CCA. While it is generally accepted that the *P-A* relationship of arteries closely resembles an exponential function in the physiological range of pressure (Gavish and Izzo, 2016), the subject-specific *P-A* relationships might not be exactly exponential, especially in young subjects at low pressures (Vande Geest et al., 2004). It is therefore possible that, for some subjects, the mechanistic method failed to accurately predict the relationship between BP and cPWV. It is, however, unlikely that this has significantly affected the cPWV-normalization since similar methods showed good ability in predicting changes in both local and regional PWV, given a BP change (Spronck et al., 2015b; Pucci et al., 2020).

CONCLUSION

We concluded that mild hypertension does not chronically affect the stiffness of the CCA wall, at least in the middle-aged subjects without target organ damage.

Assuming an exponential *P-A* relationship, we proposed a method that allows for determining arterial stiffness, as PWV, independently of BP. The proposed method is non-invasive and provides a subject-specific normalization of PWV which could be implemented in the clinical setting. The results warrant further investigations to establish the potential clinical utility of the method.

DATA AVAILABILITY STATEMENT

The raw data supporting the conclusions of this article will be made available by the authors, upon reasonable request.

ETHICS STATEMENT

The studies involving human participants were reviewed and approved by Comitato Etico di Area Vasta Nord Ovest (reference number: 3146/2010), Italy. The patients/participants provided their written informed consent to participate in this study.

AUTHOR CONTRIBUTIONS

AG contributed to the conceptualization, data analysis, manuscript drafting, and editing. AG and AK developed the analytical method. AK, CP, JC, and MK contributed to the conceptualization, manuscript editing, and project supervision. CM contributed to the data acquisition and management. All authors contributed to the article and approved the submitted version.

FUNDING

This study was partially supported by an Innovative Medicines Initiative (IMI-EU) grant "Surrogate markers for Micro- and Macrovascular hard endpoints for innovative diabetes tools: SUMMIT." AG was supported by Addenbrooke's Hospital (Cambridge, United Kingdom) (Grant No. 10696100).

REFERENCES

Alastruey, J. (2011). Numerical assessment of time-domain methods for the estimation of local arterial pulse wave speed. *J. Biomech.* 44, 885–891.

Armentano, R., Megnien, J. L., Simon, A., Bellenfant, F., Barra, J., and Levenson, J. (1995). Effects of hypertension on viscoelasticity of carotid and femoral arteries in humans. *Hypertension* 26, 48–54. doi: 10.1161/01.hyp.26.1.48

Borlotti, A., Khir, A. W., Rietzschel, E. R., De Buyzere, M. L., Vermeersch, S., and Segers, P. (2012). Noninvasive determination of local pulse wave velocity and wave intensity: changes with age and gender in the carotid and femoral arteries of healthy human. *J. Appl. Physiol.* 113, 727–735. doi: 10.1152/japplphysiol.00164.2012

Boutouyrie, P., Boumaza, S., Challande, P., Lacolley, P., and Laurent, S. (1998). Smooth muscle tone and arterial wall viscosity: an *in vivo*/*in vitro* study. *Hypertension* 32, 360–364. doi: 10.1161/01.hyp.32.2.360

Boutouyrie, P., Tropeano, A. I., Asmar, R., Gautier, I., Benetos, A., Lacolley, P., et al. (2002). Aortic stiffness is an independent predictor of primary coronary events in hypertensive patients: a longitudinal study. *Hypertension* 39, 10–15. doi: 10.1161/hy0102.099031

Bramwell, J. C., Hill, A. V., and McSwiney, B. A. (1923). The velocity of the pulse wave in man in relation to age as measured by the hot-wire sphygmograph. *Heart* 10, 233–255.

Brandts, A., Van Elderen, S. G. C., Tamsma, J. T., Smit, J. W. A., Kroft, L. J. M., Lamb, H. J., et al. (2012). The effect of hypertension on aortic pulse wave velocity in type-1 diabetes mellitus patients: assessment with MRI. *Int. J. Cardiovasc. Imaging* 28, 543–550. doi: 10.1007/s10554-011-9841-2

Campos Arias, D., Stergiopulos, N., Rodríguez Moliner, T., and Segers, P. (2019). Mapping the site-specific accuracy of loop-based local pulse wave velocity estimation and reflection magnitude: a 1D arterial network model analysis. *Physiol. Meas.* 40:075002. doi: 10.1088/1361-6579/ab15aa

Cardoso, C. R. L., Salles, G. C., and Salles, G. F. (2019). Prognostic impact of aortic stiffness in patients with resistant hypertension. *Hypertension* 73, 728–735. doi: 10.1161/HYPERTENSIONAHA.118.12367

Chiesa, S. T., Masi, S., Shipley, M. J., Ellins, E. A., Fraser, A. G., Hughes, A. D., et al. (2019). Carotid artery wave intensity in mid- to late-life predicts cognitive decline: the Whitehall II study. *Eur. Heart J.* 40, 2300–2309. doi: 10.1093/eurheartj/ehz189

Cruickshank, J. K., Riste, L., Anderson, S. G., Wright, J. S., Dunn, G., and Gosling, R. G. (2002). Aortic pulse-wave velocity and its relationship to mortality in diabetes and glucose intolerance: an integrated index of vascular function? *Circulation* 106, 2085–2090. doi: 10.1161/01.cir.0000033824.02722.f7

Desamericq, G., Tissot, C. M., Akakpo, S., Tropeano, A. I., Millasseau, S., and MacQuin-Mavier, I. (2015). Carotid-femoral pulse wave velocity is not increased in obesity. *Am. J. Hypertens.* 28, 546–551. doi: 10.1093/ajh/hpu190

Diaz, A., Tringler, M., Wray, S., Ramirez, A. J., and Cabrera Fischer, E. I. (2018). The effects of age on pulse wave velocity in untreated hypertension. *J. Clin. Hypertens.* 20, 258–265. doi: 10.1111/jch.13167

Feng, J., and Khir, A. W. (2010). Determination of wave speed and wave separation in the arteries using diameter and velocity. *J. Biomech.* 43, 455–462. doi: 10.1016/j.jbiomech.2009.09.046

Gavish, B., and Izzo, J. L. (2016). Arterial stiffness: going a step beyond. *Am. J. Hypertens.* 29, 1223–1233. doi: 10.1093/ajh/hpw061

Giannattasio, C., Salvi, P., Valbusa, F., Kearney-Schwartz, A., Capra, A., Amigoni, M., et al. (2008). Simultaneous measurement of beat-to-beat carotid diameter and pressure changes to assess arterial mechanical properties. *Hypertension* 52, 896–902. doi: 10.1161/HYPERTENSIONAHA.108.116509

Giudici, A., Khir, A. W., Reesink, K. D., Delhaas, T., and Spronck, B. (2021a). Five years of cardio-ankle vascular index (CAVI) and CAVI0. *J. Hypertens.* 39, 2128–2138. doi: 10.1097/HJH.0000000000002928

Giudici, A., Khir, A. W., Szafron, J. M., and Spronck, B. (2021b). From uniaxial testing of isolated layers to a tri-layered arterial wall: a novel constitutive modelling framework. *Ann. Biomed. Eng.* 49, 2454–2467. doi: 10.1007/s10439-021-02775-2

Giudici, A., Palombo, C., Kozakova, M., Morizzo, C., Penno, G., Jamagidze, G., et al. (2021c). Non-invasive carotid pressure-diameter loops to identify viscoelastic properties in ageing, hypertension and type 2 diabetes. *J. Hypertens.* 39, 2307–2317. doi: 10.1097/HJH.0000000000002918

Giudici, A., Palombo, C., Morizzo, C., Kozakova, M., Cruickshank, J. K., Wilkinson, I. B., et al. (2021d). Transfer-function-free technique for the noninvasive determination of the human arterial pressure waveform. *Physiol. Rep.* 9:e15040. doi: 10.14814/phy2.15040

Giudici, A., Wilkinson, I. B., and Khir, A. (2021e). Review of the techniques used for investigating the role elastin and collagen play in arterial wall mechanics. *IEEE Rev. Biomed. Eng.* 14, 256–269. doi: 10.1109/RBME.2020.3005448

Huybrechts, S. A. M., Devos, D. G., Vermeersch, S. J., Mahieu, D., Achten, E., de Backer, T. L. M., et al. (2011). Carotid to femoral pulse wave velocity: a comparison of real travelled aortic path lengths detrmined by MRI and superficial measurments. *J. Hypertens.* 29, 1577–1582. doi: 10.1097/HJH.0b013e3283487841

Khir, A. W., and Parker, K. H. (2005). Wave intensity in the ascending aorta: effects of arterial occlusion. *J. Biomech.* 38, 647–655. doi: 10.1016/j.jbiomech.2004.05.039

Krasny, W., Magoariec, H., Morin, C., and Avril, S. (2017). Kinematics of collagen fibers in carotid arteries under tension-inflation loading. *J. Mech. Behav. Biomed. Mater.* 77, 718–726. doi: 10.1016/j.jmbbm.2017.08.014

Laurent, S., Caviezel, B., Beck, L., Girerd, X., Billaud, E., Boutouyrie, P., et al. (1994). Carotid artery distensibility and distending pressure in hypertensive humans. *Hypertension* 23, 878–883. doi: 10.1161/01.hyp.23.6.878

Laurent, S., Cockcroft, J., Van Bortel, L., Boutouyrie, P., Giannattasio, C., Hayoz, D., et al. (2006). Expert consensus document on arterial stiffness: methodological issues and clinical applications. *Eur. Heart J.* 27, 2588–2605. doi: 10.1093/eurheartj/ehl254

Laurent, S., Katsahian, S., Fassot, C., Tropeano, A.-I., Gautier, I., Laloux, B., et al. (2003). Aortic stiffness is an independent predictor of fatal stroke in essential hypertension. *Stroke* 34, 1203–1206. doi: 10.1161/01.STR.0000065428.03209.64

Li, Y., Giudici, A., Wilkinson, I. B., and Khir, A. W. (2021). Towards the non-invasive determination of arterial wall distensible properties: new approach using old formulae. *J. Biomech.* 115:110102. doi: 10.1016/j.jbiomech.2020.110102

Ma, Y., Choi, J., Hourlier-Fargette, A., Xue, Y., Chung, H. U., Lee, J. Y., et al. (2018). Relation between blood pressure and pulse wave velocity for human arteries. *Proc. Natl. Acad. Sci. U.S.A.* 115, 11144–11149.

Maritz, M., Fourie, C. M., Van Rooyen, J. M., Huisman, H. W., and Schutte, A. E. (2016). Carotid characteristics of black South Africans with five-year sustained hypertension. *Cardiovasc. J. Afr.* 27, 262–269. doi: 10.5830/CVJA-2016-059

Meinders, J. M., and Hoeks, A. P. G. (2004). Simultaneous assessment of diameter and pressure waveforms in the carotid artery. *Ultrasound Med. Biol.* 30, 147–154. doi: 10.1016/j.ultrasmedbio.2003.10.014

Moens, A. I. (1878). *Die Pulskurve*. Leiden: E.J. Brill.

Najjar, S. S., Scuteri, A., Shetty, V., Wright, J. G., Muller, D. C., Fleg, J. L., et al. (2008). Pulse wave velocity is an independent predictor of the longitudinal increase in systolic blood pressure and of incident hypertension in the baltimore longitudinal study of aging. *J. Am. Coll. Cardiol.* 51, 1377–1383. doi: 10.1016/j.jacc.2007.10.065

Park, J., Na, Y., Jang, Y., Park, S. Y., and Park, H. (2020). Correlation of pre-hypertension with carotid artery damage in middle-aged and older adults. *Int. J. Environ. Res. Public Health* 17, 1–13. doi: 10.3390/ijerph17207686

Pucci, G., Bart, S., Avolio, A. P., Tap, L., Vaudo, G., Anastasio, F., et al. (2020). Age-specific acute changes in carotid-femoral pulse wave velocity with head-up tilt. *Am. J. Hypertens.* 33, 1112–1118. doi: 10.1093/ajh/hpaa101

Rabben, S. I., Stergiopulos, N., Hellevik, L. R., Smiseth, O. A., Slørdahl, S., Urheim, S., et al. (2004). An ultrasound-based method for determining pulse wave velocity in superficial arteries. *J. Biomech.* 37, 1615–1622. doi: 10.1016/j.jbiomech.2003.12.031

Segers, P., Mahieu, D., Kips, J., Rietzschel, E., De Buyzere, M., De Bacquer, D., et al. (2009). Amplification of the pressure pulse in the upper limb in healthy, middle-aged men and women. *Hypertension* 54, 414–420. doi: 10.1161/HYPERTENSIONAHA.109.133009

Shirai, K., Utino, J., Otsuka, K., and Takata, M. (2006). A novel blood pressure-independent arterial wall stiffness parameter; cardio-ankle vascular index (CAVI). *J. Atheroscler. Thromb.* 13, 101–107. doi: 10.5551/jat.13.101

Spronck, B. (2021). Disentangling arterial stiffness and blood pressure. *Hear. Lung Circ.* 30, 1599–1601. doi: 10.1016/j.hlc.2021.05.086

Spronck, B., Avolio, A. P., Tan, I., Butlin, M., Reesink, K. D., and Delhaas, T. (2017a). Arterial stiffness index beta and cardio-ankle vascular index inherently depend on blood pressure but can be readily corrected. *J. Hypertens.* 35, 98–104. doi: 10.1097/HJH.0000000000001132

Spronck, B., Delhaas, T., Butlin, M., Reesink, K. D., and Avolio, A. P. (2017b). Options for dealing with pressure dependence of pulse wave velocity as a measure of arterial stiffness: an update of cardio-ankle vascular index (CAVI) and CAVI0. *Pulse* 5, 106–114. doi: 10.1159/000479322

Spronck, B., Heusinkveld, M. H. G., Donders, W. P., de Lepper, A. G. W., Op't Roodt, J., Kroon, A. A., et al. (2015a). A constitutive modeling interpretation of the relationship among carotid artery stiffness, blood pressure, and age in hypertensive subjects. *Am. J. Physiol. Heart Circ. Physiol.* 308, H568–H582. doi: 10.1152/ajpheart.00290.2014

Spronck, B., Heusinkveld, M., Vanmolkot, F., Roodt, J. O., Hermeling, E., Delhaas, T., et al. (2015b). Pressure-dependence of arterial stiffness: potential clinical implications. *J. Hypertens.* 33, 330–338. doi: 10.1097/HJH.0000000000000407

The Reference Values for Arterial Stiffness' Collaboration (2010). Determinants of pulse wave velocity in healthy people and in the presence of cardiovascular risk factors: "establishing normal and reference values". *Eur. Heart J.* 31, 2338–2350. doi: 10.1093/eurheartj/ehq165

Uejima, T., Dunstan, F. D., Arbustini, E., Łoboz-Grudzień, K., Hughes, A. D., Carerj, S., et al. (2019). Age-specific reference values for carotid arterial stiffness estimated by ultrasonic wall tracking. *J. Hum. Hypertens.* 34, 214–222.

Valbusa, F., Angheben, A., Mantovani, A., Zerbato, V., Chiampan, A., Bonapace, S., et al. (2019). Increased aortic stiffness in adults with chronic indeterminate Chagas disease. *PLoS One* 14:e0220689. doi: 10.1371/journal.pone.0220689

van der Bruggen, M., Spronck, B., Bos, S., Heusinkveld, M., Taddei, S., Ghiadoni, L., et al. (2021). Pressure-corrected carotid stiffness and Young's modulus: evaluation in an outpatient clinic setting. *Am. J. Hypertens.* 34, 737–743. doi: 10.1093/ajh/hpab028

Vande Geest, J. P., Sacks, M. S., and Vorp, D. A. (2004). Age dependency of the biaxial biomechanical behavior of human abdominal aorta. *J. Biomech. Eng.* 126, 815–822. doi: 10.1115/1.1824121

Williams, B., Mancia, G., Spiering, W., Agabiti Rosei, E., Azizi, M., Burnier, M., et al. (2018). 2018 ESC/ESH Guidelines for the management of arterial hypertension. *Eur. Heart J.* 39, 3021–3104.

Conflict of Interest: JC was a past president of the ARTERY (Association for Research into Arterial Structure and Physiology) society. MK was responsible for clinical studies at Esaote SpA (Genova, Italy).

The remaining authors declare that the research was conducted in the absence of any commercial or financial relationships that could be construed as a potential conflict of interest.

Publisher's Note: All claims expressed in this article are solely those of the authors and do not necessarily represent those of their affiliated organizations, or those of the publisher, the editors and the reviewers. Any product that may be evaluated in this article, or claim that may be made by its manufacturer, is not guaranteed or endorsed by the publisher.

APPENDIX

The tube law proposed (Eq. 1 in the main manuscript text) by Meinders and Hoeks (2004) relates changes in pressure (P) to those in the cross-sectional area (assumed circular: $A = \pi D^2/4$):

$$P(D) = P_{\text{ref}} e^{\gamma_0 \left(\frac{D^2}{D^2_{\text{ref}}} - 1 \right)}, \tag{A1}$$

where P_{ref} is a reference pressure, D_{ref} is the arterial diameter at P_{ref}, and γ_0 is an arterial stiffness index.

The Bramwell-Hill equation (Bramwell et al., 1923) indicates that pulse wave velocity (PWV) at a given pressure level P_c can be expressed as a function of the slope of the tangent to the P-D^2 relationship at P_c.

$$\text{PWV}(P_c) = \sqrt{\frac{D^2}{\rho} \left. \frac{\text{d}P}{\text{d}D^2} \right|_{P_c}}, \tag{A2}$$

where $\rho = 1,060\ \text{kg/m}^3$ is the blood density.

Given Eq. A1, the derivative term in Eq. A2 can be rewritten as follows:

$$\left. \frac{\text{d}P}{\text{d}D^2} \right|_{P_c} = \frac{\text{d}}{\text{d}D^2} \left[P_{\text{ref}} e^{\gamma_0 \left(\frac{D^2}{D^2_{\text{ref}}} - 1 \right)} \right] = \frac{P_{\text{ref}} \gamma_0}{D^2_{\text{ref}}} e^{\gamma_0 \left(\frac{D_c^2}{D^2_{\text{ref}}} - 1 \right)}, \tag{A3}$$

where D_c is the diameter value corresponding to the pressure level P_c [i.e., $P_c = P(D_c)$]. Inverting Eq. A1 to express diameter as a function of pressure leads to the following relationship:

$$D = D_{\text{ref}} \sqrt{1 + \frac{\ln\left(\frac{P}{P_{\text{ref}}} \right)}{\gamma_0}}, \tag{A4}$$

so that D_c becomes as follows:

$$D_c = D_{\text{ref}} \sqrt{1 + \frac{\ln\left(\frac{P_c}{P_{\text{ref}}} \right)}{\gamma_0}}. \tag{A5}$$

Substituting Eq. A5 in Eq. A3 yields as follows:

$$\left. \frac{\text{d}P}{\text{d}D^2} \right|_{P_c} = \frac{P_{\text{ref}} \gamma_0}{D^2_{\text{ref}}} e^{\gamma_0 \left(\frac{\ln\left(\frac{P_c}{P_{\text{ref}}} \right)}{\gamma_0} \right)} = \frac{P_c \gamma_0}{D^2_{\text{ref}}}. \tag{A6}$$

Replacing the derivative in Eq. A1 with Eq. A6 and rearranging using Eq. A5 then leads to Eq. A7 (corresponding to Eq. 3 in the main manuscript text):

$$\text{PWV}(P_c)^2 = \frac{D_c^2}{\rho} \frac{P_c \gamma_0}{D^2_{\text{ref}}} = \left(1 + \frac{\ln\left(\frac{P_c}{P_{\text{ref}}} \right)}{\gamma_0} \right) \frac{P_c \gamma_0}{\rho} = \frac{P_c \gamma_0}{\rho} + \frac{P_c}{\rho} \ln\left(\frac{P_c}{P_{\text{ref}}} \right). \tag{A7}$$

Frontiers in Physiology

Understanding how an organism's components work together to maintain a healthy state

The second most-cited physiology journal, promoting a multidisciplinary approach to the physiology of living systems - from the subcellular and molecular domains to the intact organism and its interaction with the environment.

Discover the latest Research Topics

See more →

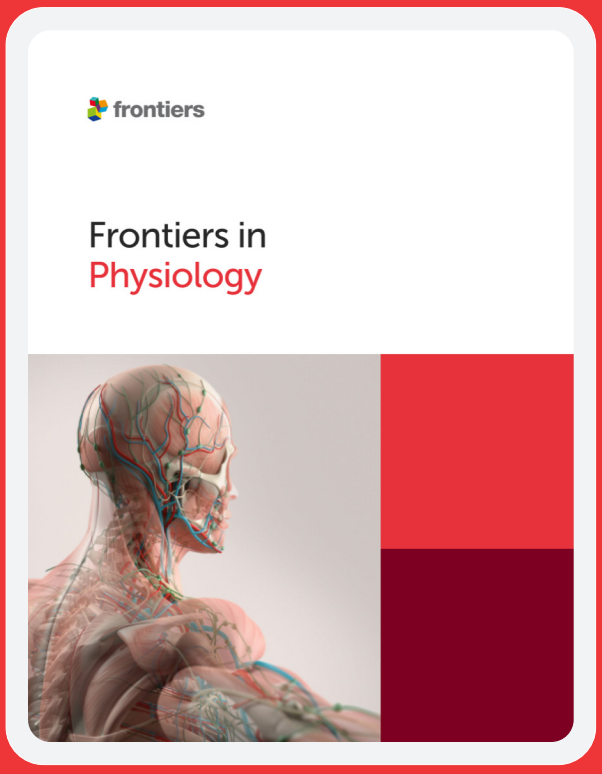

Frontiers

Avenue du Tribunal-Fédéral 34
1005 Lausanne, Switzerland
frontiersin.org

Contact us

+41 (0)21 510 17 00
frontiersin.org/about/contact